University of New Mexico
UNM Digital Repository

Earth and Planetary Sciences ETDs | Electronic Theses and Dissertations

7-2-1986

Long-Term Tributary Adjustments To Base-Level Lowering, Northern Rio Grande Rift, New Mexico

Keith Irvin Kelson

Follow this and additional works at: https://digitalrepository.unm.edu/eps_etds

Part of the Geology Commons

Recommended Citation

Kelson, Keith Irvin. "Long-Term Tributary Adjustments To Base-Level Lowering, Northern Rio Grande Rift, New Mexico." (1986). https://digitalrepository.unm.edu/eps_etds/296

This Thesis is brought to you for free and open access by the Electronic Theses and Dissertations at UNM Digital Repository. It has been accepted for inclusion in Earth and Planetary Sciences ETDs by an authorized administrator of UNM Digital Repository. For more information, please contact disc@unm.edu.

THE UNIVERSITY OF NEW MEXICO
ALBUQUERQUE, NEW MEXICO 87131

Policy on Use of Theses and Dissertations

Unpublished theses and dissertations accepted for master's and doctor's degrees and deposited in the University of New Mexico Library are open to the public for inspection and reference work. *They are to be used only with due regard to the rights of the authors.* The work of other authors should always be given full credit. Avoid quoting in amounts, over and beyond scholarly needs, such as might impair or destroy the property rights and financial benefits of another author.

To afford reasonable safeguards to authors, and consistent with the above principles, anyone quoting from theses and dissertations must observe the following conditions:

1. Direct quotations during the first two years after completion may be made only with the written permission of the author.

2. After a lapse of two years, theses and dissertations may be quoted without specific prior permission in works of original scholarship provided appropriate credit is given in the case of each quotation.

3. Quotations that are complete units in themselves (e.g., complete chapters or sections) in whatever form they may be reproduced and quotations of whatever length presented as primary material for their own sake (as in anthologies or books of readings) ALWAYS require consent of the authors.

4. The quoting author is responsible for determining "fair use" of material he uses.

This thesis/dissertation by Keith Irvin Kelson has been used by the following persons whose signatures attest their acceptance of the above conditions. (A library which borrows this thesis/dissertation for use by its patrons is expected to secure the signature of each user.)

NAME AND ADDRESS	DATE

Keith Irvin Kelson
Candidate

Geology
Department

This thesis is approved, and it is acceptable in quality and form for publication on microfilm:

Approved by the Thesis Committee:

, Chairperson

Accepted:

Asst. *Dean, Graduate School*

July 2, 1986
Date

LONG-TERM TRIBUTARY ADJUSTMENTS TO BASE-LEVEL LOWERING, NORTHERN RIO GRANDE RIFT, NEW MEXICO

By

KEITH IRVIN KELSON

B.A., University of California, Santa Barbara, 1983

THESIS

Submitted in Partial Fulfillment of the
Requirements for the Degree of
Master of Science in Geology

The University of New Mexico
Albuquerque, New Mexico

July, 1986

To Jane,
my wife and best friend,
for direction, unlimited encouragement
and love

ACKNOWLEDGEMENTS

I would like to thank all of the members of my thesis committee, Drs. Stephen G. Wells, Leslie D. McFadden, and Robyn Wright, for moral support and valuable comments; I would like to thank especially Dr. Wells for pointing out this problem, for encouragement, and for asking pertinent questions. The Student Research Allocation Committee of the University of New Mexico provided partial funding for this project, which is greatly appreciated. Acknowledgement is also due to Danny Ruiz and Ted Lucero of the Taos field office of the Soil Conservation Service, and to Linda Beal of the U. S. Geological Survey, Water Resources Division, for providing large amounts of data. Chris Menges, John Wesling, and Keith Taylor of the Department of Geology, University of New Mexico, all provided valuable field assistance, discussion, debate, and friendship throughout the course of this research. My deepest thanks go to my wife, Jane, for field assistance, for pulling me out of the rain, for moral and financial support, and most of all, for love.

LONG-TERM TRIBUTARY ADJUSTMENTS TO BASE-LEVEL LOWERING, NORTHERN RIO GRANDE RIFT, NEW MEXICO

Keith Irvin Kelson

B.A. Geological Sciences, University of California, Santa Barbara, 1983
M.S. Geology, University of New Mexico, 1986

ABSTRACT

Late Cenozoic (post-3.6 Ma) entrenchment of the Rio Grande in northern New Mexico formed a gorge over 200 m deep and induced different types of fluvial adjustments on two adjacent tributaries. Rio Hondo (drainage area 181 km^2) has a concave-up long-profile and flows in a narrow valley containing six Quaternary strath terraces with parallel long-profiles grading to the Rio Grande. In contrast, Rio Pueblo de Taos (drainage area 1080 km^2) has a convex-up long-profile and flows in a wide valley containing four strath terraces which do not grade to the Rio Grande. Although smaller in drainage area, Rio Hondo has adjusted to base-level fall by continued entrenchment, whereas Rio Pueblo de Taos has produced a 140 m-high nickpoint.

Differences between the two watershed's present-day hydrologic parameters relate to source-area lithology and apparently explain differences in long-term fluvial adjustments. The Rio Hondo watershed is developed in gneiss and granite, and produces higher unit discharge and higher bankfull discharge than the Rio Pueblo de Taos watershed, which is underlain by sandstone and shale. Stream power and shear stress data suggest that higher bedload transport rates and larger bedload grain sizes exist on Rio Hondo during bankfull discharge. These differences coupled with the distinct valley morphologies suggest that, over long

periods of time, Rio Hondo has had sufficient stream power to transport its bedload, erode vertically, and keep pace with downcutting on the Rio Grande. Rio Pueblo de Taos has apparently expended its energy via lateral migration rather than vertical erosion. Alternating periods of incision and lateral erosion on both streams may also be linked to hydrologic changes resulting from climatic changes. The present-day hydrologic parameters of these two watersheds suggest that bedrock lithology strongly influences: 1) the duration and magnitude of discharge events, 2) stream power, 3) sediment load, and 4) the relative sensitivity of each basin to base-level change.

TABLE OF CONTENTS

INTRODUCTION.....1
Problem.....1
Purpose.....2
Study Area.....2
Climate and Vegetation.....6
Geologic Setting.....8
Previous Work.....12

METHODS.....15
Field Methods.....15
Laboratory and Office Methods.....20

RESULTS.....29
Present-day Fluvial System.....29
Water Discharge Characteristics.....29
Runoff Generation.....34
Bankfull Discharge.....41
Bed Material Characteristics.....46
Sediment Transport Parameters.....54
Basin Morphometry.....59
Geomorphic Surfaces and Deposits.....72
Geomorphic Surfaces in the Rio Hondo Valley.....73
Sedimentology of Rio Hondo Fluvial Deposits.....79
Soil Properties of Geomorphic Surfaces in the Rio Hondo Valley.....86
Geomorphic Surfaces in the Rio Pueblo de Taos Valley.....91
Sedimentology of Rio Pueblo de Taos Fluvial Deposits.....104
Soil Properties of Geomorphic Surfaces in the Rio Pueblo de Taos Valley.....107

DISCUSSION.....110
Factors Controlling Present-day Fluvial Hydrology 110
Water Inputs.....110
Infiltration Capacities.....111
Storage Capabilities.....115
Summary.....119
Sediment Transport in the Present-day Fluvial Systems.....119
Sediment Transport in Channels Draining Crystalline Terrane.121
Sediment Transport in Channels Draining Sedimentary Terrane.125
Present-day Longitudinal Profiles.....129
Quaternary Fluvial System.....132
Age Relationships of Geomorphic Surfaces.....132
The Critical-power Threshold.....134
Rio Hondo Stream Power/Critical Power Relations.....135
Rio Pueblo de Taos Stream Power-Critical Power Relations....139
Long-term Fluvial System Adjustments to External Variables.....141
Influences of Time.....141
Effects of Relief and Lithology During the Quaternary.....143
Effects of Base-level Lowering.....143
Effects of Base-level Lowering on Rio Hondo.....144
Effects of Base-level Lowering on Rio Pueblo de Taos...146

TABLE OF CONTENTS (continued)

Effects of Climatic Change.....148
Effects of Climatic Change on Rio Hondo.....148
Effects of Climatic Change on Rio Pueblo de Taos.....152
Effects of Mountain-front Tectonic Activity.....156
Complex Responses of the Fluvial Systems.....157
Summary.....158
Grade and Equilibrium in Rivers on the Taos Plateau.....159
Fluvial Geomorphic History.....161

CONCLUSIONS.....164

APPENDICES.....166

A. Methods and assumptions used in snowmelt-runoff water budget calculations.....166

B. XSECTION: Pascal-language program for calculation of water discharge using slope-area method, for IBM-compatible microcomputer.....170

C. Classification and field descriptions of soils in the Rio Hondo and Rio Pueblo de Taos valleys below the Sangre de Cristo mountain front, near Taos, New Mexico.....178

D. Method of calculating normalized values for carbonate morphology in the Relative Profile Development index.....190

E. Mean annual discharges of selected U. S. Geological Survey streamflow gaging stations in Colorado, Utah, Wyoming, and New Mexico.....191

F. Mean monthly snowmelt, rainfall, evapotranspiration, runoff, and water storage in six drainage basins near Taos, NM.....193

G. Number and lengths of stream links in six small drainage basins near Taos, New Mexico.....195

H. Calculations of the Relative Profile Development index (Harden, 1982) for soil profiles described in the Rio Hondo and Rio Pueblo de Taos valleys.....197

REFERENCES.....203

LIST OF FIGURES

Figure 1. Photograph of the Rio Grande gorge, taken looking south (downstream) from the Rio Grande Gorge Bridge. Note absence of distinct fluvial terraces.....3

Figure 2. General geologic map of the two watersheds in the study area. (after Gruner, 1920; Dane and Bachman, 1965; Miller et al., 1976; Reed et al., 1983).....4

Figure 3. Longitudinal-profiles of active Rio Hondo and Rio Pueblo de Taos channels between the Sangre de Cristo mountain front and the Rio Grande. (^) denotes mountain front.....7

Figure 4. Map of the Rio Grande rift region, showing location of study area. Fine stipple = rift-related basin; coarse stipple = structural or topographic high. (after Manley, 1979).....9

Figure 5. Diagrammatic cross-section through the Taos Plateau volcanic field showing inferred structure of the Rio Grande rift; Q = Quaternary surficial deposits, Toa = olivine andesite, Tse Servilleta Basalt, Ts = Tertiary rift sediments, Tb = pre-rift basalt flows, Ta = pre-rift andesitic flows and breccias, Tg = pre-rift granitic intrusions, pT = pre-Tertiary rocks. (after Lipman and Mehnert, 1979). Horizontal scale: 1 cm = 3 km.....10

Figure 6. Map showing geomorphic regions and station locations of bed-material and channel morphology measurements. Geomorphic regions are based on areas containing similar channel and physiographic properties; Table 20 contains characteristics of streams within each region. Regions are: (I) streams draining crystalline terrane above the mountain front, (II) Rio Hondo between the mountain front and its basalt gorge, (III) Rio Hondo in its basalt gorge, (IV) streams draining sedimentary terrane above the mountain front, (V) stream reaches between the mountain front and the Rio Pueblo de Taos basalt gorge, and (VI) Rio Pueblo de Taos in its basalt gorge.....17

Figure 7. Variation of precipitation with elevation at climatic stations within and near the study area. Periods of record: Taos (T) 1889-1954; Cerro (C), 1910-1954; San Cristobal (SC), 1948-1954; Red River (RR), 1906-1954; Taos Canyon (TC), 1910-1943; Anchor Mine (AM), 1911-1920. Data from State Engineer Office (1956). ■ = April, + = May, ◆ = June, ▲ = July.....22

Figure 8. Variation of mean daily temperature with elevation at climatic stations within and near the study area. Periods of record: Taos (T) 1892-1954; Cerro (C), 1911-1954; San Cristobal (SC), 1948-1954; Red River (RR), 1910-1954. Data from State Engineer Office (1956). ■ = April, + = May, ◆ = June, ▲ = July.....23

Figure 9. Variation of average snowpack water content on April 1 with elevation, for snow courses within and near the study area. Data from: Red River Pass, Red River Pass #2, Hematite Park,

Twining, Taos Canyon, Palo, Tres Ritos, Alamitos, Cordova, and Taos Powderhorn (Washichek et al., 1972; Washichek et al., 1978).....24

Figure 10. Discharge per unit area duration curves at six U.S.G.S. streamflow gaging stations near Taos. RH = Rio Hondo near Valdez; RL = Rio Lucero near Arroyo Seco; RPT = Rio Pueblo de Taos near Taos; RGR = Rio Grande del Rancho near Talpa; RC = Rio Chiquito near Talpa; RFT = Rio Fernando de Taos near Taos. RH and RL drain predominantly granite and gneiss; RGR, RC, and RFT drain sandstone and shale; RPT drains about 70% sedimentary and about 30% crystalline lithologies.....31

Figure 11. Mean daily discharge (m^3/s) from April 1 to July 31, 1973, for six U.S.G.S. streamflow gaging stations in the study area. All plots have the same scales. Stations are same as those in Table 3.....33

Figure 12. Plot of mean annual discharge (Qa) against drainage area (A) for basins in New Mexico, Colorado, Utah, and Wyoming. Criteria for basin selection: 1) basins underlain by greater than 85% crystalline or sedimentary terrane, 2) minor or no upstream diversions, 3) perennial flow, and 4) a gaged record longer than seven years. See Appendix E for references.....35

Figure 13. Mean monthly snowmelt (A), runoff (B), rainfall (C), and evapotranspiration (D); for the Rio Hondo (□), Rio Lucero (+), Rio Pueblo de Taos (◇), Rio Fernando de Taos (△), Rio Chiquito (×), and Rio Grande del Rancho (▽) basins.....37

Figure 14. Mean daily discharge per unit drainage area ($m^3/s/km^2$) from April 1 to July 31, 1973, for six gaging stations in the study area.....39

Figure 15. Mean monthly change in basin storage for the Rio Hondo (□), Rio Lucero (+), Rio Pueblo de Taos (◇), Rio Fernando de Taos (△), Rio Chiquito (×), Rio Grande del Rancho (▽) basins. Storage change calculated by subtracting runoff and evapotranspiration losses from snowmelt and rainfall inputs.....40

Figure 16. Bankfull discharge plotted against drainage area for surveyed sites. The least-squares regression curves have coefficients of correlation (r) of 0.896 (crystalline) and 0.935 (sedimentary).....48

Figure 17. Relative frequency plot of bed-material grain sizes on streams draining crystalline and sedimentary terrane. Note coarser grain sizes in channels draining crystalline rocks.....51

Figure 18. Plot of bed-material grain size against distance from drainage divide.....52

Figure 19. Relative frequency plot of clast lithologies in bed-material samples. GN = gneiss, GR = granite, RHY = rhyolite and andesite, SCH = schist, OX = other crystalline lithologies

(including basalt, amphibolite, and massive quartz), SS = sandstone, CG = conglomerate, SH = shale. To allow comparison with Figure 31, data is from sites 30, 31, and 32 along Rio Hondo, and from sites 29, 33, and 34 along Rio Pueblo de Taos (see Plates 1 and 2 for locations).....53

Figure 20. Plot of largest bed-material clast and of 5th largest bed-material clast in each bed-material sample against mean grain size. High r value for 5th largest clast data suggests that the 5th largest clasts are moveable bed material; whereas, the low r value for largest clast data implies that the largest clasts are usually mot moved.....55

Figure 21. Plot of stream power against distance from drainage divide.....61

Figure 22. Plot of cumulative percent of drainage area above a given elevation for six drainage basins in the study area. The two basins underlain by crystalline rocks (Rio Hondo and Rio Lucero) have more drainage area within high elevation zones than basins underlain by sedimentary rocks.....62

Figure 23. Variations in Vf ratios (valley floor width/valley depth) with distance from the mountain front. High Vf ratios reflect valleys having wide floors relative to valley depth. (A) Rio Hondo, (B) Rio Lucero, (C) Rio Chiquito, (D) Rio Fernando de Taos.....65

Figure 24. Hypsometric curves for six basins above the Sangre de Cristo mountain front.....68

Figure 25. Long-profiles of Rio Hondo and six major tributaries to Rio Pueblo de Taos. See Figure 2 for locations and underlying rock types. (^) denotes mountain front. Vertical arrangement of long-profiles is for clarity; y-axis does not represent elevation.....71

Figure 26. Schematic cross-valley profiles of the Rio Hondo valley. (A) approximately 9 km above the Rio Hondo-Rio Grande junction, where strath terraces are cut into basin-fill deposits. (B) approximately 2 km above the Rio Hondo-Rio Grande junction, where strath terraces are cut into basalt. Thicknesses of terrace deposits are approximate.....74

Figure 27. Photograph of the Rio Hondo valley, showing several fluvial terraces. Photograph taken looking northwest from Highway 3. RH = present-day Rio Hondo, RGG = Rio Grande gorge, see Plate 1 for descriptions of map units Qt3, Qt4, Qt5, Qt6, Qt7, and Q8.....75

Figure 28. Long-profiles of geomorphic surfaces flanking Rio Hondo below the mountain front. (^) denotes mountain front. Solid lines represent continuous surfaces. See Plate 1 for locations of cross-section measurement sites 30, 31, and 32.....78

Figure 29. Photograph of deposits associated with surface Qt4,

exposed in roadcut 3.7 km west of Valdez (see Plate 1). Note that terrace gravels unconformably overlie finer grained basin-fill deposits. Hammer is about 30 cm long.....82

Figure 30. Relative frequency plot of coarse grain size fractions of terrace deposits in the Rio Hondo (A) and Rio Pueblo de Taos (B) valleys below the mountain front.....84

Figure 31. Relative frequency plot of clast lithologies in deposits associated with surfaces Qt2 through Qt7 in the Rio Hondo and Rio Pueblo de Taos valleys. GN = gneiss, GR = granite, RHY = rhyolite and andesite, SCH = schist, OX = other crystalline lithologies (including basalt, amphibolite, and massive quartz), SS = sandstone, CG = conglomerate, SH = shale. Compare with Figure 19. (see Plates 1 and 2 for locations).....85

Figure 32. Cumulative numerical percent plot of coarse grain-size fractions of deposits associated with surfaces Qt2 through Qt7 in the Rio Hondo (□) and Rio Pueblo de Taos (+) valleys, and of deposits associated with surface Q1p (◆). Note that deposits associated with surface Q1p are finer grained than deposits associated with younger geomorphic surfaces.....87

Figure 33. Relative Profile Development indices (Harden, 1982) for soils in the (A) Rio Hondo and (B) Rio Pueblo de Taos valleys. Top of wide-ruled bar shows minimum; top of narrow-ruled bar shows maximum. N.D. = no data.....90

Figure 34. Schematic cross-valley profiles below the mountain front. (A) Rio Pueblo de Taos near Ranchito, (B) Arroyo Seco above Los Cordovas, (C) Rio Grande del Rancho near Ranchos de Taos, (D) Rio Pueblo de Taos below Los Cordovas. Strath terraces in (A), (B), and (C) are cut into basin-fill deposits; surfaces Qt3 and Qt4 in (D) are cut into basalt. Thicknesses of terrace deposits are approximate. Arrows indicate confluences of Arroyo Seco and Rio Grande del Rancho with Rio Pueblo de Taos. Diagrams are arranged to show that Arroyo Seco and Rio Grande del Rancho flow into Rio Pueblo de Taos near Los Cordovas.....94

Figure 35. Photograph of the Arroyo Seco valley, showing geomorphic surfaces Q1p, Qt2, Qt4, and Q8. Photograph taken looking northwest about 3 km above the Arroyo Seco-Rio Pueblo de Taos junction. AS = present-day Arroyo Seco, See Plate 2 for descriptions of map units.....96

Figure 36. Long-profiles of geomorphic surfaces flanking (A) Arroyo Seco near Los Cordovas (B) Rio Grande del Rancho below the mountian front, and (C) Rio Pueblo de Taos below Taos. Solid lines represent continuous geomorphic surfaces. See Plate 2 for locations of cross-section measurement sites 29, 33, and 34.....99

Figure 37. Long-profiles of geomorphic surfaces flanking Rio Grande del Rancho between the mountian front and Ojo Sarco Canyon (see Plate 3). Solid lines represent continuous geomorphic

surfaces. (^) denotes mountain front.....103

Figure 38. Deposits associated with surface Qt2 exposed in gravel pit at site PC11 (see Plate 2). Note well-developed soil and terrace gravels unconformably overlying fine-grained basin-fill deposits (lower right).....106

Figure 39. Photograph of the Rio Hondo valley at the mountain front, showing narrow valley that lacks significant amounts of valley fill alluvium. Note bedrock outcrops on steep hillslopes. Photograph taken looking east from surface Qlp above the village of Valdez.....113

Figure 40. Photograph of the Rio Fernando de Taos valley showing large amounts of valley fill alluvium and shallow hillslopes. Photograph taken looking southeast above the Rio Fernando-Las Tienditas Creek junction.....114

Figure 41. Long-profile of the Lake Fork branch of Rio Hondo, showing inferred distribution of glacial deposits and inferred groundwater flow paths. W = Williams Lake, T = village of Twining (Taos Ski Valley). Reach 24 was dry on September 22, 1984, although reach 25 contained about 0.75 m^3/s. No tributaries enter between the two sites.....117

Figure 42. Changes in stage for a discharge of 1.42 m^3/s at (A) U.S.G.S. station 08267500 and (B) U.S.G.S. station 08268500. Similar trends exist for higher discharges at both sites. See Figure 6 for locations.....123

Figure 43. Changes in stage at three U.S.G.S. streamflow gaging stations in the Rio Pueblo de Taos basin. (A) U.S.G.S. station 08275500; stages are for 0.71 m^3/s. (B) U.S.G.S. station 08275300; stages are for 2.83 m^3/s. (C) U.S.G.S. station 08276300; stages are for 2.83 m^3/s. Similar trends exist at higher and lower discharges at all three sites. See Figure 6 for locations.....126

Figure 44. Photograph of the Rio Pueblo de Taos valley on the Taos Plateau, showing wide valley floor and low relief. Photograph taken looking west from mountain front facet near Rio Fernando de Taos. RPT = present-day Rio Pueblo de Taos.....128

Figure 45. Arithmetic plot of regression curves from data in Figure 16, showing higher increase in discharge in basins underlain by crystalline rocks.....131

Figure 46. Diagrammatic sketch and graphs of stream power and critical power for an arid rocky drainage basin (from Bull, 1979)....136

Figure 47. Diagrammatic sketches of stream power and critical power along Rio Hondo and Rio Pueblo de Taos. (A) present-day system, representing dominant mode of behavior along both streams. (B) past conditions, representing less prevalent mode of behavior. Stream power curves are based on Figure 21. Critical power curves

are estimated based on negligible changes in hydraulic roughness as estimated by Manning n-values (Tables 4 and 5), and differences in bed-material grain sizes along Rio Pueblo de Taos and Rio Hondo (Fig. 17).....138

Figure 48. (A) Cross-section of paleochannel in deposits associated with surface Qt6 exposed in Highway 3 roadcut 0.4 km north of Arroyo Hondo. Estimated bankfull discharge = 110 m^3/s (see text). (B) Channel cross-section at site 31, 1.0 km west of Arroyo Hondo, plotted at same scale as (A). Estimated bankfull discharge = 10.9 m^3/s. See Plate 2 for locations.....151

Figure 49. Schematic representation of inferred aggradation and degradation through time. Change from stability to degradation on Rio Hondo is shown as being contemporaneous with change from degradation to stability on Rio Pueblo de Taos; these events may not have been synchronous.....162

Figure A1. Methods used to calculate monthly water storage changes in six basins within the study area. P = precipitation, M = snowmelt, L = evapotranspiration loss, R = runoff, S = storage change.....167

LIST OF TABLES

Table 1. The status of drainage basin variables during time spans of decreasing duration. Cyclic time represents geologic time, during which there is continual removal of material from a drainage basin. Graded time represents a span of perhaps hundreds of years, during which fluvial changes fluctuate about an average condition. Steady time is perhaps days or hours, during which channel morphology remains essentially constant. (from Schumm and Lichty, 1965).....15

Table 2. Parent material characteristics used in calculating Relative Profile Development indices (Harden, 1982), for soil profiles described in the Rio Hondo and Rio Pueblo de Taos drainage basins. Data from samples of modern alluvium (see Appendix C). Soil profile SP23 was described on Qt6 near Los Cordovas (see Plate 2).....28

Table 3. Discharge data for six U.S.G.S. streamflow gaging stations in the study area, as of Water Year 1984. Note higher discharges per unit area for basins draining crystalline rocks. xtln = crystalline, sed = sedimentary. See Figure 6 for station locations.....30

Table 4. Channel characteristics and bankfull flow properties at sites draining crystalline terrane. Qbf = bankfull discharge. See Plate 1 and Figure 6 for locations.....42

Table 5. Channel characteristics and bankfull flow properties at sites draining sedimentary terrane. Qbf = bankfull discharge. See Plate 2 and Figure 6 for locations.....43

Table 6. Width, area, velocity, and discharge values calculated from field surveys and measured by U.S.G.S. personnel. See Figure 6 for locations. Measurement 409 at gage 08275300 probably represents overbank flow.....45

Table 7. Bankfull flood frequency data for sites measured at or near U.S.G.S. gaging stations. Qbf = bankfull discharge. See Figure 6 for locations.....47

Table 8. Bed-material grain size parameters of channels draining crystalline and sedimentary terrane. See Figure 6 for locations.....49

Table 9. Means of the five and ten largest clasts in random bed-material samples. See Plates 1 and 2 for locations.....57

Table 10. Selected channel and bankfull flow properties and dimensionless shear stress values for channels draining crystalline and sedimentary terranes. T*c50 = 0.031, T*c90 = 0.015 (Andrews, 1984). ! indicates values close to critical values. Regions are shown in Figure 6.....58

Table 11. Selected bankfull hydraulic characteristics in channels draining crystalline and sedimentary terrane. Fluid density

assumed to be 1.00 g/cm^3 in stream power calculations. Regions are shown in Figure 6.....60

Table 12. Summary of basin morphometry data for six basins in the Sangre de Cristo mountains near Taos. Data for Rio Grande del Rancho includes data from Rito de la Olla tributary. xtln = crystalline, sed = sedimentary.....64

Table 13. Summary of morphometry data for long-profiles from drainage divide to the confluence with a higher order stream. Coefficients of determination (r^2) are for logarithmic, exponential, and power function best-fit curves to long-profiles. * indicates highest r^2 values of three curves. Rito de la Olla is a large tributary to Rio Grande del Rancho above the mountain front.....70

Table 14. Heights (m) of geomorphic surfaces above the modern floodplain, in the Rio Hondo and Rio Pueblo de Taos valleys below the Sangre de Cristo mountain front. The Arroyo Seco, Rio Grande del Rancho, and Rio Pueblo de Taos valleys all join near Los Cordovas, which is about 10.7 km upstream of the Rio-Grande-Rio Pueblo de Taos junction. See Plates 1 and 2 for valley locations.....77

Table 15. Gradients (m/km) of long-profiles of geomorphic surfaces in the Rio Hondo and Rio Pueblo de Taos valleys below the Sangre de Cristo mountain front. The Arroyo Seco, Rio Grande del Rancho, and Rio Pueblo de Taos valleys all join near Los Cordovas, which is about 10.7 km upstream of the Rio-Grande-Rio Pueblo de Taos junction.....80

Table 16. Grain size characteristics of fluvial deposits in the Rio Hondo and Rio Pueblo de Taos valleys below the mountain front. Deposits associated with surface $Q1_p$ occur in both valleys; data from these deposits are presented separately due to distinctness from other deposits (see text). See Plates 1 and 2 for site locations.....83

Table 17. Selected soil characteristics for soil profiles described in the Rio Hondo and Rio Pueblo de Taos valleys. See Plates 1 and 2 for profile locations. Dashes (--) indicate that property was not present in soil profile.....88

Table 18. Summary of selected soil properties used in identification of map units. Range in properties is for one to five soil profiles per geomorphic surface.....92

Table 19. Summary of flow properties, channel properties, and valley morphology in Regions I to VI (see Fig. 6).....122

LIST OF PLATES (in pocket)

1. Map of fluvial geomorphic units along Rio Hondo below the Sangre de Cristo mountain front, near Taos, New Mexico

2. Map of fluvial geomorphic units along Rio Pueblo de Taos, Arroyo Seco, Rio Grande del Rancho, and Rio Fernando de Taos, near Taos, New Mexico

3. Map of fluvial geomorphic units along Rio Grande del Rancho between the Sangre de Cristo mountain front and Ojo Sarco Canyon, near Taos, New Mexico

INTRODUCTION

Problem

Discharge and stream power influence fluvial system response to external stimuli (such as base-level or climatic change) (Leopold and Bull, 1979), and therefore may affect longitudinal-profile shape and position after a stream has experienced base-level or climatic change. Therefore, present-day hydrologic parameters can be used to investigate adjustments of long-profiles. Long-profile adjustments in fluvial systems involve changes in streambed elevation, channel gradient, and profile shape (Richards, 1982). Streambed elevation is influenced by aggradation and degradation, which can be produced by changes in base-level elevation (Bull, 1979) or sediment yield/streamflow ratios (Richards, 1982). Channel gradient is influenced by water discharge (Gilbert, 1877; Mackin, 1948) and the size and amount of bed material being transported (Hack, 1957; Rubey, 1952). Long-profile shape may be a function of: 1) discharge (Wheeler, 1979), 2) bed-material size (Hack, 1957), and 3) underlying lithology (Shepherd, 1979). Because changes in channel gradient and long-profile shape result from local changes in streambed elevation, processes which result in aggradation or degradation largely control long-profile adjustments.

Aggradation and degradation along a stream may be a result of processes that act at base level, which John Wesley Powell defined as the ultimate level to which a landscape could be denuded (Ritter, 1978). Leopold and Bull (1979) defined base level as the elevation at which potential energy is not further transformed into kinetic energy, and found that local base levels can control upstream channel elevations for limited periods of time.

In the northern Rio Grande rift, base level for Rio Grande tributaries has been lowered due to downcutting of the Rio Grande through late Cenozoic (4.5 to 3.6 Ma) basalt (Fig. 1). This lowering has produced the Rio Grande Gorge, which is over 200 m deep, and has initiated long-profile adjustments along tributaries. Two adjacent tributaries, Rio Hondo and Rio Pueblo de Taos, show significant differences in long-profile, valley morphology, and stream terrace sequences, which reflect different responses to base-level fall. Therefore, this setting enables evaluation of fluvial adjustments of long-profile, local gradient, and sediment transport capabilities in response to base-level fall, and assessment of factors which have controlled the distinct fluvial adjustments on the two tributaries.

Purpose

The primary purpose of this research is to determine the factors which have controlled long-term longitudinal profile development, valley morphology, and terrace sequence production in the Rio Hondo and Rio Pueblo de Taos drainage basins. Specifically, this research addresses: 1) the influence of source-area lithology on runoff production, 2) the geomorphic evolution of the Rio Hondo and Rio Pueblo de Taos valleys since initiation of downcutting along the Rio Grande, and 3) the relative sensitivities of the two basins to base-level lowering.

Study Area

The study area is composed of the Rio Hondo and Rio Pueblo de Taos drainage basins located in southeastern Taos County, New Mexico (Fig. 2). Both streams head on the western side of the Sangre de Cristo Mountains, flow onto the piedmont alluvium and basalt of the Taos Plateau, and drain

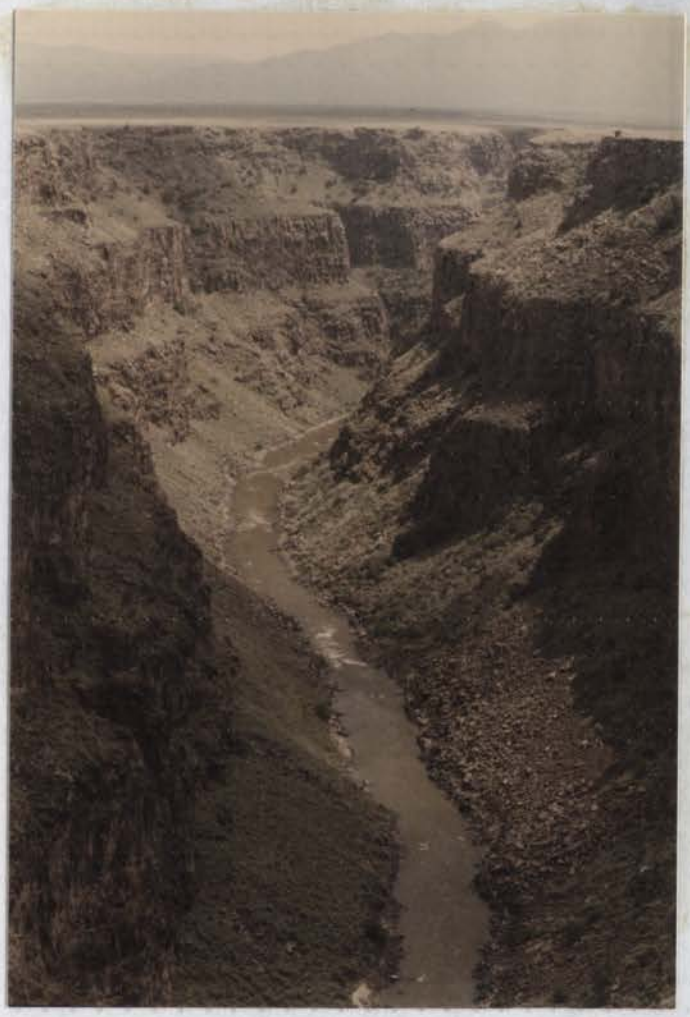

Figure 1. Photograph of the Rio Grande gorge, taken looking south (downstream) from the Rio Grande Gorge Bridge. Note absence of distinct fluvial terraces.

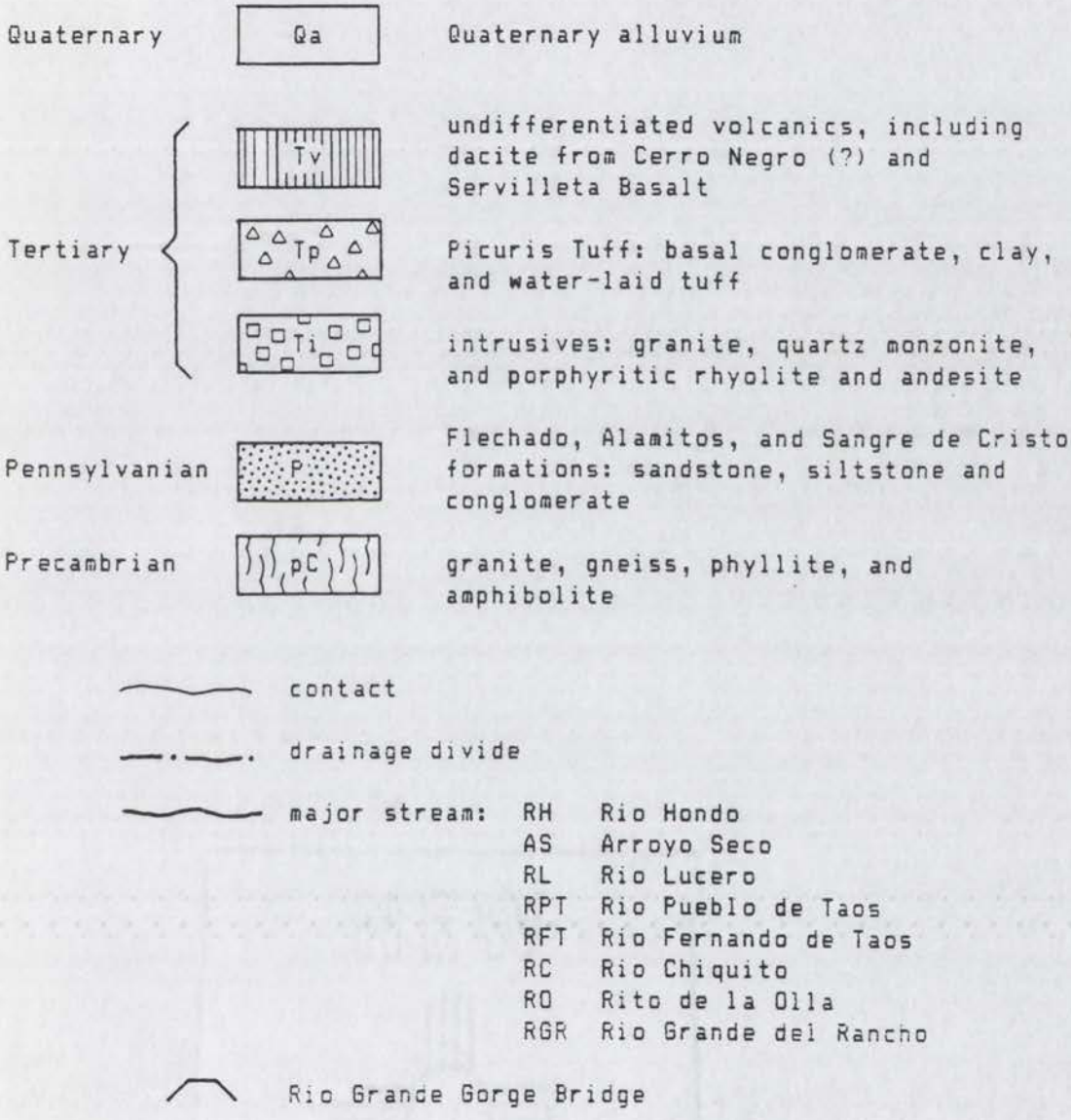

Figure 2. General geologic map of the two watersheds in the study area. (after Gruner, 1920; Dane and Bachman, 1965; Miller et al., 1976; Reed et al., 1983)

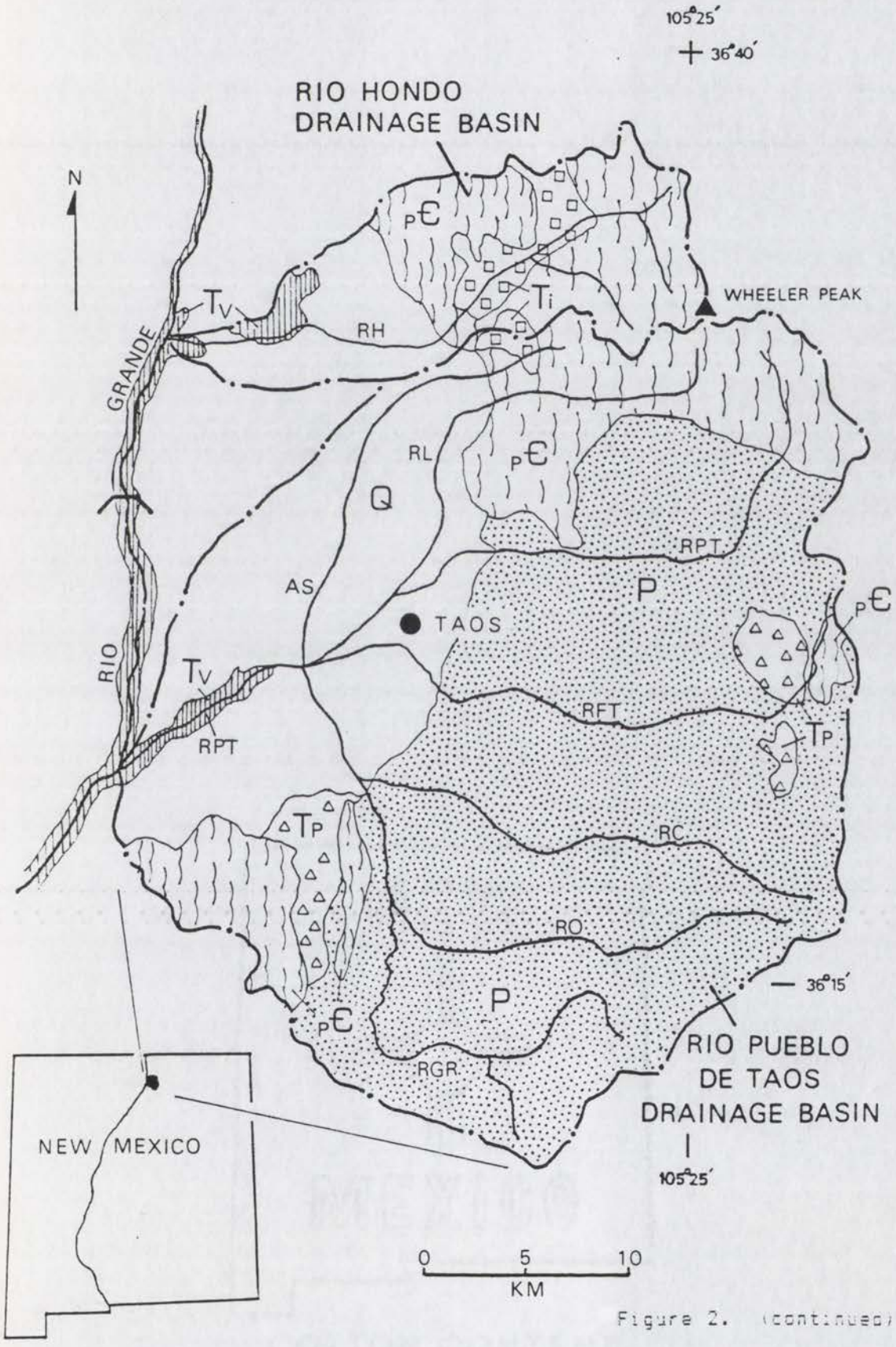

Figure 2. (continued)

to the Rio Grande (Fig. 2). The perennial Rio Hondo flows west 33 km, draining an area of 181 km². The drainage area has 2040 m of relief and includes Wheeler Peak, the highest peak in New Mexico (elevation 4010 m). Rio Pueblo de Taos flows west 56 km, draining an area of 1080 km². Several perennial tributaries drain this basin, which has total relief of 2150 m.

Significant differences in source-area lithology, long-profiles, valley morphology, and terrace sequences exist between the two drainages. Above the Sangre de Cristo mountain front, the Rio Hondo basin is underlain predominantly by gneiss and granite; however, sandstone and shale underlie the majority of the Rio Pueblo de Taos basin above the mountain front. Rio Hondo, below the mountain front, flows in a narrow valley containing six fluvial terraces. The Rio Hondo long-profile below the mountain front is straight and steep, having a gradient of 23 m/km (Fig. 3). Below the mountain front, Rio Pueblo de Taos has a convex-up long-profile and flows in a broad valley containing three fluvial terraces. The Rio Pueblo de Taos long-profile decreases in gradient from about 16 to 3 m/km, but then increases in gradient to 84 m/km within 2 km of the Rio Grande (Fig. 3).

Climate and Vegetation

Present-day climate and vegetation throughout the study area vary considerably with elevation. Annual precipitation ranges from 315 mm at Taos to over 530 mm in the subhumid mountains, and mean annual temperature ranges from about 4.0°C in the mountains to 8.6°C at Taos (State Engineer Office, 1956). Precipitation in both basins falls mostly as winter snow or convectional summer rain.

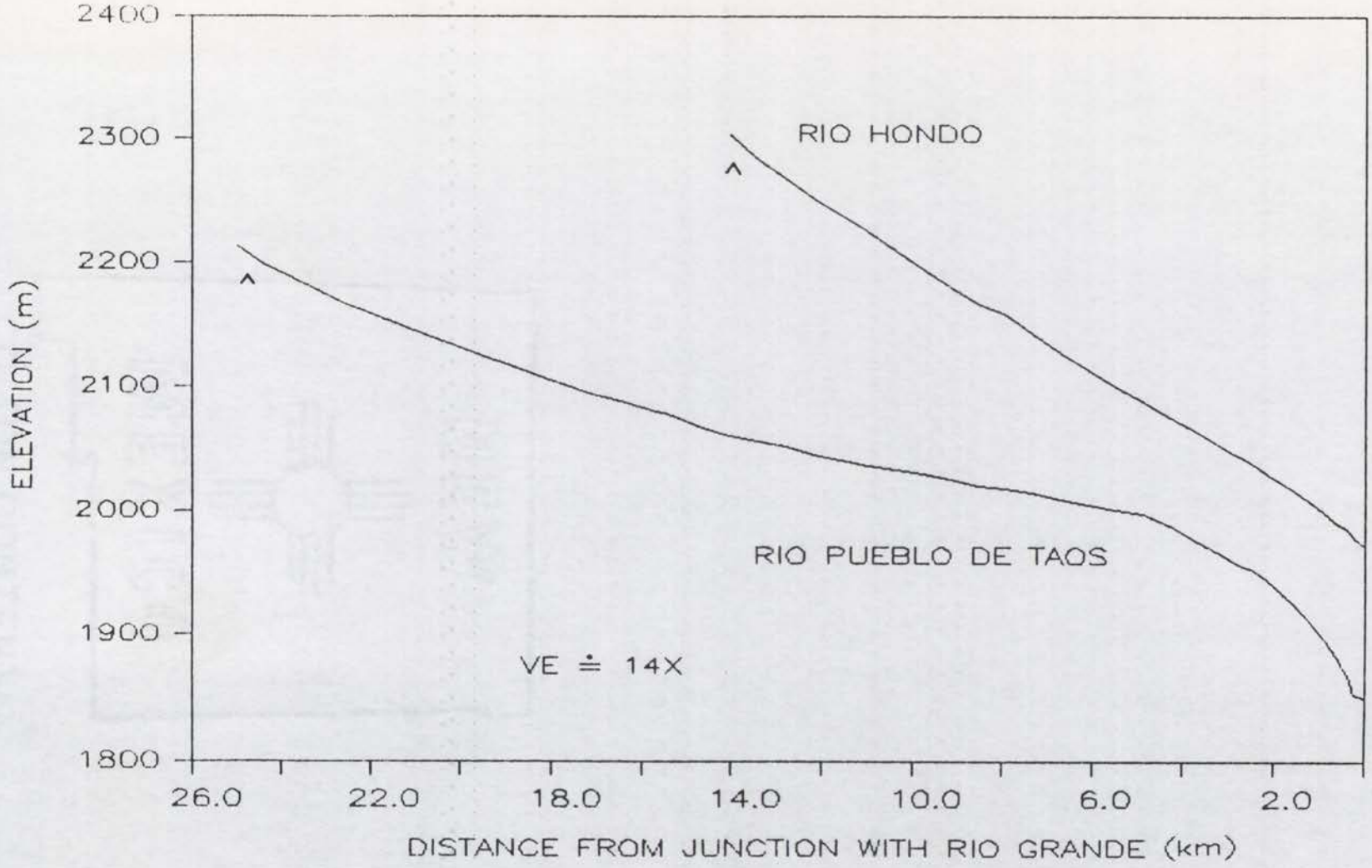

Figure 3. Longitudinal-profiles of active Rio Hondo and Rio Pueblo de Taos channels between the Sangre de Cristo mountain front and the Rio Grande. (^) denotes mountain front.

Vegetation consists of pine (Pinus ponderosa), fir (Picea taxifolia), and aspen (Populus tremuloides) in the mountains, and piñon (Pinus edulis), and juniper (Juniperus monosperma) and sagebrush (Artemesia sp.) on the plateau (Dixon, 1962). Many stream terraces are used for grazing or agriculture.

Geologic Setting

Rio Hondo and Rio Pueblo de Taos flow west out of the Sangre de Cristo Mountains near Taos, New Mexico, and onto the Taos Plateau (Fig. 2). The Taos Plateau comprises the southern portion of the San Luis Basin (Fig. 4), which is a fault-block basin in the northern Rio Grande structural trough filled with approximately 5 km of Oligocene and younger basin fill (Kelley, 1956; Fig. 5). The Sangre de Cristo fault zone marks the eastern basin margin, and normal faults along the Tusas Mountains bound the western margin of the basin (Manley, 1982; Fig. 5). Chapin and Seager (1975) hypothesized that rifting began in late Oligocene time.

McCalpin (1982) documented that near Alamosa, Colorado, Quaternary movement in the active Sangre de Cristo fault zone consisted of alternating periods of rapid uplift and tectonic quiescence. However, the post-Pinedale uplift rate is approximately equal to the long-term average rate of 0.3 mm/yr (McCalpin, 1982). Near Taos, the Sangre de Cristo fault zone has been less active in the late Quaternary (Personius and Machette, 1984). These workers mapped several north-trending, Pliocene to latest Pleistocene normal faults on the Taos Plateau which offset basalt strata, alluvial fans, and basin-fill deposits. Offset on the Sangre de Cristo fault zone in this area ranges from 4 to 18 m; all scarps indicate recurrent movement with the most recent rupture in the middle or late Pleistocene. Deformation on the plateau also includes

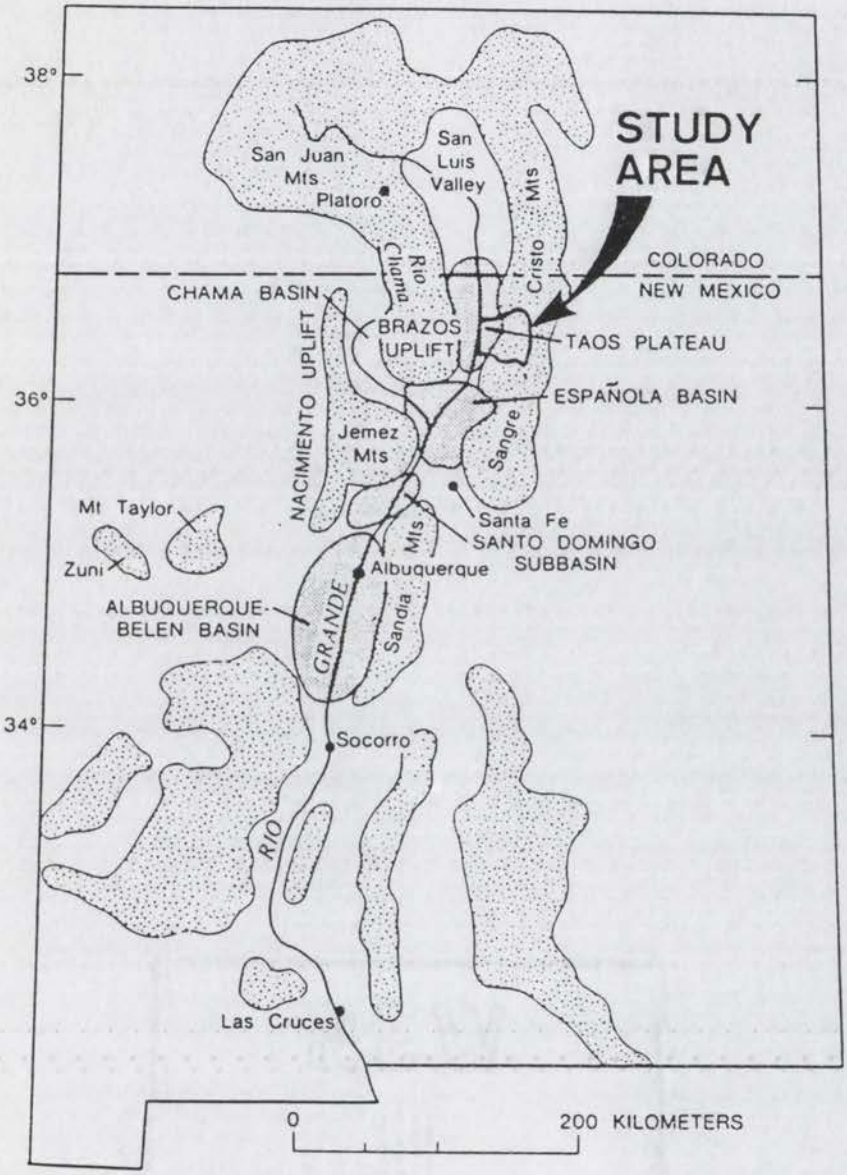

Figure 4. Map of the Rio Grande rift region, showing location of study area. Fine stipple = rift-related basin; coarse stipple = structural or topographic high. (after Manley, 1979)

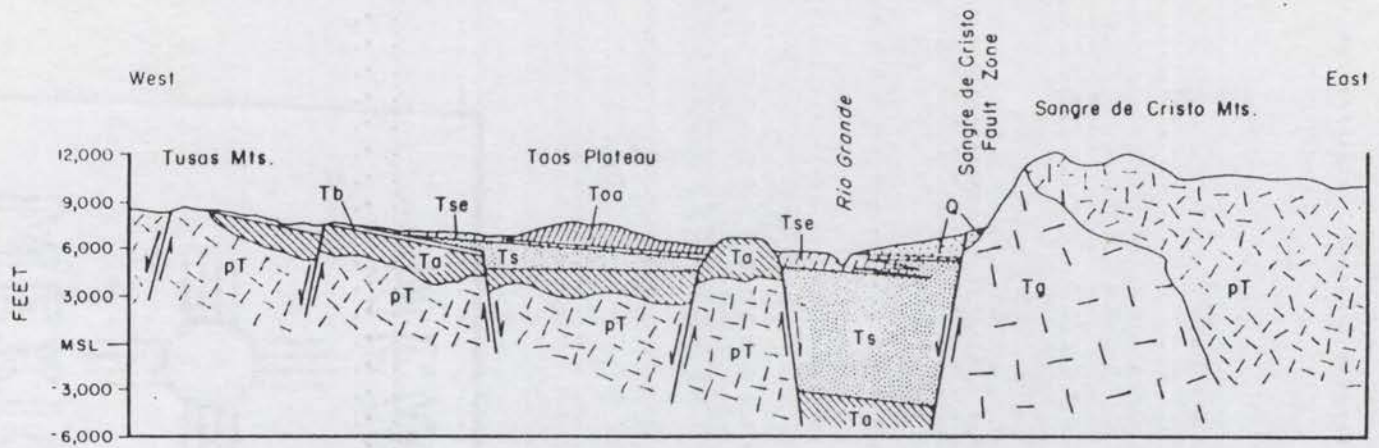

Figure 5. Diagrammatic cross-section through the Taos Plateau volcanic field showing inferred structure of the Rio Grande rift; Q = Quaternary surficial deposits, Toa = olivine andesite, Tse Servilleta Basalt, Ts = Tertiary rift sediments, Tb = pre-rift basalt flows, Ta = pre-rift andesitic flows and breccias, Tg = pre-rift granitic intrusions, pT = pre-Tertiary rocks (after Lipman and Mehnert, 1979). Horizontal scale: 1 cm = 3 km.

formation of a broad, northeast-trending arch, which has affected drainage patterns of small ephemeral streams between Rio Hondo and Rio Pueblo de Taos (Muehlberger, 1979; Peterson, 1981).

Lithologic units above the mountain front have been mapped by Gruner (1920), Dane and Bachman (1965), Clark and Read (1972), and Reed et al. (1983). These studies indicate that Precambrian granite, gneiss, phyllite, and amphibolite, and Tertiary granite, quartz monzonite, rhyolite, and andesite underlie the Rio Hondo, Arroyo Seco, and Rio Lucero drainage basins (Fig. 2). It should be noted that, of the basins underlain by crystalline terrane, Rio Hondo flows directly to the Rio Grande, but Arroyo Seco and Rio Lucero flow onto the plateau and to Rio Pueblo de Taos.

The majority of the Rio Pueblo de Taos drainage basin above the Sangre de Cristo mountain front is underlain by Paleozoic shales, sandstones, and conglomerates of the Flechado, Alamitos, and Sangre de Cristo formations (Miller et al., 1963). The contact between sedimentary and crystalline terranes lies within the Rio Pueblo de Taos drainage above the mountain front, and has been mapped as partly faulted, partly depositional (Gruner, 1920; Dane and Bachman, 1965; Reed et al., 1983). Locally, Tertiary Picuris Tuff crops out (Fig. 2), which is composed of basal conglomerate overlain by poorly consolidated water-laid tuff (Miller et al., 1963).

Servilleta Basalt underlies piedmont alluvium on the plateau (Fig. 5) and is exposed in the Rio Hondo, Rio Pueblo de Taos, and Rio Grande gorges. K-Ar age-dates of this unit range from 4.5 to 3.6 Ma (Lipman and Mehnert, 1979). Detailed stratigraphic analyses by Peterson (1981) and Leininger (1982) indicate that four discrete packages of Servilleta

Basalt flows occur between the Rio Hondo and Rio Pueblo de Taos gorges and are separated by fairly continuous gravel interbeds. Volcanism appears to have occurred in discrete, voluminous pulses, separated by periods of fluvial deposition (Peterson, 1981).

Pleistocene glaciation varied between the two drainage basins. Glacial deposits in the Rio Hondo drainage indicate Bull Lake, Pinedale, and Neoglacial ice advances (Richmond, 1962; Clark and Read, 1972). Although pre-Bull Lake glacial outwash occurs north of Taos in the northern San Luis Valley (McCalpin, 1982), and may be present in the study area, no pre-Bull Lake moraines have been identified near Taos. Approximately 30% of the Rio Hondo basin area has been glaciated, based on topographic map and aerial photograph interpretation, field observation, and mapping by Reed et al. (1983). Glacial deposits occur in the Long Canyon and Lake Fork valleys and extend to an elevation of about 2700 m (Reed et al., 1983). Approximately 9% of the total area above the mountain front draining to Rio Pueblo de Taos has been glaciated, most of which lies in the Rio Lucero and Rio Pueblo de Taos drainages. Glacial deposits comprise valley floors in headwater portions of these two drainages and extend to an elevation of about 2900 m (Clark and Read, 1972).

Previous Work

Upson (1939) applied the name Taos Plateau to the piedmont and alluvial plain areas near Taos, and Lambert (1966) first described the late Cenozoic geology of the Taos-Questa area. Lambert (1966, p. 47) found fresh, unweathered gravel veneers overlying yellowish, weathered sandy gravel alluvium in the vicinity of Taos, and suggested that these

veneers represent channel deposits of laterally eroding, "nearly graded or graded" streams. He noted variable amounts of alluvial fan and piedmont surface dissection and suggested that the "three or four alluvial and/or bedrock terraces" (1966, p. 47) present along perennial streams on the Plateau are probably late Pleistocene to Recent in age. These terraces cannot be traced upstream to glacial deposits in the Sangre de Cristo Mountains (Lambert, 1966).

Detailed mapping of gravel lenses between Servilleta Basalt flows (Peterson, 1981) indicates that the courses of major rivers near Taos have not shifted appreciably since the early phases of volcanism. North-trending faults and topographically high volcanic flows determined the course of the Rio Grande near Taos (Peterson, 1981). Manley (1981) determined that Rio Grande downcutting post-dates extrusion of late Pliocene basalt flows in the northern Española Basin. Kottlowski (1958) suggested that incision of the Rio Grande is due to integration of upper and lower reaches near El Paso, Texas.

Several field and experimental studies have shown that base-level lowering may induce degradation and/or aggradation in upstream reaches (Born and Ritter, 1970; Schumm and Parker, 1973; Pickup, 1975; Begin et al., 1981). However, Leopold and Bull (1979) showed that aggradation and degradation may occur regardless of base-level fall, and suggested that the response of a stream to base-level lowering may be related to the stream's ability to erode a local base level. This supports conclusions made by Brush and Wolman (1960), who found that if a stream is capable of "easily" transporting its bed material, a long-profile nickpoint is eroded quickly. Bull (1979) and Leopold and Bull (1979) used a ratio between the amount of stream power available relative to the amount of

power needed to transport sediment (the stream power/critical power ratio) to qualitatively assess channel erosion or deposition, and hence the ability of a stream to respond to base-level or climatic change.

Bedrock geology is one of four independent variables that may significantly influence fluvial systems at the cyclic time scale (millions of years, see Table 1). Lithology may influence discharge production via infiltration processes (Schumm, 1977), and bed-material size via different erodibilities and sediment size contributions (Hack, 1957; Brush, 1961). Hack (1957), Miller (1958), and Leopold et al. (1964) have shown that local stream gradient is related to discharge and bed-material size, suggesting that lithology may significantly influence channel gradient and long-profile shape (Hack, 1957) and thus fluvial response to base-level fall.

Climatic fluctuations may also produce major changes in river behavior (Schumm, 1977; Leopold and Bull, 1979). Glaciation influences hydrologic conditions by producing large amounts of water and sediment which overwhelm the ability of a stream to remove the imposed load (Fahnestock, 1963). Schumm (1977) described possible river responses to climatic change in areas unaffected by glaciation. For example, in unglaciated basins containing perennial streams, change to a cooler, wetter climate will generally result in erosion, assuming no changes in other independent variables (Schumm, 1977). This is based on estimated relations between mean annual runoff and precipitation (Langbein and Schumm, 1958) and on relations between mean annual sediment yield and precipitation (Schumm, 1965).

Table 1. The status of drainage basin variables during time spans of decreasing duration. Cyclic time represents geologic time, during which there is continual removal of material from a drainage basin. Graded time represents a span of perhaps hundreds of years, during which fluvial changes fluctuate about an average condition. Steady time is perhaps days or hours, during which channel morphology remains essentially constant. (from Schumm and Lichty, 1965)

	Status of variables during designated time spans		
Drainage basin variables	Cyclic	Graded	Steady
Time	Independent	Not relevant	Not relevant
Initial relief	Independent	Not relevant	Not relevant
Geology (lithology, structure)	Independent	Independent	Independent
Climate	Independent	Independent	Independent
Vegetation (type and density)	Dependent	Independent	Independent
Relief or volume of system above base level	Dependent	Independent	Independent
Hydrology (runoff and sediment yield per unit area within system)	Dependent	Independent	Independent
Drainage network morphology	Dependent	Dependent	Independent
Hillslope morphology	Dependent	Dependent	Independent
Hydrology (discharge of water and sediment from system)	Dependent	Dependent	Dependent

METHODS

Field Methods

Present-day fluvial system characteristics were quantified utilizing channel cross-section and slope surveys and bed-material and terrace deposit sampling. Channel-geometry and bed-slope surveys were performed at 34 sites in the Rio Hondo and Rio Pueblo de Taos drainage basins, in order to estimate bankfull discharge and to quantify channel form at bankfull stage (Fig. 6). Field techniques followed procedures given by Benson and Dalrymple (1967) for the slope-area method of discharge calculation.

Channel-geometry measurement sites were selected based on accessibility, location within the drainage basin, ease of identification of bankfull stage, straightness of reach, and uniformity of reach characteristics. Most sites lacked significant channel bars or pool-riffle sequences. Measured reaches were approximately 50 m long, with 2 or 3 cross-sections located where bankfull stage was best identifiable. Measurements made at sites 1 to 5 (Fig. 6) were not utilized due to extreme discrepancies in bankfull area between cross-sections, probable hydraulic jumps within the reaches, and possible bedrock channel control. Other measurements (at sites 9, 15, 18, 23, 27, and 28) were not used due to recent channel incision and/or suspected incorrect identification of bankfull stage.

Bed material at each channel geometry measurement site was sampled using techniques outlined by Wolman (1954). Lithology, rounding, and intermediate diameter (b-axis) were measured for greater-than-2 mm fractions only. Less-than-2 mm fractions of bed material in these coarse-bed mountain streams are minor components of the bed material,

Figure 6. Map showing geomorphic regions and station locations of bed-material and channel morphology measurements. Geomorphic regions are based on areas containing similar channel and physiographic properties; Table 19 contains characteristics of streams within each region. Regions are: (I) streams draining crystalline terrane above the mountain front, (II) Rio Hondo between the mountain front and its basalt gorge, (III) Rio Hondo in its basalt gorge, (IV) streams draining sedimentary terrane above the mountain front, (V) stream reaches between the mountain front and the Rio Pueblo de Taos basalt gorge, and (VI) Rio Pueblo de Taos in its basalt gorge.

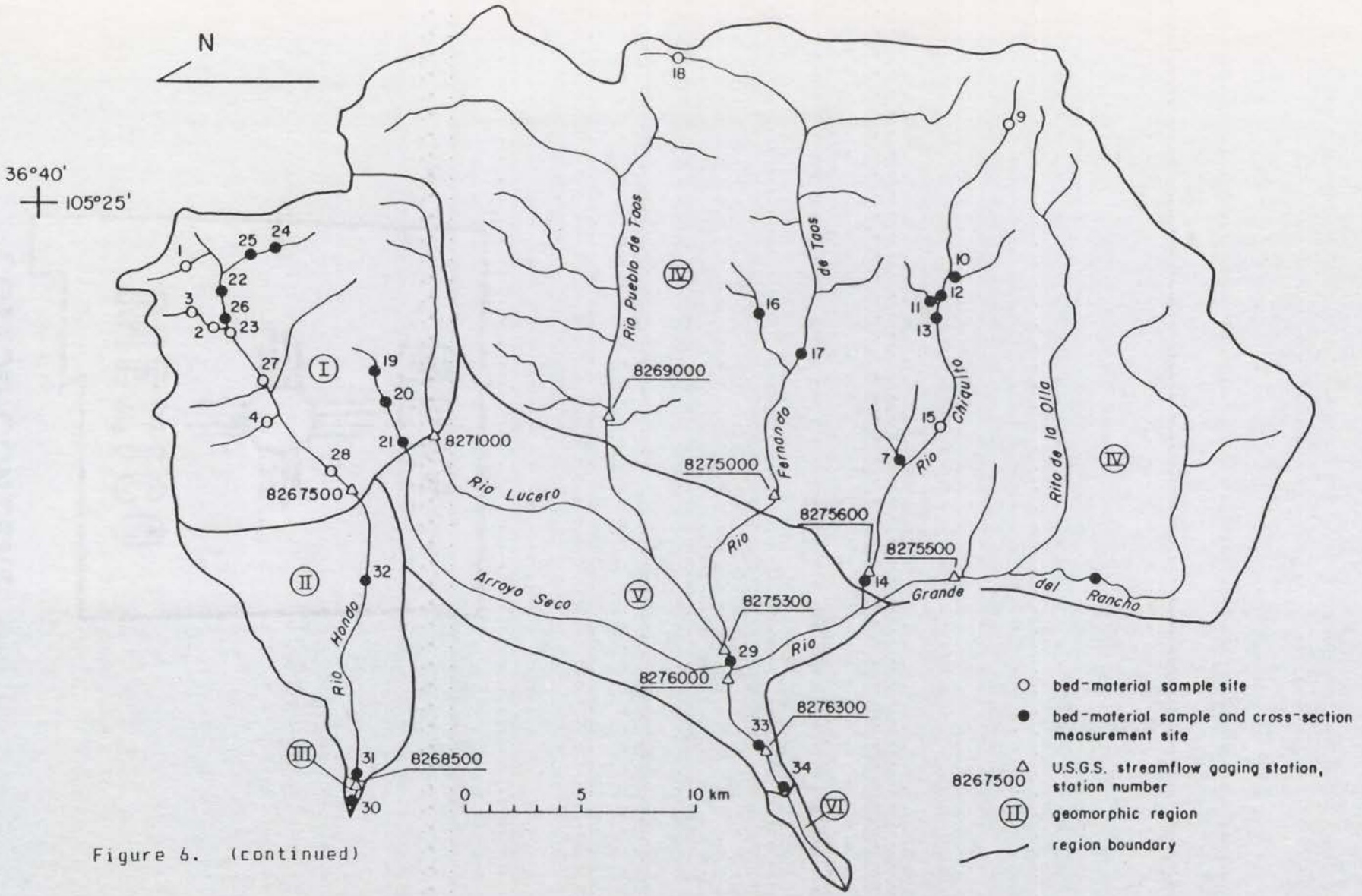

Figure 6. (continued)

comprising probably less than 5% by weight of the total bed material. At least 50 clasts were measured at each of the sites, which were located throughout the study area (Fig. 6).

Several investigators have used the term *geomorphic surface* to describe a landform or group of landforms produced during an interval of time when local climate and base-level controls were relatively constant (see Gile et al., 1981, p. 24). In this study, geomorphic surfaces are defined as genetically related landforms produced during a definite interval of time and having certain pedologic properties. Most geomorphic surfaces mapped in stream valleys are fluvial terraces; exceptions are local valley-border surfaces and alluvial fans. Geomorphic surfaces have been informally designated by numbers from 1 (the highest, oldest surface) to 8 (the modern floodplain) (see Plates 1 and 2). For example, the second highest surface is designated as surface Qt2 where it occurs as a fluvial terrace, and as Q2 where it occurs as another type of landform (e.g., valley-border surface) produced during the same interval of time as Qt2.

Mapping was confined to major valleys between the mountain front and confluences with the Rio Grande. Initial identification of geomorphic surfaces utilized black and white aerial photographs taken in 1973 (approximate scale: 1:18,000), and was based on land surface relief and tonal qualities of the photographs. Field delineation of fluvial terraces relied on heights above the modern floodplain, soil properties, and terrace longitudinal profiles. Limited land access precluded detailed investigation of terraces on Taos Pueblo Indian lands and on low terraces in cultivated portions of the Rio Pueblo de Taos valley.

Twenty-four soil profiles were described using Soil Survey Staff

(1975) nomenclature, in hand-dug pits, roadcuts, gravel pits and other excavations. Most soil profiles were described to at least Ck horizons; unaltered C horizons were not reached at many sites, including roadcuts exposing over 200 cm of soil. Soil profiles were described at sites free of erosion, deposition, and agricultural impact; agriculture severely limited the number of potentially undisturbed soil-description sites.

Valley transects were also used to help identify and correlate stream terraces. In the Rio Hondo valley, surface heights above the modern floodplain could be accurately estimated from topographic maps due to sufficient relief between units. However, due to relatively low relief in the Rio Pueblo de Taos valley system, valley transects using a hand-level and pace method were necessary to estimate terrace heights above the active stream channel.

Pebble counts were performed to quantify lithology, rounding, and intermediate diameter of greater-than-2 mm clasts in terrace deposits. At least 50 clasts were sampled at each site, along vertical transects spaced between 1 and 3 m apart. Roadcut locations determined measurement sites; very few deposits associated with lower geomorphic surfaces were sampled due to limited exposure.

Laboratory and Office Methods

Several laboratory methods were employed to quantify both present-day and Quaternary fluvial systems in the study area. The present-day hydrologic system has been documented by the Water Resources Division of the U. S. Geological Survey, which maintains, or has maintained, ten streamflow gaging stations within the study area. This agency provided partial duration and annual series data, daily streamflow values, stage-discharge relations, and selected current-meter measurements for each

station.

Snowmelt-runoff water budgets were analyzed in an attempt to understand discharge production processes within the mountainous study basins. Water balance equations take the general form: Input - Output = Storage Changes (Todd, 1980), and can be modified for snowmelt conditions to (Viessman et al., 1977):

$$P + M - R - L = S \qquad (1)$$

where P = net rainfall, M = snowmelt, R = runoff, L = losses to evapotranspiration, and S = storage changes. Storage changes include changes in soil moisture and changes in channel, depression, detention, snowpack, and groundwater storage (Viessman et al., 1977). For the months of April through July, average monthly values of precipitation, snowmelt, and evapotranspiration losses were estimated from climatic data collected at stations within and near the study area (Figs. 7 and 8), and equations developed for forested areas given by the U. S. Army Corps of Engineers (1956). Average April 1 snowpack water content was estimated from Figure 9. Average monthly runoff was calculated from U. S. G. S. streamflow records. Appendix A details the assumptions and the sequence of calculations used in this analysis.

Channel cross-section data were entered into a microcomputer program written by the author, which calculated channel area, hydraulic radius, conveyance, and discharge for any specified stage. Conveyance, K, was calculated using the Manning equation (Dalrymple and Benson, 1967); for metric units, K is defined as

$$K = (1/n) * A * R^{2/3} \qquad (2)$$

where n is Manning's roughness coefficient, A is cross-section area, and R is hydraulic radius. Discharge for a reach containing two cross-

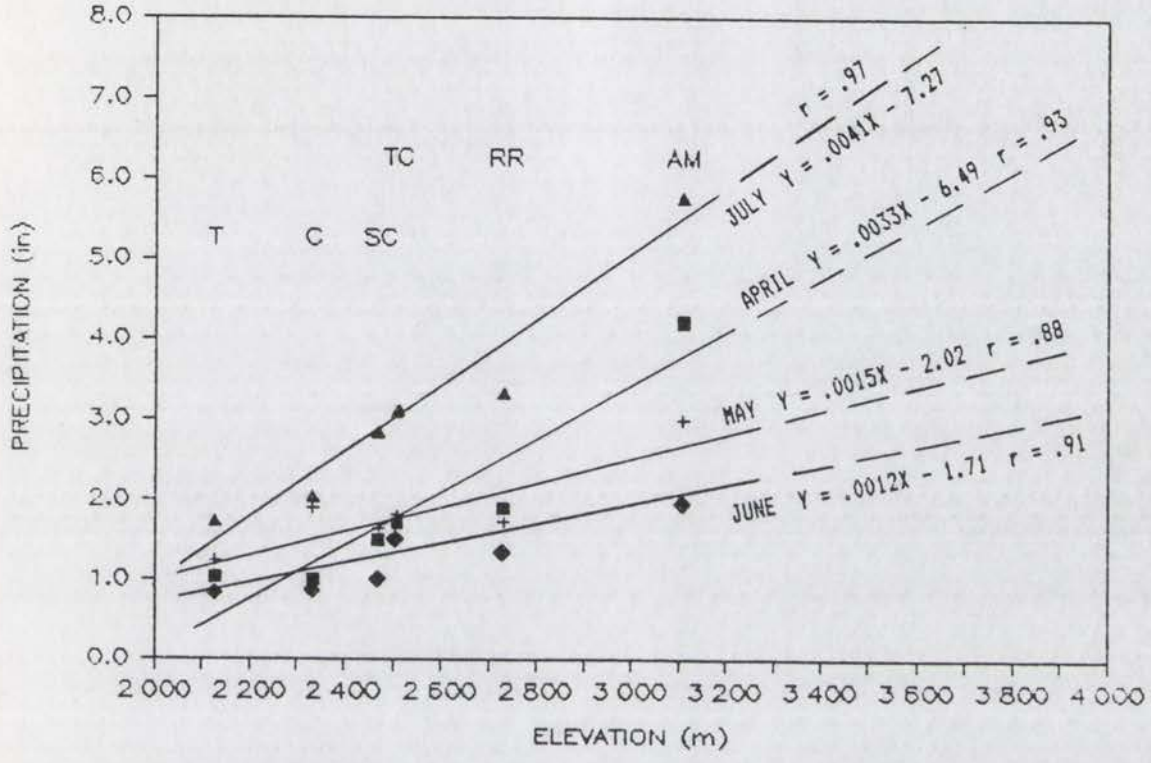

Figure 7. Variation of precipitation with elevation at climatic stations within and near the study area. Periods of record: Taos (T) 1889-1954; Cerro (C), 1910-1954; San Cristobal (SC), 1948-1954; Red River (RR), 1905-1954; Taos Canyon (TC), 1910-1943; Anchor Mine (AM), 1911-1920. Data from State Engineer Office (1956). ■ = April, + = May, ◆ = June, ▲ = July.

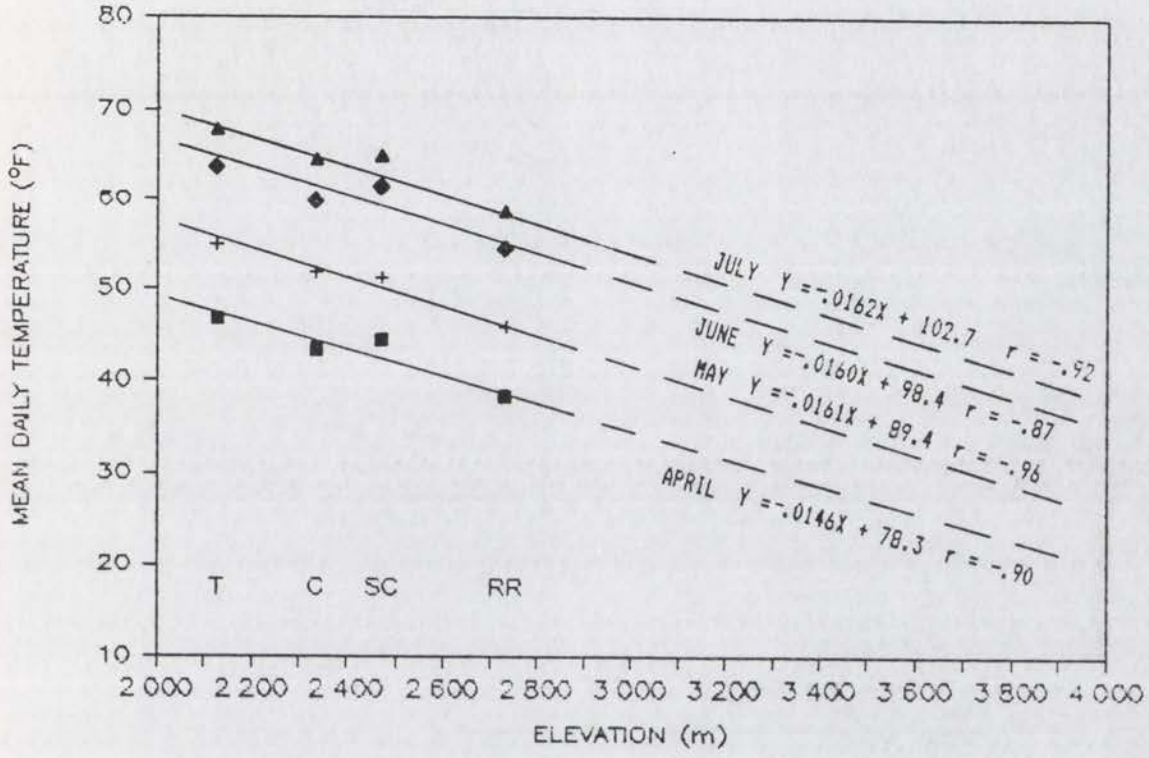

Figure 8. Variation of mean daily temperature with elevation at climatic stations within and near the study area. Periods of record: Taos (T) 1892-1954; Cerro (C), 1911-1954; San Cristobal (SC), 1948-1954; Red River (RR), 1910-1954. Data from State Engineer Office (1956). ■ = April, + = May, ◆ = June, ▲ = July.

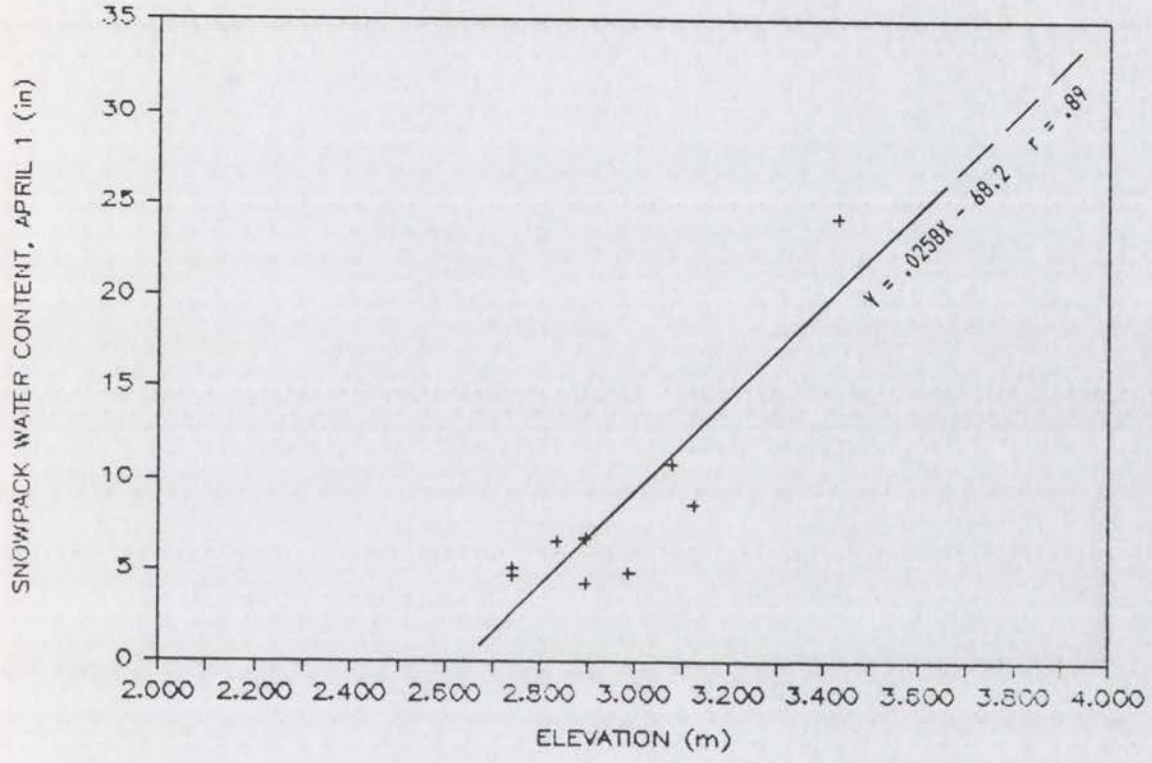

Figure 9. Variation of average snowpack water content on April 1 with elevation, for snow courses within and near the study area. Data from: Red River Pass, Red River Pass #2, Hematite Park, Twining, Taos Canyon, Palo, Tres Ritos, Alamitos, Cordova, and Taos Powderhorn (Washichek et al., 1972; Washichek et al., 1978).

sections was computed as (Dalrymple and Benson, 1967):

$$Q = (K_1 * K_2 * S)^{1/2} \quad (3)$$

where S is friction slope. It was assumed that flow does not accelerate or decelerate in the measured reaches, and that channel cross-section area remained relatively rigid at bankfull discharge. Therefore, flow was assumed to be steady and uniform (e.g., no changes in the velocity profile take place through time or in a downstream direction). These assumptions allow bed slope to be substituted for friction slope in the calculation of discharge (Maizels, 1983). Manning's roughness coefficient was estimated by visual comparison with photographs of reaches of known n-value (Barnes, 1967). The computer program used for discharge calculations (XSECTION) is given in Appendix B.

Shields (1936; see Andrews, 1984) showed that hydraulic conditions required to initiate motion of bed material could be described by the dimensionless shear stress T^*_i,

$$T^*_i = \frac{D*S}{(p_s/p_w - 1)d_i} \quad (4)$$

where D is mean flow depth, S is bed slope, p_s and p_w are sediment and fluid densities, respectively, and d_i is the particle diameter that is coarser than i^{th}% of the surface bed material (Andrews, 1984). In 24 coarse-bed rivers in Colorado having properties very similar to those near Taos, Andrews (1984) found that the average threshold dimensionless shear stress for d_{50} (T^*_{c50}) was 0.031. The average threshold dimensionless shear stress for d_{90} (T^*_{c90}) was calculated using data given by Andrews (1984). This value is equal to 0.015. Calculations using equation (4) assumed p_s = 2.65 g/cm^3 and p_w = 1.00 g/cm^3.

Drainage basin morphometry was analyzed using 1:24,000-scale

topographic maps; measurements include drainage density (D_d) and drainage frequency (F) (Melton, 1958) and Vf ratios (Bull and McFadden, 1977). Basin hypsometry and the hypsometric integral (Schumm, 1956) were determined using 1:100,000-scale topographic maps. Area and length measurements were made using a digitizing computer.

Calculation of drainage density and frequency is highly dependent on scale and drainage net delineation (Goudie, 1981). For this study, drainage lines were stopped at contour crenulations which had width/depth ratios less than 2. Streams were ordered according to the Strahler (1957) method.

Long-profile concavity (C) is defined in this study as 1 - K, where K is the area under a %height-%distance curve. High C values represent long-profiles which are very concave. Stream profiles from the basin divide to the next higher-order stream were used in determining C values. Linear, logarithmic, exponential, and power function curve-fitting to modern and terrace long-profiles used equations given by Shepherd (1985). Correlation of geomorphic surfaces was also based on terrace long-profiles, which were digitized from 1:15,840-scale topographic maps. Elevations of surfaces derived from valley transects and field mapping on topographic maps were projected to a valley axis, from which a stream distance was determined.

Correlation of discontinuous stream terraces within each basin and between the Rio Hondo and Rio Pueblo de Taos basins is based largely on relative soil-profile development. The semi-quantitative Relative Profile Development (RPD) index (Harden, 1982) was employed to compare soil profiles and to help correlate surficial units. For this index, parent material characteristics must be known. Soil profiles which

reached unaltered C horizons (SP11, SP14, and SP19, see Plates 1 and 2), had C-horizon colors, dry consistences, and textures very close to those of modern alluvium (SP13 and SP17, see Appendix C). These deposits contained no soil structure, clay films, or calcium carbonate (Table 2). Color, texture, and dry consistence at depth in profile SP23 differed from properties in other profiles, and may reflect differences in parent material (Table 2).

Possible sources of calcium carbonate found in soil profiles include aerosolic sources after deposition (Gile et al., 1966) and rare limestone interbeds in Paleozoic sediments in the southern portion of the Rio Pueblo de Taos basin. Limestone clasts were not found in any pebble counts, bed-material samples, or soil pits below the mountain front, and composed less than 2% of bed material in reaches draining the scarce limestone outcrops above the mountain front. Therefore, calcium carbonate found in soil profiles was assumed to be derived entirely from aerosolic sources after deposition. A detailed index for carbonate accumulation was developed to introduce carbonate morphologic properties into the RPD index. Appendix D shows the technique used to calculate the index, which is intended to be analogous to Harden's (1982) clay film index.

Table 2. Parent material characteristics used in calculating Relative Profile Development indices Harden (1982), for soil profiles described in the Rio Hondo and Rio Pueblo de Taos drainage basins. Data from samples of modern alluvium (see Appendix C). Soil profile SP23 was described on unit Qt6 near Los Cordovas (see Plate 2).

	Dry Color	Moist Color	Texture	Stickiness	Plasticity	Dry Consistence	Clay Films	Structure	Calcium Carbonate
All profiles (except SP23)	10YR 6/3	10YR 4/3	loamy sand	nonsticky	nonplastic	loose	none	none	none
Profile SP23	10YR 6/3	10YR 4/3	silt loam	slightly sticky	slightly plastic	slightly hard	none	none	none

RESULTS

Present-day Fluvial System

Water Discharge Characteristics

In order to investigate influences of lithology on present-day discharge characteristics, several hydrologic parameters were analyzed. Data from ten U. S. Geological Survey streamflow gaging stations in the study area indicate that significant differences in several discharge properties exist between basins underlain by crystalline rocks and basins underlain by sedimentary rocks (Table 3). Substantial diversions for agriculture exist on all streams below the mountain front; however, six of the ten gaging stations lie upstream of the mountain front and are unaffected by diversions. Only data from these six stations were analyzed.

Differences in discharge and discharge per unit area between areas draining different rock types exist at low, medium, and high flows (Table 3). Low flow can be represented by the flow which is equaled or exceeded 90% of the time (Q_{90}, Hely and Olmstead, 1963). Q_{90} per unit drainage area (A) in crystalline terrane is nearly an order of magnitude higher than in sedimentary terrane (Table 3). Mean annual discharge (Qa) is higher in crystalline terrane than in sedimentary terrane, as is unit discharge (Qa/A). High discharge, represented by the mean annual flood (Qma), is also higher for stations on rivers draining crystalline terrane. In addition, the mean-annual-flood recurrence interval is lower for stations draining crystalline bedrock, indicating that the mean annual flood is both higher and more frequent at these sites.

These flow duration characteristics are summarized in Figure 10. Discharge normalized by drainage area for any given flow frequency (e.g.,

Table 3. Discharge data for six U.S.G.S. streamflow gaging stations in the study area, as of Water Year 1984. Note higher discharges per unit area for basins draining crystalline rocks. xtln = crystalline, sed = sedimentary. See Figure 6 for station locations.

Dominant basin lithology	Station number	Station name	Years of Record	A	Qa	Qma	Qa/A	Q90/A	Q50/A	Qma/A	Qma R.I.
xtln	08267500	Rio Hondo Near Valdez	50	93.8	0.963	5.24	0.010	0.0029	0.0053	0.056	2.80
	08271000	Rio Lucero Near Arroyo Seco	56	43.0	0.611	3.68	0.014	0.0035	0.0075	0.086	2.40
70% sed											
30% xtln	08269000	Rio Pueblo de Taos Near Taos	50	173	0.804	6.57	0.005	0.0009	0.0017	0.038	2.96
sed	08275000	Rio Fernando de Taos Near Taos	19	186	0.178	2.21	0.001	< 0.0001	0.0003	0.012	3.23
	08275500	Rio Grande del Rancho Near Talpa	32	215	0.558	4.79	0.003	0.0005	0.0010	0.022	2.92
	08275600	Rio Chiquito Near Talpa	24	95.8	0.225	2.95	0.002	0.0006	0.0011	0.031	2.60
			mean :		crystalline:		0.012	0.0032	0.0064	0.071	2.60
					sedimentary:		0.002	0.0004	0.0008	0.022	2.92

KEY-- Q90: discharge equaled or exceeded 90% of the time (m^3/s)
Q50: discharge equaled or exceeded 50% of the time (m^3/s)
Qma: mean annual flood (average of all annual peaks) (m^3/s)
Qa: mean annual discharge (m^3/s)
A: drainage area (km^2)
R.I.: recurrence interval (yr)

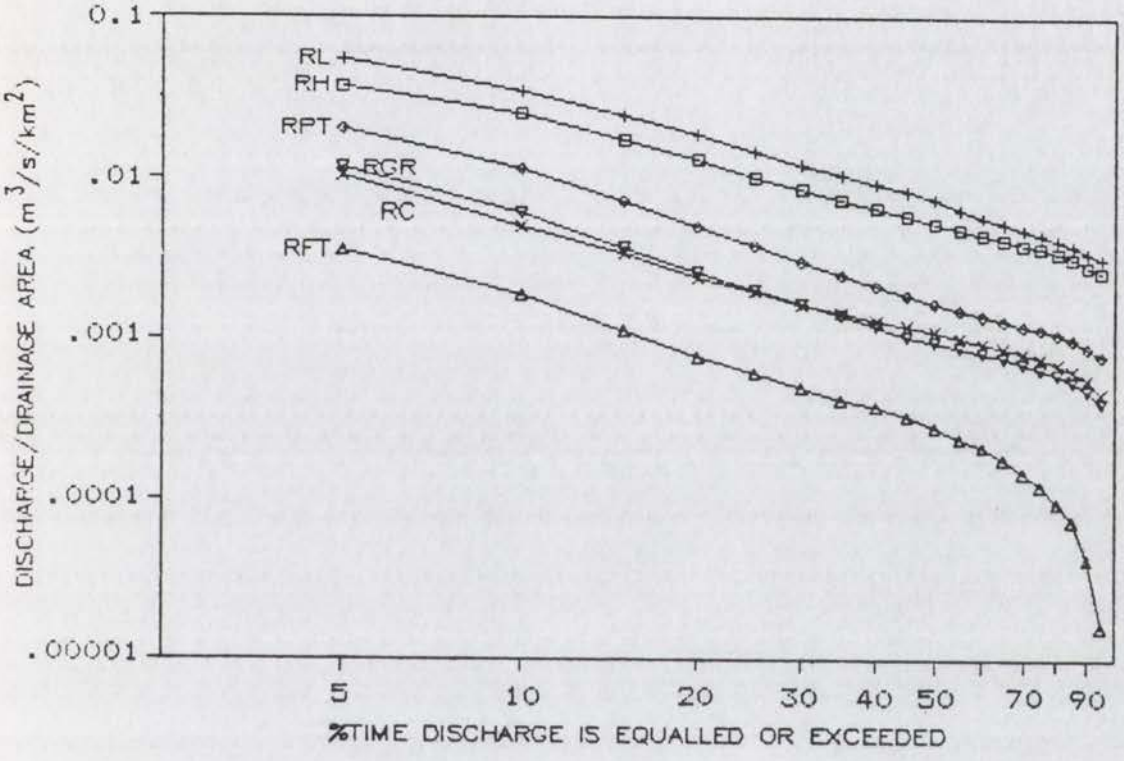

Figure 10. Discharge per unit area duration curves at six U.S.G.S. streamflow gaging stations near Taos. RH = Rio Hondo near Valdez; RL = Rio Lucero near Arroyo Seco; RPT = Rio Pueblo de Taos near Taos; RGR = Rio Grande del Rancho near Talpa; RC = Rio Chiquito near Talpa; RFT = Rio Fernando de Taos near Taos. RH and RL drain predominantly granite and gneiss; RGR, RC, and RFT drain sandstone and shale; RPT drains about 70% sedimentary and about 30% crystalline lithologies.

Q_{50}, Q_{90}) at stations draining crystalline bedrock are substantially higher than at stations draining sedimentary rocks. Also, a given discharge per unit area occurs much more often at the stations draining crystalline bedrock. Thus, discharge per unit area is both higher and more frequent for stations draining crystalline rocks.

Notably, data from Rio Pueblo de Taos near Taos, which drains both crystalline and sedimentary rocks, plots between data from streams draining crystalline terrane and streams draining sedimentary terrane (Fig. 10). Values of unit discharge and mean annual flood per unit area for Rio Pueblo de Taos near Taos are also intermediate between values for crystalline and sedimentary terranes (Table 3).

In the Taos area, spring runoff due to snowmelt produces the largest annual discharge events and approximately 75% of the total annual discharge. Hydrographs for the six gaging stations unaffected by diversions were plotted for April, May, June, and July of several years. Although hydrographs vary from year to year, hydrographs from 1973 show typical discharge characteristics of streams in the study area (Fig. 11). The six hydrographs can be classified into three groups, each containing two hydrographs. Rio Pueblo de Taos and Rio Grande del Rancho usually peak early in the spring (Fig. 11a), and produce hydrographs with relatively steep limbs. Flow on these two streams recedes significantly by mid-June, and the base-flow component of discharge is usually large by early July.

Rio Fernando de Taos and Rio Chiquito produce hydrographs shaped similar to those of Rio Pueblo de Taos and Rio Grande del Rancho (Fig. 11b), but these have shallower limbs and are lower in peak discharge. Peaks in mid-May are common, and base-flow usually dominates discharge by

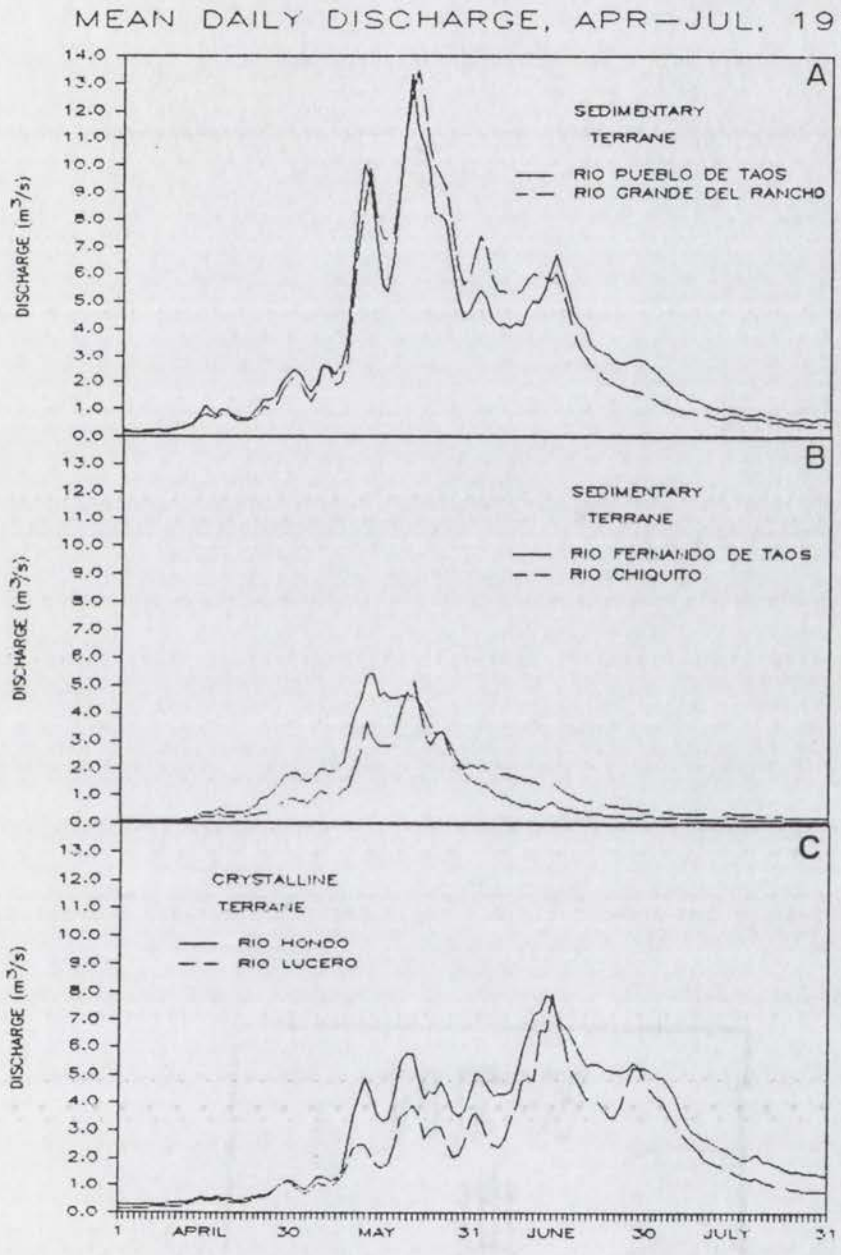

Figure 11. Mean daily discharge (m^3/s) from April 1 to July 31, 1973, for six U.S.G.S. streamflow gaging stations in the study area. All plots have the same scales. Stations are same as those in Table 3.

mid-June.

Rio Hondo and Rio Lucero hydrographs comprise the third group (Fig. 11c). Spring runoff on Rio Hondo and Rio Lucero typically consists of a series of peaks which increase in magnitude until about mid-June, with a more gradual recession occuring late in the spring, usually about mid-July. Hydrographs are not as steep-limbed as in the other two groups, and high discharges are generally maintained throughout June and into July. In some years, discharge on Rio Hondo and Rio Lucero increases in response to late June or early July thunder showers, while no increase occurs at the other stations. In summary, hydrographs for stations on rivers draining crystalline terrane indicate that high snowmelt discharges are maintained for longer periods of time than on rivers draining sedimentary terrane.

Runoff Generation

In order to assess the effect of lithology on runoff generation in the study area, two methods have been employed: (1) compilation of mean annual discharge data for a sample population of gaged streams in the Rocky Mountains, and (2) a detailed water-budget analysis of six gaged drainage basins in the study area.

Data from 54 gaging stations within the Rocky Mountains indicate that relatively high runoff production in crystalline terrane is not limited to the study area (Fig. 12). These data were collected from gaging stations draining basins underlain homogeneously by either crystalline or sedimentary rock types (see Appendix E). Effects of glaciation and topographic relief were not addressed in data collection, and variations in, for example, the median basin elevation or percent of basin area affected by glaciation may account for some data scatter.

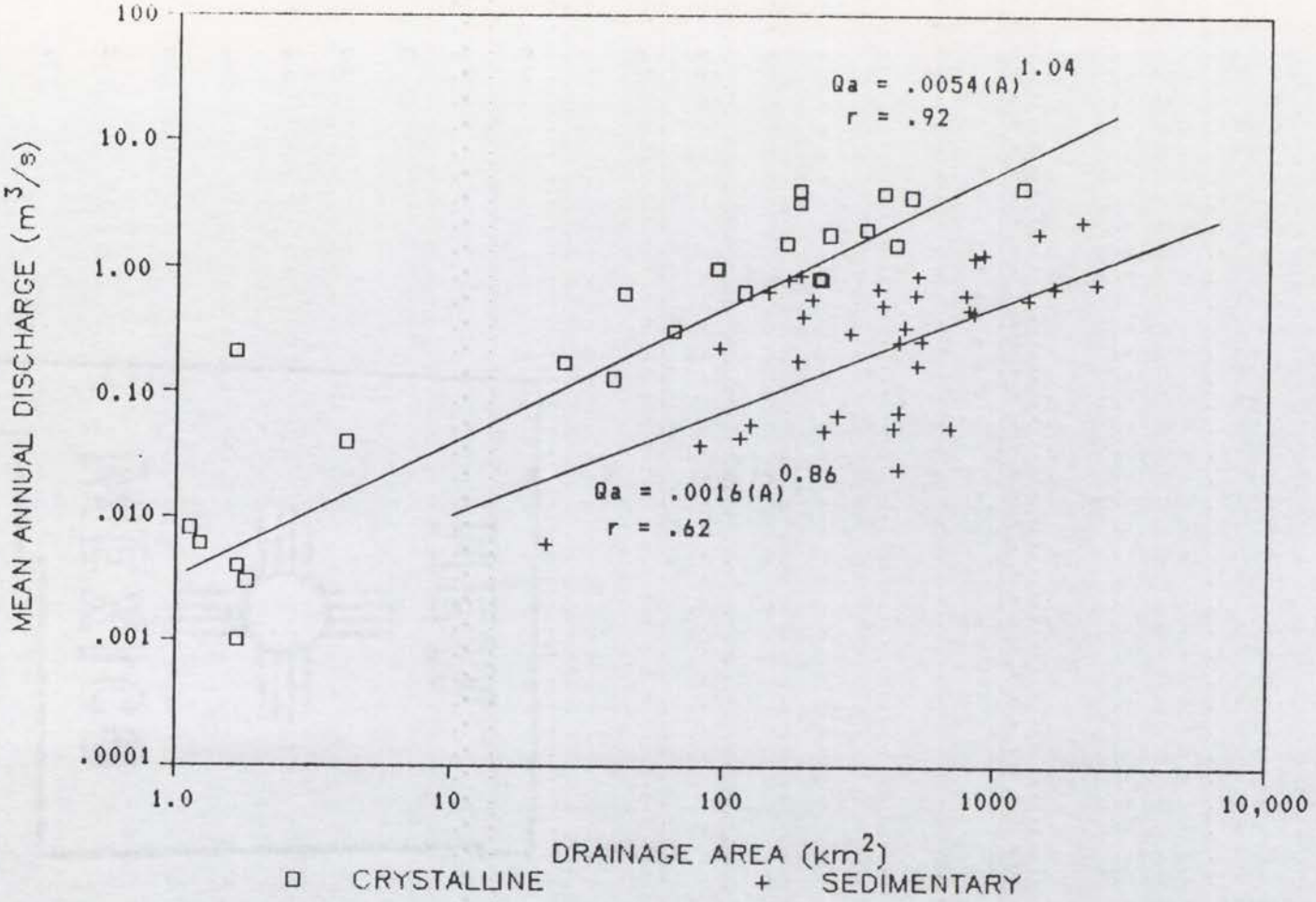

Figure 12. Plot of mean annual discharge (Qa) against drainage area (A) for basins in New Mexico, Colorado, Utah, and Wyoming. Criteria for basin selection: 1) basins underlain by greater than 85% crystalline or sedimentary terrane, 2) minor or no upstream diversions, 3) perennial flow, and 4) a gaged record longer than seven years. See Appendix E for references.

For each of six gaged basins near Taos, components of the snowmelt-runoff water budget have been calculated using climatologic and hydrologic indices (see Methods). Results of these calculations are shown in Figure 13 and summarized in Appendix F. Rio Hondo and Rio Lucero show substantially higher amounts of total snowmelt, and a later snowmelt peak (Fig. 13a), than the other four basins. Snow depth data (Washichek et al., 1972; Washichek et al., 1978) and field observations during two summers indicate that snow remains in the upper elevations of Rio Hondo and Rio Lucero through June and into July; whereas, the other basins usually lose their snowpack by the end of June.

Runoff trends parallel snowmelt trends (Fig. 13b), with peaks occurring during May in sedimentary terrane and during June in crystalline terrane. Data from individual years also show these trends (Fig. 14). Rainfall differs only slightly between the two lithologically distinct groups (Fig. 13c), and differences in evapotranspiration losses are small between the six basins (Fig. 13d).

Monthly storage changes in each basin are calculated by subtracting runoff and evapotranspiration losses from snowmelt and rainfall inputs (equation (1)), and are shown in Figure 15. Notably, April storage changes are lower in the Rio Hondo and Rio Lucero basins than in the other basins, although contributions to storage are relatively high in June and July (Fig. 15). In the sedimentary terrane, relatively high amounts of water are added to storage in April, but contributions to storage decrease through spring. Little moisture is added to storage in basins underlain by sedimentary rocks during June (Fig. 15). July additions to storage in these basins coincide with rainfall increases (Fig. 13c).

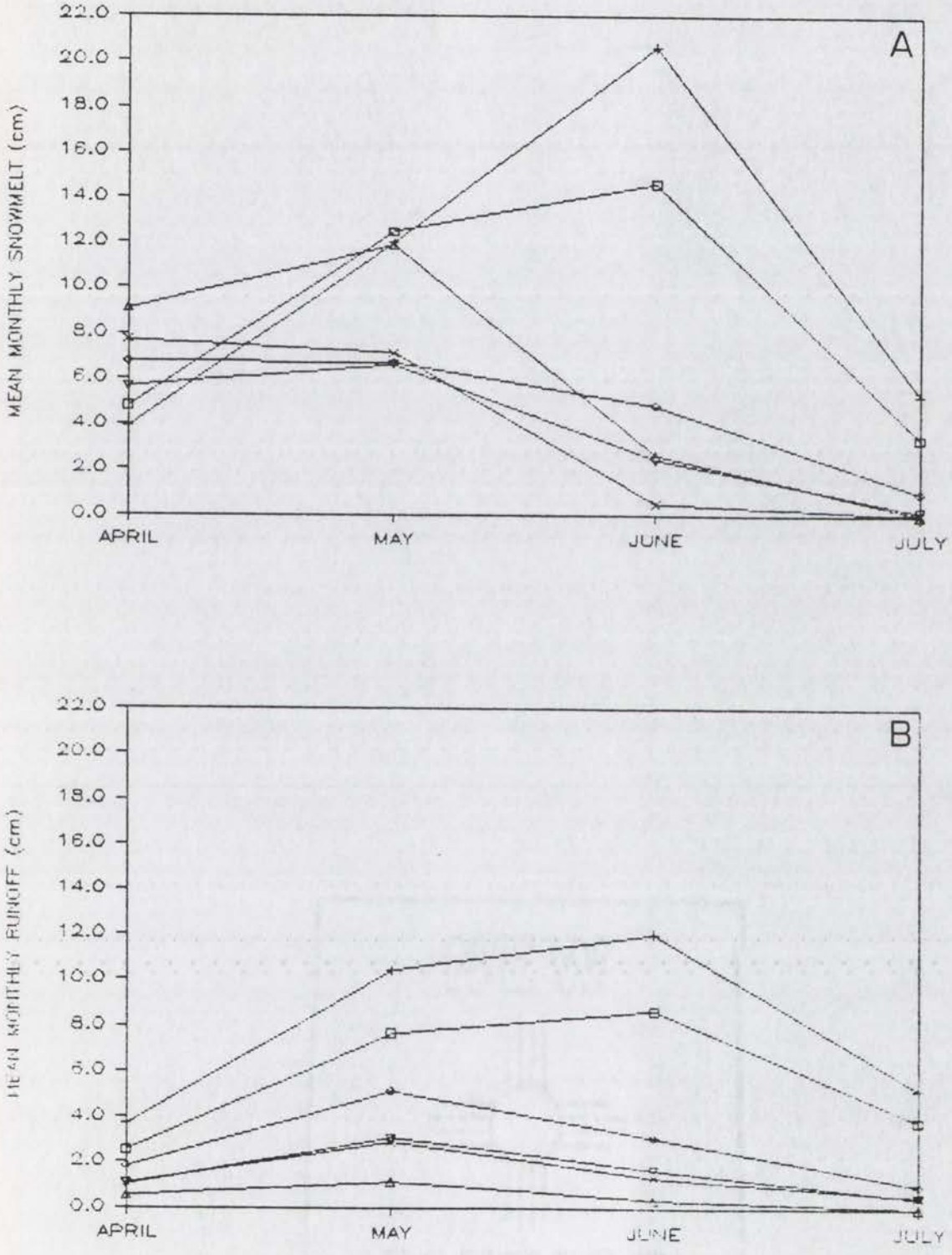

Figure 13. Mean monthly snowmelt (A), runoff (B), rainfall (C), and evapotranspiration (D); for the Rio Hondo (□), Rio Lucero (+), Rio Pueblo de Taos (◇), Rio Fernando de Taos (△), Rio Chiquito (x), and Rio Grande del Rancho (▽) basins.

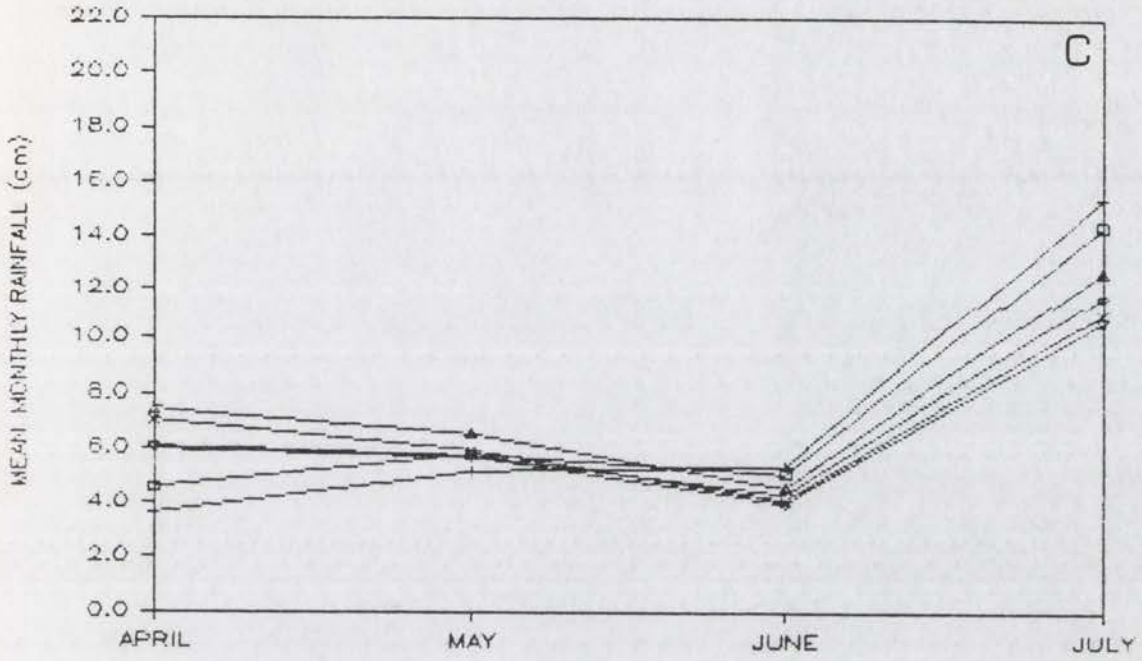

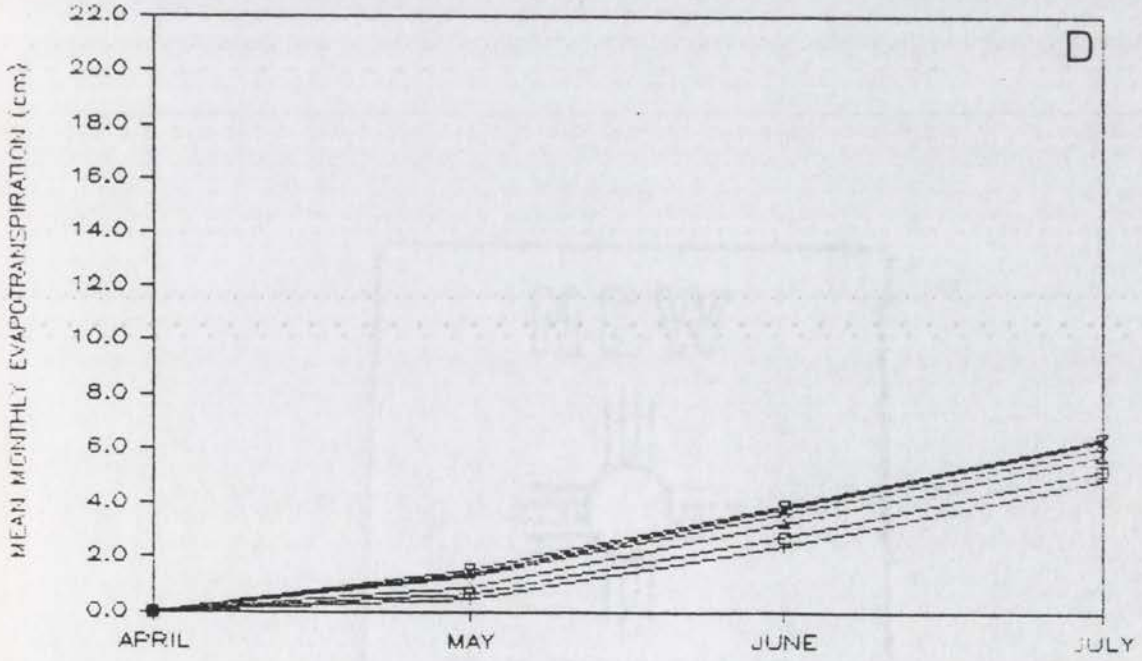

Figure 13. (continued)

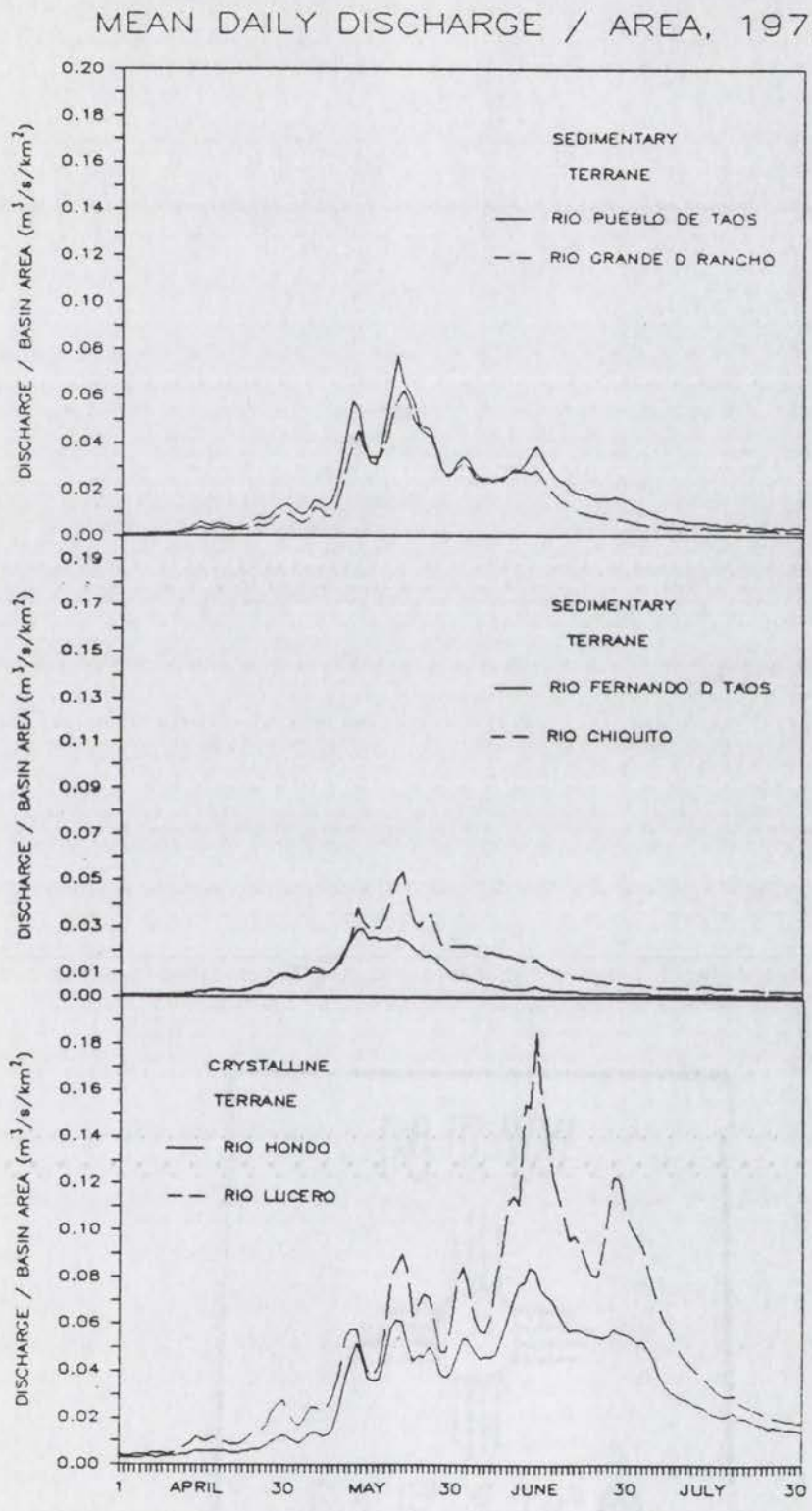

Figure 14. Mean daily discharge per unit drainage area ($m^3/s/km^2$) from April 1 to July 31, 1973, for six gaging stations in the study area.

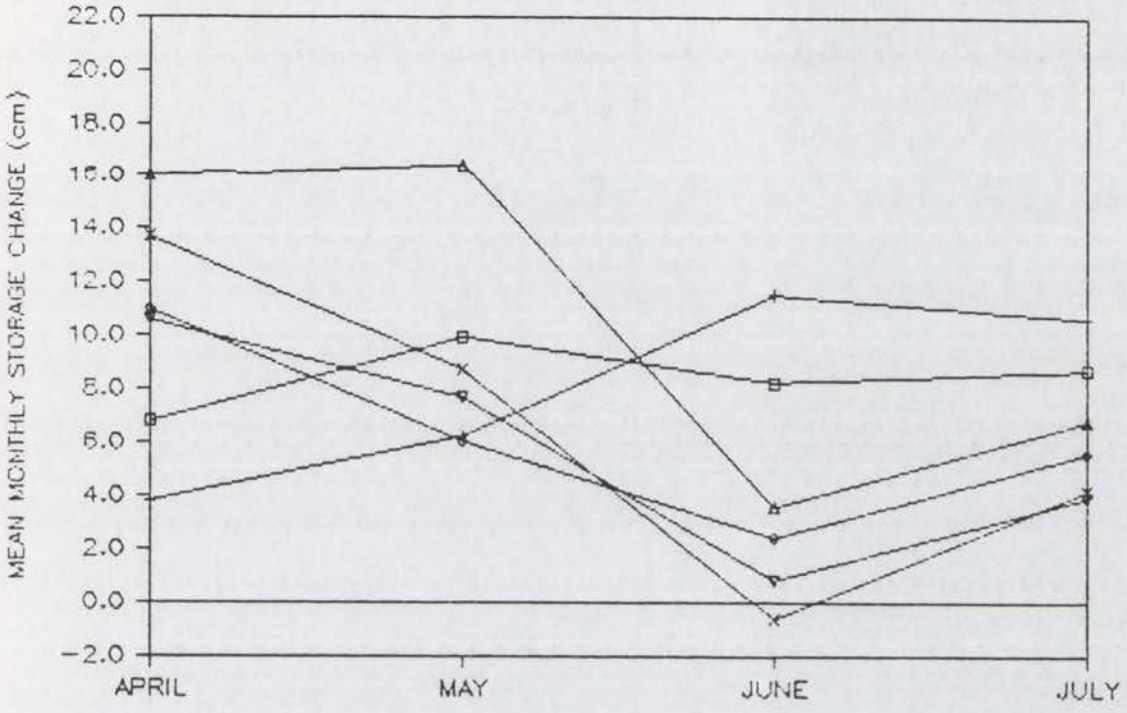

Figure 15. Mean monthly change in basin storage for the Rio Hondo (□), Rio Lucero (+), Rio Pueblo de Taos (◇), Rio Fernando de Taos (△), Rio Chiquito (x), Rio Grande del Rancho (▽) basins. Storage change calculated by subtracting runoff and evapotranspiration losses from snowmelt and rainfall inputs.

Bankfull Discharge

A flow characteristic commonly used to compare streams is bankfull discharge, which "just fills the section of an alluvial channel without overtopping the banks" (Richards, 1982, p. 135). Bankfull discharge (Q_{bf}) has often been deemed as the 'dominant' event which controls channel form. Q_{bf} was calculated from field surveys at 22 sites in the study area (Tables 4 and 5). Field measurement of bankfull discharge by indirect surveys may contain substantial error due to difficult identification of bankfull stage, post-Q_{bf} channel modification, and assumptions of steady, uniform flow necessary for discharge calculation (Williams, 1978; Maizels, 1983). However, the validity of Q_{bf} calculations used in this study can be verified by two independent methods, outlined below.

First, three cross-sections were measured at or near U. S. G. S. gaging stations, and therefore the calculated bankfull channel areas and velocities can be compared to current-meter measurements made by the U. S. G. S. at discharges close to calculated Q_{bf} values. Table 6 shows calculated and measured values of channel width, area and velocity at similar discharges. Reasonable agreement exists between calculated and measured values at two of the three sites; causes for discrepancies in area and velocity at site 14 (Rio Chiquito near Talpa) are unknown. In general, however, Q_{bf} values appear to be reasonable based on current-meter measurement data.

A second verification of Q_{bf} values incorporates flood-frequency data derived from the gaging stations. Dunne and Leopold (1978) suggest that Q_{bf} is equaled or exceeded 0.9% of the time. Calculated bankfull discharges from the measured sites have exceedence percents ranging from

Table 4. Channel characteristics and bankfull flow properties at sites draining crystalline terrane. Qbf = bankfull discharge. See Plate 1 and Figure 6 for locations.

Site	Drainage area (km^2)	Reach Qbf (m^3/s)	Manning's Roughness Coefficient	Bed Slope (m/m)	Cross-section	Qbf (m^3/s)	Bankfull Area (m^2)	Hydraulic Radius (m)	Width (m)	Mean Depth (m)	Width: Depth Ratio	Velocity (m/s)	Conveyance (m^3/s)	Froude No.
19	4.3	1.03	0.045	0.1303	26 m	0.96	0.44	0.14	2.86	0.15	19.1	2.18	2.65	1.80
					36.7 m	1.11	0.48	0.15	2.94	0.16	17.9	2.31	3.09	1.84
20	7.0	2.21	0.045	0.0926	7 m	2.21	0.81	0.25	2.84	0.29	9.9	2.72	7.26	1.61
21	8.2	2.86	0.044	0.0679	2 m	3.00	1.14	0.30	3.86	0.32	11.2	2.63	11.5	1.49
					26 m	2.74	0.99	0.32	2.77	0.36	7.7	2.76	10.5	1.47
22	24.1	7.98	0.048	0.0458	11 m	7.35	2.88	0.43	6.26	0.46	13.6	2.55	34.3	1.20
					18 m	8.66	3.21	0.47	6.49	0.50	13.1	2.69	40.5	1.22
24	6.8	2.81	0.053	0.1142	10 m	2.74	1.06	0.26	3.90	0.27	14.4	2.59	8.11	1.59
					25 m	2.88	1.09	0.27	3.92	0.28	14.1	2.65	8.54	1.60
25	10.9	5.06	0.051	0.0851	15 m	4.86	1.72	0.35	4.54	0.38	12.0	2.83	16.7	1.47
					25 m	5.25	1.87	0.34	5.18	0.36	14.3	2.81	18.0	1.50
26	29.5	3.49	0.047	0.0297	30 m	3.42	1.85	0.36	4.75	0.39	12.2	1.85	19.8	0.95
					39 m	3.57	2.07	0.32	6.03	0.34	17.6	1.72	20.7	0.94
30	180	11.4	0.048	0.0232	26 m	12.5	5.12	0.67	6.90	0.74	9.3	2.43	81.7	0.90
					45 m	10.4	4.73	0.58	7.45	0.63	11.7	2.20	68.3	0.89
31	172	10.8	0.044	0.0137	17 m	11.3	6.54	0.52	12.0	0.54	22.1	1.73	96.7	0.75
					33 m	10.3	6.12	0.50	11.9	0.52	23.0	1.67	87.6	0.74
32	110	10.8	0.043	0.0210	10 m	10.3	4.77	0.51	9.86	0.54	18.5	2.16	71.0	0.94
					21 m	11.3	5.11	0.53	9.19	0.56	16.5	2.20	77.8	0.94

Table 5. Channel characteristics and bankfull flow properties at sites draining sedimentary terrane. Qbf = bankfull discharge. See Plate 2 and Figure 6 for locations.

Site	Drainage area (km^2)	Reach Qbf (m^3/s)	Manning's roughness coefficient	Bed slope (m/m)	Cross-section	Qbf (m^3/s)	Bankfull area (m^2)	Hydraulic radius (m)	Width (m)	Mean depth (m)	Width: depth ratio	Velocity (m/s)	Conveyance (m^3/s)	Froude No.
6	70.1	1.10	0.038	0.0124	11 m	1.18	1.15	0.21	5.48	0.21	26.1	1.02	10.60	0.71
					35 m	1.02	1.06	0.19	5.55	0.19	29.1	0.96	9.20	0.70
7	13.5	0.21	0.040	0.0476	7 m	0.18	0.15	0.10	1.40	0.11	12.9	1.20	0.83	1.16
					15 m	0.23	0.19	0.11	1.60	0.12	13.8	1.26	1.07	1.16
10	6.9	0.58	0.050	0.0565	3 m	0.60	0.35	0.21	1.10	0.32	3.4	1.69	2.51	0.95
					7.5 m	0.57	0.38	0.18	1.74	0.22	8.0	1.51	2.39	1.03
11	4.3	0.27	0.043	0.0682	11 m	0.29	0.18	0.13	1.15	0.16	7.3	1.59	1.10	1.27
					14 m	0.25	0.17	0.13	1.12	0.15	7.6	1.54	0.97	1.27
12	43.5	0.95	0.043	0.0124	10 m	0.72	0.82	0.20	3.77	0.22	17.2	0.87	6.46	0.59
					23 m	1.26	1.06	0.31	2.89	0.37	7.9	1.19	11.3	0.62
13	47.8	1.00	0.043	0.0190	3 m	0.73	0.66	0.20	3.01	0.22	13.7	1.10	5.28	0.75
					6 m	1.38	0.98	0.29	2.94	0.33	8.8	1.41	10.0	0.78
14	97.5	2.26	0.043	0.0411	10 m	2.37	1.26	0.25	4.80	0.26	18.3	1.88	11.7	1.18
					20 m	2.13	0.99	0.31	2.49	0.40	6.3	2.17	10.6	1.10
16	4.8	0.50	0.045	0.0404	12 m	0.45	0.30	0.19	1.18	0.26	4.6	1.48	2.22	0.93
					20 m	0.55	0.34	0.22	0.98	0.35	2.9	1.63	2.76	0.88
17	120	4.62	0.042	0.0281	10 m	3.99	1.93	0.37	4.79	0.40	11.8	2.06	23.8	1.04
					27 m	5.34	2.38	0.42	5.06	0.47	10.8	2.24	31.8	1.04

Table 5. (continued)

Site	Drainage area (km^2)	Reach Qbf (m^3/s)	Manning's roughness coefficient	Bed slope (m/m)	Cross-section	Qbf (m^3/s)	Bankfull area (m^2)	Hydraulic radius (m)	Width (m)	Mean depth (m)	Width: depth ratio	Velocity (m/s)	Conveyance (m^3/s)	Froude No.
29	555	10.0	0.040	0.0051	9.7 m	9.74	7.74	0.59	12.7	0.61	20.7	1.26	136	0.52
					35 m	10.3	7.84	0.63	11.9	0.66	18.2	1.31	144	0.52
33	984	18.7	0.041	0.0037	15 m	15.5	12.1	0.80	14.6	0.83	17.5	1.28	254	0.45
					35 m	19.6	15.3	0.80	18.4	0.83	22.1	1.28	321	0.45
					45 m	16.8	14.9	0.66	15.6	0.95	16.4	1.13	275	0.37
34	1010	12.5	0.040	0.0077	11 m	11.1	7.70	0.53	14.0	0.55	25.5	1.45	127	0.62
					25 m	14.6	9.31	0.61	15.0	0.62	24.2	1.57	167	0.64
					35 m	11.7	8.19	0.52	15.2	0.54	28.4	1.42	133	0.62

Table 6. Width, area, velocity and discharge values calculated from field surveys and measured by U.S.G.S. personnel. See Figure 6 for locations. Measurement 409 at gage 08275300 probably represents overbank flow.

Site	Cross-section	CALCULATED VALUES Width (m)	Area (m^2)	Velocity (m/s)	Discharge (m^3/s)	MEASURED VALUES Measurement date	number	Width (m)	Area (m^2)	Velocity (m/s)	Discharge (m^3/s)
	Rio Pueblo de Taos Near Ranchito 08275300										
29	9.7 m	12.68	7.74	1.26	9.74	5/9/79	409	23.48	9.09	1.20	10.94
	35 m	11.94	7.84	1.31	10.27	6/26/79	414	10.06	6.73	1.38	9.32
	Rio Chiquito Near Talpa 08275600										
14	10 m	4.80	1.26	1.88	2.37	5/9/79	417	5.79	2.22	1.06	2.36
	20 m	2.49	0.99	2.17	2.13	5/27/80	435	4.88	2.23	1.07	2.39
						5/29/80	436	6.86	2.37	0.94	2.23
	Rio Pueblo de Taos Below Los Cordovas 08276300										
33	15 m	14.55	12.11	1.28	15.45	5/27/80	431	15.24	10.28	1.70	18.28
	35 m	18.35	15.26	1.28	19.55	5/27/83	471	16.16	12.64	1.78	22.53
	45 m	15.59	14.85	1.13	16.75						

0.80% to 1.05% of the time (Table 7). Dunne and Leopold (1978) also state that Q_{bf} has a recurrence interval (based on annual series data) of between 1.5 and 3.0 yr, and Q_{bf} recurrence intervals from this study are between 2.0 and 5.0 yr. Calculated Q_{bf} values are therefore reasonable based on flow-frequency data. Although the one site on Rio Hondo (below Arroyo Hondo, site 31) has a higher Q_{bf} recurrence interval than sites draining sedimentary rocks, flow duration curves (Fig. 10) suggest that bankfull discharges per unit area are equaled or exceeded a greater percentage of time at sites draining crystalline terrane.

Bankfull discharge tends to increase with drainage area, if seepage losses are negligible (Richards, 1982). This allows a third check on calculated discharges. For example, three measurements made on Arroyo Seco show discharge increases from the upstream site (site 19, Q_{bf} = 1.03 m^3/s) to the intermediate site (site 20, Q_{bf} = 2.21 m^3/s), to the downstream site (site 21, Q_{bf} = 2.86 m^3/s). Q_{bf} increases similarly in the downstream direction on other streams. A log-log plot of Q_{bf} *versus* drainage area indicates that Q_{bf} is substantially higher for a given drainage area on streams draining areas underlain by crystalline bedrock (Fig. 16).

Bed Material Characteristics

Channels throughout the study area contain predominately poorly-sorted, pebble, cobble, and boulder bed material. Mean grain sizes of each sample site are given in Table 8. A Student's t-test (Mendenhall and Sincich, 1984) performed on 976 and 900 samples from channels draining crystalline and sedimentary terranes, respectively, indicates that mean grain size in channel bed material in crystalline terrane is significantly higher at the α = .005 level. Relative frequency

Table 7. Bankfull flood frequency data for sites measured at or near U.S.G.S. gaging stations. Qbf = bankfull discharge. See Figure 6 for locations.

Basin lithology	Site	Station number	Station name	Drainage area (km^2)	Qbf (m^3/s)	% time exceeded	Average # days/yr exceeded	Approx. Qbf recurrence interval (yr)
Sedimentary	14	08275600	Rio Chiquito Near Talpa	95.8	2.26	1.05	3.8	2.0
	29	08275300	Rio Pueblo de Taos Near Ranchito	516	10.0	0.93	3.4	3.7
	33	08276300	Rio Pueblo de Taos Below Los Cordovas	984	18.7	1.01	3.7	2.3
Crystalline	31	08268500	Arroyo Hondo At Arroyo Hondo	172	10.8	0.80	2.9	5.0

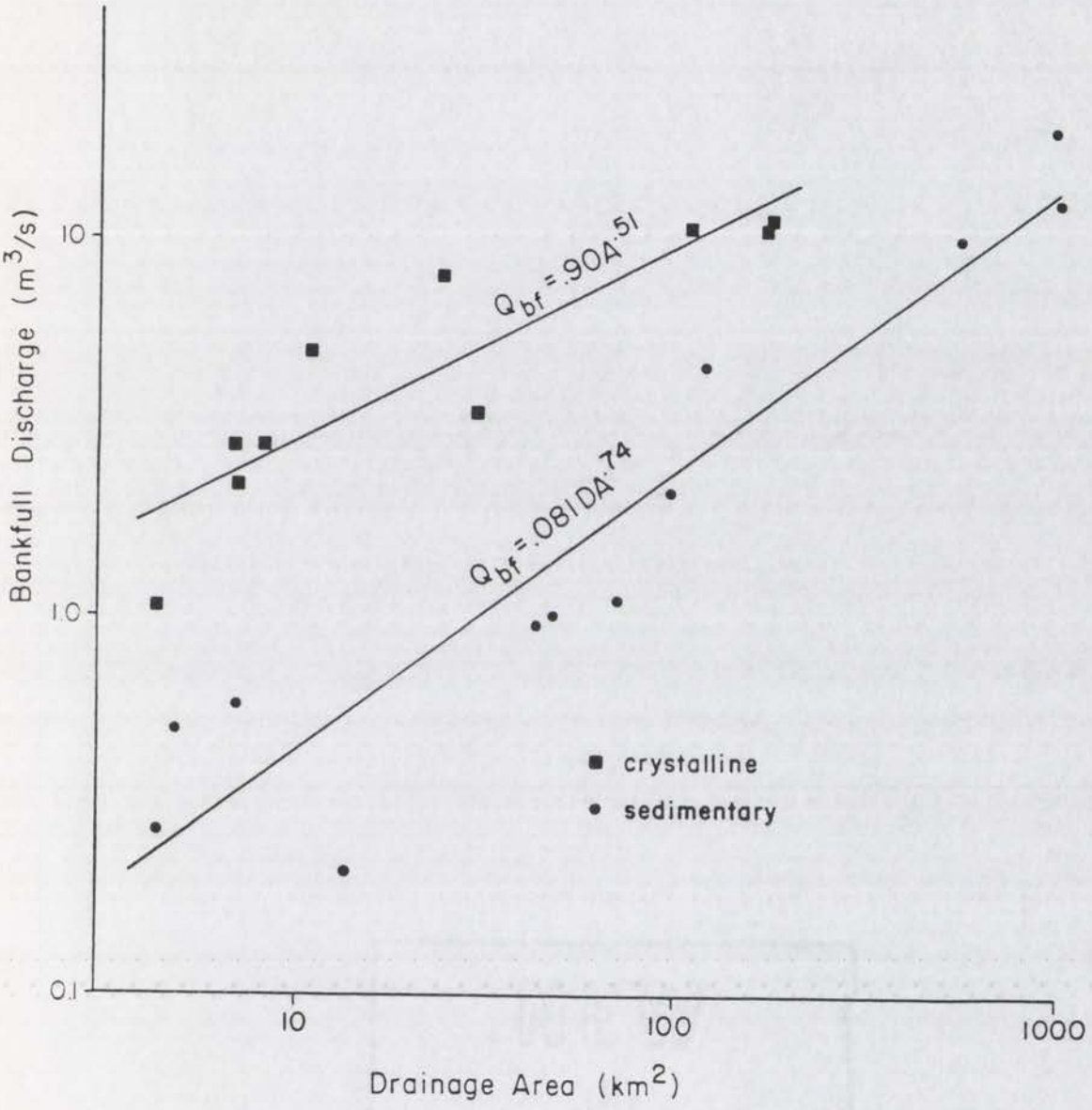

Figure 16. Bankfull discharge plotted against drainage area for surveyed sites. The least-squares regression curves have coefficients of correlation (r) of 0.896 (crystalline) and 0.935 (sedimentary).

Table 8. Bed-material grain-size parameters of channels draining crystalline and sedimentary terrane. See Figure 6 for locations.

CHANNELS DRAINING CRYSTALLINE TERRANE

Site	# samples	Mean grain size (mm)	Largest clast (mm)	5th largest clast (mm)	10th largest clast (mm)
1	51	143	480	294	222
2	51	239	990	600	400
3	50	188	860	370	299
4	68	114	430	262	227
19	53	143	450	297	271
20	48	164	528	345	243
21	48	132	357	259	225
22	52	118	580	236	172
23	66	161	1040	476	248
24	52	191	700	400	338
25	52	155	500	340	265
26	63	98	355	257	159
27	62	168	825	347	284
28	83	114	400	233	213
30	60	142	900	236	200
31	61	100	685	191	156
32	56	134	420	225	199
	(976) mean:	145	618	316	242

CHANNELS DRAINING SEDIMENTARY TERRANE

Site	# samples	Mean grain size (mm)	Largest clast (mm)	5th largest clast (mm)	10th largest clast (mm)
6	77	48	123	90	82
7	61	70	635	166	136
9	76	64	364	140	111
10	53	90	231	196	136
11	48	87	280	157	138
12	55	124	315	141	122
13	58	70	450	220	177
14	59	139	426	260	215
15	62	122	500	231	204
16	52	80	318	188	127
17	55	133	1250	267	190
18	63	90	312	217	194
29	59	103	335	195	151
33	69	107	465	256	177
34	53	48	134	85	73
	(900) mean:	91	409	187	149

histograms of the two sample populations (Fig. 17) illustrate that channels draining crystalline terrane have larger mean grain-sizes than those draining sedimentary terrane. Most individual site data do not demonstrate normal distributions, although overall sample populations approximate normality (Fig. 17).

Grain sizes may be related to distance from headwater divide (Hack, 1957; Miller, 1958), and therefore the areal distribution of sample sites can affect sample population distributions. For instance, more sample sites in headwater regions may bias a population toward the coarse end, if grain size decreases with distance downstream. In this study, attempts were made to have approximately equal percentages of sample sites in headwater regions in crystalline and sedimentary terranes. Figure 18 indicates that there is considerable variablity of mean grain size with distance downstream on streams draining both terranes.

Bed-material lithologies were also noted in the field. Figure 19 shows the relative frequency distribution of present-day bed-material lithologies in Rio Hondo and Rio Pueblo de Taos channels downstream from the mountain front. Most bed material in Rio Hondo is composed of either gneiss or granite. Rio Pueblo de Taos channels below the mountain front drain mostly sedimentary rocks (about 60% by area), smaller areas underlain by crystalline rocks (about 10% by area, in the Arroyo Seco, Rio Lucero, and Rio Pueblo de Taos drainages), and some areas (about 30%) underlain by Quaternary and late Tertiary(?) deposits derived from both crystalline and sedimentary terrane. The relative frequency distribution of Rio Pueblo de Taos bed material (below the mountain front) indicates contributions from all sources. About 60% of Rio Pueblo de Taos bed material is composed of crystalline rocks (Fig. 19), although only 10% of

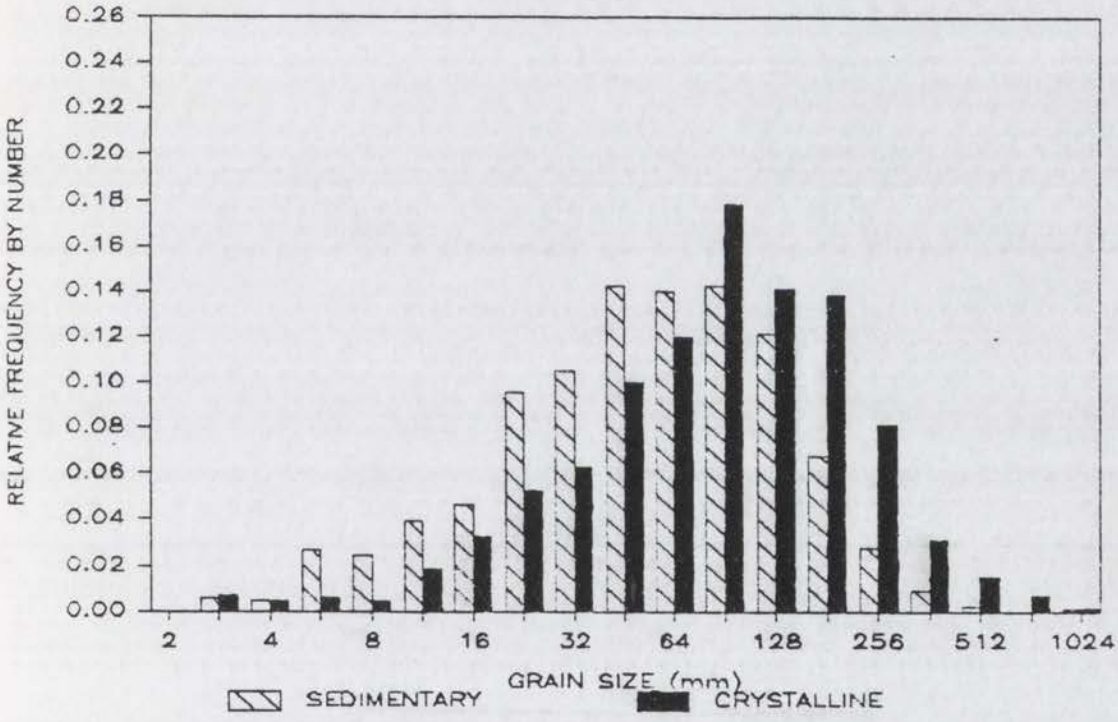

Figure 17. Relative frequency plot of bed-material grain sizes on streams draining crystalline and sedimentary terrane. Note coarser grain sizes in channels draining crystalline rocks.

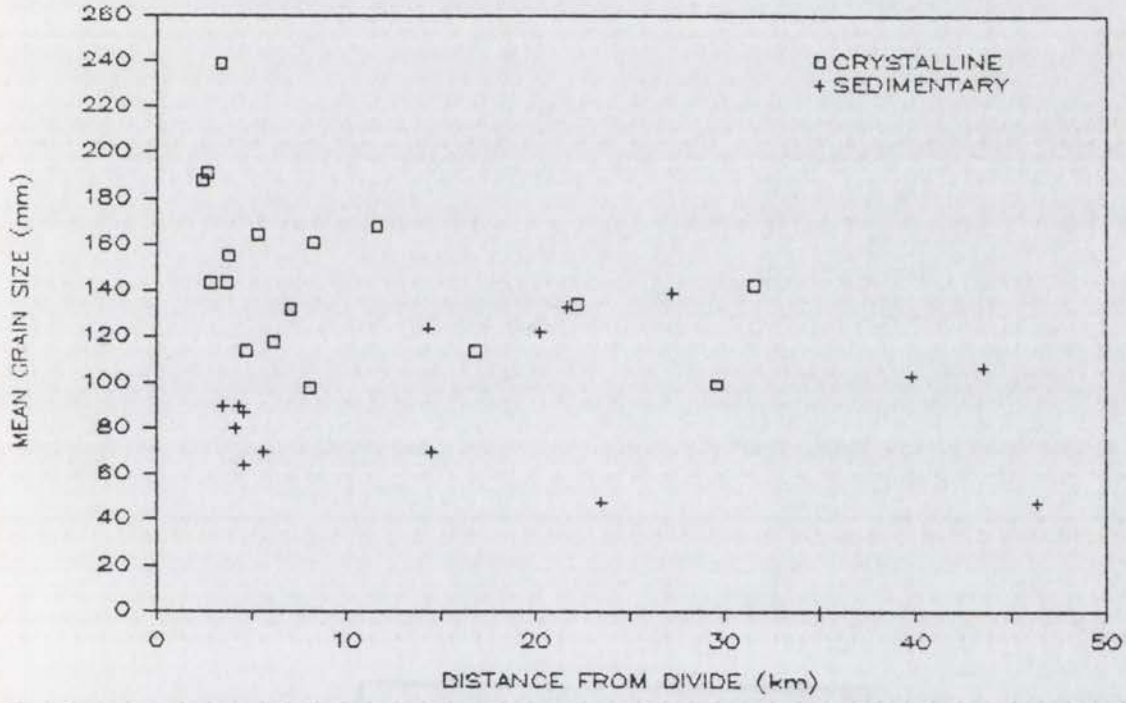

Figure 18. Plot of bed-material grain size against distance from drainage divide.

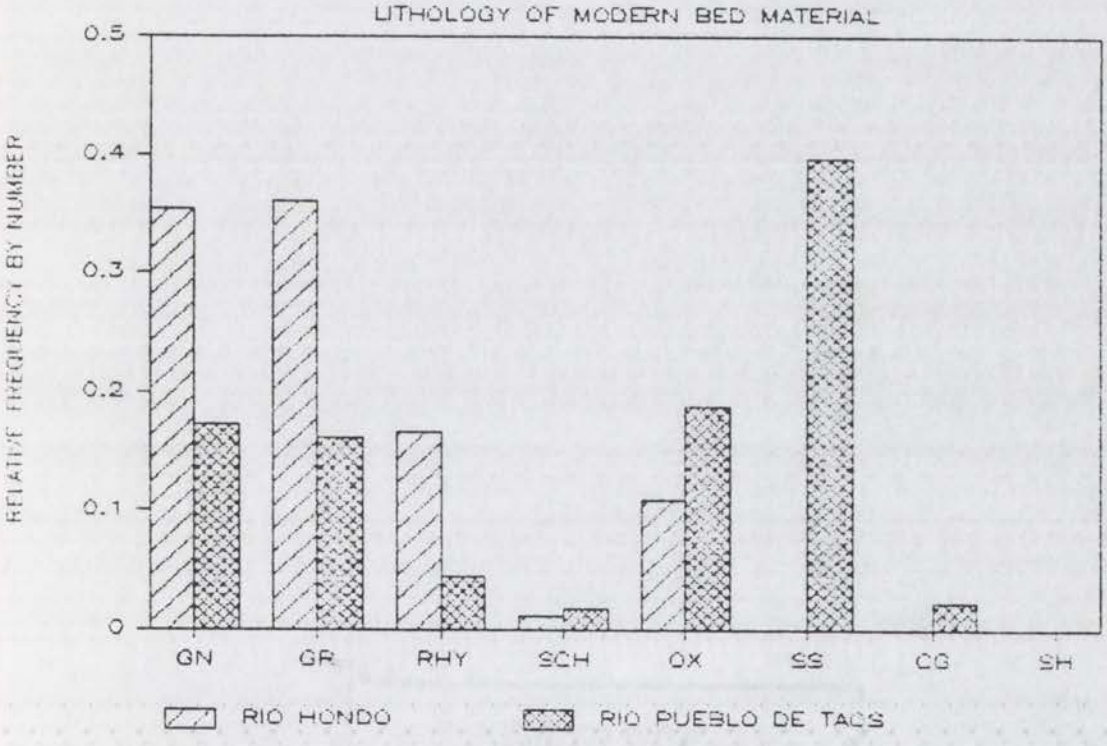

Figure 19. Relative frequency plot of clast lithologies in bed-material samples. GN = gneiss, GR = granite, RHY = rhyolite and andesite, SCH = schist, OX = other crystalline lithologies (including basalt, amphibolite, and massive quartz), SS = sandstone, CG = conglomerate, SH = shale. To allow comparison with Figure 21, data is from sites 30, 31, and 32 along Rio Hondo, and from sites 29, 33, and 34 along Rio Pueblo de Taos (see Plates 1 and 2 for locations).

the drainage area (at sample site 34, see Fig. 6) is underlain by these lithologies. In contrast, about 40% of bed material at 34 is composed of sedimentary rocks, although 60% of the drainage area is underlain by these lithologies (Fig. 19).

Sediment Transport Parameters

A main goal of this study is to assess sediment transport capabilities of streams draining the two lithologic terranes. Flow competence, dimensionless shear stress, and stream power data are presented here, and these data sets will be used later to compare transport conditions within the study area.

Flow competence is a measure of a stream's ability to transport sediment, and can be defined as the maximum particle size transportable (Baker and Ritter, 1975). In order to compare competence data between streams, it must be shown that there is sediment available which is larger than the stream's competence, that the measured clast was transported, and that the channel bed is not armoured (Baker and Ritter, 1975; Pickup, 1975).

Field observations indicate that hillslopes in both basins contribute material to channels which is not transported. Abundant clast imbrication indicates that the majority of bed material is not "lag", and can probably be transported at high flow. An attempt has been made to detect bed armouring in Taos streams by plotting the largest and 5th largest clasts against mean grain size (Fig. 20). Abundant imbrication suggests that much of the bed material is transported in Taos streams, and thus mean grain sizes are probably determined by the moveable bed-material fraction. Correlation ($r = .90$) between mean grain size and 5th

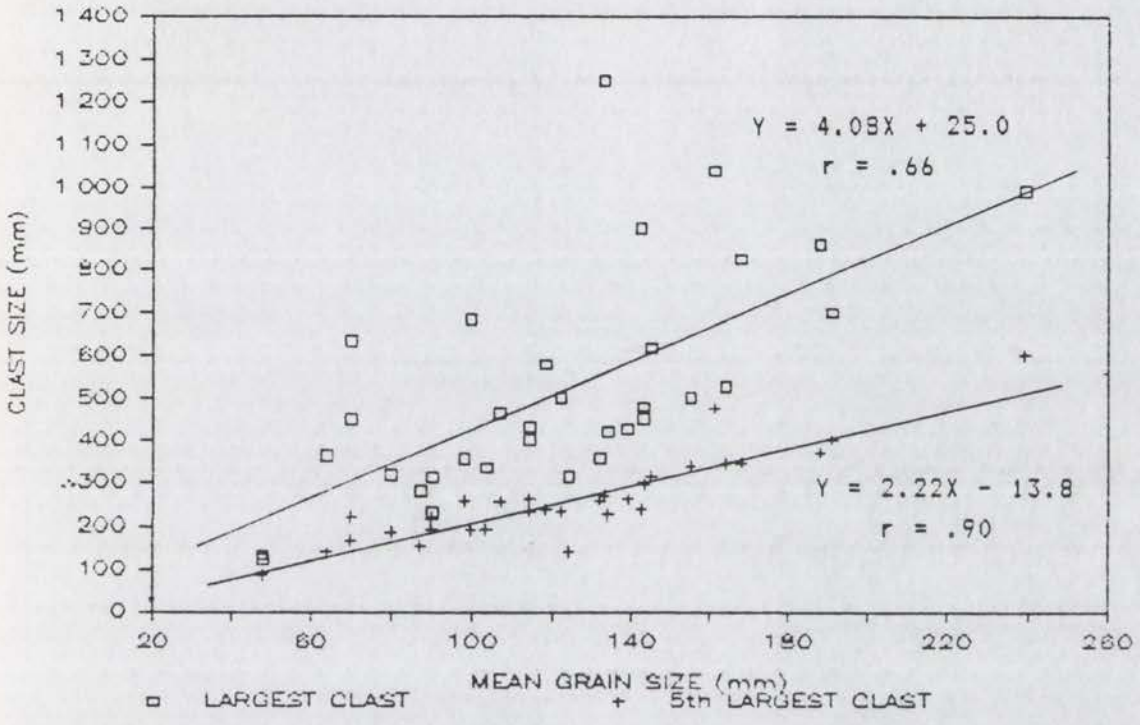

Figure 20. Plot of largest bed-material clast and of 5th largest bed-material clast in each bed-material sample against mean grain size. High r value for 5th largest clast data suggests that the 5th largest clasts are moveable bed material; whereas, the low r value for largest clast data implies that the largest clasts are usually not moved.

largest clast indicates that the 5th largest clasts are part of the moveable distribution (Fig. 20); a lower degree of correlation (r = .66) between mean grain size and largest clast suggests that the largest clasts are not moved, except perhaps in extreme floods. In addition, Pickup (1975) notes that armouring is insignificant in naturally degrading stream channels because new sediment supplies derived from upstream erosion are always available, which may be the case in streams on the Taos Plateau.

For this study, competence has been estimated by averaging the five and ten largest clasts in a random bed-material sample. Scott and Gravlee (1968) and Costa (1983) have used similar measures to estimate flow parameters. Table 9 shows that higher mean values of D_{5x} and D_{10x} (averages of the five and ten largest clasts, respectively) were found at sites draining crystalline terrane. Thus, streams draining crystalline rocks have higher competences than those draining sedimentary terrane.

Dimensionless shear stress values (T^*_{50} and T^*_{90}) were calculated for 32 reaches near Taos using equation (4) (Table 10), and in almost all instances, T^*_{c50} (= 0.031, see Methods) was exceeded at bankfull discharges. For reaches draining crystalline rocks, the mean bankfull T^*_{50} value is 0.159, whereas for reaches draining sedimentary rocks the mean value is 0.098. In additon, T^*_{c90} was exceeded by bankfull discharge at most sites (Table 10). Thus, transport of the majority of the bed-material distributions can occur at Q_{bf} in both stream systems. However, imbrication, particle clustering (Brayshaw, 1985), non-uniform flow characteristics, and less effective transport conditions away from the channel center (Parker, 1978) probably also influence entrainment of d_{50} and d_{90} during bankfull events.

Table 9. Means of the five and ten largest clasts in random bed-material samples. See Plates 1 and 2 for locations.

channels draining crystalline terrane			channels draining sedimentary terrane		
Site	Mean of 5 largest clasts (mm)	Mean of 10 largest clasts (mm)	Site	Mean of 5 largest clasts (mm)	Mean of 10 largest clasts (mm)
1	358	303	6	104	95
2	728	620	7	310	231
3	518	429	9	214	165
4	329	282	10	211	184
19	348	314	11	215	180
20	405	338	12	188	158
21	290	264	13	323	259
22	360	282	14	334	283
23	727	527	15	330	270
24	573	468	16	255	203
25	428	362	17	387	311
26	306	244	18	273	238
27	510	404	29	235	202
28	280	250	33	332	260
30	477	349	34	101	90
31	311	238			
32	309	240			
mean:	427	348		254	209
σ:	139	107		82	63

Table 10. Selected channel and bankfull flow properties and dimensionless shear stress values for channels draining crystalline and sedimentary terranes. T*c50 = 0.031, T*c90 = 0.015 (Andrews, 1984). ! indicates values close to critical values. Regions are shown in Figure 6.

Region	Site	Bankfull mean depth (m)	Slope (m/m)	D50 (mm)	D90 (mm)	T*50	T*90
Channels draining crystalline terrane							
I	19	0.16	0.130	77	217	0.164	0.058
I	20	0.29	0.093	108	211	0.151	0.077
I	21	0.34	0.068	81	187	0.173	0.075
I	22	0.48	0.046	66	171	0.202	0.078
I	24	0.28	0.114	90	296	0.215	0.065
I	25	0.37	0.085	74	236	0.258	0.081
I	26	0.36	0.030	55	147	0.118	0.044
III	30	0.68	0.023	64	204	0.149	0.047
II	31	0.53	0.014	56	126	0.079	0.035
II	32	0.55	0.021	84	164	0.083	0.043
					mean:	0.159	0.060
Channels draining sedimentary terrane							
IV	6	0.20	0.012	29	58	0.052	0.026
IV	7	0.12	0.048	25	115	0.138	0.030
IV	10	0.27	0.057	56	129	0.165	0.072
IV	11	0.16	0.068	45	129	0.147	0.051
IV	12	0.30	0.012	37	101	0.061	0.022
IV	13	0.28	0.019	77	162	0.042	0.020
IV	14	0.33	0.041	93	182	0.088	0.045
IV	16	0.30	0.040	39	132	0.188	0.056
IV	17	0.44	0.028	56	191	0.134	0.039
V	29	0.64	0.005	65	132	0.030!	0.015!
V	33	0.87	0.004	54	148	0.036!	0.013!
V	34	0.57	0.008	28	56	0.095	0.047
					mean:	0.098	0.036

Erosion and deposition in channels is dependent on the relative magnitudes of power needed to transport the average sediment load and stream power available to transport the load (Bull, 1979). Stream power is the rate at which a stream loses its potential energy as it flows down a channel, as described by the equation (Bagnold, 1966):

$$\Omega = pgQS \quad (5)$$

where Ω is stream power, p = fluid density, g is acceleration of gravity, Q is discharge, and S is slope. Values of stream power in channels draining crystalline terrane are higher than those draining sedimentary rocks (Table 11). Notably, stream power in the headwaters of streams draining crystalline terrane is relatively high (Fig. 21), but is lower further downstream. Stream power in streams draining sedimentary terrane is relatively low and does not systematically change downstream.

The total power supply per unit bed area (or unit stream power, w) influences bedload transport rates (Bagnold, 1977). Unit stream power can be written as Ω/W, where W is flow width (Bagnold, 1966). Average w for reaches draining crystalline rocks is about 490 N/m/s. Average unit stream power for reaches draining sedimentary rocks is about 140 N/m/s (Table 11).

Basin Morphometry

The purposes of this section are to present results of basin form measurements and to compare morphologies of basins underlain by different lithologies in order to investigate of the effects of lithology on discharge production, sediment production, and drainage basin evolution.

As shown earlier, elevation affects precipitation and temperature, and therefore influences the amount of water input to hillslope, groundwater and fluvial systems. Figure 22 shows the cumulative percent

Table 11. Selected bankfull hydraulic characteristics in channels draining crystalline and sedimentary terrane. Fluid density assumed to be 1.00 g/cm^3 in stream power calculations. Regions are shown in Figure 6.

Channels draining crystalline terrane						
Region	Site	Bankfull discharge (m^3/s)	Slope (m/m)	Width (m)	Stream power (N/s)	Unit stream power (N/m/s)
I	19	1.03	0.130	2.90	1313	453
I	20	2.21	0.093	2.84	2016	710
I	21	2.86	0.068	3.32	1907	574
I	22	7.98	0.046	6.38	3600	564
I	24	2.81	0.114	3.91	3142	804
I	25	5.06	0.085	4.86	4218	868
I	26	3.49	0.030	5.39	1027	191
III	30	11.4	0.023	7.18	2571	358
II	31	10.8	0.014	11.9	1483	125
II	32	10.8	0.021	9.02	2224	247
mean:					2350	489
σ:					981	246

Channels draining sedimentary terrane						
Region	Site	Bankfull discharge (m^3/s)	Slope (m/m)	Width (m)	Stream power (N/s)	Unit stream power (N/m/s)
IV	6	1.10	0.012	5.52	129	23
IV	7	0.21	0.048	1.50	99	66
IV	10	0.58	0.056	1.42	319	225
IV	11	0.27	0.068	1.14	180	158
IV	12	0.95	0.012	3.33	112	34
IV	13	1.00	0.019	2.98	186	62
IV	14	2.26	0.041	3.64	909	250
IV	16	0.50	0.040	1.08	196	181
IV	17	4.62	0.028	4.92	1269	258
V	29	10.0	0.005	12.3	490	40
V	33	18.7	0.004	16.2	734	45
V	34	12.5	0.008	14.8	981	67
mean:					467	117
σ:					388	87

Above the mountain front Channels draining crystalline terrane						
mean:					2460	595
σ:					1117	213

Above the mountain front Channels draining sedimentary terrane						
mean:					378	140
σ:					394	89

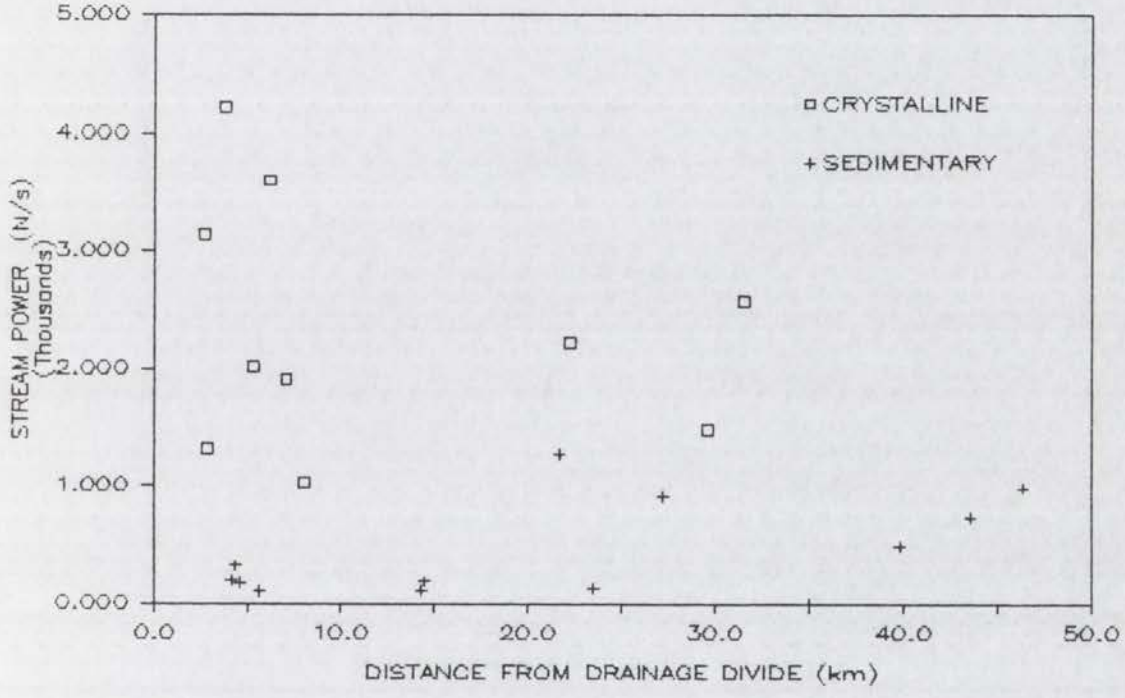

Figure 21. Plot of stream power against distance from drainage divide.

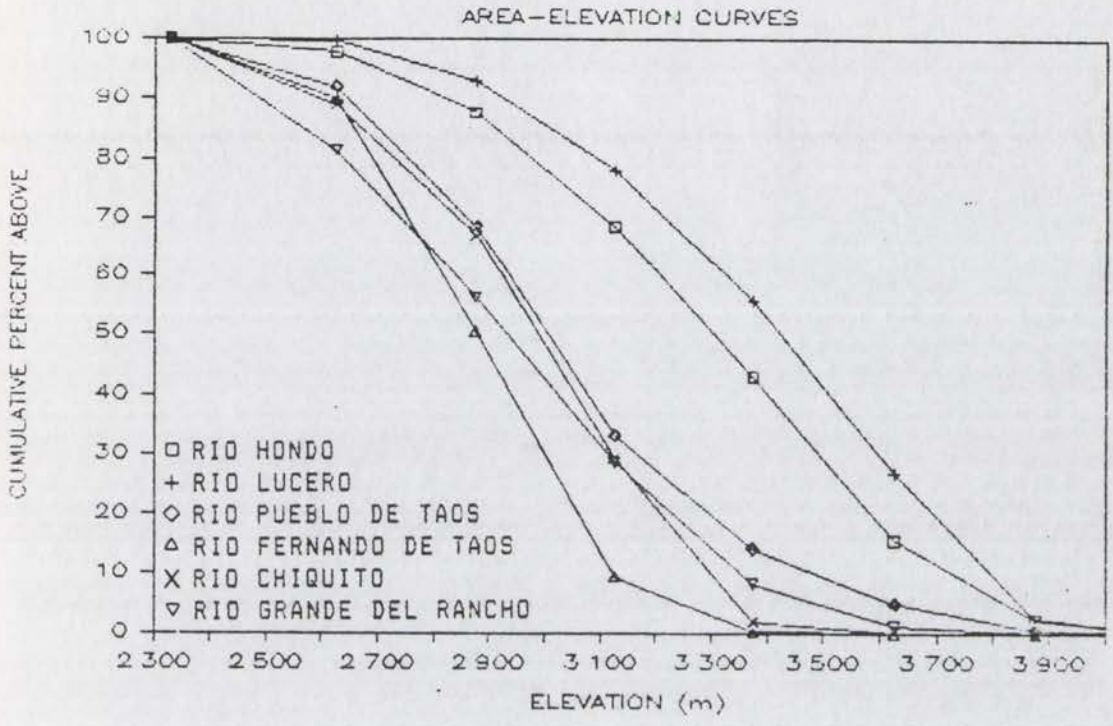

Figure 22. Plot of cumulative percent of drainage area above a given elevation for six drainage basins in the study area. The two basins underlain by crystalline rocks (Rio Hondo and Rio Lucero) have more drainage area within high elevation zones than basins underlain by sedimentary rocks.

of area above a given elevation for six basins in the Taos Range. Basins underlain by crystalline rocks tend to have larger percentages of drainage area within higher elevation zones. Median basin elevations range from 3300 to 3120 m in crystalline terrane, and from 2870 to 3000 m in sedimentary terrane.

Table 12 contains relief and relief ratio (or average basin slope; basin relief divided by basin length) data for the study area. Basins underlain by crystalline bedrock have higher relief and higher relief ratios than basins underlain by sedimentary bedrock. High relief ratios in the study area are therefore associated with steep hillslopes and narrow, deep valleys, whereas basins with low relief ratios typically have shallow hillslopes and wide valleys.

Vf ratios (Bull and McFadden, 1977) provide a quantitative measure of valley form by comparing valley floor width to mean valley depth. In four basins Vf ratios have been determined at intervals of 1/20th of total stream length, in order to compare valley morphologies within and between basins (Fig. 23). Vf ratios tend to be lower in areas underlain by crystalline rocks than in areas underlain by sedimentary rocks (Table 12).

Rio Hondo, Rio Lucero and Rio Chiquito have low Vf values all along their courses (Fig. 23), with the exception of slightly higher values in the Rio Hondo and Rio Lucero headwaters. In these headwater valleys, Vf ratios average 0.82 on Rio Hondo and 1.54 on Rio Lucero, and reflect valleys underlain by glacial material. Valleys are also much wider in the glaciated regions (average: 420 m). Topographic map and aerial photograph interpretation suggest that the Rio Pueblo de Taos valley is similar to the Rio Hondo and Rio Lucero valleys: wide, glacial deposit-

Table 12. Summary of basin morphometry data for six basins in the Sangre de Cristo mountains near Taos.
Data for Rio Grande del Rancho includes data from Rito de la Olla tributary. xtln = crystalline, sed = sedimentary

Dominant basin lithology	Basin	Relief (m)	Relief/ length ratio	Drainage density (km/km^2)	Drainage frequency ($\#/km^2$)	Hypsometric integral	Mean valley floor width (m)	Mean valle depth (m)	Mean Vf
xtln	Rio Hondo	1575	0.08	3.10	5.52	0.49	47	353	0.17
	Rio Lucero	1498	0.11	2.44	3.86	0.45	55	255	0.28
	mean:	1537	0.10	2.91	5.05	0.47			
sed	Rio Fernando de Taos	1160	0.04	2.56	4.25	0.50	130	98	1.86
	Rio Chiquito	1229	0.05	2.42	4.54	0.51	60	128	0.44
	Rio Grande del Rancho	1442	0.03	2.37	4.25	0.42	--	--	--
	mean:	1277	0.04	2.45	4.31	0.48			
70% sed 30% xtln	Rio Pueblo de Taos	1785	0.07	--	--	0.38	--	--	--

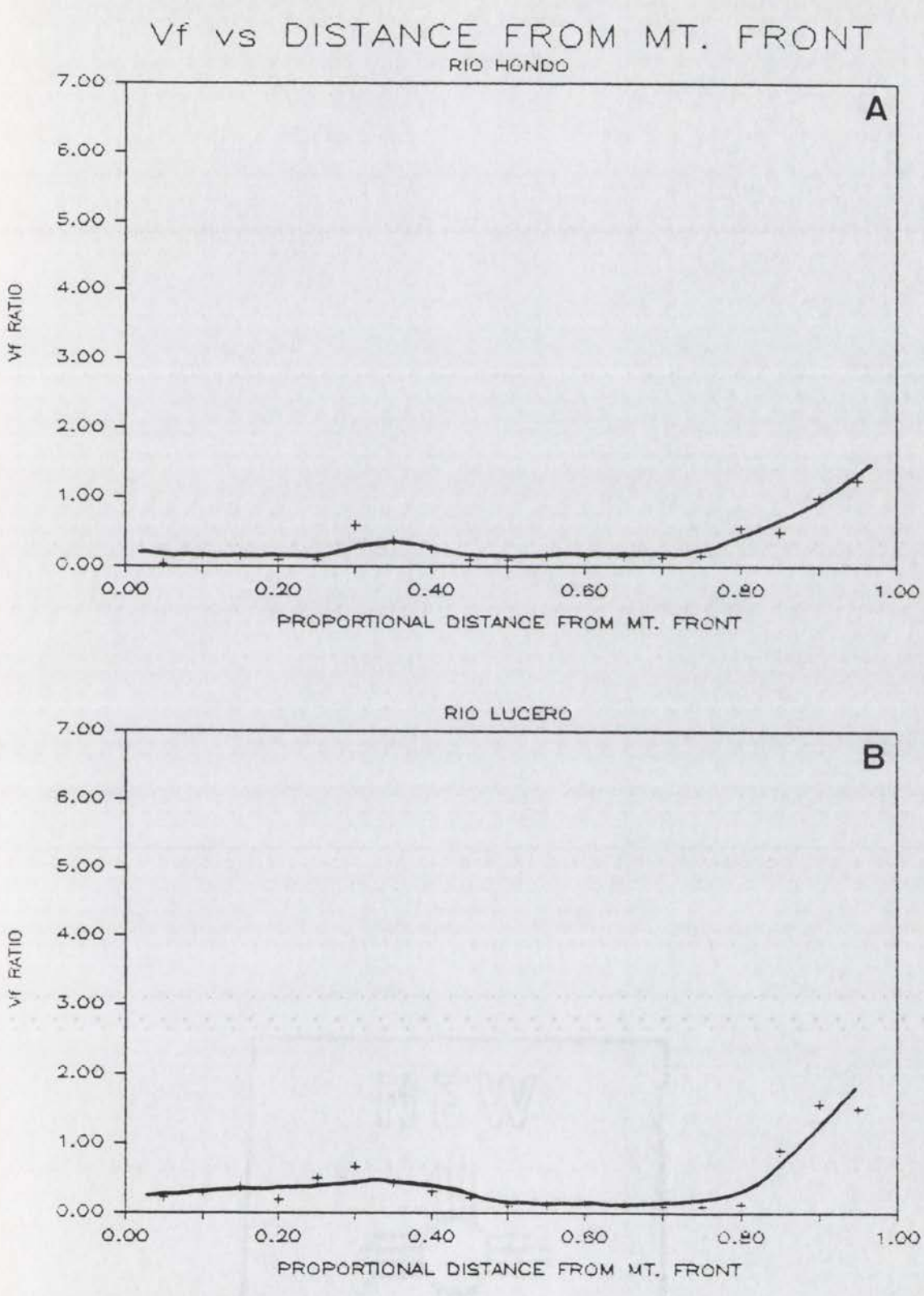

Figure 23. Variations in Vf ratios (valley floor width/valley depth) with distance from the mountain front. High Vf ratios reflect valleys having wide floors relative to valley depth. (A) Rio Hondo, (B) Rio Lucero, (C) Rio Chiquito, (D) Rio Fernando de Taos.

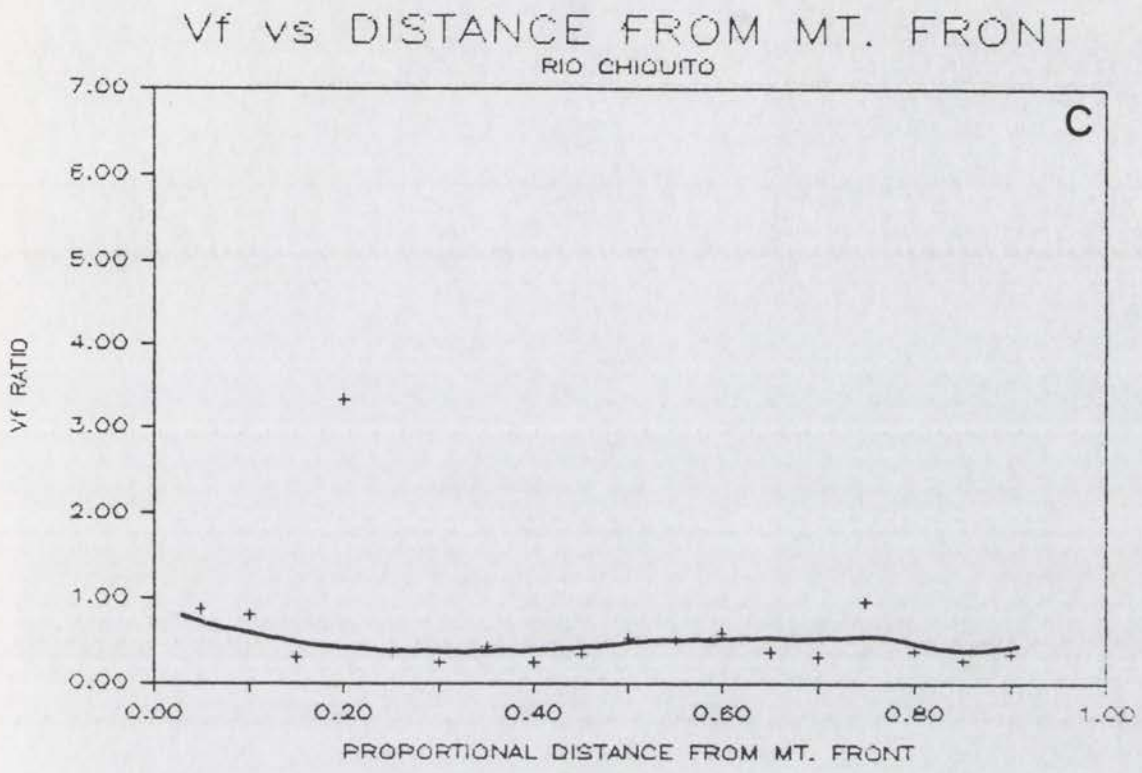

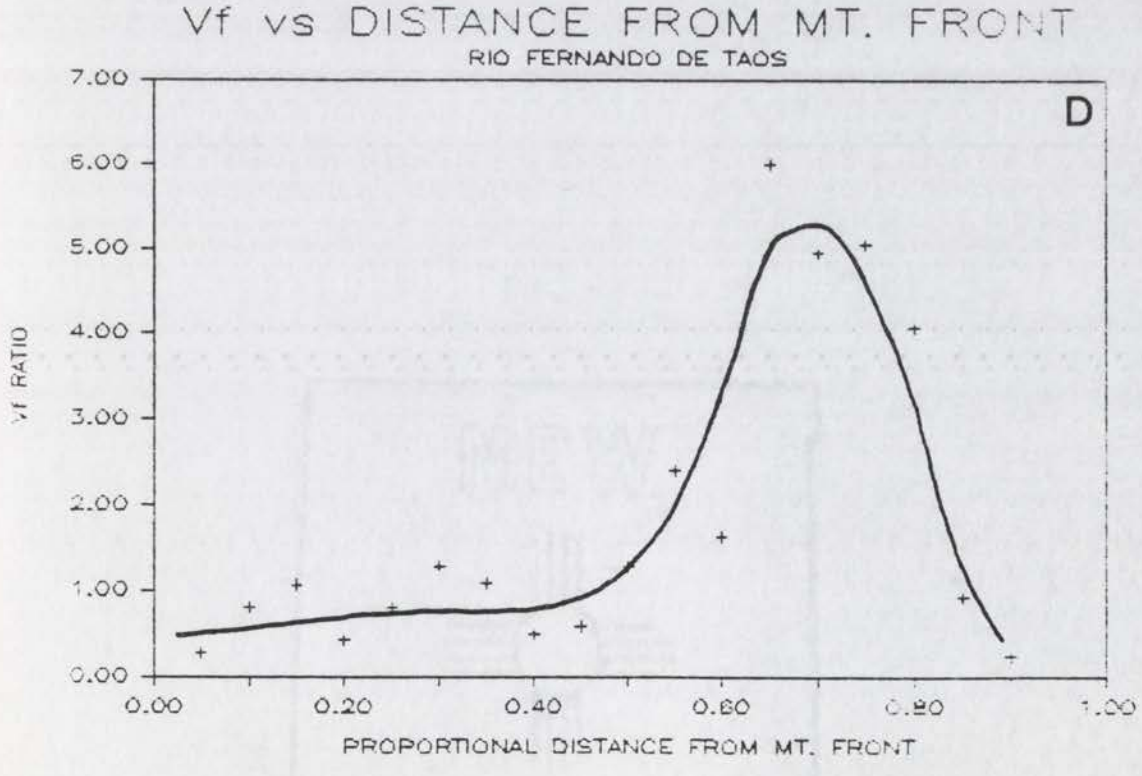

Figure 23. (continued)

floored headwater valleys and narrow, deep valleys between glacial deposits and the mountain front.

Vf ratios in the Rio Fernando de Taos basin are generally higher than those in other measured basins, reflecting wider valley morphology. Vf values are highest about 70% of the distance upstream (Fig. 23d), corresponding to a broad valley containing significant amounts of alluvium. Large amounts of valley fill also exist in the fairly wide Rio Grande del Rancho valley above the mountain front.

Valley morphology is closely linked to channel network morphology, which can be quantified by two parameters: drainage density (D_d, total stream length per unit area) and drainage frequency (F, total number of stream links per unit area). D_d and F values in the study area are higher in basins underlain by crystalline rocks than in basins underlain by sedimentary rocks (Table 12). A Student's t-test was performed on D_d values from 96 3rd-order drainage basins (21 in crystalline terrane and 75 in sedimentary terrane), which showed that crystalline terrane has higher drainage density than sedimentary terrane, at the $\alpha = .005$ level of significance. Data used in calculating D_d and F are presented in Appendix G.

The hypsometric integral represents the area under the hypsometric curve (Schumm, 1956) and allows quantification of basin-area relations. Hypsometric curves for six major drainages in the study area are plotted in Figure 24, and corresponding integrals are given in Table 12. Neither curves nor integrals differ substantially between the two lithologic terranes, although Rio Pueblo de Taos, which is underlain by both rock types, has a slightly lower integral.

Three analyses have been employed to quantitatively describe long-

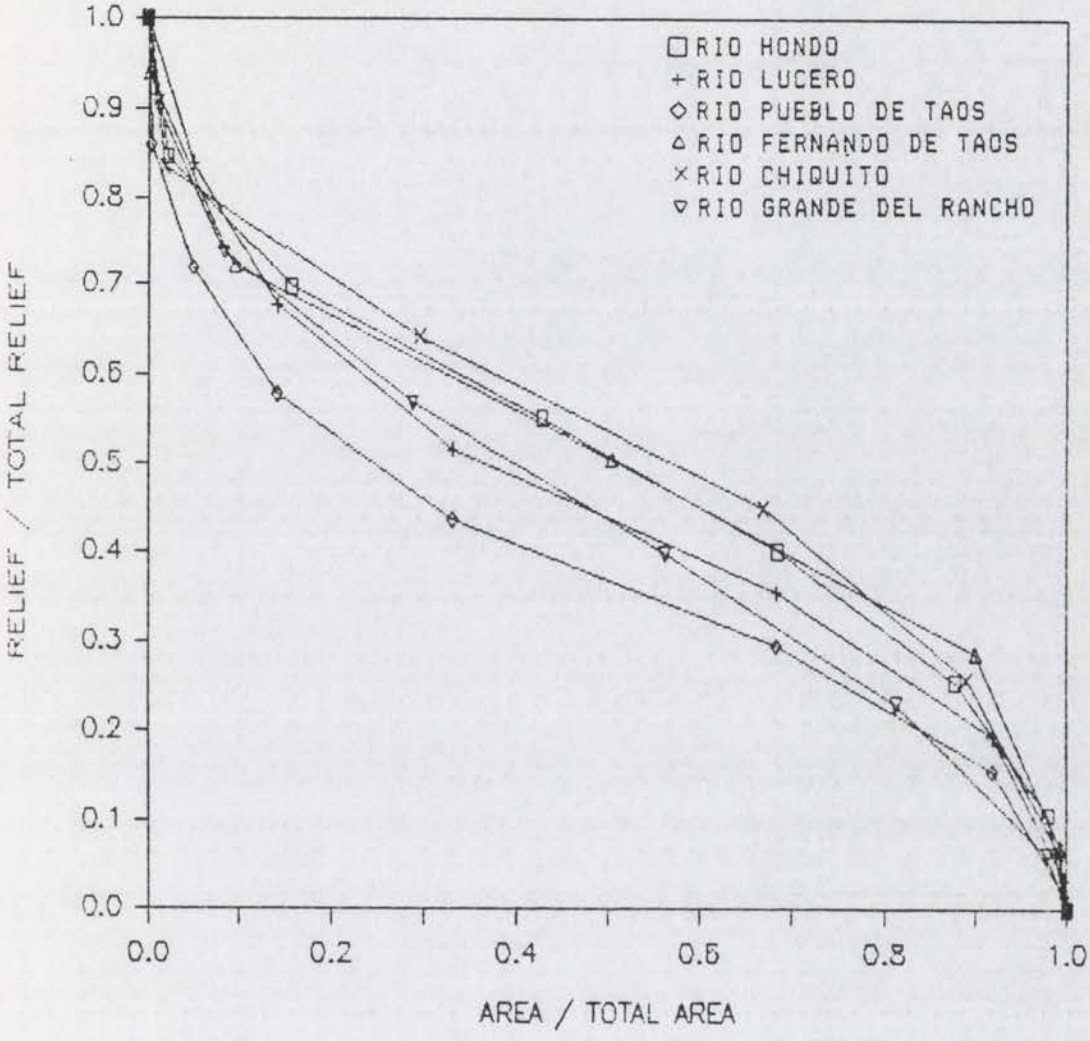

Figure 24. Hypsometric curves for six basins above the Sangre de Cristo mountain front.

profiles of the present-day streams and to compare these profiles between lithologic regions. These are: 1) a dimensionless concavity index (C); 2) least-squares exponential, logarithmic, and power function curve-fitting to long-profiles; and 3) least-squares power curve-fitting to slope-distance data. Basins underlain by crystalline rocks have higher values of C than those underlain by sedimentary rocks (Table 13). Rio Pueblo de Taos, which contains crystalline rocks in its source areas but sedimentary rocks downstream (Dane and Bachman, 1965), has the highest C value in the study area.

Least-squares exponential, logarithmic, and power function regression curves were fit to long-profiles using equations given by Shepherd (1985). The coefficients of determination (r^2) for these curves are given in Table 13. Most coefficients are high for both the exponential and logarithmic curves, but low for the power function curves. Three groups can be distinguished in these data. First, basins underlain by sedimentary rocks (Rio Fernando de Taos, Rio Chiquito, Rio Grande del Rancho, and Rio Pueblo de Taos) have profiles best described by logarithmic curves (Table 13, see also Fig. 25). Second, basins underlain by crystalline rocks and flowing to Rio Pueblo de Taos (Arroyo Seco and Rio Lucero) have profiles best described by exponential functions, which are asymptotic to the distance axis (Shepherd, 1985). Third, the Rio Hondo, underlain by crystalline rocks and flowing to the Rio Grande, is best described by a logarithmic curve (Table 13).

Shepherd (1985) and Hack (1957) used the first derivative of the long-profile, with slope instead of height on the ordinate, to analyze long-profiles. Hack (1957) expresses the slope-distance relation as a power function,

Table 13. Summary of morphometry data for long-profiles from drainage divide to the confluence with a higher order stream. Coefficients of determination (r^2) are for logarithmic, exponential, and power function best-fit curves to long-profiles. * indicates highest r^2 value of three curves. Rito de la Olla is a large tributary to Rio Grande del Rancho above the mountain front (see Fig. 1).

Dominant basin lithology	Stream	Concavity (C)	Coefficient of determination (r^2) Log.	Exp.	Power	$n^\dagger$	$k^\dagger$	$r^\dagger$
xtln	Rio Hondo	0.74	.92 *	.88	.57	-0.76	0.288	-.94
	Arroyo Seco	0.75	.95	.96 *	.65	-0.72	0.239	-.87
	Rio Lucero	0.72	.81	.94 *	.48	-0.59	0.215	-.87
	mean:	0.74						
sed	Rio Fernando de Taos	0.62	.95 *	.81	.54	-0.61	0.125	-.84
	Rio Chiquito	0.68	.88 *	.88	.57	-0.38	0.102	-.84
	Rio Grande del Rancho	0.62	.92 *	.90	.54	-0.53	0.139	-.74
	Rito de la Olla	0.65	--	--	--	--	--	--
	mean:	0.64						
70% sed 30% xtln	Rio Pueblo de Taos	0.76	.99 *	.80	.57	-0.84	0.304	-.84

† from equation (slope) = k (length)^n, (Hack, 1957). r is coefficient of correlation.

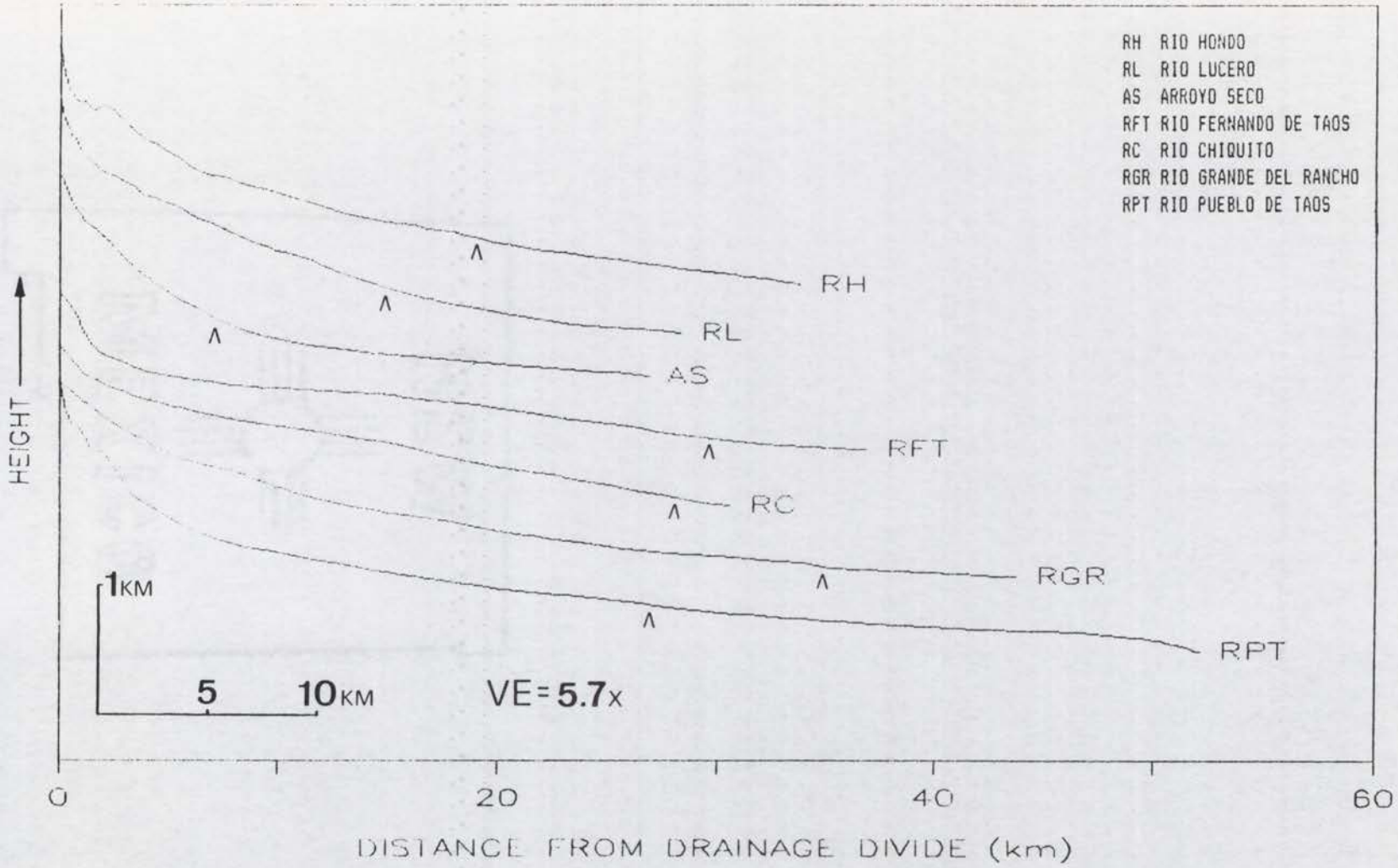

Figure 25. Long-profiles of Rio Hondo and six major tributaries to Rio Pueblo de Taos. See Figure 2 for locations and underlying rock types. (^) denotes mountain front. Vertical arrangement of long profiles is for clarity; y-axis does not represent elevation.

$$S = kL^n \quad (6)$$

where S is channel slope at a point on the profile, L is stream length at the same point, measured fron the drainage divide, and k and n are constants. Power function curves were fit to slope-distance data in the study area, using least-squares linear regression of $\log_{10}$-transformed data. Coefficients of correlation (r) and values of k and n for the fitted curves are given in Table 13. Values of n for long-profiles underlain by crystalline rocks are generally more negative than n-values for profiles underlain by sedimentary rocks. Notably, Rio Pueblo de Taos has a more negative n-value than other long-profiles in the area (Table 13). As values of highly negative n-values indicate pronounced long-profile concavity (Hack, 1957), these data also show that long-profiles in crystalline terrane tend to be more concave than those in sedimentary terrane.

In summary, basin morphometry data indicates differences in area-elevation distributions, relief, average basin slope, drainage density, drainage frequency, and long-profile concavity between the two lithologic terranes. Hypsometric data do not appear to be different between basins draining crystalline rocks and basins draining sedimentary rocks.

Geomorphic Surfaces and Deposits

Interpretation of paleohydrologic conditions and geomorphic histories in the Rio Hondo and Rio Pueblo de Taos drainage basins necessitates mapping and characterizing Quaternary geomorphic surfaces and their associated deposits. Plates 1 and 2 show the distribution of geomorphic surfaces within major stream valleys below the mountain front. Valleys above the mountain front were investigated on a reconnaissance

scale only, with the exception of the Rio Grande del Rancho valley (Plate 3). Field investigations of geomorphic surfaces within the Rio Hondo and Rio Pueblo de Taos valleys below the mountain front included: 1) field mapping, 2) measurement of deposit grain sizes and lithologies using random pebble counts, and 3) soil descriptions. Geomorphic surfaces within the Rio Grande del Rancho valley above the mountain front were also mapped in detail (Plate 3).

Geomorphic Surfaces in the Rio Hondo Valley

Below the Sangre de Cristo mountain front, eight geomorphic surfaces occur in the Rio Hondo valley, which consists of three valley sections separated by two bedrock constrictions (Plate 1). The constrictions are composed of dacite probably derived from Cerro Negro (Peterson, 1981), a small volcanic cone about 1 km north of Rio Hondo (Plate 1). A schematic representation of geomorphic surfaces in the Rio Hondo valley is given in Figure 26. Figure 27 also illustrates relationships of surfaces within the Rio Hondo valley. Geomorphic surfaces are described below in order of decreasing heights above the modern floodplain.

Near Rio Hondo, surface Q1 is composed of two subunits: the surface sloping west on the plateau (surface $Q1_P$), and the surface sloping south near the Rio Grande (surface $Qt1_{RG}$) (Plate 1). Surface $Q1_P$ is the slightly dissected, continuous piedmont surface (the "alluvial plain" of Lambert, 1966, p. 48) between Rio Hondo and Rio Pueblo de Taos. Surface $Qt1_{RG}$ occurs discontinuously as the tops of dissected hills north of Rio Hondo, although it is continuous on the west side of the Rio Grande gorge from north of Rio Hondo to as far south as Pilar. Surface $Qt1_{RG}$ is probably a depositional terrace formed by the Rio Grande, based on clast lithologies, crude imbrication, and proximity to the Rio Grande.

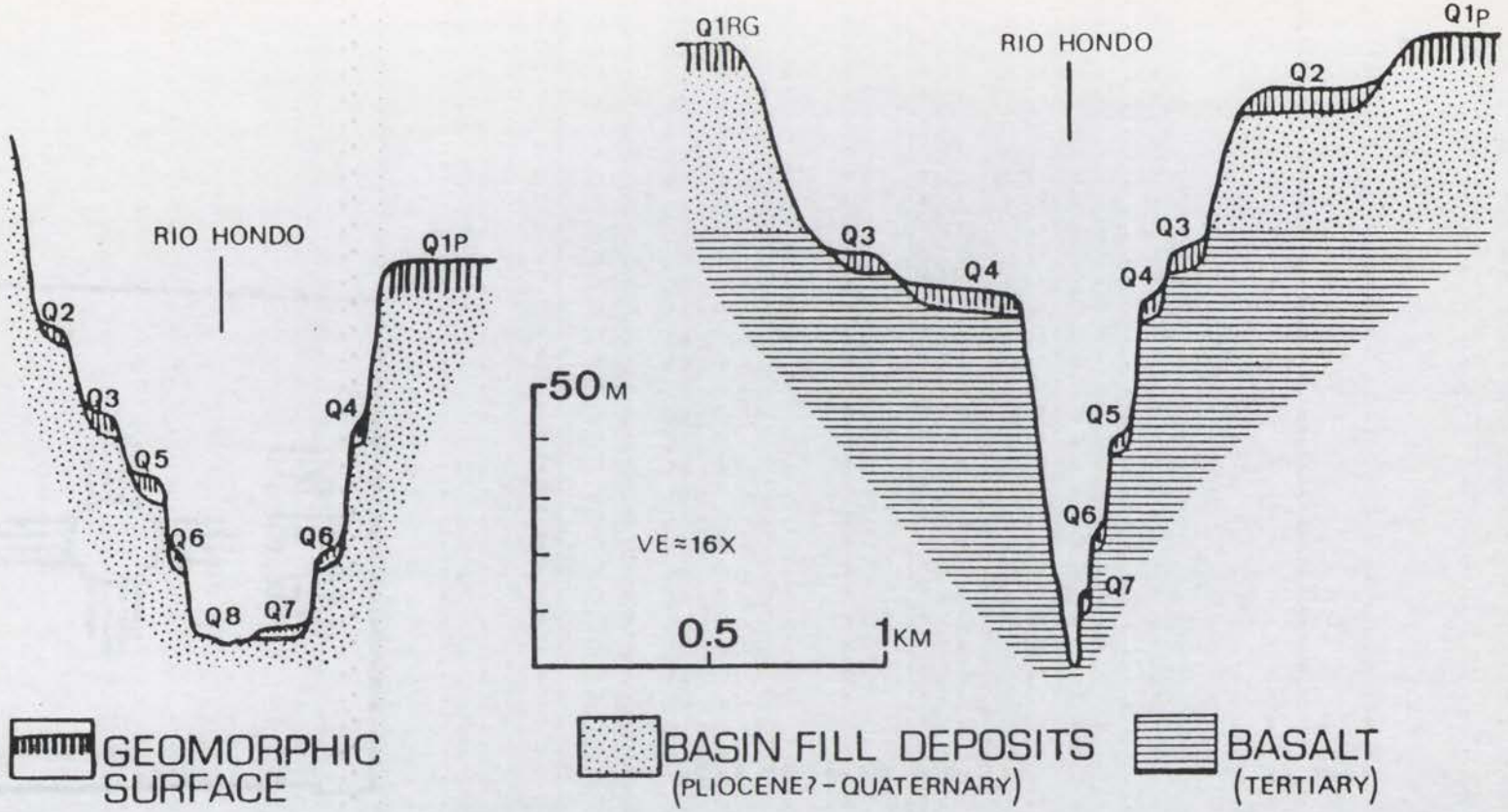

Figure 26. Schematic cross-valley profiles of the Rio Hondo valley. (A) approximately 9 km above the Rio Hondo-Rio Grande junction, where strath terraces are cut into basin-fill deposits. (B) approximately 2 km above the Rio Hondo-Rio Grande junction, where strath terraces are cut into basalt. Thicknesses of terrace deposits are approximate.

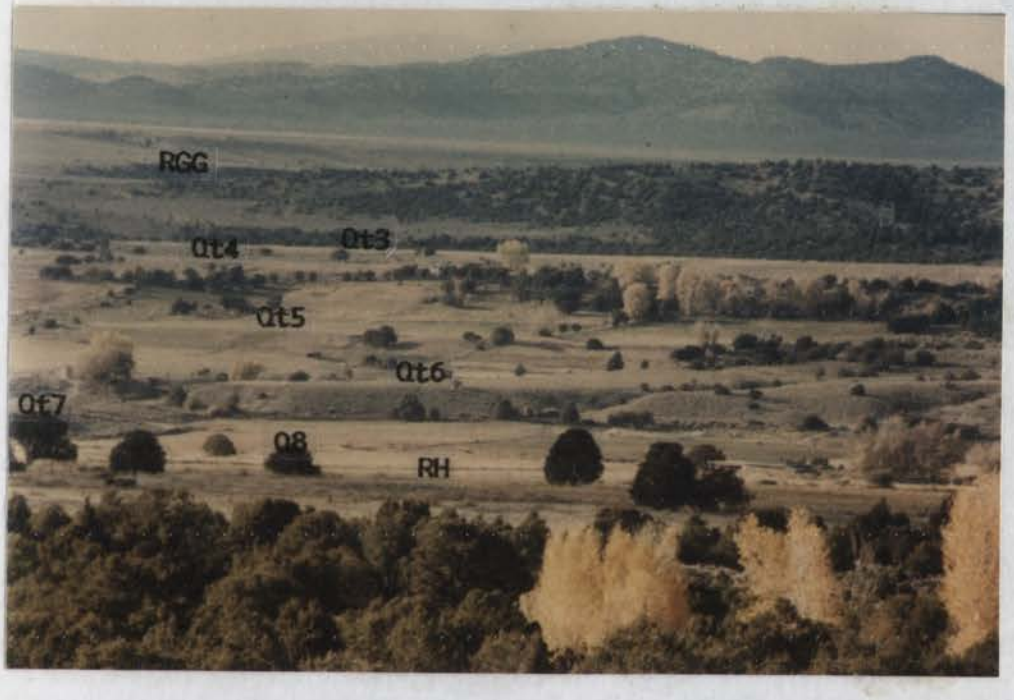

Figure 27. Photograph of the Rio Hondo valley, showing several fluvial terraces. Photograph taken looking northwest from Highway 3. RH = present-day Rio Hondo, RGG = Rio Grande gorge, see Plate 1 for descriptions of map units Qt3, Qt4, Qt5, Qt6, Qt7, and Q8.

Surface 2 (Qt2) does not occur along Rio Hondo close to the mountain front (near the village of Valdez), and exists only as narrow terrace remnants between the two dacite bedrock constrictions (Plate 1). Near the Rio Grande and southwest of the village of Arroyo Hondo, this surface is continuous and inset into surface Qls_{P}. About 8 to 10 m separate surfaces Qls_{P} and Qt2 (Table 14). Surfaces Qts_{RG} and Qt2 both overlie the uppermost layer of Servilleta Basalt near the Rio Grande gorge (Fig. 28).

Surfaces Qt3, Qt4, and Qt5 do not occur near Valdez, but all occur discontinuously between the two bedrock constrictions and in the Arroyo Hondo valley (Plate 1). Two very localized rock-cut terraces occur in the valley constriction below Valdez; these are straths formed on dacite, and appear to be remnants of surfaces Qt4 and Qt5 based on heights above the active stream channel.

Surface 6 (Q6 and Qt6) is relatively continuous all along the Rio Hondo. North of Rio Hondo and near Valdez, surface Q6 occurs as dissected alluvial-fan surface remnants. The height of surface Q6 above the Rio Hondo decreases from about 75 m near the mountain front to about 27 m above the first bedrock constriction, where it grades into Qt6 terrace remnants. In the Arroyo Hondo valley, surface Qt6 is a continuous terrace, consistently 27 m $\pm$ 2 m above Rio Hondo (Plate 1, Table 14).

Surface Qt7 and the modern floodplain (surface Q8) are also continuous within the Rio Hondo valley. Surface Qt7 occurs about 9 m above the floodplain, except at the downstream end of the Arroyo Hondo valley, where it is about 14 m above the active stream channel (Table 14). Surface Q8 is continuous from the mountain front to elevation 2038 m (6685 ft), where Rio Hondo leaves the Arroyo Hondo valley and enters

Table 14. Heights (m) of geomorphic surfaces above the modern floodplain, in the Rio Hondo and Rio Pueblo de Taos valleys below the Sangre de Cristo mountain front. The Arroyo Seco, Rio Grande del Rancho, and Rio Pueblo de Taos valleys all join near Los Cordovas, which is about 10.7 km upstream of the Rio Grande-Rio Pueblo de Taos junction. See Plates 1 and 2 for valley locations.

Rio Hondo valley

Geomorphic surface	8.9 km above Rio Grande	5.5 km above Rio Grande	2.0 km above Rio Grande
Q1	82	88	120
Qt2	70	--	110
Qt3	58	58	70
Qt4	46	44	61
Qt5	37	32	40
Qt6	27	27	27
Qt7	9	9	14
Q8	0	0	0

Rio Pueblo de Taos valley system

Geomorphic surface	Arroyo Seco valley	Rio Grande del Rancho valley	Rio Pueblo de Taos valley	8.0 km above Rio Grande	4.8 km above Rio Grande	at Rio Grande
Q1	27	--	40	49	67	210
Qt2	12	26	18	29	37	181
Qt3	--	--	--	23	27	--
Qt4	8	12	--	15	18	--
Qt6	--	6	--	9	6	--
Q8	0	0	0	0	0	0

* affected by faulting

ALL HEIGHTS IN METERS

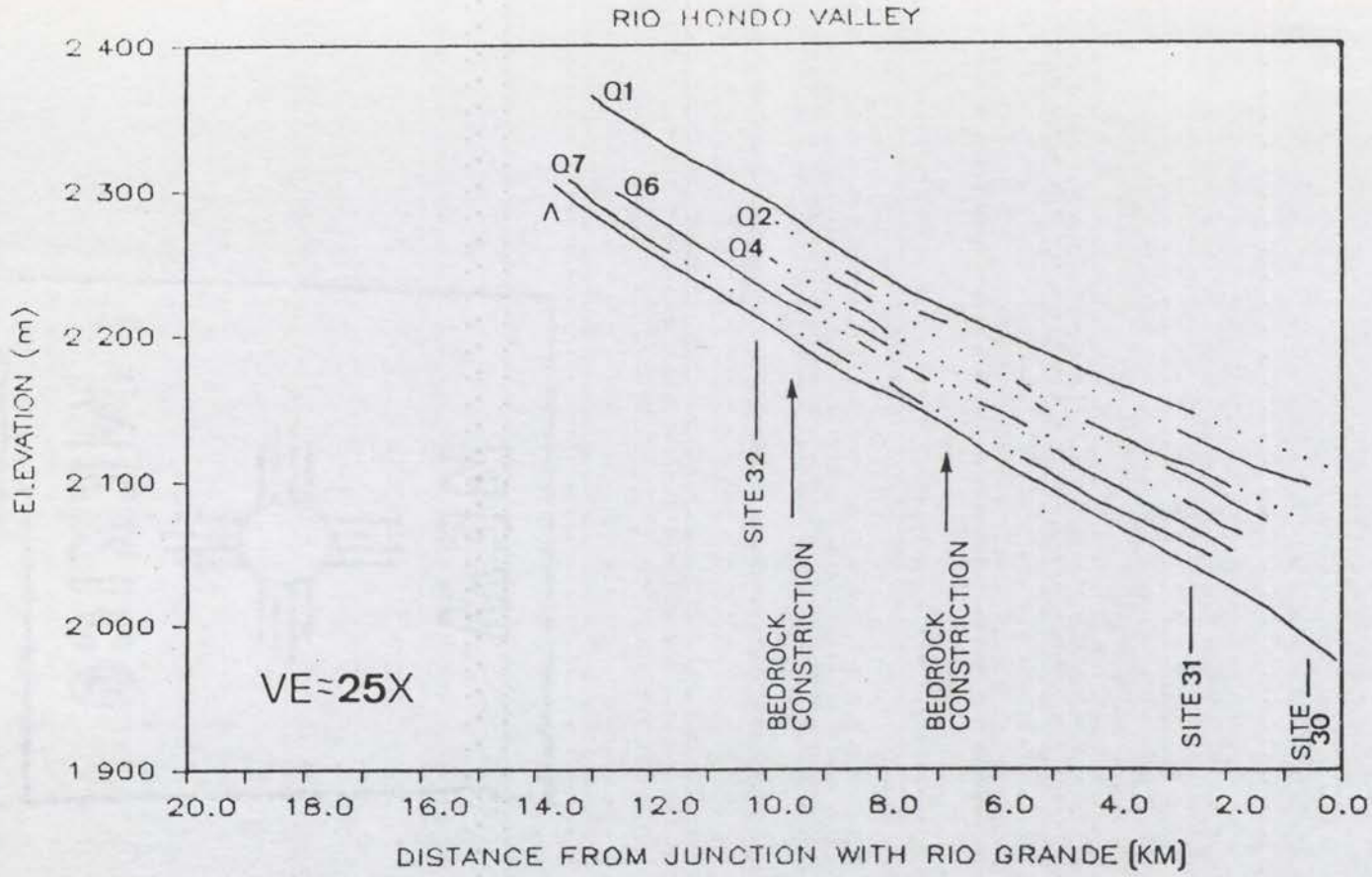

Figure 28. Long-profiles of geomorphic surfaces flanking Rio Hondo below the mountain front. (^) denotes mountain front. Solid lines represent continuous surfaces. See Plate 1 for locations of cross-section measurement sites 30, 31, and 32.

the basalt gorge.

All eight geomorphic surfaces are juxtaposed southwest of the village of Arroyo Hondo (Plate 1). Notably, each surface is further to the east and lower in elevation than the next older surface. Surfaces Qt_P and Qt2 extend west to the Rio Grande gorge and lie above the uppermost layer of Servilleta Basalt (Fig. 26). Surfaces Qt3 through Qt7 are strath terraces formed on basalt, and each tread is about 10 to 20 m below the next older terrace tread. Due to the spatial arrangement of terrace treads, progressively older terraces have long-profiles which extend further downstream, as shown in Figure 28.

Geomorphic surfaces flanking Rio Hondo have nearly parallel long-profiles, although surfaces Qt_P and Qt2 diverge slightly near the Rio Hondo mouth (Fig. 28). These two surfaces are slightly higher above the active channel near the Rio Grande than they are upstream (Table 14). Long-profile gradients are lower on surface Qt_P (20 m/km) than on surfaces Qt6, Qt7, and Q8 (23 m/km) (Table 15), indicating slight long-profile divergence. Long-profile gradients decrease slightly in a downstream direction (Table 15), although a high (30 m/km) active channel gradient in the basalt gorge (near site 30) indicates slight long-profile convexity. However, geomorphic surfaces in the Rio Hondo valley have long-profiles which are nearly parallel, straight, and steep.

Sedimentology of Rio Hondo Fluvial Deposits

Quaternary fluvial deposits are only exposed in the Rio Hondo valley at a few roadcuts and gravel pits which allow limited observations. Surfaces Qt2 through Qt7 cannot be distinguished by deposit characteristics. Deposits associated with surfaces Qt2 through Qt7 lack

Table 15. Gradients (m/km) of long-profiles of geomorphic surfaces in the Rio Hondo and Rio Pueblo de Taos valleys below the Sangre de Cristo mountain front. The Arroyo Seco, Rio Grande del Rancho, and Rio Pueblo de Taos valleys all join near Los Cordovas, which is about 10.7 km upstream of the Rio Grande-Rio Pueblo de Taos junction.

Rio Hondo valley

Geomorphic surface	overall gradient	10.1 km upstream of Rio Grande	2.5 km upstream of Rio Grande	0.6 km upstream of Rio Grande
Q1	20	22	16	16
Qt2	19	23	16	16
Qt3	21	24	22	--
Qt4	21	26	22	--
Qt5	21	23	23	--
Qt6	23	21	22	--
Qt7	23	23	20	--
Q8	23	25	21	30

Rio Pueblo de Taos valley system

Geomorphic surface	Arroyo Seco valley	Rio Grande del Rancho valley	Rio Pueblo de Taos valley	10.8 km upstream of Rio Grande	7.5 km upstream of Rio Grande	5.0 km upstream of Rio Grande
Q1	11	--	10	*	*	3
Qt2	14	14	10	--	3	3
Qt3	--	--	--	--	6	6
Qt4	15	12	--	8	6	6
Qt6	--	12	--	9	7	7
Q8	15	13	12	9	7	7

* affected by faulting

ALL GRADIENTS IN METERS PER KILOMETER

bedding, are poorly-sorted, crudely-imbricated, and are composed primarily of unaltered subrounded to subangular clasts (Fig. 29). Color of the less-than-2 mm fraction approximates the color of recent alluvium (10YR 6/3 dry). Mean grain size (b-axis) ranges from 59 cm to 83 cm (Table 16); the grain-size distribution of all sampled Rio Hondo deposits (combined) approximates normality (Figure 30a), although individual sample site distributions do not. Notably, deposits associated with surfaces Qt2 and Qt3 contain clasts which are slightly more altered than clasts in other deposits. The limited number of exposures precludes collection of a larger pebble-count grain-size data base.

Deposits associated with surfaces Qt2 through Qt7 contain predominantly gneiss and granite clasts (Fig. 31). However, fan deposits north of Valdez (Plate 1) are composed primarily of angular quartzite pebbles. These relatively fine-grained, bedded deposits are the "gravelly silt facies" of Lambert (1966, p. 46). Deposits associated with surfaces Qt2 through Qt7 in the Rio Hondo valley system range in thickness from approximately 2 to 6 m, as estimated from the few exposures that show terrace deposits unconformably overlying basalt or older basin-fill deposits.

In places, deposits associated with surfaces Qt2 through Qt7 unconformably overlie the "yellowish, weathered sandy gravel facies" of Lambert (1966, p. 46). These older deposits are also associated with surface $Q1_P$, and can be distinguished from other deposits by degree of clast alteration, matrix color, bedding, and smaller grain sizes. Most granitic clasts within these deposits are grussified, schists are altered to clay minerals, and other clasts are fractured. Matrix material is

Figure 29. Photograph of deposits associated with surface Qt4, exposed in roadcut 3.7 km west of Valdez (see Plate 1). Note that terrace gravels unconformably overlie finer grained basin-fill deposits. Hammer is about 30 cm long.

Table 16. Grain-size characteristics of fluvial deposits in the Rio Hondo and Rio Pueblo de Taos valleys below the mountain front. Deposits associated with surface Qlp occur in both valleys; data from these deposits are presented separately due to distinctness from other deposits (see text). See Plates 1 and 2 for site locations.

Rio Hondo valley

Geomorphic surface	Site	n	Mean grain size (mm)	Largest clast (mm)	5th largest clast (mm)	10th largest clast (mm)
Qt3	PC 3	56	61	236	132	98
Qt4	PC 5	53	83	278	220	138
Qt4	PC 19	52	59	195	134	110
Qt5	PC 7	54	59	270	155	105
Qt6	PC 18	52	71	303	176	120
Qt7	PC 9	61	67	284	161	132
	ALL	328	67			

Rio Pueblo de Taos valley

Geomorphic surface	Site	n	Mean grain size (mm)	Largest clast (mm)	5th largest clast (mm)	10th largest clast (mm)
Qt2	PC 11	51	44	174	105	73
Qt2	PC 12	60	65	206	176	131
Qt2	PC 17	52	60	173	152	104
Qt4	PC 13	53	52	264	163	84
Qt4	PC 15	65	91	340	239	157
Qt4?	PC 14	59	68	293	173	133
Q8	PC 16	26	46	205	91	36
	ALL	366	63			

Deposits associated with surface Qlp

Geomorphic surface	Site	n	Mean grain size (mm)	Largest clast (mm)	5th largest clast (mm)	10th largest clast (mm)
Qlp	PC 4	57	43	173	115	82
Qlp	PC 8	52	45	150	105	76
Qlp	PC 10	56	24	63	54	36
	ALL	165	37			

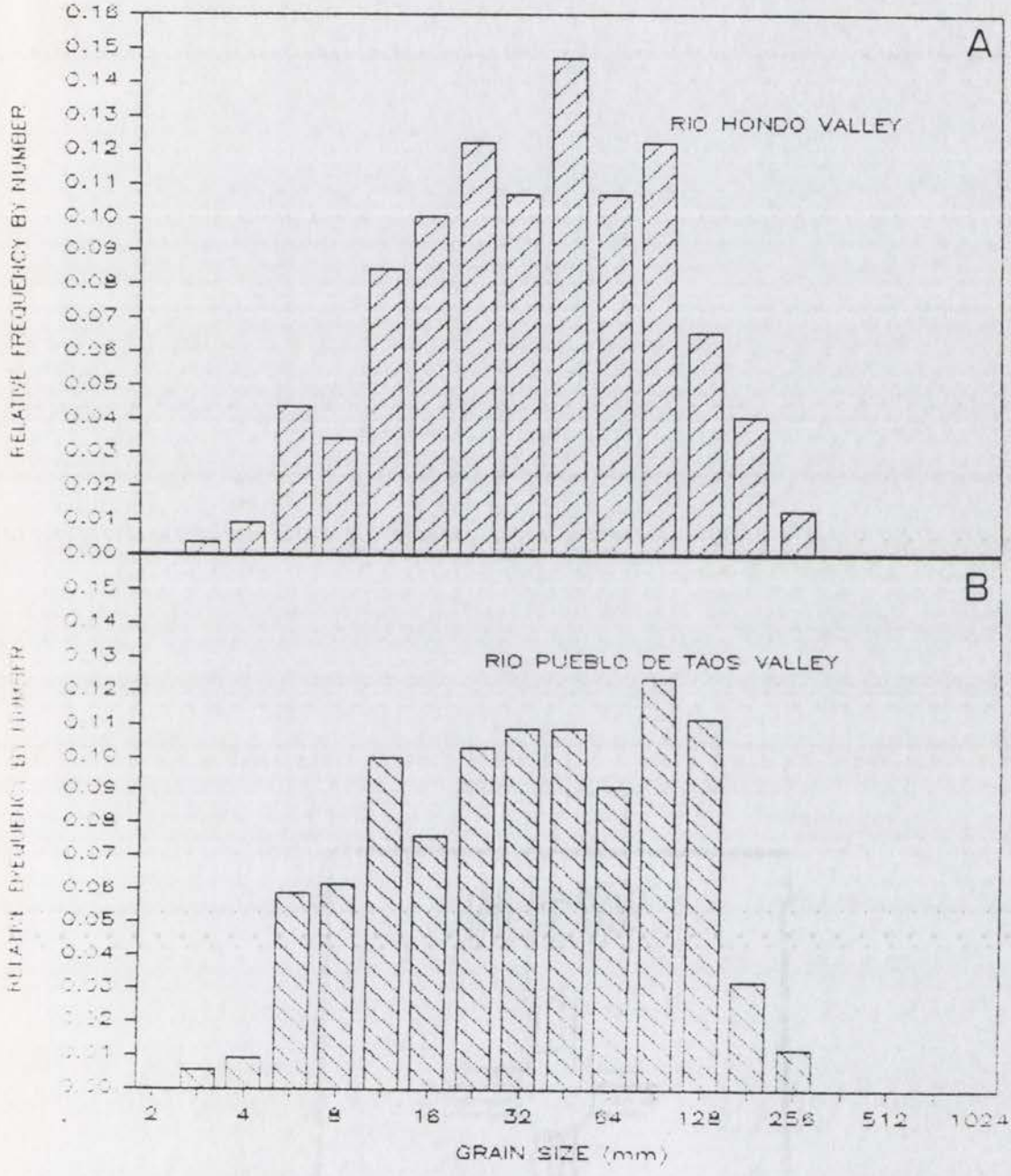

Figure 30. Relative frequency plot of coarse grain size fractions of terrace deposits in the Rio Hondo (A) and Rio Pueblo de Taos (B) valleys below the mountain front.

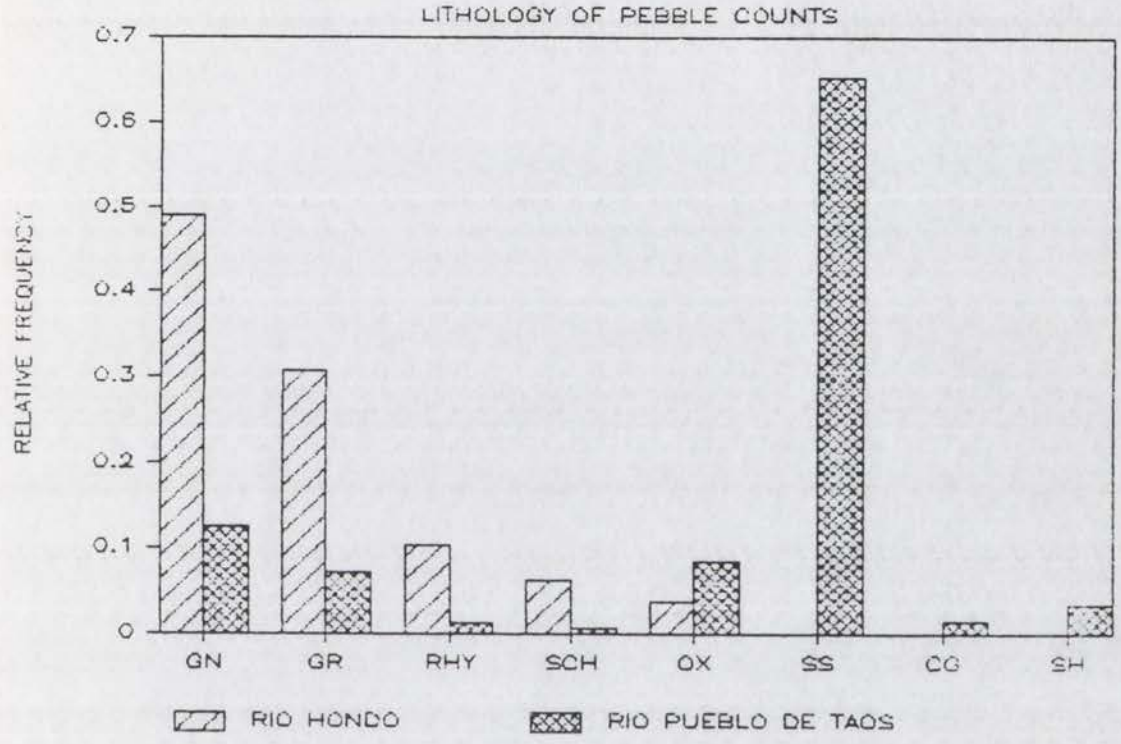

Figure 31. Relative frequency plot of clast lithologies in deposits associated with surfaces Qt2 through Qt7 in the Rio Hondo and Rio Pueblo de Taos valleys. GN = gneiss, GR = granite, RHY = rhyolite and andesite, SCH = schist, OX = other crystalline lithologies (including basalt, amphibolite, and massive quartz), SS = sandstone, CG = conglomerate, SH = shale. Compare with Figure 19. (see Plates 1 and 2 for locations).

discolored by oxidation, and black manganese oxide (?) stains clasts and cuts across bedding. Bedding is common in surface $Qt1_P$ deposits, and mean grain size of the greater-than-2 mm grains is lower than that of other deposits (Table 16). The grain size distribution of these deposits is finer than deposits associated with younger surfaces (Fig. 32). The thickness of these deposits is unknown, but is at least 80 m based on exposures south of Valdez and in the valley between the two bedrock constrictions.

Deposits associated with surface $Qt1_{RG}$ are composed of lithologies not found within the Rio Hondo basin, including sandstones and altered volcanics. Crude imbrication and clast lithologies suggest deposition by the ancestral south-flowing Rio Grande. These deposits are approximately 25 to 30 m thick.

Soil Properties of Geomorphic Surfaces in the Rio Hondo Valley

In order to aid in identification and correlation of geomorphic surfaces, fourteen soil profiles were described in the Rio Hondo valley system (see Appendix C for descriptions, Plate 1 for locations). Within the Rio Hondo valley, selected soil-profile properties were used to identify geomorphic surfaces, although final identification of surfaces employed soil characteristics, terrace long-profiles, and surface heights above the active stream channel. Soil properties used to identify and differentiate the geomorphic surfaces include stage of carbonate development, depth to the Ck-horizon, B-horizon morphology, and the Relative Profile Development (RPD) index (Harden, 1982) (Table 17).

Stage of carbonate development (Gile et al., 1966; Birkeland, 1984) is relatively high (stage IV) for soils developed on surface $Qt1_P$, intermediate (stage III to II) for soils formed on surfaces Qt3, Qt4, and

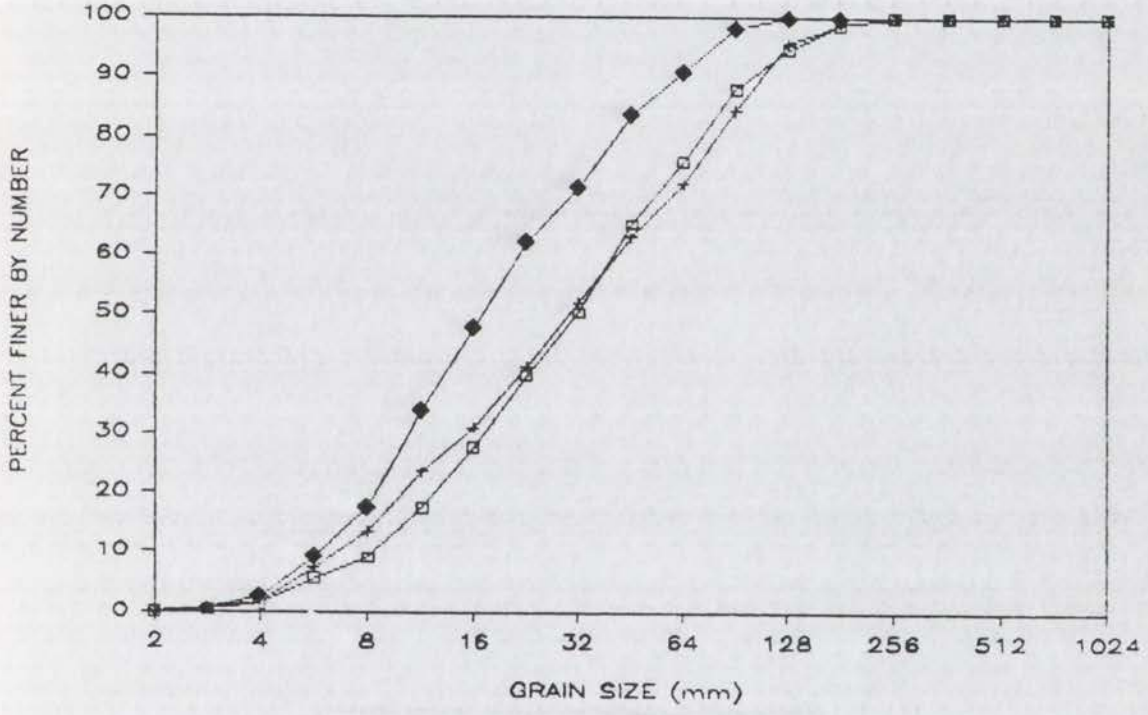

Figure 32. Cumulative numerical percent plot of coarse grain-size fractions of deposits associated with surfaces Qt2 through Qt7 in the Rio Honda (□) and Rio Pueblo de Taos (+) valleys, and of deposits associated with surface Qlp (◆). Note that deposits associated with surface Qlp are finer grained than deposits associated with younger geomorphic surfaces.

Table 17. Selected soil characteristics for soil profiles described in the Rio Hondo and Rio Pueblo de Taos valleys. See Plates 1 and 2 for profile locations. Dashes (--) indicate that property was not present in soil profile.

Rio Hondo valley

Geomorphic surface	Soil profile	A-horizon thickness (cm)	B-horizon thickness (cm)	Bt-horizon thickness (cm)	Bt hue	K-horizon thickness (cm)	Depth to Ck-horizon (cm)	Carbonate stage†	RPD index (unit-cm)
Qlp	SP 14	13	29	29	8.25 YR	86	128	IV	42.6
Qt3	SP 5	5	34	34	7.5 YR	48	87	III	34.8
Qt3	SP 12	5	75	23	7.5 YR	--	80	III	25.0
Qt3	SP 2	13	56	24	8.25 YR	--	85	III	20.6
Qt4	SP 1	14	69	59	10 YR	--	83	II +	24.0
Qt4	SP 10	6	49	49	8.25 YR	38	93	III	24.4
Qt5	SP 3	11	62	62	10 YR	--	73	III	24.2
Qt5	SP 9	8	55	35	10 YR	--	73	II	18.8
Qt5	SP 15	10	45	--	10 YR	--	55	II	15.0
Qt6	SP 7	3	60	14	7.5 YR	--	63	II	16.2
Qt7	SP 11	18	35	--	--	--	--	--	9.6
Q8	SP 13	--	--	--	--	--	--	--	0.0

Rio Pueblo de Taos valley

Geomorphic surface	Soil profile	A-horizon thickness (cm)	B-horizon thickness (cm)	Bt-horizon thickness (cm)	Bt hue	K-horizon thickness (cm)	Depth to Ck-horizon (cm)	Carbonate stage†	RPD index (unit-cm)
Qt2	SP 19 *	12	15	--	10 YR	54	81	IV	--
Qt2	SP 20	8	84	84	7.5 YR	12	104	III	41.7
Qt4	SP 18	11	43	26	10 YR	46	100	III	35.1
Qt4	SP 21	4	57	61	7.5 YR	14	?	III	--
Qt4	SP 22	10	60	60	7.5 YR	50	?	III	--
Qt6	SP 23	8	79	45	10 YR	--	87	II	23.2
Q8	SP 17	--	--	--	--	--	--	--	0.0

†Carbonate stages after Gile et al. (1966)
*Upper horizons probably affected by erosion

Qt5, and relatively low (stage II) in unit Qt6 soils (Table 17). Soils developed on surfaces Qt7 and Q8 show no carbonate accumulation. Although carbonate stage varies between units, correlation based on this property alone is not definitive.

Depth to the Ck-horizon in Rio Hondo soils was used as a substitute for depth of weathering (Gillam et al., 1984). Soils developed on surface $Q1_P$ have high depth-to-Ck values (128 cm, see Table 17), and soils formed on surfaces Qt3 and Qt4 have Ck-horizon depths between 80 and 95 cm. Soils developed on surfaces Qt5 and Qt6 have Ck-horizon depths between 55 and 73 cm; surfaces Qt7 and Q8 do not have Ck-horizons.

Other individual soil-profile properties, such as A- or B-horizon thickness, were not useful for distinguishing surficial units (Table 17). However, surface $Q1_P$ can be identified based on a thin B-horizon, and surface Q8 lacks a B-horizon. B-horizon morphology was useful in identifying surface Qt7, which has a cambic B, as opposed to argillic B-horizons in soils formed on surfaces $Q1_P$ through Qt6.

A semi-quantitative index of soil development formulated by Harden (1982) can be used to combine several soil characteristics into a single number for comparative purposes. The Relative Profile Development (RPD) index calculated from Rio Hondo soil-profile descriptions decreases from soils developed on surface $Q1_P$ to soils formed on surface Q8 (Fig. 33). Geomorphic surfaces in the Rio Hondo valley can be divided into 5 groups based on RPD-index values. Surface $Q1_P$ soils have high RPD values (>40 unit-cm, Table 17). Soils formed on surfaces Qt3 and Qt4 have RPD values between 20 and 35 unit-cm, and are somewhat more developed than surface Qt5 and surface Qt6 soils, which have RPD values between 15 and 25 unit-

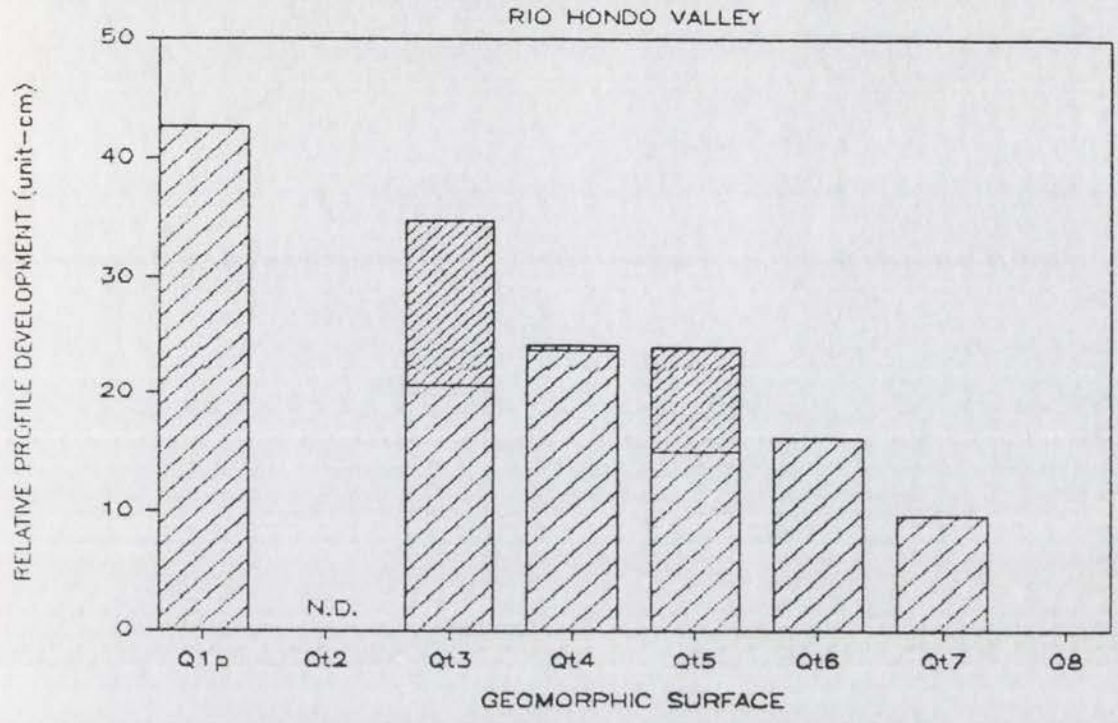

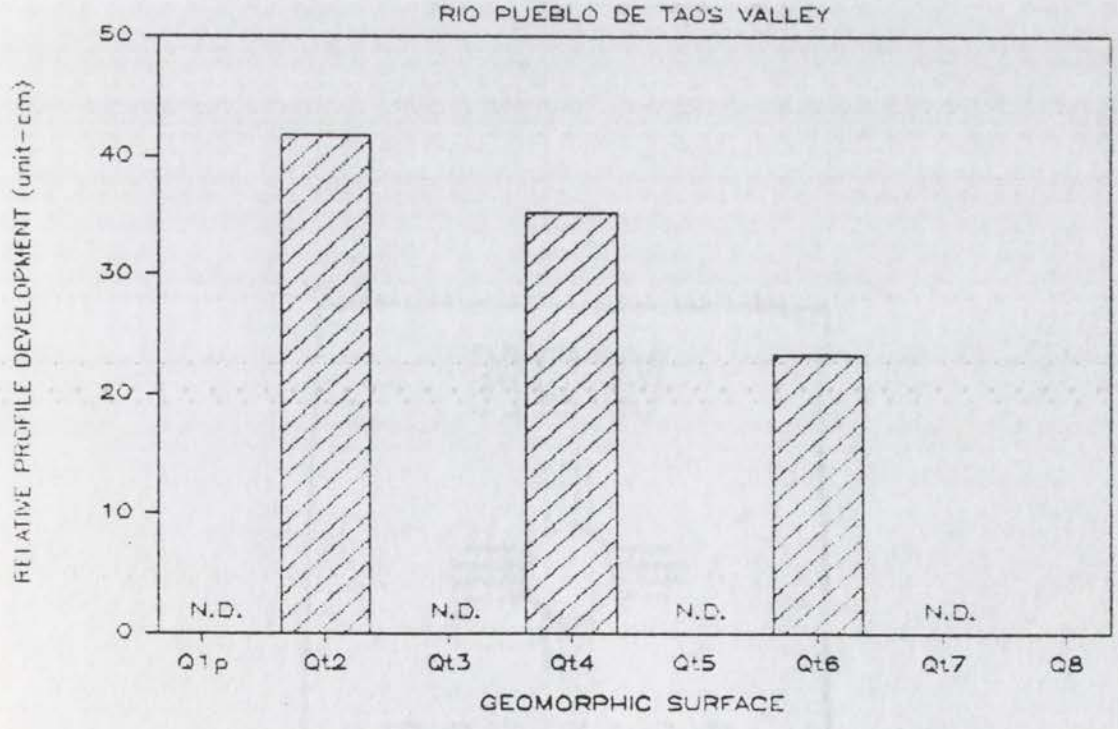

Figure 33. Relative Profile Development indices (Harden, 1982) for soils in the (A) Rio Hondo and (B) Rio Pueblo de Taos valleys. Top of wide-ruled bar shows minimum; top of narrow-ruled bar shows maximum. N.D. = no data.

cm. Surface Qt7 soils have RPD values of about 10 unit-cm, and surface Q8 has no pedogenic alteration (Fig. 33). Data used in calculating these values are presented in Appendix H.

In summary, no single parameter derived from field descriptions of soils can be used to definitively identify geomorphic surfaces in the Rio Hondo valley system. However, use of several parameters in combination enables identification and therefore correlation of units. Table 18 summarizes the soil characteristics used to distinguish between surficial units. Notably, surface Qi_P can be distinguished based on its well-developed calcic horizon. Surfaces Qt3 and Qt4 have soil characteristics which are similar, but have better developed carbonate morphology and higher RPD values than surfaces Qt5 and Qt6. Distinction between surfaces Qt3 and Qt4, and between surfaces Qt5 and Qt6, requires reliance on height above the active stream channel, terrace long-profiles, and relief differences from more easily identifiable units. Surface Qt7 can be distinguished based on its cambic B horizon and lack of carbonate accumulation. The modern floodplain (surface Q8) is distinguished by lack of soil development, proximity to Rio Hondo, and recent depositional features.

Geomorphic Surfaces in the Rio Pueblo de Taos Valley

The Rio Pueblo de Taos and its major tributaries flow for about 20 km on the Taos Plateau in broad, cultivated valleys. Rio Lucero joins Rio Pueblo de Taos west of Taos, but Arroyo Seco, Rio Fernando de Taos, and Rio Grande del Rancho all join Rio Pueblo de Taos just upstream of Los Cordovas (Plate 2). Terraces flanking Arroyo Seco, Rio Pueblo de Taos (below Taos), and Rio Grande del Rancho were mapped in detail, due

Table 18. Summary of selected soil properties used in identification of map units. Range in properties for one to five profiles per geomorphic surface.

Geomorphic surface & profiles used	B horizon properties			Carbonate horizon properties (Bk, Ck, K)				RPD index (range)
	type	thickness (cm)	clay films	Maximum stage	Morphology on clast bottoms	Morphology in matrix	Cement.	
Qt1 (SP14)	argillic	~30	continuous, thin to moderate on peds, pore walls and clasts	IV	continuous, thick coatings	none	strong	> 40
Qt2 (SP19, SP20)	argillic	~85	continuous, thin to moderate on peds, pore walls and clasts	IV	continuous, thin to moderate coatings	many fine to coarse nodules and mottles	strong	> 40
Qt3 (SP2, SP5, SP12)	argillic	55-85	very discontinuous to continuous, thin to moderate on peds, pore walls and clasts	III	very discontinuous to continuous, very thin to thick coatings	very fine to fine nodules	weak to strong	20-35
Qt4 (SP1, SP10, SP18, SP21, SP22)	argillic	45-70	very discontinuous to continuous, thin to moderate on peds, pore walls and clasts	III	very discontinuous to continuous, thin to thick coatings	few fine nodules; common fine mottles	none to weak	25-35
Qt5 (SP3, SP9, SP15)	argillic	45-65	discontinuous, thin on peds, pore walls and clasts	II	discontinuous to continuous, thin to mod. coatings	very few fine filaments and nodules	none	15-25
Qt6 (SP7, SP23)	argillic	60-80	discontinuous to continuous, thin on peds, pore walls and clasts	II	discontinuous to continuous, thin to thick coatings	very few fine filaments and nodules	none	15-25
Qt7 (SP11)	cambic	~35	none	--	none	none	none	~10

to terrace continuity in these valleys. In other valleys, land access was restricted, and terraces as interpreted from aerial photographs were not easily distinguishable due to low relief between terraces as well as agricultural and urban modifications. Field observations indicate that terraces in the unmapped valleys (Rio Lucero and Rio Pueblo de Taos above Taos) are traceable into terraces in mapped valleys.

Geomorphic surfaces in the Rio Pueblo de Taos basin have been numbered according to correlative surfaces in the Rio Hondo basin, based on deposit and soil characteristics, and field relationships. Problems in correlation between the two basins are discussed below (see Discussion). Geomorphic surfaces in the Arroyo Seco, Rio Grande del Rancho, and Rio Pueblo de Taos valleys below the mountain front, and in the Rio Grande del Rancho valley above the mountain front, are described below. Figure 34 is a schematic representation of terrace relationships in this area.

Surfaces $Q1_P$, Qt2, Qt4, and Q8 occur in the wide, straight Arroyo Seco valley above its confluence with Rio Pueblo de Taos (Plate 2, Fig. 35). Surface $Q1_P$ is the continuous, slightly dissected piedmont surface described above; in this region it slopes to the southwest, as does the Arroyo Seco valley. This appears to be an aggradational surface.

About 2.4 km upstream of the junction of Arroyo Seco with Rio Pueblo de Taos, basalt strata confine Arroyo Seco (Plate 2). Where the basalt crops out, surfaces Qt2 and Qt4 are strath terraces which are associated with fluvial deposits less than 3 m thick. Near Rio Pueblo de Taos, surface Qt4 from the Arroyo Seco valley grades continuously into Rio Pueblo de Taos surface Qt4 remnants (Plate 2), which in conjunction with soil profile descriptions enabled correlation of Arroyo Seco surfaces

Figure 34. Schematic cross-valley profiles below the mountain front. (A) Rio Pueblo de Taos near Ranchito, (B) Arroyo Seco above Los Cordovas, (C) Rio Grande del Rancho near Ranchos de Taos, (D) Rio Pueblo de Taos below Los Cordovas. Strath terraces in (A), (B), and (C) are cut into basin-fill deposits; surfaces Qt3 and Qt4 in (D) are cut into basalt. Thicknesses of terrace deposits are approximate. Arrows indicate confluences of Arroyo Seco and Rio Grande del Rancho with Rio Pueblo de Taos. Diagrams are arranged to show that Arroyo Seco and Rio Grande del Rancho flow into Rio Pueblo de Taos near Los Cordovas.

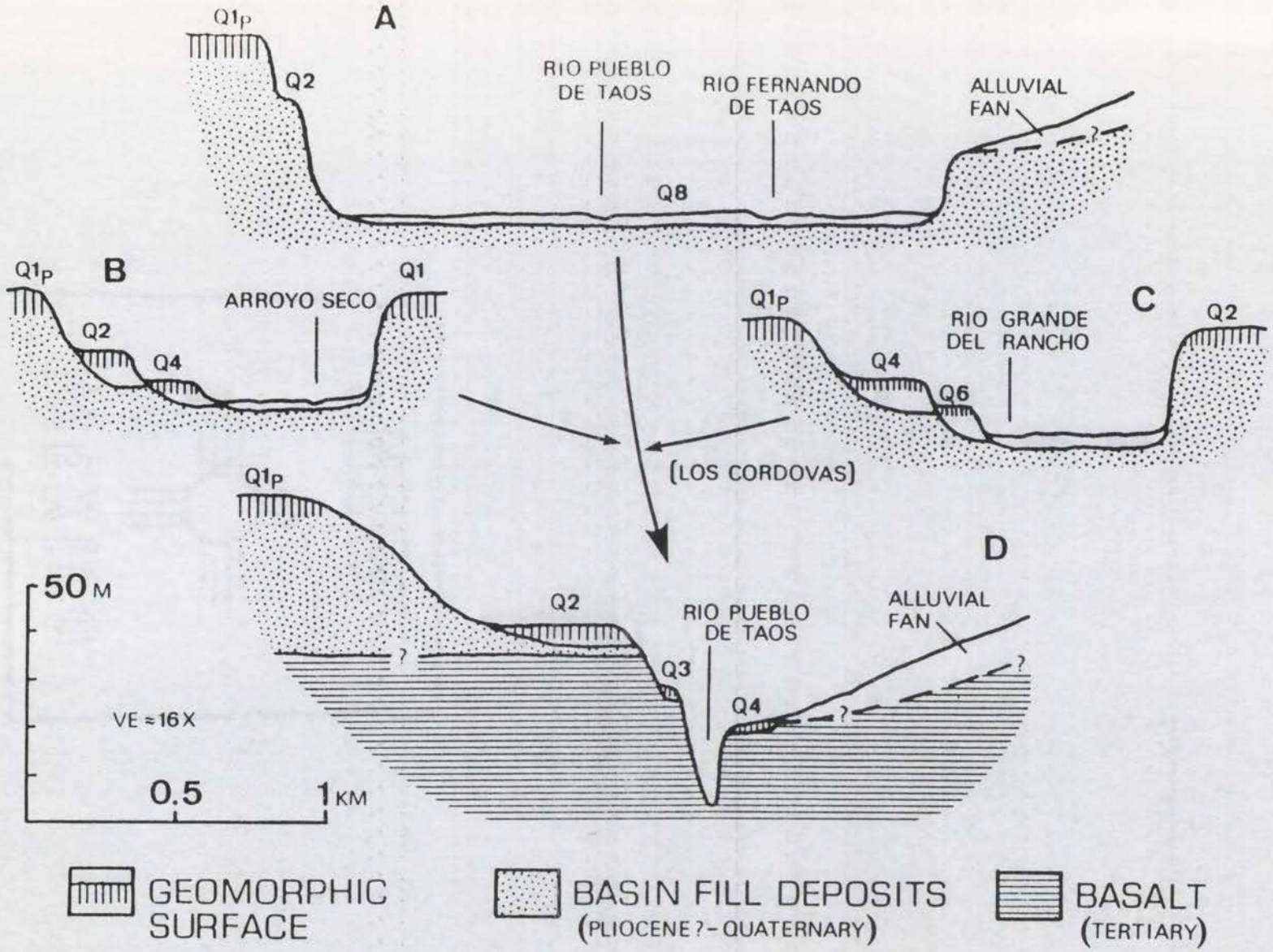

Figure 34. (continued)

Figure 35. Photograph of the Arroyo Seco valley, showing geomorphic surfaces Q1p, Qt2, Qt4, and Q8. Photograph taken looking northwest about 3 km above the Arroyo Seco-Rio Pueblo de Taos junction. AS = present-day Arroyo Seco. See Plate 2 for descriptions of map units.

with those on Rio Pueblo de Taos. Above the basalt strata, surfaces Qt2 and Qt4 may be either depositional or strath terraces.

Heights of surfaces $Q1_P$, Qt2, and Qt4 above the modern Arroyo Seco floodplain are given in Table 14. These are average heights, however, and do not indicate the downstream long-profile divergence of the terraces (Fig. 36a). Between Highway 3 and the mountain front (northeast of the boundary of Plate 2), relief between surfaces $Q1_P$, Qt2, Qt4, and Q8 gradually decreases to less than 1 m. Long-profile divergence in the Arroyo Seco valley is also shown by the lower gradients on surface $Q1_P$ (11 m/km) than on unit Q8 (15 m/km) (Table 15). Long-profiles of surfaces in the Arroyo Seco valley are generally straight, although unit Q8 has a pronounced convexity just above the Rio Pueblo de Taos confluence (Fig. 36a).

The wide, straight Rio Grande del Rancho valley contains continuous portions of surfaces Qt2, Qt4, Qt6, and Q8 (Plate 2). Surfaces Qt2 and Qt4 grade into terraces along the Rio Pueblo de Taos near the village of Los Cordovas. Southwest of Rio Grande del Rancho, unit Qt2 (known here as Llano Quemado) is a strath terrace formed on deposits associated with surface $Q1_P$, based on an exposure at site PC11 (Plate 2). Exposures on the northeast side of the valley indicate that surface Qt4 is a strath terrace also formed on basin-fill deposits. Surface Qt6 in this valley occurs as a 1.5 km-long terrace near the Rio Pueblo de Taos confluence (Plate 2), and lies only 6 m above the modern floodplain (Table 14). Long-profiles of surfaces in the Rio Grande del Rancho valley are generally parallel (Fig. 36b).

Very few stream terraces occur in the Rio Pueblo de Taos valley above the Los Cordovas confluence (Plate 2). To the northwest of the

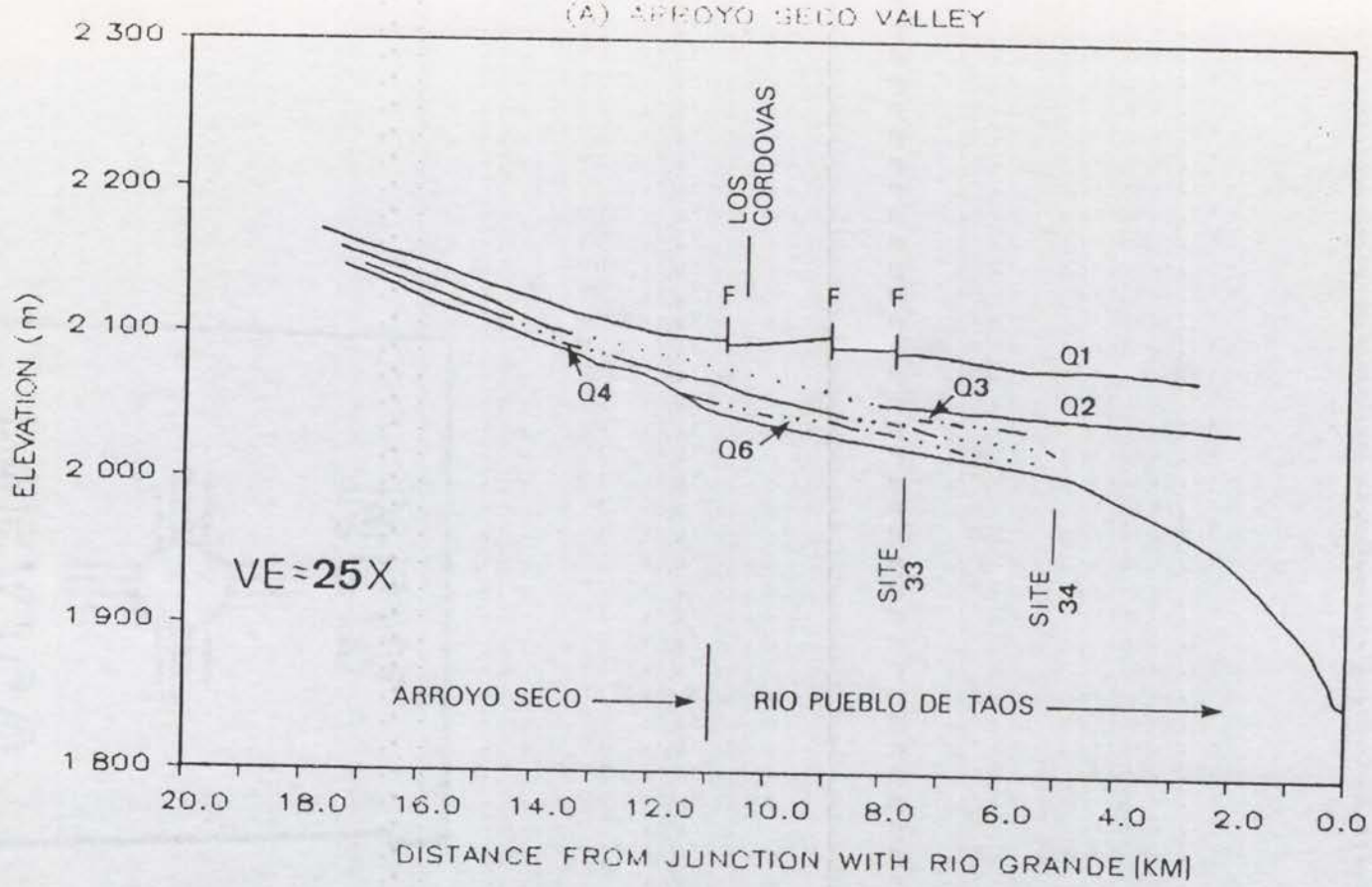

Figure 36. Long-profiles of geomorphic surfaces flanking (A) Arroyo Seco near Los Cordovas (B) Rio Grande del Rancho below the mountian front, and (C) Rio Pueblo de Taos below Taos. Solid lines represent continuous geomorphic surfaces. See Plate 2 for locations of cross-section measurement sites 29, 33, and 34.

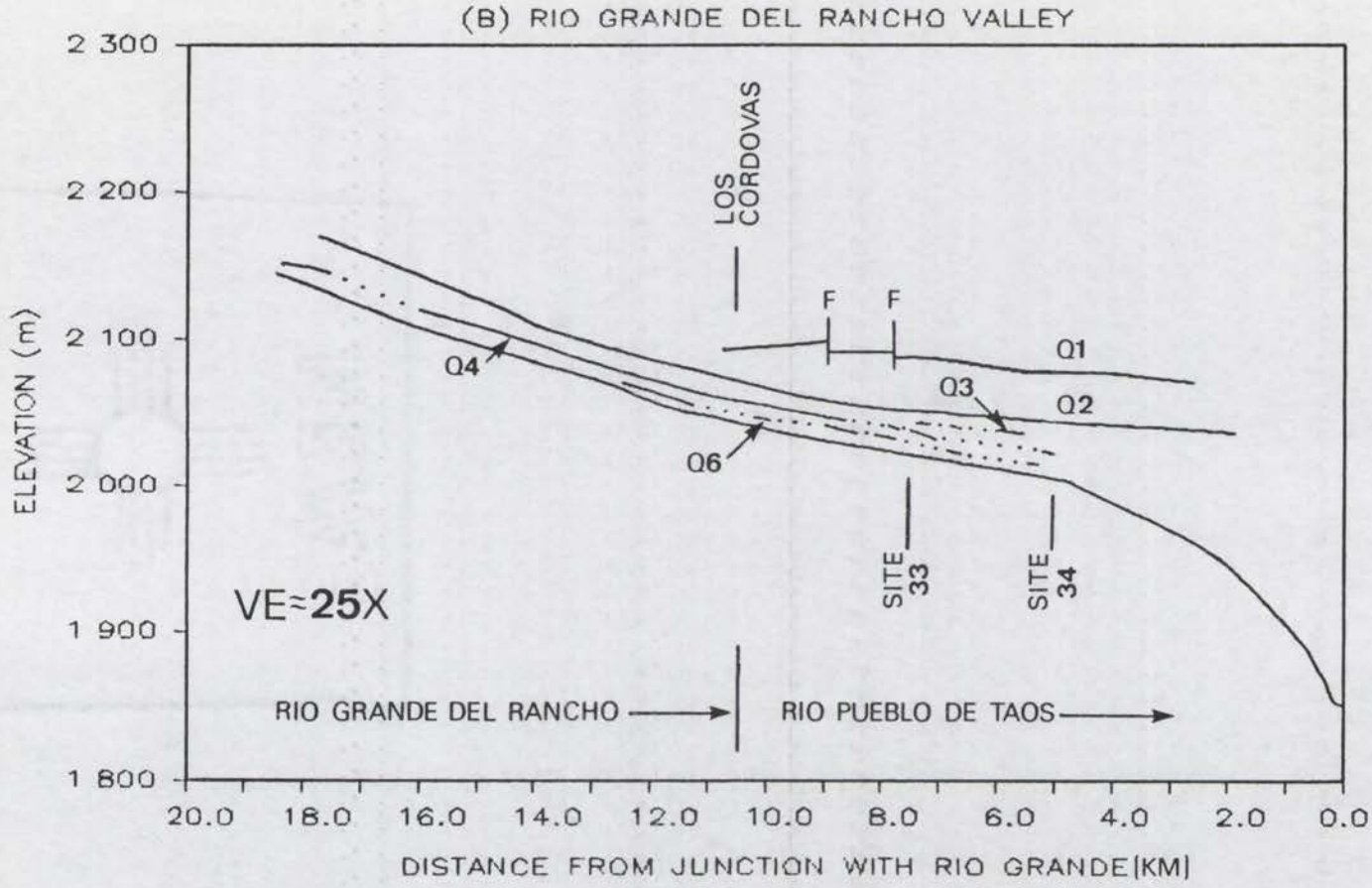

Figure 36. (continued)

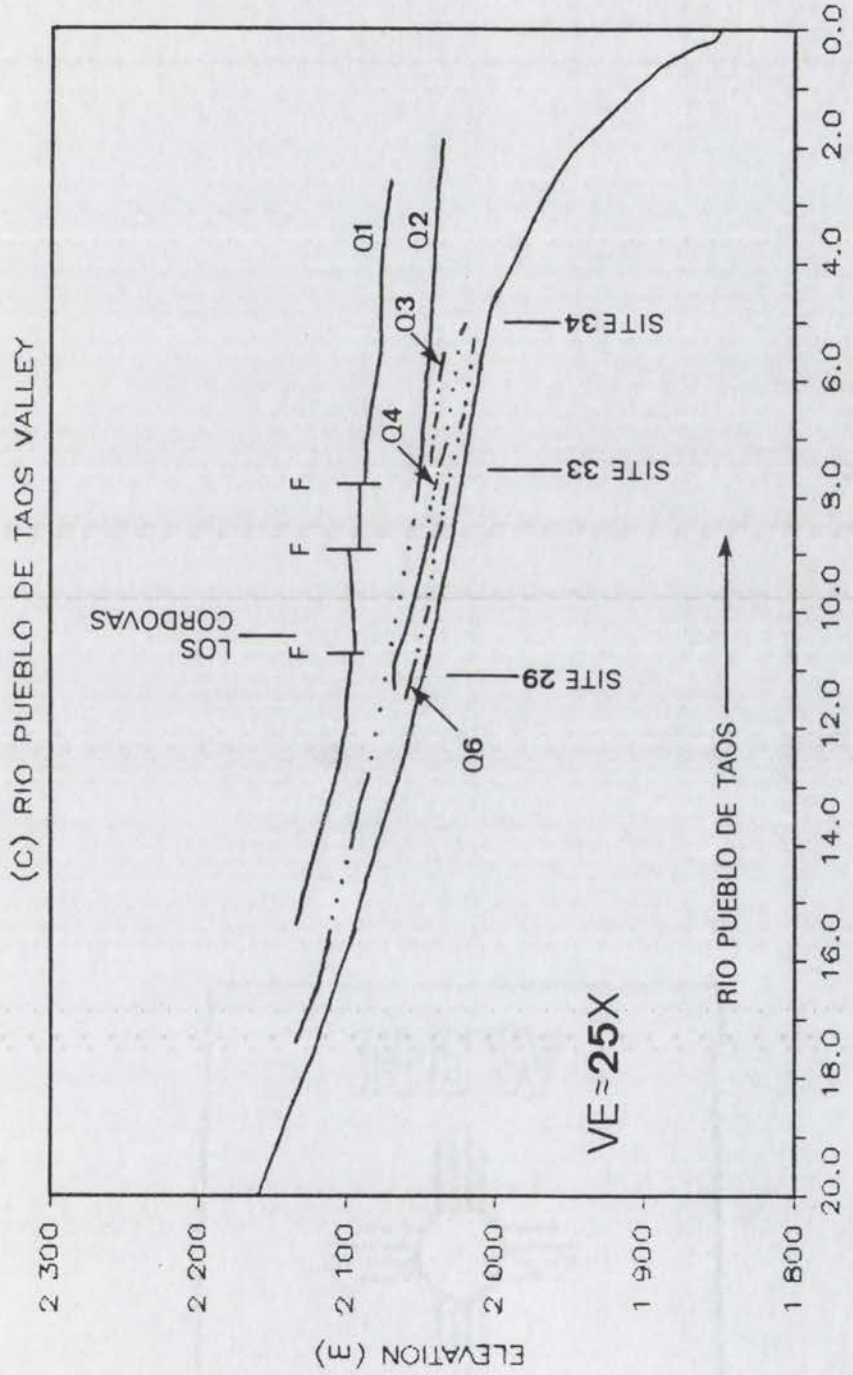

Figure 36. (continued)

present-day channel, surface $Qt1_P$ is continuous with surface $Qf1_P$ as described for the Arroyo Seco valley. The town of Taos is built on a remnant of surface Qt2 which is 18 m above the modern floodplain (Table 14) and associated with a 2 m-thick gravel deposit. These gravels unconformably overlie deposits similar to those associated with surface $Qf1_P$; thus, Qt2 is a strath terrace in this area. Further downstream, between the villages of Ranchito and Los Cordovas (see Plate 2), surface Qt2 is cut into surface $Qf1_P$ deposits and contains no gravel veneer. Long-profiles of surfaces in this portion of the Rio Pueblo de Taos valley are slightly divergent (Fig. 36c).

Below the confluence of Arroyo Seco, Rio Grande del Rancho and Rio Pueblo de Taos, valley morphology, terrace continuity, and terrace gradients change substantially. The Rio Pueblo de Taos valley in this area is narrow relative to valleys above the confluence, and the stream is confined by basalt on the north and alluvial fans on the south (Fig. 34). Although surfaces $Qf1_P$, $Qt1_{RG}$, and Qt2 are well preserved on the north side of the valley, surfaces Qt3, Qt4, and Qt6 are very discontinuous. Surfaces Qt3, Qt4, and Qt6 are straths developed on basalt, and are associated with thin (less than 2 m) gravel deposits. Surface Qt3(?) occurs downstream of the confluence, but only as three very localized straths. Identification of these terraces as unit Qt3 remnants is based solely on relief differences between units Qt2 and Qt4; access for soil profile descriptions was not available. No stream terraces exist within the narrow basalt gorge near the Rio Pueblo de Taos mouth, although $Qt1_{RG}$ and Qt2 continue nearly to the Rio Grande gorge, and lie above the uppermost layer of Servilleta Basalt (Fig. 34).

Three faults noted by Lambert (1966) and Personius and Machette

(1984) juxtapose Servilleta Basalt and Ql_p gravels north of Rio Pueblo de Taos near Los Cordovas (Plate 2). Offset appears to be less than 10 m; the western fault blocks are relatively down-dropped (Fig. 36c). Surface Qt2 and younger surfaces are not offset. Personius and Machette (1984) noted that movement on these faults may as be as old as early Pleistocene or as young as middle (?) Pleistocene, but did not indicate reliable age control for surface offset.

Long-profiles of surfaces downstream of Los Cordovas are shown in Figure 36. Gradients of long-profiles below the confluence at Los Cordovas are slightly lower than long-profiles in the valleys above the confluence (Table 15). Both Arroyo Seco and Rio Grande del Rancho show abrupt changes in present-day long-profiles at the Los Cordovas confluence (Fig. 36a and b). Long-profiles of surfaces below the confluence are divergent, with gradients on surfaces Ql_p and Qt2 (3 m/km) being lower than those on surfaces Qt6 and Q8 (7 m/km) (Table 15). It should be noted that gradients on all long-profiles of surfaces in the Rio Pueblo de Taos valley system are substantially lower than those in the Rio Hondo valley.

Geomorphic surfaces above the mountain front in the Rio Grande del Rancho valley were mapped in detail upstream to Ojo Sarco Canyon (Plate 3). Soil development on the two lowermost map units indicate that these geomorphic surfaces probably correlate with surfaces Qt6 and Qt7 elsewhere in the study area. Surface Qt7 in the Rio Grande del Rancho valley near Fort Burgwin lies about 8 to 12 m above the modern floodplain, and grades into tributary fans derived from Ojo Sarco Canyon and Rito de la Olla (Plate 3). Surface Qt6 lies about 18 to 24 m above the modern floodplain (Fig. 37), and occurs as a discontinuous strath

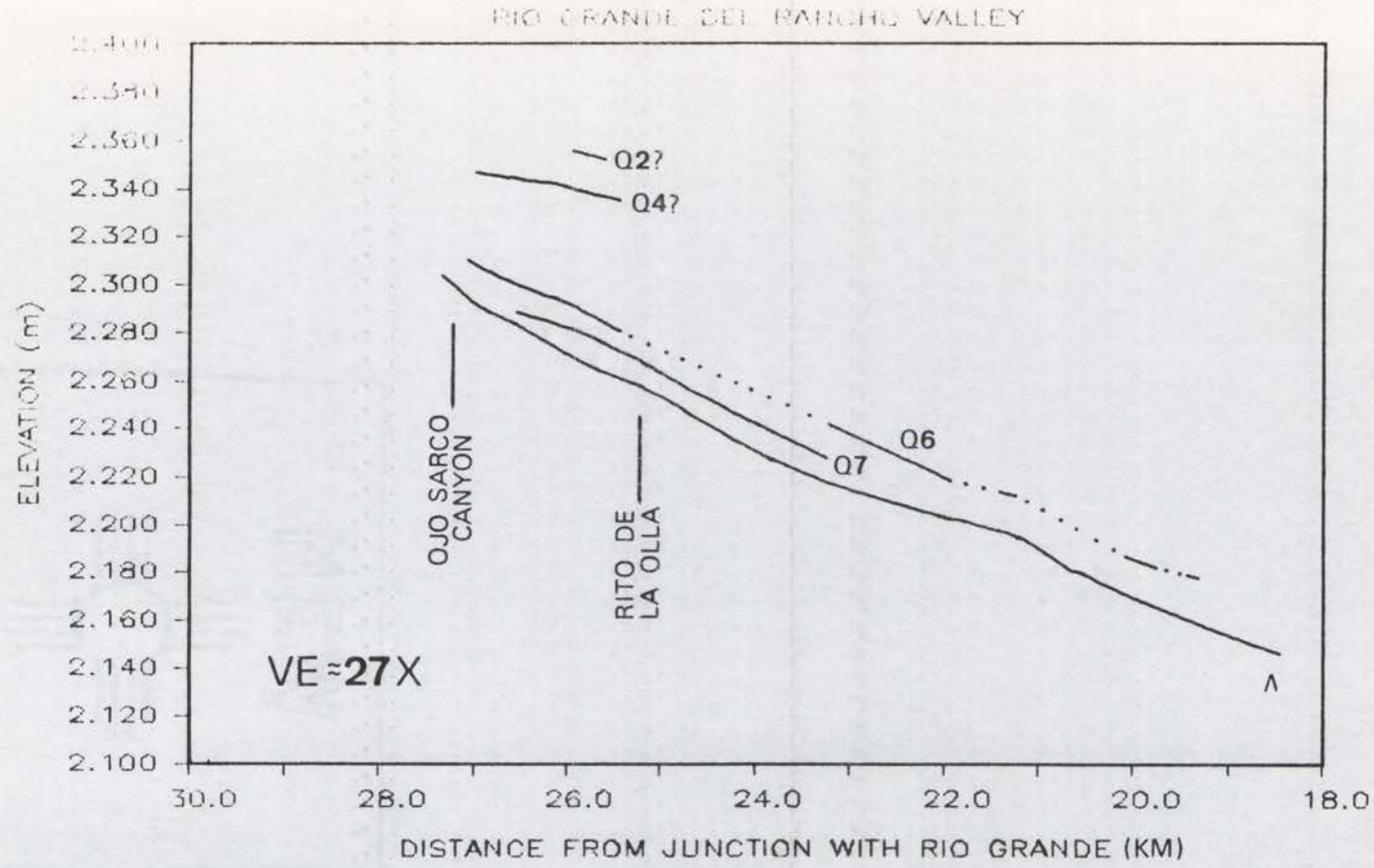

Figure 37. Long-profiles of geomorphic surfaces flanking Rio Grande del Rancho between the mountian front and Ojo Sarco Canyon (see Plate 3). Solid lines represent continuous geomorphic surfaces. (^) denotes mountain front.

terrace formed on Paleozoic sedimentary rocks in the northern (downstream) end of the valley, and as a depositional(?) terrace near Ojo Sarco Canyon.

Two other terrace remnants are recognized near Ojo Sarco Canyon and Rito de la Olla; the lower of these appears to be a remnant of surface Qt4(?) based on soil development. This terrace remnant occurs as a highly discontinuous strath formed on Tertiary Picuris Tuff and Paleozoic sedimentary rocks, and lies about 50 to 70 m above the modern floodplain. Near the mouth of Rito de la Olla, abundant fluvial gravels occur on a flat-toppped hill (elevation about 2355 m (7725 ft)) about 100 m above the modern floodplain. This terrace remnant may be equivalent to surface Qt2 (Plate 3), but lack of soil data precludes correlation. Several benches which are not overlain by gravel occur throughout the valley. Sandstone strata apparently uphold these features, which do not appear to be fluvial terraces.

Long-profiles of surfaces in the Rio Grande del Rancho valley above the mountain front are shown in Figure 37. A convexity exists in both surface Qt6 and the present-day long-profile about 2.6 km above the mountain front, where the valley narrows. Surface Qt6 occurs only as isolated terrace remnants below the profile convexity (Plate 3). No surfaces are continuous across the mountain front. Based on surface heights above the active stream channel, offset on surface Qt6 at the mountain front fault is about 10 m.

Sedimentology of Rio Pueblo de Taos Fluvial Deposits

Exposures of fluvial deposits in the Rio Pueblo de Taos valley are uncommon. Low relief between surfaces and few roadcuts limit the number of exposures of deposits associated with surfaces $Qt1_P$, Qt2, and Qt4;

exposures of surface Qt6 deposits were not found. Pebble-count data cannot be used to distinguish deposits of units Qt2 and Qt4. In general, these deposits are poorly-sorted, crudely-imbricated, and are composed primarily of unaltered subrounded to subangular clasts (Fig. 38). Color of the less-than-2 mm fraction approximates that of modern alluvium (10YR 6/3 dry). Mean grain size (b-axis) ranges from 44 mm to 91 mm (Table 16), a range which is not significantly different from that in Rio Hondo deposits. Grain size distributions of individual sample sites and of all unit Qt2 and Qt4 deposits do not approximate normal distributions (Fig. 30b). As in the Rio Hondo basin, more exposures and a larger data base are necessary to refine pebble-count grain-size data.

Rio Pueblo de Taos terrace deposits contain predominantly sandstone clasts (Fig. 31). At most sites, sandstone clasts are abundant (74% to 98% by frequency). However, at site PC17 (see Plate 2), a relatively high percentage of crystalline clasts (64%) was found; these clasts were probably derived from crystalline rocks in the Rio Lucero and Rio Pueblo de Taos basins.

Deposit thicknesses in the Rio Pueblo de Taos basin are difficult to determine due to limited exposure. However, exposures at sites PC11, PC12, PC13, and PC17 (Plate 2) suggest that deposits associated with surfaces Qt2 and Qt4 do not exceed 7 m in thickness. Thicknesses of unit Qt6 deposits are unknown.

Pebble-count data on deposits associated with surface Qt_P show that these deposits are distinct from other deposits in the Rio Pueblo de Taos basin (Fig. 32). Clast alteration, color of the fine-grained fraction, sorting, bedding, and grain-size distribution suggest that deposits associated with surface Qt_P in both the Rio Hondo and Rio Pueblo de Taos

Figure 38. Deposits associated with surface Qt2 exposed in gravel pit at site PC11 (see Plate 2). Note well-developed soil and terrace gravels unconformably overlying fine-grained basin-fill deposits (lower right).

basins are from the same population, and are distinct from younger deposits inset into deposits associated with surface Ql_p.

Soil Properties of Geomorphic Surfaces in the Rio Pueblo de Taos Valley

In order to correlate geomorphic surfaces along Rio Pueblo de Taos to surfaces in the Rio Hondo valley, ten soil profiles were described in the Rio Pueblo de Taos valley system (see Appendix C for descriptions, Plate 2 for locations). Three of these ten profiles have not been used in correlating surfaces: 1) SP16, which was affected by erosion of upper horizons, 2) SP24, which was located on the downthrown side of a mountain front fault and had been affected by erosion and deposition, and 3) SP25, which was described in order to document a series of buried soils on an alluvial fan between Taos and Talpa. Table 17 provides selected characteristics of seven profiles described in the Rio Pueblo de Taos valley; see also Appendix C.

Geomorphic surfaces within the Rio Pueblo de Taos valley cannot be identified using soil characteristics alone. However, a combination of soil-profile descriptions, surface heights above the active stream channel, surface heights below surface Ql_p, and terrace long-profiles were used to identify geomorphic surfaces in the Rio Pueblo de Taos valley system. Similarly, both soil characteristics and field relations are necessary to correlate surfaces along Rio Pueblo de Taos with surfaces in the Rio Hondo basin.

Soil carbonate morphology, a property which helped differentiate surfaces along Rio Hondo, shows similar trends in the Rio Pueblo de Taos basin (Table 17). Soil profile SP19 contained a laminar, stage IV carbonate horizon; surface dissection, lack of significant clast

alteration, color of the deposit matrix, and height above the active channel indicate that this soil profile developed in unit Qt2 deposits. Soils of unit Qt4 contained stage III carbonate morphology (Table 18). Soil profile SP23 showed carbonate morphology (stage II) similar to soils of unit Qt6 in the Rio Hondo valley. Modern floodplain deposits contain no carbonate accumulation, as indicated by profile SP17 (Table 17, see also Appendix C).

Other soil properties do not enable differentiation between surfaces in the Rio Pueblo de Taos area. Surfaces in the Rio Pueblo de Taos valley cannot be distinguished using depth to the Ck-horizon, although surface Qt6 deposits tend to have smaller Ck-horizons than surface Qt2 and Qt4 deposits (Table 17). Thickness of B-horizons appears to be lower in unit Qt4 soil profiles than in unit Qt2 and unit Qt6 soil profiles along the Rio Pueblo de Taos (Table 17). Soil profile SP19, which has a B-horizon thickness of only 15 cm, was described in a gravel pit and appeared to be affected by erosion and/or human activity.

Values of the Relative Profile Development (RPD) index (Harden, 1982) for soils of surfaces $Qt1_P$, Qt2, Qt4, and Qt6 show a relationship similar to that found in the Rio Hondo basin (Fig. 33). The surface Qt2 soil has a higher RPD value than the surface Qt4 soil, which has a higher value than the surface Qt6 soil (Table 17). Data from soil profiles SP21 and SP22 were excluded from Figure 33 because neither soil profile reached a Ck-horizon. Also, data from soil profile SP19, which was affected by erosion, could not be used to calculate RPD values.

Continuity of surfaces $Qt1_{RG}$ and Qt2 along the western rim of the Rio Grande gorge from Rio Hondo to Rio Pueblo de Taos and of surface $Qt1_P$ on the plateau supports the correlation of surfaces between the Rio Hondo

and Rio Pueblo de Taos valleys. Soil characteristics in the Rio Pueblo basin may be less diagnostic in distinguishing surfaces due to: 1) variability in soil properties, which may be higher in Rio Pueblo soils, 2) the low number of soil profiles described per surface, and/or 3) slight parent material differences.

DISCUSSION

Factors Controlling Present-day Fluvial Hydrology

In the Sangre de Cristo mountains near Taos, spring snowmelt produces virtually all high discharge events and is probably the main source of water eventually reaching stream systems via subsurface flow. Between 69 and 78 percent of total annual runoff at the six gaging stations above the mountain front occurs from April to July. Therefore, in order to interpret the hydrologic differences between the crystalline and sedimentary terranes in the study area, it is important to assess snowmelt-runoff relationships above the mountain front.

Discharge production due to a given water input (e.g., rainstorm, snowmelt) results from the interaction of input and catchment properties (Baker, 1977; Richards, 1982). Input rates from snowmelt depend on snowpack water content, temperature, and rainfall, which in turn are highly dependent on elevation (Figs. 7, 8, and 9). A basin's ability to produce runoff depends primarily on the infiltration capacity of bedrock and surficial materials (Yair and Lavee, 1985), and storage capabilities of lakes and valley-fill aquifers. Discharge hydrograph shapes within the study area are therefore a function of input rates and amounts, infiltration rates, and basin storage, which are discussed below.

Water Inputs

Meltwater and rainfall inputs to the crystalline and sedimentary terranes vary in timing and magnitude, primarily due to distributions of basin area within elevation zones (Fig. 22). Basins underlain by sedimentary rocks have relatively low median basin elevations, and snowmelt peaks in May. Most of the snowpack has been melted before the end of June (Fig. 13a). In the crystalline terrane, however,

temperatures sufficient to melt the snowpack (and permit rainfall instead of snowfall) are not attained in large portions of drainage area at high elevations until June. Above-freezing average temperatures in June coupled with large amounts of available water as snow at high elevations result in large amounts snowmelt during June (Fig. 13a). By the end of July in an average year, the majority of snow present in the crystalline terrane has melted, as shown by Figure 13a.

In all of the basins, rainfall inputs supplement snowmelt inputs, and are also controlled by basin-elevation distributions. For example, higher elevations in the crystalline terrane results in more convective summer rainfall and less evapotranspiration in these basins. Thus, the distribution of drainage area within elevation zones greatly influences the overall amount of meltwater and rainwater inputs available for either runoff or infiltration.

Relief determines the amount of basin area within high elevation zones, and therefore influences present-day hydrologic conditions by controlling differences in water inputs. Higher resistance to erosion of crystalline rocks may have resulted in the differences in relief and relief/length ratios (Table 12) between the two terranes in the study area. Therefore, lithology has probably had a direct effect on area-elevation relationships; this implies that present-day differences in climate and relief between the two terranes in the study area may be indirectly linked to lithology.

Infiltration Capacities

Infiltration capacities and storage capabilities may interact with water inputs to influence the shape and magnitude of the discharge

hydrograph. Previous workers have shown that infiltration capacity can vary depending on lithology and surficial materials (Yair and Lavee, 1985; Wells and Jercinovic, 1983), and that runoff production may be affected by the distribution and areal extent of surficial cover (Dunne and Black, 1970). In addition, infiltration capacity may vary through time, given excess water input (Horton, 1933; Selby, 1982). Quantification of the areal and temporal variations of infiltration rates within the study area was not within the scope of this project; however, field observations and basin morphometry provide data which suggest that lithology controls infiltration, and therefore runoff production.

In the drainages underlain by crystalline rocks, the narrow valley floors (Fig. 39) contain only small amounts of fill, except above elevation 2900 m, where glacial deposits are extensive (Richmond, 1962). Unweathered bedrock outcrops of gneiss and granite and thin colluvium comprise the steep hillslopes in these basins (Reed et al., 1983). During snowmelt conditions of excess water input, infiltration capacities are probably controlled by the underlying crystalline bedrock, and thus are probably low. Therefore, runoff produced from a given water input is probably relatively high. Data from gaged basins in the Rocky Mountains supports the postulation that, in general, crystalline rocks promote relatively high runoff (Fig. 12).

In the drainages underlain by sedimentary rocks, valley floors are typically wide, and contain significant amounts of alluvium (Fig. 40). Hillslopes are generally not as steep as those in the crystalline terranes (indicated by lower relief ratios, Table 12) and are mantled with thin colluvium. Outcrops of sandstone and conglomerate are common. During snowmelt conditions of excess water input, infiltration capacities

Figure 39. Photograph of the Rio Hondo valley at the mountain front, showing narrow valley that lacks significant amounts of valley fill alluvium. Note bedrock outcrops on steep hillslopes. Photograph taken looking east from surface Qlp above the village of Valdez.

Figure 40. Photograph of the Rio Fernando de Taos valley showing large amounts of valley fill alluvium and shallow hillslopes. Photograph taken looking southeast above the Rio Fernando-Las Tienditas Creek junction.

in areas of thin cover or sedimentary bedrock are probably controlled by relatively high bedrock permeability. Although partial-area contributions to runoff may be significant where infiltration rates vary within a basin (Yair and Lavee, 1985; Dunne and Black, 1970), it is probably reasonable to postulate that, on the average, fairly high infiltration rates in the sedimentary terrane produce relatively low amounts of runoff. Data from sedimentary terranes throughout the Rocky Mountains also supports this postulation (Fig. 12).

The relative permeabilities of different rock and soil types can be assessed using drainage density data. For example, D_d is high in regions of impermeable soils (Schumm, 1977; Wells and Jercinovic, 1983), because low infiltration capacities result in high runoff production (Richards, 1982). Higher D_d values in crystalline terrane (Table 12) therefore suggest that these regions have lower average permeabilities, and have had higher runoff generation per unit area over long periods of time, than areas underlain by sedimentary rocks.

Storage Capabilities

Regions of high runoff production per unit area typically show relatively peaked hydrographs (Richards, 1982), which is only partially true in the study area. Hydrographs are generally steeper in sedimentary terrane than in crystalline terrane (Fig. 11), although some individual convective summer storms produce quick rises on Rio Hondo and Rio Lucero. Rio Hondo and Rio Lucero tend to maintain high discharge per unit area for long periods of time (Fig. 14), which is probably linked to June snowmelt at high elevations and water storage in headwater regions. Therefore the shape of the hydrographs appear to be influenced strongly by two factors: snowmelt distribution through space and time, and

meltwater storage in headwater regions. The former factor has already been discussed, the latter is discussed below.

Water can be stored in several basin localities, including channels, small surface depressions, lakes, and saturated and unsaturated subsurface zones (Viessman et al., 1978). Channel storage in these high-velocity meltwater streams is probably negligible, and above the mountain front depression storage is probably small. Lake storage is small in the sedimentary terranes, but lakes and glacial deposits in headwater regions of the crystalline terrane probably store significant amounts of water.

Williams Lake, a tarn in the Rio Hondo headwaters, is held in by a Neoglacial terminal moraine (Richmond, 1962), and has no outlet. As noted before, glacial deposits underlie the Rio Hondo valley floor down to Twining (elevation 2865 m) (Fig. 41). Several springs return substantial amounts of discharge to the Lake Fork branch through these deposits. Bankfull discharge at two sites underlain by these deposits (sites 24 and 25) increases downstream; lack of tributary inflow between these sites suggests that return flow significantly contributes to discharge on Rio Hondo (Fig. 41).

Glaciated regions cover about 31% and 41% of the Rio Hondo and Rio Lucero drainages, respectively, and glacial deposits probably hold the majority of stored meltwater in these basins. Storage is probably minor where these deposits are not present, due to minor amounts of valley fill (Fig. 39); the same is probably true in the Rio Lucero basin.

These relationships are supported by Figure 15, which shows that additions to storage in crystalline terrane are small in April, when the majority of snowmelt in the basins occurs at lower elevations. Storage contributions are high in June and July due to snowmelt at higher

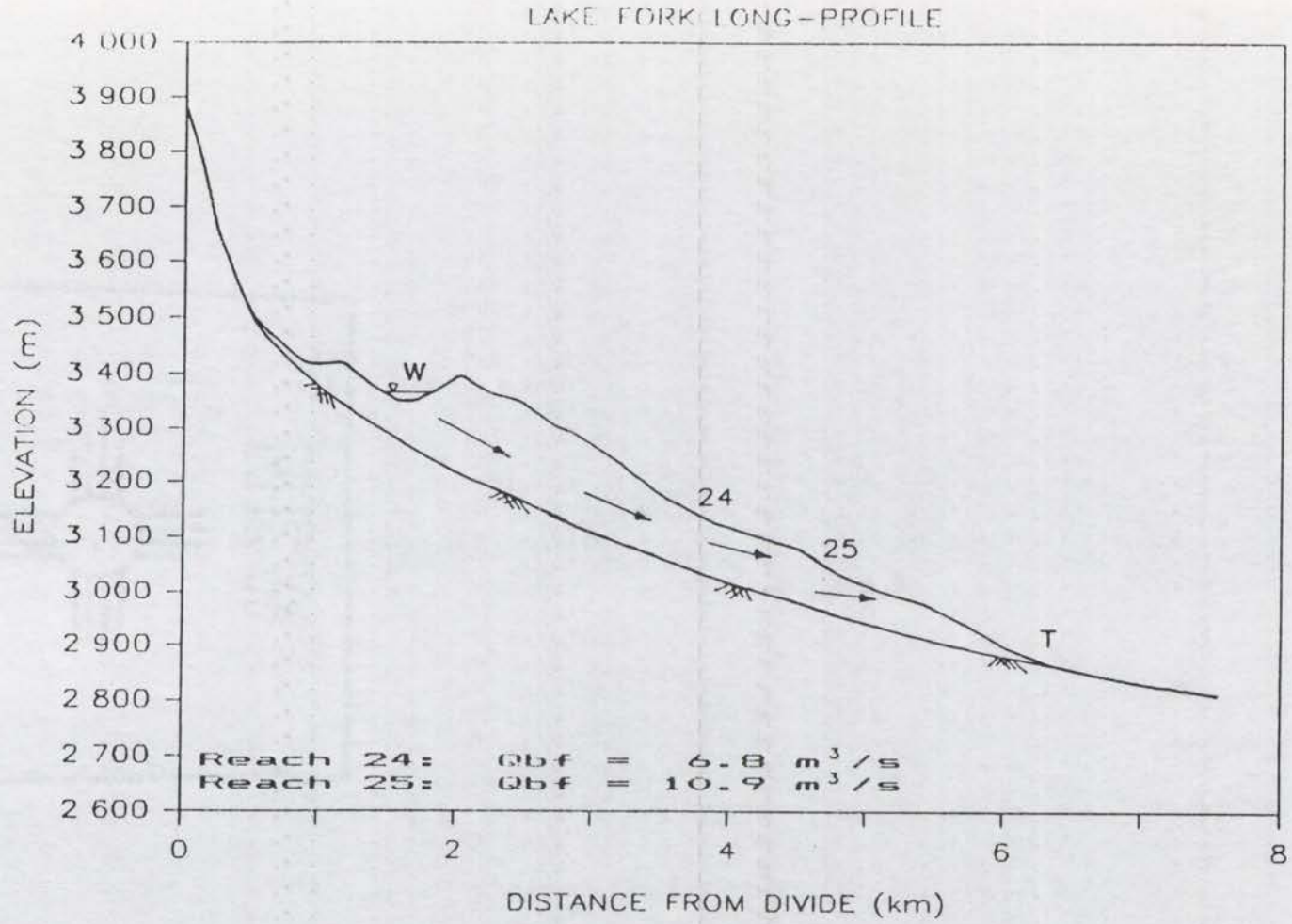

Figure 41. Long-profile of the Lake Fork branch of Rio Hondo, showing inferred distribution of glacial deposits and inferred groundwater flow paths. W = Williams Lake, T = village of Twining (Taos Ski Valley). Reach 24 was dry on September 22, 1984, although reach 25 contained about 0.75 m^3/s. No tributaries enter between the two sites.

elevations, infiltration into glacial deposits, and runoff into tarns (Fig. 15). It appears that the storage reservoirs (glacial deposits) are never saturated to the point of not being able to take on more water. Dunne and Leopold (1978, p. 203) indicate that glacial tills may have high transmissibility, although values may be low if the tills are fine-grained. The large amounts of return flow via springs in the Lake Fork valley suggest that the transmissibility of the glacial deposits is high. Continued return flow in July maintains high discharge on these basins (Fig. 14), and indicates that permanent losses to groundwater are probably low, due to impermeable bedrock underlying glacial deposits.

In contrast, glaciated regions cover about 14% and 10%, respectively, of the Rio Pueblo de Taos and Rio Grande del Rancho drainage areas above the mountain front. Glacial deposits in these basins probably also store meltwater and return discharge to channels later in the spring. Water storage contributions decrease through the spring (Fig. 15), suggesting that glacial deposits in the headwaters and broad valley-fill aquifers cannot store large amounts of water. In May, additions to storage are low, although snowmelt is high, resulting in peak discharges during this month. With the elimination of the snowpack in these basins by the end of June, additions to storage are low. Rainfall increases storage contributions in July (Fig. 15). Hydrograph shapes support this model; rising limbs are generally steep (Fig. 11), but less steep recessional limbs indicate that return flow (probably from headwater glacial deposits and tarns) occurs in mid-June.

Rio Fernando de Taos and Rio Chiquito have no glaciated regions, although trends of storage contributions in these two basins parallel trends in other basins underlain by sedimentary rocks (Fig. 15). The

high additions to storage in the Rio Fernando de Taos basin in April and May are probably due to exceptionally broad valley fills (Fig. 40), but low base flow suggests that return flow is minor (Fig. 11).

Therefore, in sedimentary terrane storage is relatively low due to the scarcity of glacial deposits, and discharge per unit area is low due to relatively permeable bedrock. It appears that permanent losses to groundwater and evapotranspiration from valley fill aquifers may be high. Consequently, base flow is low, and high discharges are not maintained throughout the spring.

Summary

It has been shown that runoff production is a function of three factors. First, area-elevation distributions control the magnitude and timing of water inputs. These distributions may be linked to lithology via relative bedrock erodibilities. Second, groundwater storage capabilities control the timing of return flow to channels. The amount of flow returned to channels is affected by underlying bedrock permeabilities. Third, bedrock permeabilites control infiltration and runoff in areas not underlain by glacial deposits. Thus, the present-day high discharges in crystalline terrane and relatively low discharges in sedimentary terrane appear to be determined directly and indirectly by lithology.

Sediment Transport in the Present-day Fluvial Systems

Bed-material sampling and channel geometry measurements enable assessment of the relative sediment-transport capabilities of active channels draining both lithologic terranes (Fig. 6). Present-day transport rates and amounts in the two terranes are estimated and

compared utilizing competence, stream power, and shear stress data.

Competence, stream power, and shear stress data suggest that channels draining crystalline rocks can transport larger bed material at higher rates than channels draining sedimentary rocks (Tables 9, 10, and 11). Bedload transport rates are dependent on the total power supplied per unit bed area (unit stream power, w) (Bagnold, 1966, 1977), and can be compared using w values. For example, w values at sites draining crystalline terrane average four times those at sites draining sedimentary rocks (Table 11), indicating that bedload transport rates are on the average about four times as high in channels draining crystalline rocks.

Bedload transport rates are also correlated with the shear stress applied to bed-material particles in excess of the critical shear stress (Andrews, 1984). In the streams studied by Andrews (1984), bed shear stress rarely exceeded critical values by more than 2.5 times, and Andrews concluded that transport rates are relatively low except in extreme floods. Near Taos, streams draining crystalline terrane have a mean T^*_{50} value over 5 times the critical value; whereas, in sedimentary terrane the mean T^*_{50} value exceeds T^*_{c50} by 3 times. These data suggest that sediment transport is probably substantial in both terranes, although higher in crystalline terrane.

In order to address sediment transport properties, the study area has been divided into six regions (Fig. 6): regions draining crystalline rocks above the mountain front (region I), below the mountain front (region II), and in the Rio Hondo basalt gorge (region III), and regions draining sedimentary rocks above the mountain front (region IV), below the mountain front (region V), and in the Rio Pueblo de Taos basalt gorge

(region VI). Table 19 provides information on each of these regions.

Sediment Transport in Channels Draining Crystalline Terrane

Channels in region I have T^*_{50} and T^*_{90} values 3 to 8 times critical values, and high unit stream power (w = 595 N/s, Table 19). Mean T^*_{50} is 0.183 (5.9 times T^*_{c50}), and mean T^*_{90} is 0.068 (4.6 times T^*_{c90}). In this region, bankfull discharge (Q_{bf}) can apparently transport most of the bed-material, and transport rates are probably high. Stage-discharge relations at a gaging station on Rio Hondo just above the mountain front (U. S. G. S. no. 08267500) show that no major changes in bed elevations have occurred over the last 30 years (Fig. 42a), although minor shifts suggest that the bed material is mobile. These data imply that most channels in this region are stable, mobile-bed channels, as described by Andrews (1984).

Several channels in region I show evidence of recent entrenchment, perhaps due to base-level fall at the Rio Hondo mouth and/or high stream power. Q_{bf} calculations were not possible at sites 1, 2, 3, 4, 23, 27, and 28 (Fig. 6), due to entrenchment and difficulty in identification of bankfull stage. For example, sites 2 and 3 are located in Gavilan Canyon, a tributary to Rio Hondo (7.7 km^2) which has entrenched about 5 m into recent alluvium in its lowermost 2 km. Lack of significant deposits below entrenched areas suggests that the material derived from incision has been rapidly transported through the basin. Thin, unweathered colluvial cover on hillslopes and channel entrenchment in this region imply that large amounts of sediment are probably supplied to the fluvial system due to hillslope processes and channel erosion. In summary, region I is characterized by high amounts of bedload transport (at

Table 19. Summary of flow properties, channel properties, and valley morphology in regions I to VI (see Fig. 6).

Region	Streams	T*50	T*90	w (N/m/s)	D5x (mm)	Vf	channel stability	inferred bedload condition at bankfull Q
Streams draining crystalline terrane								
I	Rio Hondo, Rio Lucero, Arroyo Seco	0.183	0.068	595	440	0.22	stable, unstable	mobile
II	Rio Hondo	0.081	0.039	186	394	3.16	stable	mobile
III	Rio Hondo	0.149	0.039	358	309	0.40	unstable	mobile
Streams draining sedimentary terrane								
IV	Rio Fernando de Taos, Rio Chiquito, Rio Grande del Rancho, Rio Pueblo de Taos	0.113	0.040	140	262	1.15	stable	mobile
V	Rio Pueblo de Taos	0.033	0.014	51	223	24.8	stable	immobile
VI	Rio Pueblo de Taos	--	--	--	--	0.67	unstable	mobile

KEY: T*50 : mean dimensionless shear stress for 50th percentile of bed material
T*90 : mean dimensionless shear stress for 90th percentile of bed material
w : mean unit stream power
D5x : average of means of five largest bed-material clasts
Vf : mean ratio of valley floor width to valley depth (Vf ratio, Bull and McFadden, 1977)

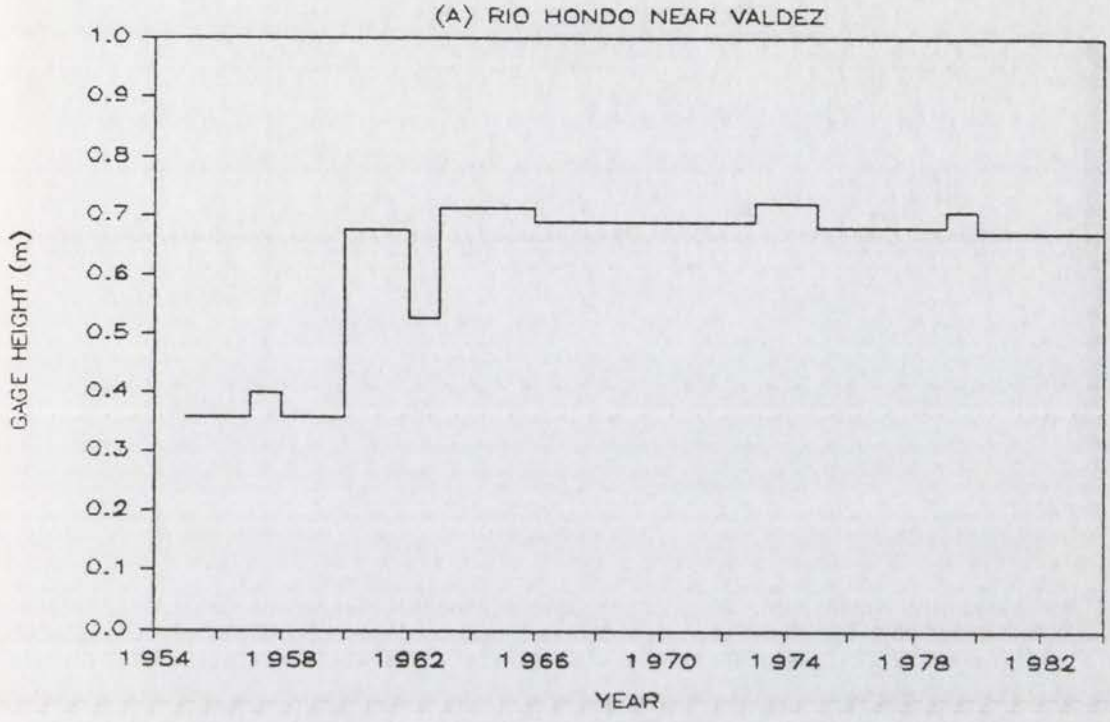

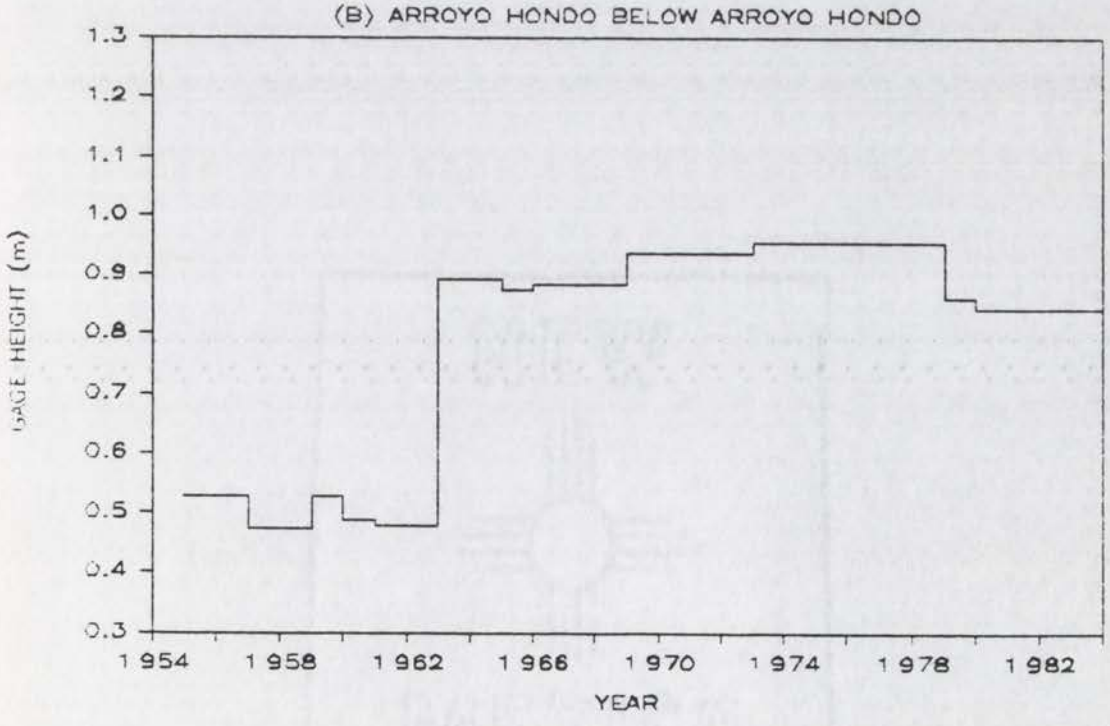

Figure 42. Changes in stage for a discharge of 1.42 m^3/s at (A) U.S.G.S. station 08267500 and (B) U.S.G.S. station 08268500. Similar trends exist for higher discharges at both sites. See Figure 6 for locations.

relatively high rates), mobile channel beds, and both stable and unstable channels.

Channels in region II, in contrast, have lower T^*_{50}, T^*_{90}, and w values than channels in region I (Table 19). Mean T^*_{50} decreases 55% from region I, and mean T^*_{90} decreases 42%. Dimensionless shear stresses are generally 2.5 times critical values, suggesting that bedload transport at Q_{bf} occurs, although at rates lower than those in region I. Stage-discharge relations at a streamflow gaging station at site 31 (Fig. 42b), show that approximately 0.4 m of deposition occurred during 1963, and minor bed elevation change has occurred since then. This data and the lack of channel entrenchment in this region suggest that the Rio Hondo has a stable, mobile-bed channel (Andrews, 1984). High stream power (Table 11) at sites 31 and 32 and lack of coarse overbank deposits in the Rio Hondo valley imply that channels in this region can transport the large bedload imposed from region I through to region III.

Region III consists of the deep, narrow basalt gorge below Arroyo Hondo, and the channel is characterized by data from site 30 (Table 19). An increase in T^*_{50} of 83% occurs between region II and site 30, and unit stream power is also high relative to values in channels in region II. Fresh hillslope colluvium and lack of a significant floodplain suggest that the channel in this region is fairly unstable. Large imbricated basalt boulders and high T* and w values suggest that the bed is mobile in this region.

In summary, all regions draining crystalline terrane appear capable of transporting imposed sediment and water discharges without substantial aggradation. Entrenchment in upstream Rio Hondo channels and lack of deposition indicate that large amounts of material can be transported

efficiently out of the basin. High unit stream power and dimensionless shear stress suggest that transport rates are high. Also, discharge duration curves (Fig. 10) imply that, due to sustained high discharge, large amounts of sediments (derived from hillslopes and channel erosion) are transported, relative to amounts transported in channels in sedimentary terrane.

Sediment Transport in Channels Draining Sedimentary Terrane

Sediment transport in streams draining sedimentary terrane shows similarities and differences with transport in streams draining crystalline terrane. In general, sediment transport rates are relatively high in channels above the mountain front (region IV), low in channels below the mountain front (region V), and high in channels in the basalt gorge (region VI). However, overall rates and amounts of transport are lower than in channels draining crystalline rocks.

Reaches in region IV have T^*_{50} and T^*_{90} values 1.3 to 6 times critical values (Table 10). Mean T^*_{50} is 3.6 times T^*_{c50} and mean T^*_{90} is 2.7 times T^*_{c90} (Table 19). At bankfull discharge, therefore, shear stresses are high enough to initiate motion of most of the bed material, although transport rates are probably lower than those in region I. Mean unit stream power in channels in region IV is less than one-fourth that in region I reaches (Table 19), implying that transport rates in region IV are less than one-fourth of the rates in region I. Stage-discharge relations at a streamflow gaging station just below 14 (Fig. 43a) show virtually no change in bed elevations in the period of record, 1958-1980. Large amounts of modern valley fill in the wide, unentrenched valleys in the Rio Fernando de Taos and Rio Grande del Rancho valleys and meandering channels suggest that degradation has not been substantial. In general,

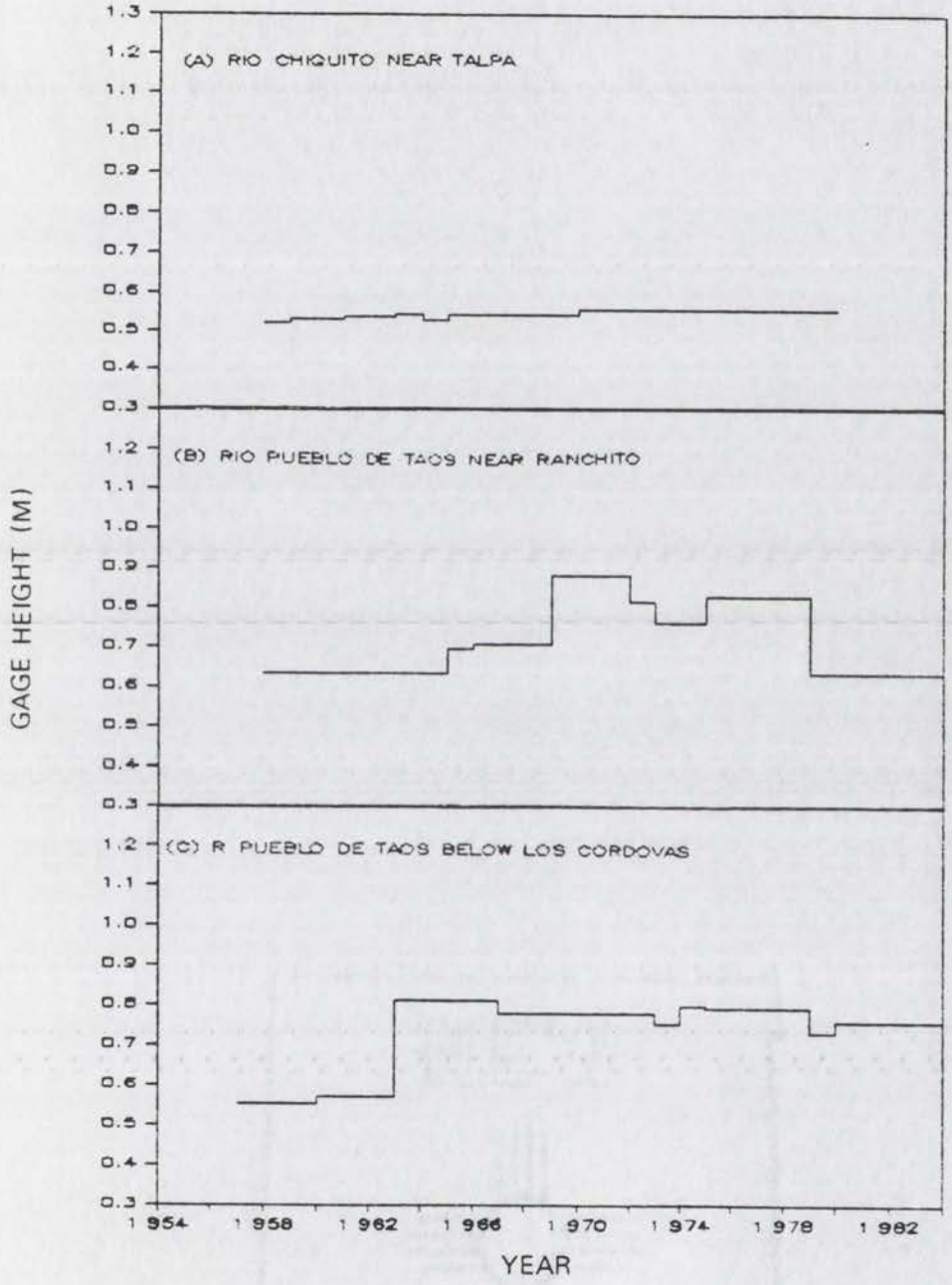

Figure 43. Changes in stage at three U.S.G.S. streamflow gaging stations in the Rio Pueblo de Taos basin. (A) U.S.G.S. station 08275500; stages are for 0.71 m^3/s. (B) U.S.G.S. station 08275300; stages are for 2.83 m^3/s. (C) U.S.G.S. station 08276300; stages are for 2.83 m^3/s. Similar trends exist at higher and lower discharges at all three sites. See Figure 6 for locations.

region IV appears to have stable, mobile-bed channels at Q_{bf}, and transport rates are probably lower than those in region I. Because Q_{bf} is equaled or exceeded only about 1% of the time (Table 7), total amounts of bedload transport are probably small.

Data for channels in region V is derived from sites 29, 33, and 34, three sites at the downstream end of the wide Rio Pueblo de Taos valley below the mountain front. Values of T^*_{50} and T^*_{90} are essentially equal to critical vaues (Table 19), suggesting that Q_{bf} can just initiate motion of bed material. Mean unit stream power is less than one-third of w in region II, suggesting transport rates in channels in region V at Q_{bf} are about one-third those in region II. Stage-discharge relations at gaging stations near sites 29 and 33 (Fig. 43) also show no major changes in bed elevation betweem 1957 and 1984, but show minor changes indicative of erosion and deposition. Thus, while bed-material is moved in these channels, substantial transport most likely occurs only at discharges above Q_{bf}. Channels in region V therefore are threshold channels, in which floods exceeding bankfull stage are necessary to transport significant amounts of bed material (Lane, 1953). Considering that Q_{bf} is equaled or exceeded on the average about 3.5 days per year (Table 7), the period during which transport occurs in these channels is short. Total amounts of bedload transport in region V are therefore probably low, relative to total amounts on the Rio Hondo at sites 31 and 32.

Geomorphic evidence indicates that substantial lateral migration has occurred in region V. For example, all of the streams in this region meander in wide, flat-floored valleys below the mountain front (Fig. 44); modern cut banks indicate that lateral migration is actively occurring.

High discharge, steep gradient and numerous plunge pools prevented

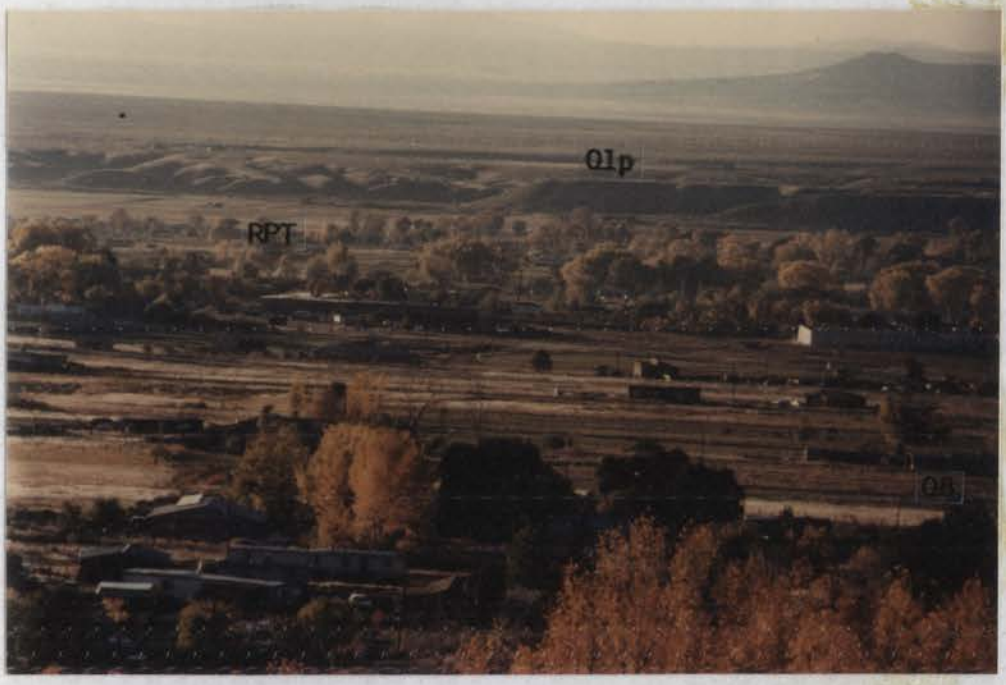

Figure 44. Photograph of the Rio Pueblo de Taos valley on the Taos Plateau, showing wide valley floor and low relief. Photograph taken looking west from mountain front facet near Rio Fernando de Taos. RPT = present-day Rio Pueblo de Taos. See Plate 2 for descriptions of geomorphic surfaces $Q1_p$ and Q8.

channel cross-section and bed-material measurement in region VI, which encompasses the Rio Pueblo de Taos gorge. Several features show that this gorge is similar to region III on the Rio Hondo. First, there is no floodplain and fresh alluvium mantles the steep hillslopes below bedrock cliffs. Second, bedload material is extremely large, including basalt boulders several meters wide. Many of these boulders are imbricated and comprise large mid-channel boulder bars. Therefore, channels in region VI are characterized by high bedload transport rates and large bedload calibre, as are channels in region III.

Present-day Longitudinal Profiles

Long-profiles are the least transient expression of fluvial processes, reflecting the influences of changes in relief (due to changes in base-level or tectonic activity), changes in climate, and the distribution of lithology (Richards, 1982; Shepherd, 1979). Because these factors generally influence fluvial systems over long periods of time (Knox, 1976), long-profiles reflect "the *general* adjustments of gradient to *average* [long-term] discharge conditions" (Richards, 1982, p. 225). Thus, because data can be collected on long-profile shape and on present-day discharge, long-profiles provide a link between present-day and past hydrologic conditions.

Hack (1957) has shown that long-profile shape is strongly influenced by underlying lithology. Hack used a power function between slope (S) and distance (L) to describe concavity, such that $S = kL^n$ (see Results). Large negative values of n indicate pronounced concavity, and large values of k indicate steep channel slopes near the drainage divide. Hack (1957) implied that different long-profile shapes between lithologic

terranes may be due to different bedrock resistances to erosion. Long-profile concavity has also been attributed to downstream increases in discharge associated with tributary inflows (Gilbert, 1877; Richards, 1982). For example, Wheeler (1979) has found that pronounced concavity in several British rivers was related to rapid downstream increases in discharge, which indicates similarity between discharges on an historical time scale and on a geologic time scale.

Near Taos, streams draining crystalline terrane have more pronounced concavity than streams draining sedimentary rocks, as indicated by higher values of the concavity index (C), and more negative values of n (Table 13). Downstream increases in discharge are also higher in crystalline terrane. Although the exponent of the present-day bankfull discharge-basin area relation for crystalline basins (0.51) is lower than for sedimentary terrane (0.74) (Fig. 16), the absolute increase in Q_{bf} is much higher, as shown by an arithmetic plot (Fig. 45). Thus, streams in the study area which are characterized by relatively high present-day discharge production have more pronounced long-profile concavity.

Rio Pueblo de Taos is underlain by crystalline rocks in its upper reaches but sedimentary rocks downstream and has the most pronounced long-profile concavity (Table 13). Discharge production is probably high in headwater regions, which are underlain by glacial deposits and crystalline terrane. However, these high discharges flow onto sandstones and shales downstream and are probably able to erode into these less resistant rock types. Thus the relatively pronounced concavity of the Rio Pueblo de Taos profile is most likely due to high discharge produced in headwater regions underlain by resistant crystalline terrane, in combination with less resistant sedimentary rocks underlying downstream

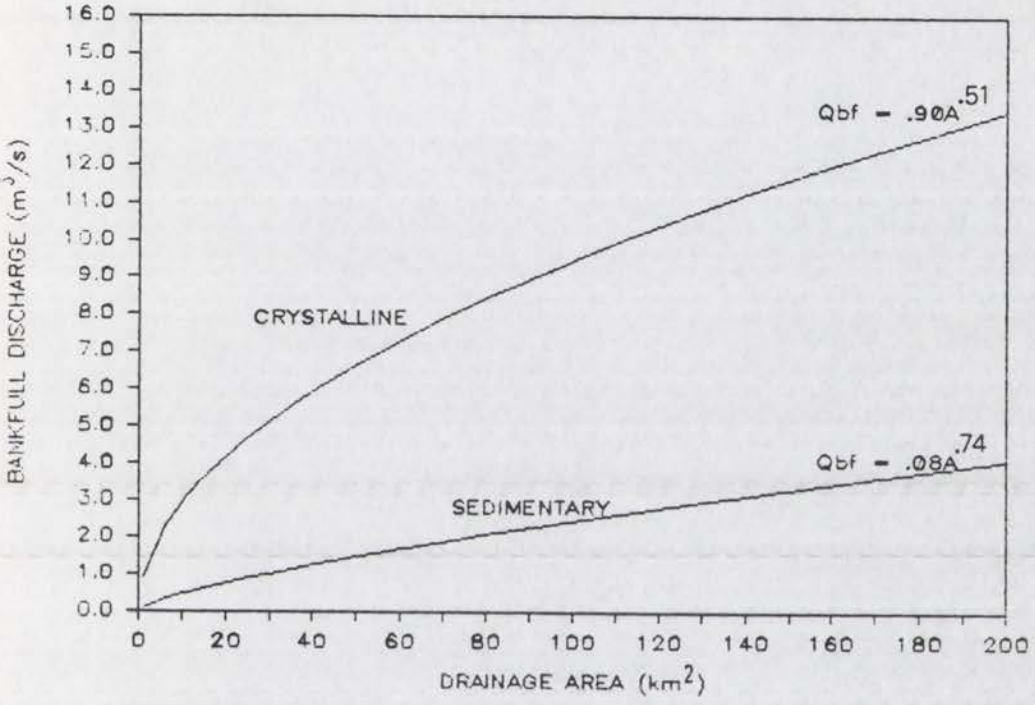

Figure 45. Arithmetic plot of regression curves from data in Figure 16, showing higher increase in discharge in basins underlain by crystalline rocks.

reaches.

In summary, streams having more pronounced concavity are those which have high discharge production. Although these streams are underlain by more resistant crystalline rocks, the relatively high runoff produced is apparently sufficient for channel incision and production of relatively concave long-profiles. Association of present-day discharge characteristics with long-profile concavity, and with underlying lithology, suggests that lithology has controlled discharge and hence long-profile shape over the geologic time scale. In conclusion, these data suggest that differences in present-day discharge characteristics in the study area have been present on the scale of thousands of years.

Quaternary Fluvial System

The Rio Hondo and Rio Pueblo de Taos drainage basins provide an opportunity to investigate the long-term effects of lithology on fluvial systems responding to similar base-level and climatic changes. Possible influences of base-level and climatic change on long-profile adjustments, terrace production, and valley morphology, as well as interpretations of the geomorphic histories of the fluvial systems are given below. The concept of critical-power thresholds (Bull, 1979) is used in an attempt to understand changes which have occurred within these fluvial systems over geologic time.

Age Relationships of Geomorphic Surfaces

In this study area soil development has been used as a tool for correlating geomorphic surfaces and as the primary relative age indicator. Few data are available concerning the absolute ages of Quaternary deposits, although one numeric age has been determined on a

lens of Tsankawi Pumice sampled in a roadcut approximately 8 km southwest of Ranchos de Taos (Izett et al., 1981). The sample was apparently taken from deposits associated with surface Ql_p (Plate 2). Izett et al. (1981) calculated a K-Ar age of 1.12 $\pm$ 0.03 Ma for the sample (no. 77W29).

Ages of other geomorphic surfaces in the Taos area are inferred on the basis of relative soil development. Surface Qt2 through Qt5 soils generally have medium to strong subangular and angular blocky B-horizon structure, and stage III to IV carbonate morphology (Appendix C). Clay films in B horizons of these soils are also well developed (Table 18). The well-developed argillic and calcic horizons of surface Qt2 soils suggest that this surface was probably formed during the early (?) to middle Pleistocene. Argillic and calcic horizons of surface Qt3, Qt4, and Qt5 soils suggest that these surfaces probably formed during the middle (?) Pleistocene. Soils formed in pre-Bull Lake alluvium in the San Luis valley are characterized by stage III to III+ carbonate morphology and strong angular blocky B-horizon structure (McCalpin, 1982), and appear to be similar to soils on surfaces Qt2 through Qt5. However, age control of pre-Bull Lake alluvium in the San Luis valley is poor (McCalpin, 1982).

Soils of unit Qt6 have stage II carbonate morphology, weak to medium subangular and angular blocky B-horizon structure, and 7.5YR and 10YR B-horizon hues (Appendix C, Table 18). Soils on Bull Lake deposits in the San Luis valley (McCalpin, 1982) have similar features. Considering the fact that the Rio Hondo basin has experienced Bull Lake and Pinedale glaciations (Richmond, 1962), it is not unreasonable to postulate that unit Qt6 soils began to develop after Bull Lake glaciation. In the Taos area, cambic horizon properties of surface Qt7 suggest that this surface

was probably abandoned during the early Holocene or latest Pleistocene. Surface Qt7 soils near Taos are comparable to soils developed on Pinedale deposits in the San Luis valley, which have ages constrained by five ^{14}C-dates (McCalpin, 1982). However, ages of geomorphic surfaces near Taos must be viewed as tentative due to poor age control.

The Critical-power Threshold

A threshold is a condition, level or stage at which a change is produced; the conditions at which a dramatic change occurs in a geomorphic system are dependent on the stress applied and the strength of the materials to which the stress is applied (Schumm, 1977). For example, initiation of bedload transport indicates that a threshold has been exceeded, which can be described by comparison of dimensionless shear stress and critical dimensionless shear stress (see above). Bull (1979) has described major fluvial adjustments in terms of the "critical-power threshold", in which stream power is equal to "critical power", or the power necessary to transport the imposed sediment load. Therefore, a stream is at the critical-power threshold when the stream power/critical power ratio is 1.0. Although stream power can be quantified (Bagnold, 1977), critical power depends on several interdependent variables, such as sediment sizes and amounts, hydraulic roughness, channel dimensions, and vegetation, and is difficult to quantify (Bull, 1979).

Bull (1979) has theorized that when the critical-power threshold is crossed, the stream system undergoes change. If the threshold is exceeded (stream power > critical power) net erosion occurs and the stream incises vertically; if these conditions are maintained long enough, the stream valley becomes narrow and V-shaped, and lacks terraces

(Fig. 46). In contrast, if stream power is less than critical power, alluviation occurs on a stream, resulting in a wide valley containing large amounts of alluvial fill. If conditions are close to the threshold, lateral erosion predominates (Fig. 46). Therefore, although only one component of the threshold ratio can be quantified, field evidence may indicate conditions above, close to, or below the threshold (Bull, 1979). These concepts can be used to interpret aggradational and degradational events which have occured along streams in the study area.

Rio Hondo Stream Power/Critical Power Relations

The relatively narrow Rio Hondo valley below the mountain front and a modern long-profile which grades to the Rio Grande suggest that this stream has been dominated by downcutting, and well-developed soils on higher terraces indicate that downcutting has occured through a long period of time. Above the mountain front, the narrow V-shaped Rio Hondo canyon and fresh hillslope colluvium suggest that substantial incision has occurred throughout the drainage basin. Nevertheless, six nearly parallel strath terraces below the mountain front and the 3 km-wide Arroyo Hondo valley indicate that downcutting has been periodically interrupted by episodes of lateral migration of the ancestral river.

Thus, it appears that stream power/critical power relations have varied through time on Rio Hondo. For example, threshold conditions apparently existed during formation of unit Qt2, but either increased stream power or decreased critical power promoted vertical erosion to the level of unit Qt3. Threshold conditions were then re-attained and Rio Hondo formed straths, on basalt near the Rio Grande and on basin-fill deposits in upstream reaches (Fig. 26). During similar threshold conditions lower terraces were formed due to lateral erosion and were

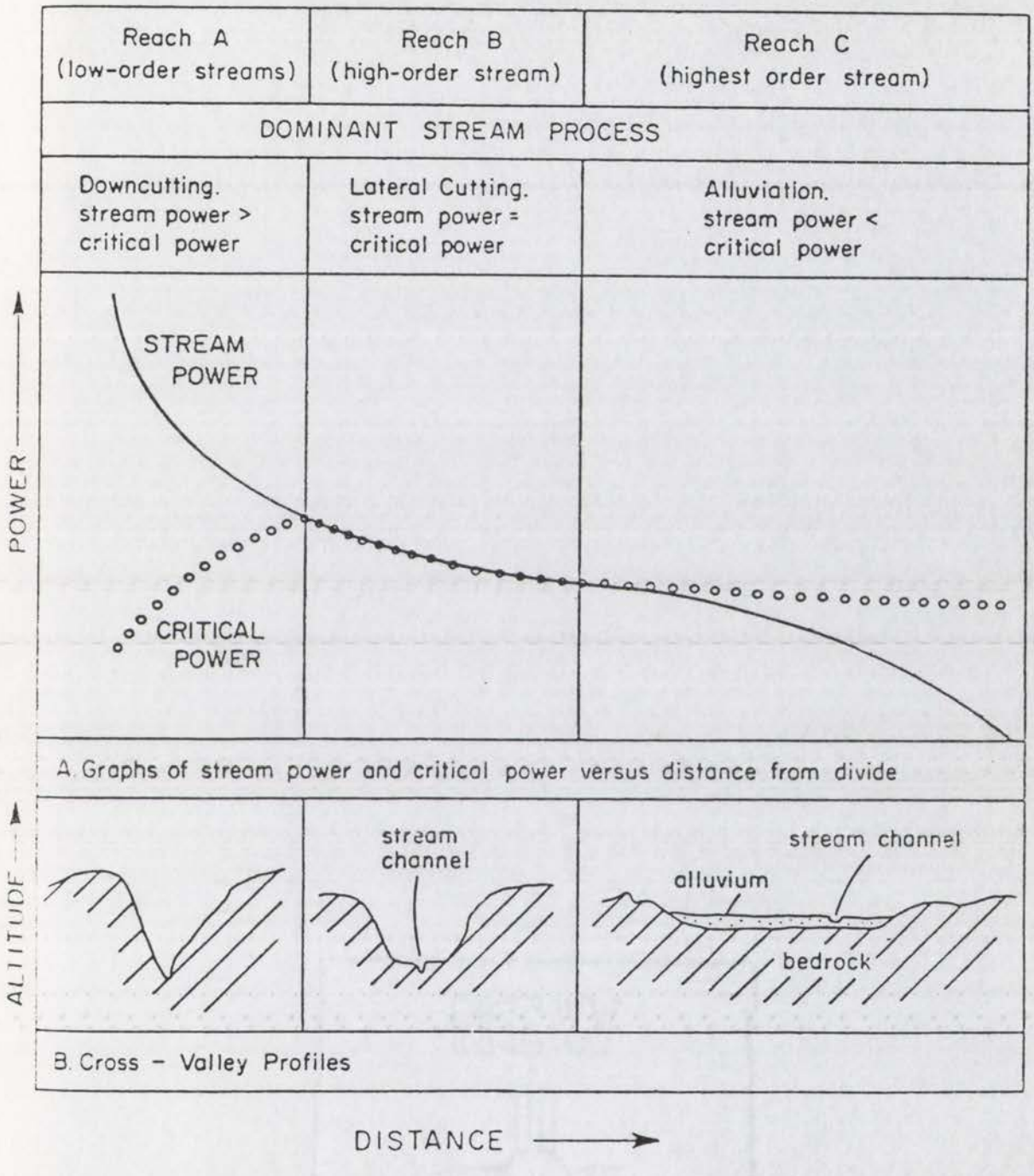

Figure 46. Diagrammatic sketch and graphs of stream power and critical power for an arid rocky drainage basin (from Bull, 1979).

later abandoned due to another exceedence of the critical-power threshold. Near the village of Arroyo Hondo (Plate 1), each cycle of floodplain formation and downcutting produced terrace treads lower in elevation and further to the east (upstream), thus producing the well-preserved sequence of inset strath terraces (Fig. 26).

Notably, the Valdez valley and the valley between the two dacitic bedrock constrictions (Plate 1) are narrow and show evidence of less lateral migration than in the Arroyo Hondo valley. For example, maximum paleofloodplain widths in the narrow middle valley (Fig. 26) could not have been wider than 1 km (as indicated by terrace widths), and were probably less than 0.5 km wide; the modern floodplain is about 100 m wide. Valley constrictions due to bedrock at both ends of the valley appear to have influenced the amount of lateral migration. Once Rio Hondo had incised into the bedrock, these constrictions apparently acted as lateral constraints, helping to preserve the terrace sequence.

Rio Hondo has therefore experienced two different modes of erosion. During periods of floodplain stability and moderate lateral migration, stream power apparently equaled critical power, and Rio Hondo was at threshold conditions. During periods of vertical erosion and floodplain abandonment, stream power exceeded critical power. Overall narrow valley morphology and narrow terraces (Fig. 26) suggest that vertical incision has dominated Rio Hondo behavior, but has been intermittently interrupted by periods of lateral erosion. It should be noted that absolute values of stream power and critical power are unknown.

These conditions can be compared to the present-day hydrologic setting. The present-day channel pattern is straight, and shows no evidence of lateral migration. In addition, dimensionless shear stress

data from all measurement sites greatly exceed critical values (Table 10), suggesting that Rio Hondo has sufficient energy to transport the imposed sediment (see above). If T^*_c values are analogous to critical power, which is reasonable because both represent conditions necessary for sediment transport, then it appears that stream power exceeds critical power in present-day channels. This relation is illustrated in Figure 47. Thus it appears that present-day conditions of high sediment transport are analogous to previous periods of downcutting and floodplain abandonment. Conversely, it appears that during times of floodplain stability and formation of terrace treads, the stream power/critical power ratio was less than the ratio present in the present-day system. Absolute values of stream power and critical power are unknown; values of stream power may have been higher during periods of floodplain stability than during periods of incision, if sediment loads were higher.

Rio Pueblo de Taos Stream Power/Critical Power Relations

Geomorphic evidence in the Rio Pueblo de Taos drainage basin suggests that stream power/critical power relations have been more complex than in the Rio Hondo basin. Above the mountain front (in region IV, see Fig. 6), two situations exist. The Arroyo Seco, Rio Lucero, Rio Pueblo de Taos, and Rio Chiquito valleys are narrow, and contain little alluvium. Apparently, stream power has consistently exceeded critical power in these basins, with downcutting predominating over lateral erosion. In contrast, the Rio Grande del Rancho valley contains at least two strath terraces above a wide valley floor (Plate 3), suggesting that both lateral erosion and downcutting have occurred in the past.

Region V (see Fig. 6) contains evidence of two modes of erosion as

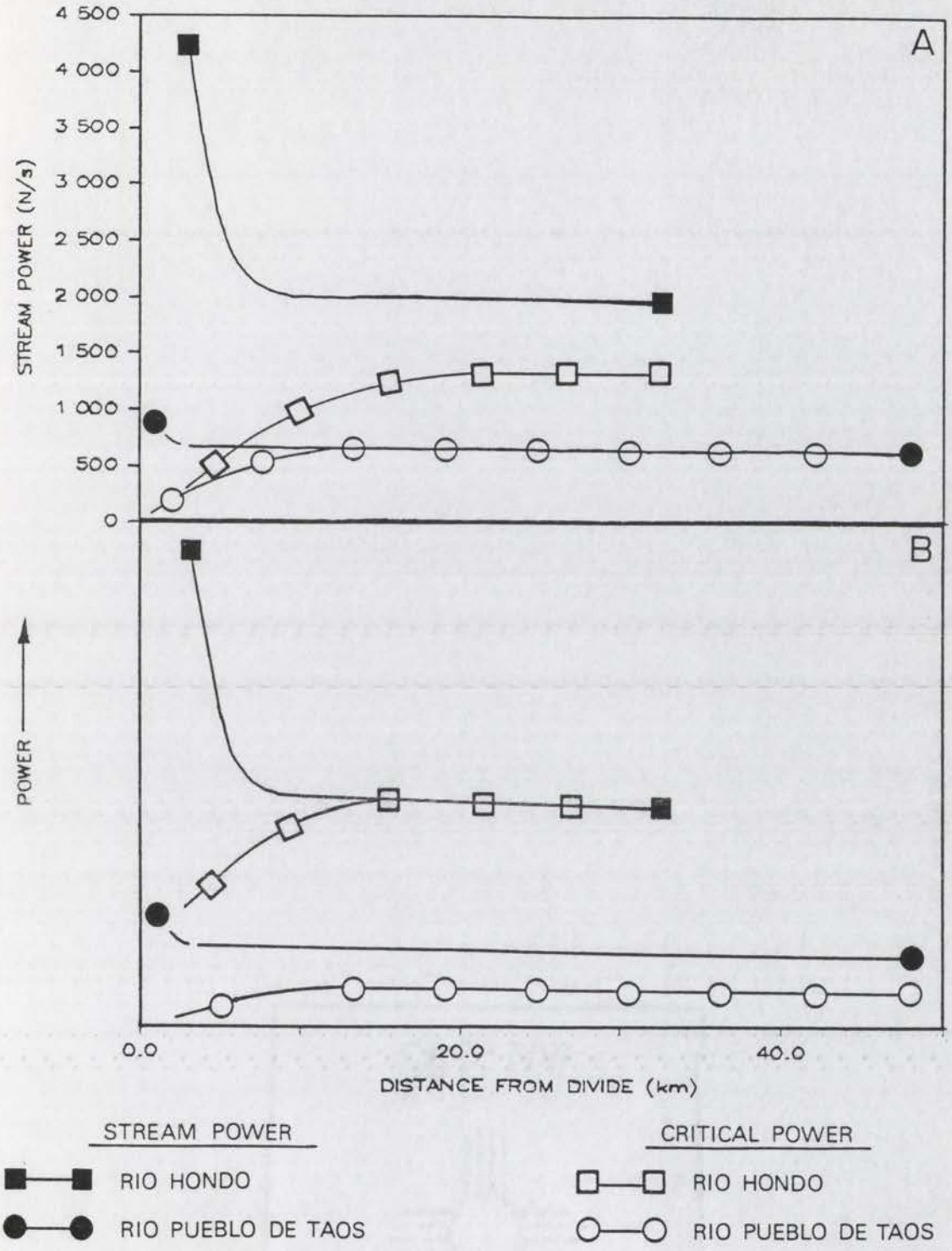

Figure 47. Diagrammatic sketches of stream power and critical power along Rio Hondo and Rio Pueblo de Taos. (A) present-day system, representing dominant mode of behavior along both streams. (B) past conditions, representing less prevalent mode of behavior. Stream power curves are based on Figure 21. Critical power curves are estimated based on negligible changes in hydraulic roughness as estimated by Manning n-values (Tables 4 and 5), and differences in bed-material grain sizes along Rio Pueblo de Taos and Rio Hondo (Fig. 17).

well. Wide valleys, few surfaces, and low relief between surfaces (Fig. 34) indicate that lateral erosion has predominated over vertical erosion. However, downcutting has induced periodic floodplain abandonment and thus terrace formation. Below the Los Cordovas confluence, divergent long-profiles of geomorphic surfaces and a slightly narrower valley suggest that downcutting has been somewhat more prevalent than above the confluence. Nevertheless, incision has been less in region V than on the Rio Hondo.

Stream power/critical power relations have apparently varied through time along main channels in region V and along Rio Grande del Rancho above the mountain front. During periods of floodplain stability and extensive lateral migration, stream power was close to critical power, and the streams were at the critical-power threshold. During periods of incision, stream power exceeded critical power, resulting in the abandonment of surfaces $Q1_p$ through Qt6. In general, wide valleys and low relief between surfaces in the Rio Pueblo de Taos system suggest that lateral erosion has been the predominant mode of stream behavior since surface $Q1_p$ time.

Several lines of evidence indicate that stream behavior on Rio Pueblo de Taos tributaries in the geologic past is comparable to present-day behavior. Wide valley floors and terraces are indicative of past floodplain stability. Active-channel lateral migration and unentrenched valley floors suggest present-day floodplain stability; in addition, dimensionless shear stress data indicate the presence of threshold channels (Lane, 1953) at sites 29 and 33 (Plate 2). If critical shear stress values are analogous to critical power (as noted above), the active channels appear to be near the critical-power threshold (Fig. 47).

Conversely, it appears that during periods of downcutting in the past, the stream power/critical power ratio exceeded present-day values.

In summary, it appears that Rio Hondo has been dominated by periods of vertical erosion, which were interrupted by periods of lateral erosion. Rio Pueblo de Taos has been dominated by periods of lateral erosion, which were interrupted by periods of downcutting. It also seems that present-day conditions reflect the predominant condition in each of the systems: exceedence of the critical-power threshold along Rio Hondo and threshold conditions along Rio Pueblo de Taos.

Long-term Fluvial System Adjustments to External Variables

The main goal of this research is to determine the factors which have produced the vastly different long-profiles, terrace sequences, and valley morphologies within the Rio Hondo and Rio Pueblo de Taos drainages. As noted above, time, relief, lithology, and climate are independent variables which affect fluvial systems at the cyclic time scale (see Table 1; Schumm and Lichty, 1965). Relief, lithology, and climate all appear to have substantial influences on present-day hydrologic conditions in the study area, and these factors must be addressed in order to investigate the production of different long-profiles, terrace sequences, and valley morphologies on Rio Hondo and Rio Pueblo de Taos during the Quaternary.

Influences of Time

Difficulties commonly arise in studying drainage basin development due to the lack of a known temporal starting point. Space-time substitutions in rapidly eroding badlands (Schumm, 1956) and documentation of network development on up-faulted lake beds (Morisawa,

1964) are examples of avoiding an unknown basin history in fluvial research.

In this study, continuous beds of 4.5 to 3.6 Ma Servilleta Basalt underlying the Taos Plateau (Peterson, 1981; see also Fig. 1) provide a known temporal control on early Quaternary base levels. The fact that surfaces Qls_P, Qtl_{RG}, and Qt2 are continuous either along the western rim of the Rio Grande gorge or on the Taos Plateau suggests that the Rio Hondo and Rio Pueblo de Taos drainages have developed on the plateau over the same amount of time. Similarity of argillic and calcic horizons in soils in both valleys (Table 18) supports this contention.

Analysis of stratigraphy within the Rio Grande, Rio Hondo and Rio Pueblo de Taos gorges (Peterson, 1981; Leininger, 1982) has revealed laterally discontinuous gravel lenses in the vicinity of Rio Hondo and Rio Pueblo de Taos. Peterson (1981) interprets these as late Tertiary alluvial fans deposited by the ancestral Rio Hondo and Rio Pueblo de Taos systems in between discrete pulses of Servilleta Basalt. Thus it appears that the position of the two streams below the mountain front has not changed since Tertiary time (Peterson, 1981).

As a drainage network evolves, area-relief relations change, which allows comparison of newly-evolved and equilibrium basins (Schumm, 1956). Schumm (1956) and Strahler (1952) found that sigmoidal hypsometric curves with integrals between .40 and .60 represent stabilized basins, in which material is being removed but area-relief relations do not change. Similarity of hypsometric curves between lithologic terranes (Fig. 24), and integrals near 0.50 (Table 12) suggest that these basins are in similar "stages" of development. In conclusion, time of development of these basins as a factor influencing discharge and sediment

characteristics is apparently not important.

Effects of Relief and Lithology During the Quaternary

Relief in the Rio Hondo and Rio Pueblo de Taos basins has probably changed through time due to uplift and erosion. However, the differences in relief between the two lithologic terranes (above the mountain front) probably has not changed since incision along the Rio Grande. Rates of uplift along the 35 km of Sangre de Cristo mountain front within the study area appear to be spatially consistent. Personius and Machette (1984) and Menges (in prep.) have collected data indicating that recurrent Pliocene-to-late Pleistocene faulting has occurred along most of the front between Rio Grande del Rancho and the piedmont north of Rio Hondo. It is reasonable to assume that the present differences in relief between the crystalline and sedimentary terranes are not due to post-Pliocene differential uplift along the mountain front. Thus the only significant change in relief which this study is concerned with has been due to incision of the Rio Grande.

It can also be assumed that lithology has not changed through time in both of the basins. Thus, through the last 1.1 Ma (based on K-Ar dates of pumice deposits associated with surface Ql_p), fluvial system changes in the study area have not been due to changes in lithology. It appears that base-level conditions and climatic changes are the major variables which have induced fluvial adjustments in the two basins.

Effects of Base-level Lowering

Base-level change can be defined as a vertical change in streambed elevation within a short reach; such a perturbation may affect upstream and downstream reaches (Leopold and Bull, 1979). Base-level lowering can

produce vertical erosion by steepening channel gradient, thereby increasing stream power relative to critical power (Bull, 1979). Periods of base-level stability allow re-attainment of threshold conditions and formation of floodplains by lateral erosion, assuming that no other independent variables change (Bull, 1979). Effects of base-level fall at the mouths of Rio Hondo and Rio Pueblo de Taos due to Rio Grande incision are discussed below.

Effects of Base-level Lowering on Rio Hondo

Bull's (1979) suggestion that base-level fall increases stream gradient and induces downcutting may not be valid on the Rio Hondo. As noted above, surface $Q1_P$ lies above Servilleta Basalt near the Rio Grande and grades to surface $Qt1_{RG}$ (Fig. 28). Surface $Q1_P$ therefore represents the Rio Hondo valley floor before entrenchment of the Rio Grande. The steep (20 m/km) long-profile of surface $Q1_P$ parallels long-profiles of lower surfaces and the modern long-profile, indicating that Rio Hondo maintained a high gradient before and after base-level fall. Thus, it appears that base-level fall has not been the cause of steep gradients of surfaces along the Rio Hondo, which are probably due to high discharges and sediment transport rates. Nevertheless, the high gradient maintained on Rio Hondo has influenced this stream's response to base-level fall: it has provided (in conjunction with high discharge) the necessary stream power to downcut through the relatively resistant basalt capping the plateau.

Other evidence indicates that base-level fall could not have been the sole factor affecting behavior of the Rio Hondo during the Quaternary period. If this stream has maintained high stream power through time, which is likely due to lithologically-controlled high discharges, then Rio

Hondo surfaces would reflect temporary stability of the Rio Grande. It appears that terraces do not occur within the Rio Grande gorge. Although preservation of terraces within the Rio Grande gorge may have been affected by abundant landslides which occur near the mouth of Rio Pueblo de Taos (see Peterson, 1981), large terrace remnants do not occur on the Rio Grande between Rio Hondo and the Rio Grande Gorge Bridge (Fig. 1), where landslides are not common. These observations suggest that downcutting along the Rio Grande may have been non-episodic. Apparently, factors other than episodic incision along the Rio Grande have induced periodic floodplain stability on Rio Hondo.

Thus, the cycle of floodplain stability and incision, which produced the strath terrace sequence, has apparently not been controlled by base-level fall. The major influence of base-level fall on Rio Hondo seems to have been to allow the stream long-profile to shift to lower elevations without affecting long-profile shape or gradient (Fig. 28). Mackin (1948, p. 498) stated that given enough time after base-level lowering, "the final adjusted profile will tend to parallel the original profile". This is supported by flume experiments performed by Begin et al. (1983), in which multiple base-level falls produced parallel long-profiles in the absence of bed armouring. Long-profile shape and gradient were not affected by the base-level falls (Begin et al., 1983, p. 54). The Rio Hondo terrace long-profiles are parallel, and are thus similar to long-profiles produced in the experimental study of Begin et al. (1983). Apparently, base-level fall has affected Rio Hondo's long-profile position in space, but has not affected long-profile shape or gradient (see Fig. 28 or Table 14).

Effects of Base-level Lowering on Rio Pueblo de Taos

Rio Pueblo de Taos has responded to base-level fall differently than Rio Hondo. The presence of a 140 m-high nickpoint between Los Cordovas and the Rio Grande indicates that this stream has not been able to keep pace with entrenchment on the master stream. It appears that Rio Pueblo de Taos is graded to a local base-level formed by basalt near the present-day long-profile nickpoint (Fig. 36). However, base-levels during periods of stability on surfaces Qt2, Qt3, Qt4, and Qt6 appear to be further downstream and higher in elevation (Fig. 36). Thus, although Rio Pueblo de Taos has experienced relatively minor lowering of local base-level, incision of the Rio Grande has not significantly influenced stream behavior.

This situation is similar to conditions on an abandoned meander loop of the San Juan River described by Leopold and Bull (1979). Aggradation and degradation has occurred within the meander loop although the San Juan River has incised 40 m, indicating that the alluvial history of the tributary was not influenced by incision along the master stream. Apparently, the Rio Pueblo de Taos alluvial history has also been unaffected by incision along its master stream.

In Leopold and Bull's (1979) study, erosion of a local base-level had no influence on the system beyond a short distance upstream. In contrast, erosion of the Rio Pueblo de Taos bedrock nickpoint may have had an effect on upstream reaches. Erosion of the basalt within the Rio Pueblo de Taos gorge has lowered local base-level; at the present-day nickpoint, the streambed has been lowered about 27 m since surface Qt2 time (Fig. 36). Divergent long-profiles of surfaces in the Arroyo Seco, Rio Lucero, and Rio Pueblo de Taos valleys indicate that the lowering of

local base-level has progressively steepened reaches upstream of the nickpoint. In context of the critical-power threshold, this lowering of local base-level probably increased stream power and possibly promoted downcutting. Although the Rio Pueblo de Taos has not been able to keep pace with incision on the Rio Grande, local base-level lowering indirectly related to Rio Grande entrenchment may have influenced the alluvial history of upstream reaches.

Differences between the responses to base-level fall on Rio Pueblo de Taos and Rio Hondo appear to be analogous to downcutting near the Wildrose Graben in eastern California (Leopold and Bull, 1979). Quaternary movement along a vertical fault has lowered base-level for several streams draining to the east side of the graben. Stream channels draining small areas above the fault have remained unentrenched, although a larger stream has been able to erode the piedmont fault scarp and has become entrenched in upstream reaches. Leopold and Bull (1979) conclude that higher discharge and stream power on the larger stream have enabled it to respond differently to the base-level fall. Although Rio Hondo has a smaller drainage area than Rio Pueblo de Taos, it has higher present-day stream power (Table 11). Apparently, high stream power over long periods of time has enabled Rio Hondo to erode the basalt near the Rio Grande, but the Rio Pueblo de Taos has not had sufficient stream power to erode the basalt nickpoint.

In conclusion, the two streams have responded differently to base-level lowering. High discharges produced by crystalline terrane has enabled the Rio Hondo to incise vertically and maintain grade with the Rio Grande. Steep, parallel long-profiles of geomorphic surfaces indicate that high stream power controlled the Rio Hondo's response to

base-level fall throughout the last 1.1 Ma. In contrast, Rio Pueblo de Taos has not been able to keep pace with Rio Grande entrenchment, possibly due to insufficient stream power, although local base-level falls have apparently promoted minor downcutting and floodplain abandonment.

Effects of Climatic Change

Climatic fluctuations may produce major changes in river activity (Schumm, 1977; Leopold and Bull, 1979), due to changes in the stream power/critical power ratio (Bull, 1979). Major Quaternary climatic shifts in the Sangre de Cristo Mountains consisted of several episodes of glaciation and deglaciation (McCalpin, 1982; Richmond, 1965). Because of considerable debate on the magnitude and timing of Quaternary precipitation and temperature shifts (Porter et al., 1983), two simplifying assumptions will be made for the purposes of this study. First, glacial periods were presumably cooler and wetter or cooler and drier than modern climates; second, interglacial periods were similar in climate to modern conditions. Possible effects of shifts between glacial and interglacial periods on Rio Hondo and Rio Pueblo de Taos behavior are discussed below.

Effects of Climatic Change on Rio Hondo

Glaciation has been relatively extensive in the Rio Hondo basin. Approximately 30% of the drainage area has been glaciated, as estimated from topographic maps, field evidence and aerial photographs. Richmond (1962) has mapped Bull Lake, Pinedale, and Neoglacial deposits along the Lake Fork branch of Rio Hondo (see also Fig. 41).

Glaciation clearly influences hydrologic conditions. Glacial

processes control downstream hydrology by producing large amounts of water and sediment which overwhelm the ability of a stream to remove the imposed load (Fahnestock, 1963), and glacial retreat usually results in significant aggradation (Fahnestock, 1963; Schumm, 1977). Following the end of glacial erosion and removal of glacial debris from a valley, incision may occur due to oversteepened valley gradients (Schumm, 1977).

On Rio Hondo, two modes of river activity have occurred: degradation and floodplain stability. Because the present-day Rio Hondo appears to be above the critical-power threshold (see above), and because interglacial climates were probably similar to modern climates, downcutting on Rio Hondo may have occurred during glacial retreat or during interglacial periods. However, evidence of significant aggradation due to high sediment loads during glacial activity does not exist. Lack of depositional terraces in the Rio Hondo valley suggests that stream power has always remained as high as or equal to critical power. During periods of lateral erosion (indicated by strath terraces), it appears that if critical power increased due to higher sediment loads, stream power was still sufficient to maintain threshold conditions (Fig. 47). If lithology has controlled high discharges during Quaternary time, as postulated above, then it is likely that Rio Hondo maintained relatively high stream power during glacial episodes. Stream power high enough to transport glacially-derived sediment loads is probably not due to base-level fall (see above). Therefore, increased "critical power" due to glacial outwash may have temporarily prevented downcutting by forcing Rio Hondo to transport large sediment loads (Fig. 47). Incision probably resumed after the glacial material was flushed from the valley.

It has been postulated that Bull Lake and Pinedale glacial deposits

influence the timing of present-day discharges along Rio Hondo. This implies that discharge hydrographs during glaciations and before the Bull Lake glacial episode were not similar to present-day hydrographs, and that present-day hydrologic conditions cannot be extrapolated into the past. However, the *timing* of present-day discharges is controlled by glacial deposits, but the *magnitude* of discharge is influenced primarily by runoff/infiltration relationships, which are ultimately controlled by underlying bedrock lithology. This is true even for areas underlain by glacial deposits; high return flow from glacial deposits underlying Lake Fork (Fig. 41) is probably ultimately linked to impermeable crystalline bedrock underlying the glacial deposits. Therefore high discharges (and high stream power) were probably present on Rio Hondo before Bull Lake time.

High paleodischarges on Rio Hondo are indicated by a paleochannel exposed in a roadcut through unit Qt6 deposits near Arroyo Hondo (Fig. 48). Q_{bf} has been estimated for this channel using a roughness coefficient calculated from the grain-size distribution (pebble count PC18) (Limerinos, 1970), and an assumed bedslope of 0.020 m/m. The estimated Q_{bf} (110 m^3/s) is over 10 times that of the present-day Q_{bf} at nearby site 31 (see Plate 1). This estimate is probably high due to difficulty in bankfull identification, as well as estimations of roughness and slope. Nevertheless, discharge and therefore sediment transport appear to have been higher during unit Qt6 time than in the present-day system.

It is possible that surfaces Qt2 through Qt7 reflect changes in hydrologic conditions due to glaciation, but better age constraints are needed. As noted above, surfaces Qt6 and Qt7 may be related to Bull

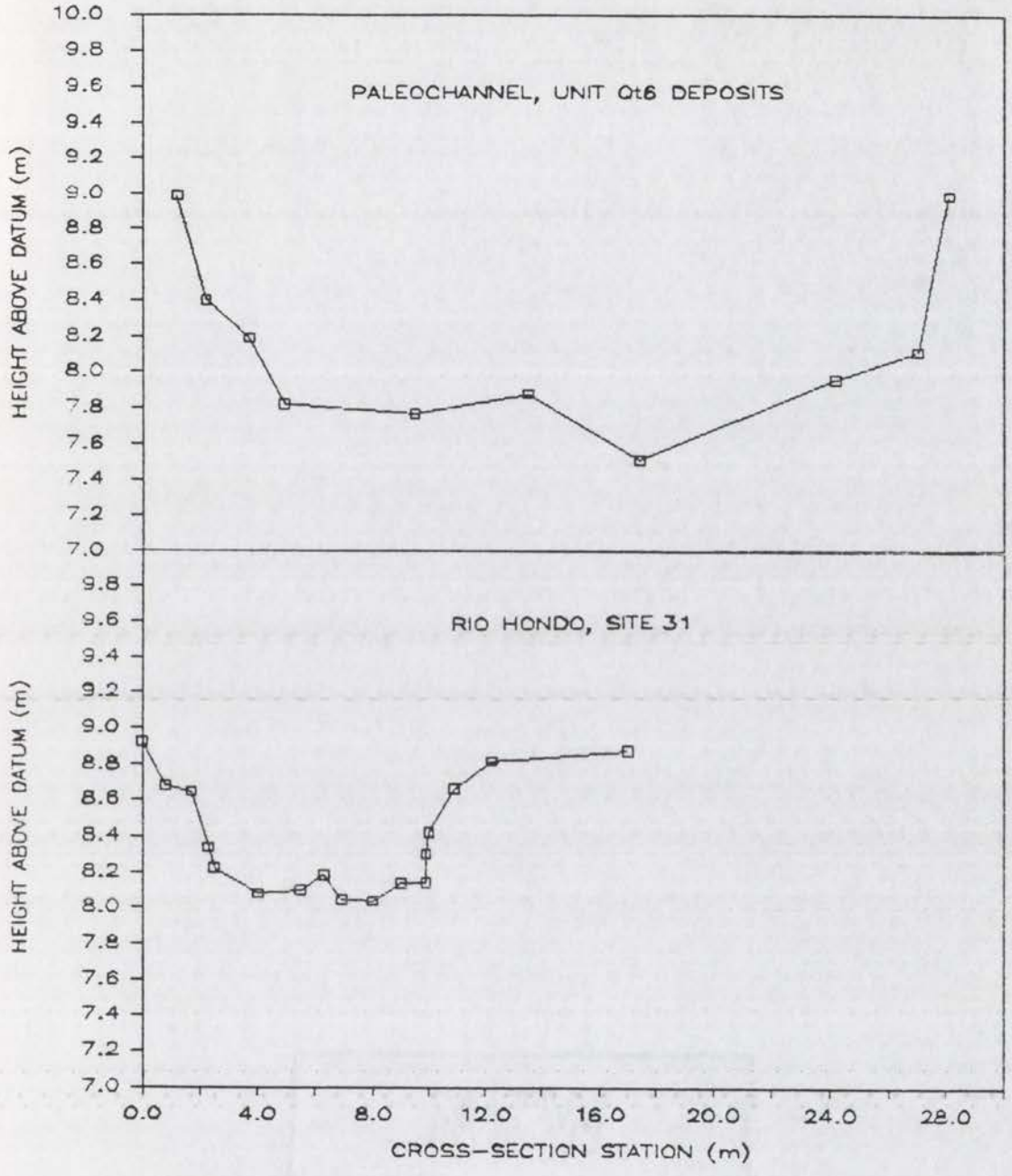

Figure 48. (A) Cross-section of paleochannel in deposits associated with surface Qt6 exposed in Highway 3 roadcut 0.4 km north of Arroyo Hondo. Estimated bankfull discharge = 110 m^3/s (see text). (B) Channel cross-section at site 31, 1.0 km west of Arroyo Hondo, plotted at same scale as (A). Estimated bankfull discharge = 10.9 m^3/s. See Plate 2 for locations.

Lake and Pinedale glaciations, respectively. Pre-Bull Lake alluvium occurs in the San Luis Valley (McCalpin, 1982). Gillam et al. (1985) found moraines of the Sacagawea Ridge glaciation near Durango, Colorado, and terrace gravels flanking the Animas River downstream of Durango which may be Cedar Ridge (?) and Washakie Point (?) outwash. Pre-Bull Lake glaciations probably occurred in the Taos Range, but geomorphic surfaces in the Rio Hondo valley cannot be linked to these glaciations.

Commonly, climatic change has been used to explain major variations in river behavior (Leopold and Bull, 1979; Gillam et al., 1984), and appears to be a probable influence (in conjunction with base-level fall) on terrace production on Rio Hondo. Lack of terraces within the Rio Grande gorge suggests that base-level fall for Rio Hondo may have been non-episodic, which suggests that Rio Hondo floodplain stability during surfaces Qt2 through Qt7 time was due to upstream or basin-wide controls. Such controls may have been changes in streamflow/sediment yield ratios produced by glaciations (Richards, 1982). In conclusion, it appears that Rio Hondo behavior during the Quaternary may have been due to effects of Quaternary climatic shifts superimposed on effects of base-level lowering.

Effects of Climatic Change on Rio Pueblo de Taos

Glaciation in the Rio Pueblo de Taos basin has been less extensive than in the Rio Hondo drainage. Approximately 9% of the total area above the mountain front has been glaciated, with about two-thirds of the glaciated region being within the Rio Lucero and Rio Pueblo de Taos drainages. Thus for most of the Rio Pueblo de Taos basin, changes to cooler climates were probably not associated with hydrologic changes linked to glacial activity.

Schumm (1977) described possible river responses to changes in climate, based on estimated hydrologic changes. For example, in unglaciated basins containing perennial streams, change to a cooler, wetter climate will generally result in erosion, assuming no changes in other independent variables (Schumm, 1977). This is based on estimated relations between mean annual runoff and precipitation (Langbein and Schumm, 1958) and on estimated relations between mean annual sediment yield and precipitation (Schumm, 1965). In a semiarid to subhumid region similar to present-day conditions in Taos, increased precipitation and decreased temperatures would probably result in increased runoff, and lower sediment yields. Channel erosion would probably result from higher streamflow/sediment yield ratios.

Along Rio Pueblo de Taos below the mountain front, two modes of river activity have occurred: floodplain stability and degradation. In contrast to the Rio Hondo system, present-day conditions suggest present floodplain stability and predominance of lateral erosion. If interglacial climates were similar to present-day climates, then lateral erosion probably predominated during interglacial periods.

If floodplain stability predominated during interglacial periods, then floodplain abandonment may have occurred during glacial periods. During periods of cooler climates, the majority of the Rio Pueblo de Taos basin was probably experiencing channel erosion due to higher runoff and lower sediment yields. Downcutting may have occurred during these periods (Fig. 47).

As noted above, however, lowering of local base-level at the Rio Pueblo de Taos long-profile nickpoint may have triggered incision. Nickpoint migration may occur in ephemeral streams underlain by valley

fill alluvium regardless of climatic change (Schumm and Hadley, 1957). However, the nickpoint for the perennial Rio Pueblo de Taos is underlain by basalt, and probably requires substantial increases in stream power in order to be lowered several meters. Increased runoff due to climatic change could provide an increase in stream power, and lower the local base-level formed by basalt bedrock. This self-enhancing mechanism may have triggered downcutting throughout the fluvial system. Thus it appears possible that the Rio Pueblo de Taos terrace sequence is a result of climatic and local base-level changes, and is only indirectly related to Rio Grande entrenchment.

Similarities between Rio Pueblo de Taos and the meander loop studied by Leopold and Bull (1979) are again apparent. These workers attributed aggradation and degradation on the meander loop to Holocene climatic changes. Incision of a master stream, as noted above, has not affected either the loop or Rio Pueblo de Taos. In both cases, then, it seems that climatic change has been the most influential variable affecting stream behavior.

Reasons for the lack of surfaces Qt5 and Qt7 on Rio Pueblo de Taos tributaries below the mountain front are uncertain. Both may have been formed but later destroyed by lateral migration, which is quite possible based on the predominance of lateral erosion in the Rio Pueblo de Taos system. Alternatively, Rio Pueblo de Taos may not have been as sensitive to the factors which produced and caused abandonment of surfaces Qt5 and Qt7 along Rio Hondo. Resolution of this uncertainty is difficult without better age control on depositional and erosional events in both watersheds.

Based on this interpretation of fluvial responses to climatic

change, terrace production in the two basins has apparently not been synchronous. For example, it appears the abandonment of surface Qt6 along Rio Pueblo de Taos may have occurred while surface Qt6 was still occupied in the Rio Hondo basin. Abandonment of the Rio Hondo surface Qt6 may have occurred during an interglacial period (after Bull Lake glaciation?), in which Rio Pueblo de Taos was characterized by lateral erosion. Correlation of surfaces between the two basins is therefore tentative without better age control, with the exception of the continuous surface $Q1_P$.

Along Rio Pueblo de Taos tributaries above the mountain front, stream behavior has apparently been more complex. For example, surfaces Qt6 and Qt7 occur as fill terraces along Rio Grande del Rancho near Ojo Sarco Canyon, but strath terrace remnants comprise unit Qt6 in downstream portions of the Rio Grande del Rancho valley (Plate 3). Also, upstream portions of the Rio Fernando de Taos valley are broad (Fig. 40) and contain significant amounts of valley fill alluvium. Downstream portions of the Rio Fernando de Taos valley (closer to the mountain front) are narrow and do not contain large amounts of valley fill alluvium. Although ages of depositional units in upstream portions of the valleys draining sedimentary rocks are unknown, it is possible that hillslope repsonses to climatic change resulted in the production of large amounts of sediment (relative to runoff) in small, low-order tributaries. Apparently, deposition in upstream valley reaches resulted from the inability of trunk streams to transport large amounts of imposed sediment. Further downstream (closer to the mountain front), the Rio Fernando de Taos and Rio Grande del Rancho main stems apparently could transport imposed sediment loads, resulting in strath terraces (along Rio

Grande del Rancho) and narrow valleys (in both systems). Therefore, deposition in response to climatic change may have occurred along tributaries to Rio Pueblo de Taos, but only in upstream portions.

Effects of Mountain-front Tectonic Activity

Vertical fault movement at a mountain front produces a base-level change for streams crossing the front and can trigger erosion and deposition along upstream and downstream reaches (Leopold and Bull, 1979; Schumm, 1977). Substantial uplift along the Sangre de Cristo mountain front has occurred since the Tertiary period (Personius and Machette, 1984), but has probably not varied along the small portion of mountain front in the study area.

Mountain-front tectonics may not have substantial effects on the production of the different long-profiles and terrace sequences in the two watersheds. In the Rio Hondo basin, base-level fall at the mountain front is probably negligible compared to the base-level fall experienced at the Rio Grande. In addition, if effects of large climatic changes have not triggered major aggradational events, it shows that the Rio Hondo has the ability to efficiently transport large amounts of sediment. Thus, relatively minor external stimuli, such as small intermittent uplift at the mountain front, probably has not influenced Rio Hondo behavior since incision of the Rio Grande.

The Rio Pueblo de Taos response to mountain front tectonic activity may be more complex, because this stream appears to be unable to keep pace with base-level fall. Lack of significant change in long-profile gradient at the mountain front along most tributaries suggests that they have been able to erode through mountain front fault scarps. However,

the Rio Grande del Rancho long-profile shows a slight convexity at the mountain front (Fig. 25). Also, offset of surface Qt6 above and below the front is about 10 m. In short, effects of mountain-front tectonics on the Rio Pueblo de Taos system is unknown. Better age control on the timing and amounts of uplift, and on aggradational and degradational events, is necessary to assess definitively the effect of tectonics on the Rio Pueblo de Taos system.

Complex Responses of the Fluvial Systems

The previous discussion is concerned primarily with "simple" fluvial system adjustments; that is, adjustments which are directly linked to changes in independent variables on the geologic time scale (Schumm and Lichty, 1965). However, Schumm (1973) and Womack and Schumm (1977) have shown that fluvial systems can have complex adjustments which are indirectly related to changes in independent variables. For example, entrenchment of a main stem may cause entrenchment along tributaries, a process which provides sediment to the main stem and may result in deposition along the master stream. Local oversteepening due to deposition then produces re-entrenchment of the main channel and propagates more changes along tributaries (Schumm, 1977). The result is several erosional and depositional terraces along the main stem, which may not correlate even within short distances in the same valley (Womack and Schumm, 1977).

Rio Hondo and Rio Pueblo de Taos do not appear to have adjusted in a complex manner to base-level and climatic changes. The fact that all terraces are straths indicates that complex cut-and-fill cycles did not occur below the mountain front. However, tributaries to the main Rio Hondo or the main Rio Pueblo de Taos tributaries were not mapped in

detail, and may show different histories than those of the main stems. Nevertheless, this study is concerned primarily with the history of the main stems, which apparently did not experience, or did not record, complex responses to base-level or climatic change.

Summary

Base-level fall and climatic change have affected the Rio Hondo and Rio Pueblo de Taos basins differently. Glaciation in the Rio Hondo basin apparently produced high sediment loads, which in conjunction with base-level fall and high discharge production resulted in lateral erosion and floodplain stability. Interglacial periods were probably characterized by degradation due to high streamflow/sediment yield ratios, as in the present-day system. It appears that high discharge, steep channel gradients, and high stream power on Rio Hondo have enabled this stream to respond to base-level fall by continued entrenchment. Rio Hondo terraces therefore appear to record climatic shifts superimposed on base-level lowering, and primarily reflect the ability of crystalline terrane to produce high runoff.

Response to climatic change in the Rio Pueblo de Taos basin was apparently different than on Rio Hondo due to lack of extensive glaciation. During glacial periods, probable high runoff/sediment yield ratios promoted incision, although total incision was less than on Rio Hondo. Interglacial periods appear to have been dominated by lateral erosion. Thus, the relative inability to incise vertically, apparently due to relatively low discharge production, prevented Rio Pueblo de Taos from keeping pace with entrenchment on the Rio Grande.

Leopold and Bull (1979, p. 195) stated, "the master stream as a

base-level has an effect only locally and has an influence that extends only a short distance up the tributary". The convex long-profile of Rio Pueblo de Taos supports this statement. However, downcutting along Rio Hondo in response to a similar base-level fall indicates that base level may influence tributaries for significant distances upstream. Apparently, a base level may affect tributary behavior if the tributary has the ability to erode the scarp or nickpoint produced by base-level fall; otherwise, other factors (such as climatic change) may be primary influences on river activity.

Therefore, it appears that discharge and stream power are primary determinants of a stream's response to base-level fall. Because discharge and stream power appear to be influenced by bedrock lithology in the study area, it seems that source-area lithology may have dramatically influenced these streams' adjustments to base-level fall. In conclusion, it appears that lithologically-controlled discharge strongly influences a basin's sensitivity to base-level change.

Grade and Equilibrium in Rivers on the Taos Plateau

The nature of an "equilibrium" or "graded" state in a fluvial system can be defined with reference to various time scales (Richards, 1982). Schumm and Lichty (1965) recognized that time and space considerations influence one's viewpoint of equilibrium and identified three time spans in which geomorphic systems may act. Many workers, notably Leopold and Maddock (1953), Hack (1957), Miller (1958), and Andrews (1979), have concentrated on short time spans, and have thus emphasized short-term equilibrium characteristics of fluvial systems. For instance, Hack (1957) and Leopold and Bull (1979) have suggested that where slope is related to bed-material grain size and discharge, the channel has

adjusted to the water and sediment imposed from upstream and is in equilibrium. Thus, data collected during short periods of time have been used to infer conditions of equilibrium on longer time scales.

Other workers, notably Bull (1979) and Schumm (1968), have attempted to infer fluvial system change by assessing longer term records, such as valley morphology and paleochannel characteristics. Bull (1979, p. 453) states that "although a tendency toward equilibrium conditions exists in streams, the attainment of graded conditions for long periods of time may be unlikely for many reaches of streams". Apparently, external inputs to fluvial systems are constantly varying, creating conditions which are conducive to change instead of attainment of equilibrium (Bull, 1979). Thus at longer time scales, river behavior is best described via the concept of thresholds. Schumm (1977) used the term "dynamic metastable equilibrium" to describe fluvial behavior over long periods of time (millions of years), which stresses that periodic erosion is due to threshold exceedence. Bull's (1979) critical-power threshold is an example; when a stream is at the critical-power threshold (when stream power/critical power = 1.0), it is in "equilibrium", and when above or below the threshold the stream is out of equilibrium (Bull, 1979).

Short-term equilibrium status on Rio Hondo and Rio Pueblo de Taos can be assessed using shear stress data. As noted before, present-day Rio Hondo is dominated by stable and unstable, mobile-bed channels (Table 19). Shear stresses exceed critical values at every measurement site, indicating probable high bedload transport at bankfull discharge. Rio Pueblo de Taos below the mountain front, on the other hand, appears to have generally stable channels and shear stresses close to critical values. Thus, Rio Hondo is probably in a degradational state and Rio

Pueblo de Taos is probably in equilibrium with imposed water and sediment discharges.

Over the scale of hundreds of thousands of years, both streams appear to have fluctuated between floodplain stability and incision. Both basins appear to have responded to the exceedence of the critical-power threshold, resulting in incision, and to have re-attained threshold conditions. Causes of changes in the relative amounts of stream power and critical power may have been base-level or climatic change. Thus, it appears that the concept of dynamic metastable equilibrium (Schumm, 1977) applies to the complex alluvial history of these watersheds.

Fluvial Geomorphic History

Determination of the exact chronology of Quaternary events along Rio Hondo and Rio Pueblo de Taos is difficult without reliable age control of aggradational and degradational events. Figure 49 schematically illustrates the postulated sequence of fluvial events in the study area. After the final late Cenozoic (post-3.6 Ma) extrusion of Servilleta Basalt on the Taos Plateau, aggradation occurred below the mountain front along the ancestral Rio Hondo and Rio Pueblo de Taos drainages, as coalescent alluvial fans sloping to the west. Aggradation proceeded to the level of surface $Q1_P$, at which time base-level for the area was the elevation of surface $Qt1_{RG}$ along the ancestral Rio Grande. A K-Ar age-date on volcanic deposits (Izett et al., 1981) associated with surface $Q1_P$ suggests that aggradation ceased sometime after 1.1 Ma.

Alternation of periods of lateral and vertical erosion dominated later events on Rio Hondo and Rio Pueblo de Taos below the mountain front. These events appear to have been nonsynchronous between the two

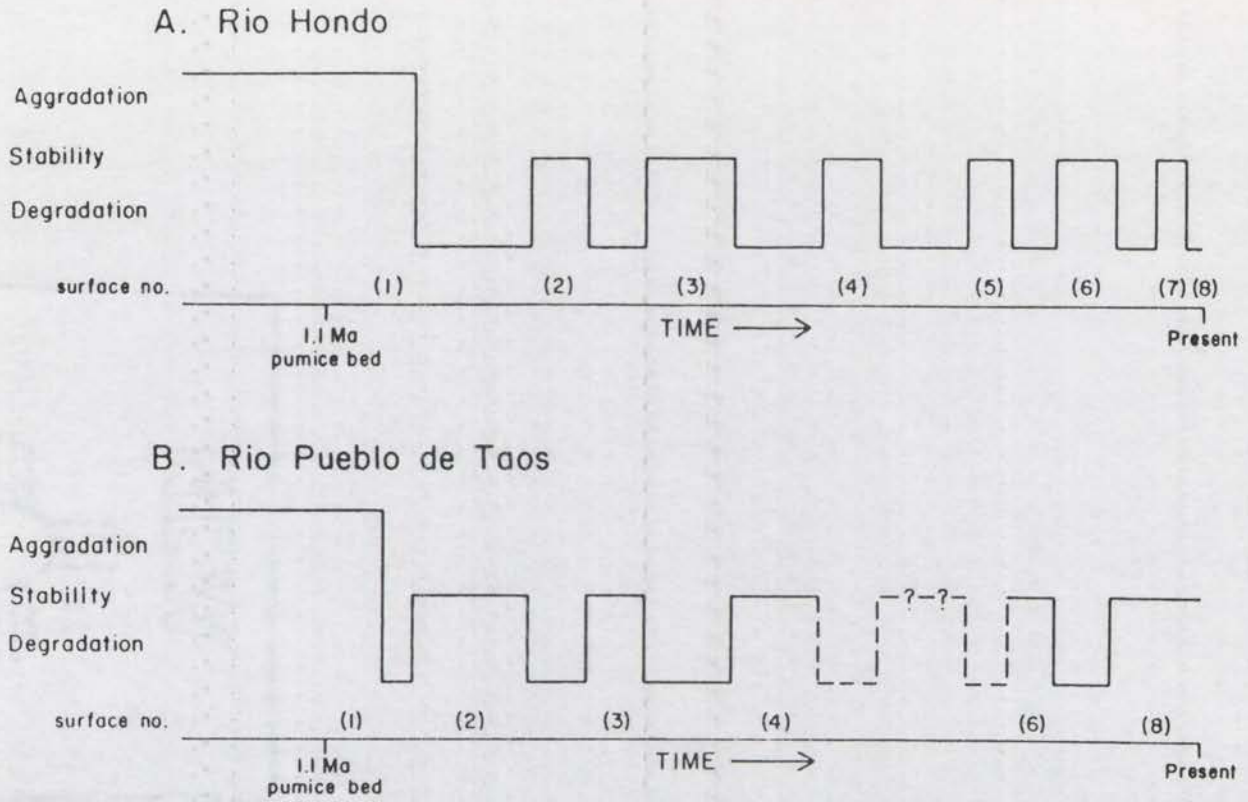

Figure 49. Schematic representation of inferred aggradation and degradation through time. Change from stability to degradation on Rio Hondo is shown as being contemporaneous with change from degradation to stability on Rio Pueblo de Taos; these events may not have been synchronous.

basins. Downcutting into basin-fill deposits along both streams lowered channels to the elevation of surface Qt2; if incision was a direct result of climatically-induced hydrologic changes, post-incision stability and lateral migration on Rio Pueblo de Taos most likely occurred as incision began on Rio Hondo (Fig. 49). Later, Rio Pueblo do Taos incised to the level of surface Qt3, which possibly coincided with a time of floodplain stability and formation of surface Qt2 on Rio Hondo. Similar alternations of vertical and lateral erosion probably occurred in the study area to at least Rio Hondo surface Qt4 time. Surface Qt5 occurs only near Rio Hondo, which probably reflects destruction of this terrace via lateral migration along Rio Pueblo de Taos.

Abandonment of surface Qt6 in the Rio Pueblo de Taos valley system may have occurred while lateral erosion was producing surface Qt6 on Rio Hondo; soil profiles suggest this may have followed Bull Lake glaciation. Surface Qt7 probably reflects a late stade of Pinedale glaciation in the Rio Hondo basin, based on soil development. Presence of surface Qt7 in the Rio Grande del Rancho valley above but not below the mountain front implies that responses to this climatic change may have been fairly localized in the Rio Pueblo de Taos watershed. The present-day Rio Hondo is characterized by high discharge production, high sediment transport and probably vertical erosion; the present-day Rio Pueblo de Taos is characterized by lateral erosion and floodplain stability.

CONCLUSIONS

1) At six streamflow gaging stations in the study area draining either crystalline or sedimentary terrane, bankfull discharge and discharge per unit area at all flow stages are higher at stations draining crystalline terrane. High discharge is sustained for longer periods of time at stations draining crystalline rocks.

2) Lithology strongly influences the duration and magnitude of present-day discharge by controlling runoff and amounts of return flow after storage in glacial deposits.

3) Bed-material grain size, competence, unit stream power and shear stress data suggest that channels draining crystalline rocks can transport larger bed material at higher rates than channels draining sedimentary rocks. Transport rates may be up to four times higher along Rio Hondo than along Rio Pueblo de Taos.

4) Basins underlain by crystalline rocks have higher relief, higher relief ratios, narrower valleys, and more drainage area within higher elevation zones than basins underlain by sedimentary rocks. Drainage density, drainage frequency, and long-profile concavity are also higher in crystalline terrane.

5) Present-day differences in discharges between the two terranes probably existed in late Quaternary time, as suggested by: a) lithologically-controlled present-day discharge characteristics, b) association of present-day discharge characteristics with stream long-profile concavity, and c) parallel long-profiles of geomorphic surfaces.

6) Six fairly continuous, nearly-parallel inset strath terraces occur in the narrow Rio Hondo valley; two discontinuous and two fairly continuous, divergent inset strath terraces occur in the wide Rio Pueblo

de Taos valley. All terrraces were formed on either late Tertiary(?)-early Quaternary basin-fill deposits or 4.5 to 3.6 Ma Servilleta Basalt.

7) The two highest geomorphic surfaces (Q1 and Qt2) overlie Servilleta Basalt, and therefore pre-date entrenchment on the Rio Grande. A K-Ar age-date of 1.12 ± 0.03 Ma (Izett et al., 1981) on deposits associated with surface $Q1_p$ indicate that the Rio Grande near Taos began entrenchment in the early Quaternary.

8) Terrace sequences indicate that Rio Hondo has been dominated by vertical erosion interrupted by periods of lateral erosion, and that Rio Pueblo de Taos has been dominated by lateral erosion interrupted by periods of vertical incision. Present-day conditions appear to reflect the dominant mode of each river's past behavior.

9) The Rio Hondo terrace sequence, longitudinal-profile, and valley morphology appear to be due to effects of climatic change superimposed on effects of base-level fall. On Rio Pueblo de Taos, these features appear to be due primarily to effects of climatic change and effects of minor local base-level lowering.

10) Rio Hondo has been able to keep pace with Rio Grande entrenchment. Base-level fall has allowed this stream's long-profile to shift to lower elevations, but has not affected long-profile gradient or shape. Similar base-level fall on Rio Pueblo de Taos has affected long-profile shape and gradient only in the lower 5 km of this stream, indicating that it could not keep pace with incision on the Rio Grande.

11) Discharge and stream power appear to be primary determinants of these streams' responses to base-level change. Because discharge and stream power are controlled by lithology, it appears that source-area lithology strongly influences a basin's sensitivity to base-level change.

APPENDIX A

Methods and assumptions used in snowmelt-runoff water budget calculations

An analysis of the snowmelt-runoff water budgets has been made in an attempt to understand discharge production processes within the mountainous study basins. Water balance equations take the general form: Input - Output = Storage Changes (Todd, 1980), and can be modified for snowmelt conditions to (Viessman et al., 1977):

$$P + M - R - L = S \qquad (A1)$$

where P = net rainfall, M = snowmelt, R = runoff, L = losses to evapotranspiration, and S = storage changes. Storage changes include changes in soil moisture and changes in channel, depression, detention, snowpack, and groundwater storage (Viessman et al., 1977).

Estimation of mean monthly precipitation requires development of elevation-precipitation curves for areas of high relief; Figure 7 shows precipitation data from six stations within or near the study area for each month characterized by substantial snowmelt. Each study basin was divided into seven 250-m elevation zones, and mean monthly precipitation for the midpoint of each zone was calculated using relations shown in Figure 7. Multiplying these values by the percentage of basin area within each zone provided areally weighted mean monthly precipitation values for each zone, which were then summed to obtain a weighted mean monthly precipitation (P) for each basin (Fig. A1).

Snowmelt is a function of several factors (Viessman et al., 1977), but in heavily forested areas which experience rainfall (and therefore cloud cover) during snowmelt, such as in the Taos Range, snowmelt can be

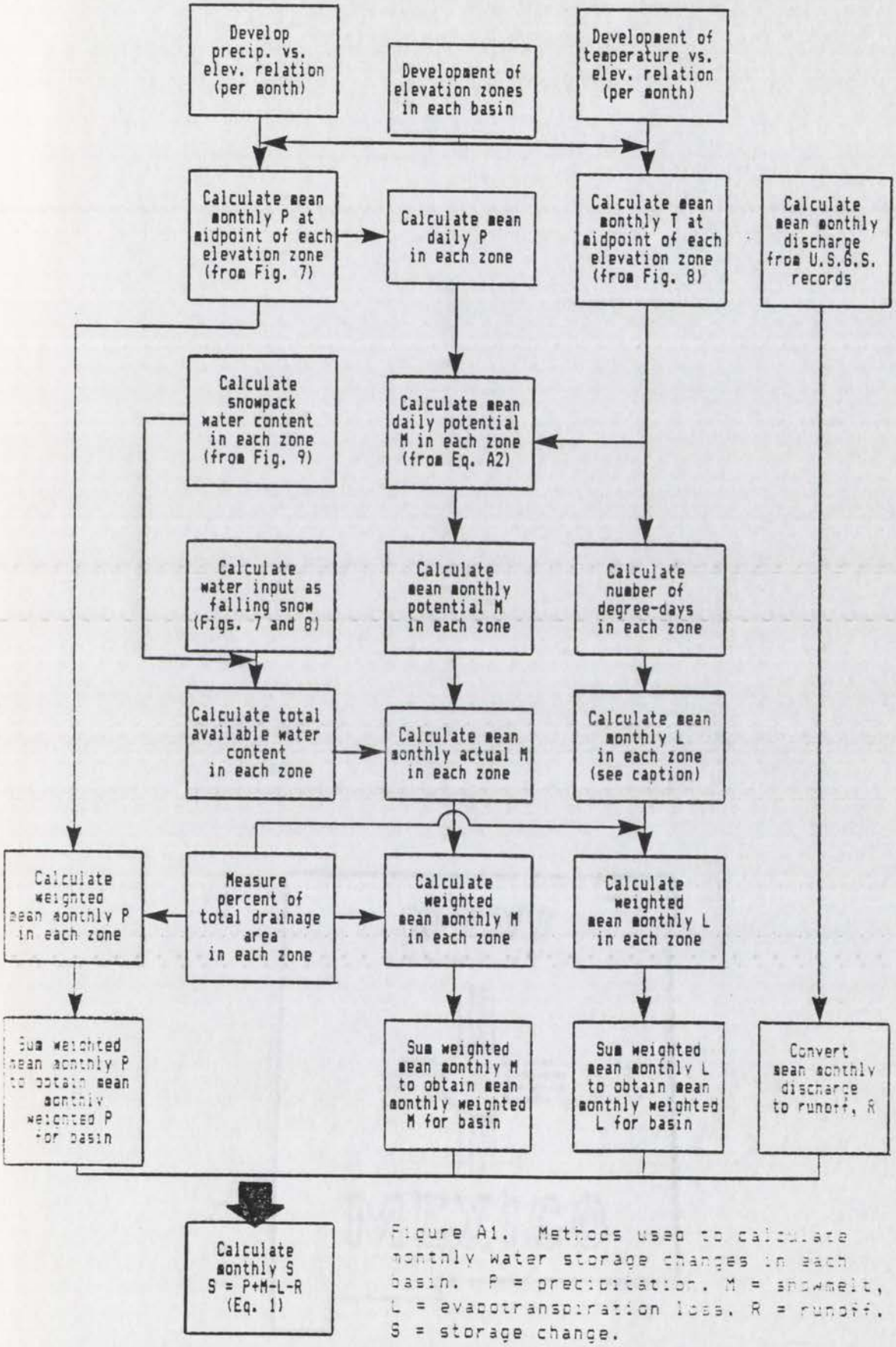

Figure A1. Methods used to calculate monthly water storage changes in each basin. P = precipitation, M = snowmelt, L = evapotranspiration loss, R = runoff, S = storage change.

estimated using the equation (U. S. Army Corps of Engineers, 1956):

$$M = (0.074 + 0.007*P)*(T - 32) + 0.05 \qquad (A2)$$

where M = daily snowmelt (in/day), P = rainfall (in/day), and T = temperature of saturated air at 10-ft level (°F). Effects of elevation on temperature require development of temperature-elevation curves for each month of interest. Figure 8 shows these relations for the period April-July, using data from four nearby stations (State Engineer Office, 1956). Mean monthly temperature was calculated for the midpoint of each elevation zone; these values were used in equation (A2) to calculate mean daily potential snowmelt and hence mean monthly potential snowmelt for each zone (Fig. A1). Actual snowmelt may be more or less than potential snowmelt; the difference is dependent on: (1) loss of snowpack due to melting, and (2) additions to the snowpack from snowfall. These possibilities are addressed below.

The Soil Conservation Service maintains several snow depth and water content measurement sites within and near the study area (Washichek et al., 1972; Washichek et al., 1978). Measurements near April 1 of each year allow estimation of available water within each basin at this time. Figure 9 shows the variation of snowpack water content on April 1 with elevation; using this relation, the amount of available water at the midpoint of each elevation zone has been estimated. Additions to this water mass from post-April 1 snowfall occurs usually during April and May, and generally only at higher elevation; elevation zones which have precipitation (Fig. 7) and mean monthly temperatures lower than 32°F were assumed to have snowfall. Therefore, snowmelt and rainfall values of zero were used in further calculations involving these zones. In addition, a water content of 10% (Viessman et al., 1977) was assumed for

the snowfall, and water contents of 0.10 * P for each elevation zone were then added to the actual April 1 water content for the zones as derived from the relation in Figure 8 (see Fig. A1).

On April 1, then, the average amount of available water as measured by the Soil Conservation Service is increased (at higher elevations only) by snowfall, and decreased (at low elevations) by snowmelt. At low elevations the potential monthly snowmelt is subtracted from the available water content each month until the snowpack is gone. At high elevation, subtraction from potential snowmelt values begins when snowfall ceases (usually in May or June), and continues until the snowpack is gone. Calculations indicate that only the uppermost elevation zone (above 3750 m) contains water left as snow at the end of July, which agrees with field observations. Net monthly snowmelt values per elevation zone are then weighted by percentage of basin area in that zone, and then summed to obtain a mean monthly basin snowmelt (M) value (Fig. A1).

Monthly evapotranspiration losses for each elevation zone were determined from graphical relationships given by the U. S. Army Corps of Engineers (1956), which use the number of degree-days above 32°F per month as a heat index. Mean monthly basin evapotranspiration (L) were determined by areal weighting (Fig. A1). Monthly runoff (R) values was calculated from U.S.G.S. streamflow records. Using values of P, M, L, and R, changes in storage (S) have been calculated by equation (A1).

Assumption of linear dependence of precipitation, temperature and available snowpack water content on elevation may not be justified. Extrapolation of the curves to high elevations may also introduce error to the calculations.

APPENDIX B

XSECTION: Pascal-language program

for calculation of water discharge using slope-area method

(for IBM-compatible microcomputers)

```
program xsection;
  var
    Count, StaNoLB, StaNoRB, h, i, j, k, l                    : integer;
    Thal, Atot, W, D, F, R, P, N, S, C, V, CON, Fr            : real;
    LBSta, RBSta, ThalSta, Bf                                 : real;
    Site                                                      : string[40];
    Choice                                                    : string[1];
    Sta, Elev          : array[0..40] of real;

{*****************************************************************************}

  procedure CreateFile;
    var
      Station, Elevation        : real;
      StaFile, ElevFile         : file of real;
      StaFileName, ElevFileName : string[12];

    begin

      i:=0; j:=0;

      write ('Enter name of the new file for cross-section station data:  ');
      readln(StaFileName);  writeln;
      assign(StaFile, StaFileName);
      rewrite(StaFile);

      write ('How many stations does this site have?  ');  readln(Count);
      writeln;
      writeln ('Enter data beginning with left bank; Remember to use metric!');
      writeln;
      writeln ('Enter rod station (distance from 0m on x-s tape)');

      for i:= 1 to Count do
        begin
          write ('     for station number  ', i, ':   ');  readln(Station);
          writeln;
          Sta[i] := Station;
          write(StaFile, Station);
        end;
      close(StaFile);

      write ('Enter name of the new file for elevation data:  ');
      readln(ElevFileName);  writeln;
      assign(ElevFile, ElevFileName);
      rewrite(ElevFile);

      for j := 1 to Count do
        begin
          write ('Enter elevation at station ', j,':   ');  readln(Elevation);
          writeln;
          Elev[j] := Elevation;
          write(ElevFile, Elevation);
        end;
      close(ElevFile);
    end;                    {end procedure          }

{*****************************************************************************}

  procedure ReadFile;
    var
      Station, Elevation        : real;
      StaFile, ElevFile         : file of real;
      StaFileName, ElevFileName : string[12];
```

```
    begin
      i:=0;
      write ('What data file is to be used for cross-section station data?  ');
        readln(StaFileName);  writeln;
        assign(StaFile, StaFileName);
        reset(StaFile);
      Count := filesize(StaFile);

      write ('What data file is to be used for elevation data?  ');
        readln(ElevFileName);  writeln;
        assign(ElevFile, ElevFileName);
        reset(ElevFile);

      for i := 1 to Count do
        begin
          read(StaFile, Station);
            Sta[i] := Station;
          read(ElevFile, Elevation);
            Elev[i] := Elevation;
        end;

      close(StaFile);  close(ElevFile);
    end;                                  {end procedure            }

{*****************************************************************************}

  procedure input1;

    begin
     writeln ('This program requires elevations at each cross-section station,');
     writeln ('  bankfull elevation, thalweg elevation, local slope, and a ');
     writeln ('  Manning''s n-value.');
     writeln;
     writeln ('This program assumes that the bankfull water surface is level ');
     writeln ('  across the section.');
     writeln;
     writeln ('Products include area of bankfull channel, discharge of this');
     writeln ('  channel calculated using Manning''s equation, channel top width,');
     writeln ('  mean channel depth, and channel width to depth ratio.  ');
     writeln ('  It will print out all of the entered and calculated data.');
     writeln;
     writeln ('First, enter the name of the sample site:  ');
       readln (Site);  writeln;
     writeln ('Next, indicate how you would like to input data.');
       writeln ('    Type ''u'' (and then Return) to Use an existing file, or');
       writeln ('    type ''c'' (and then Return) to Create and store data in a new file.');
     readln(Choice);  writeln;
       if Choice = 'u' then ReadFile;
       if Choice = 'c' then CreateFile;

     write ('Enter bankfull elevation:  '); readln (Bf);  writeln;
    end;

{*****************************************************************************}
```

```
procedure stage;

  var
    Slope, B : real;
    Change   : boolean;

  begin
    Change := false;
    Thal   := 1000;

    for h := 1 to Count do                    { finds minimum elevation}
      begin
      if Elev[h] < Thal then Thal := Elev[h]
      end;

    for i := 1 to Count do                    { finds station of min. elev.}
      begin
      if Elev[i] = Thal then ThalSta := i
      end;

    for j := 1 to Count do
      begin

        if Elev[j] = Bf then
          begin

            if j < ThalSta then
              begin
                StaNoLB := j;
                LBSta := Sta[j];
              end;

            if j > ThalSta then
              begin
                StaNoRB := j;
                RBSta := Sta[j];
              end;
          end;

        if Elev[j] > Bf then
          begin
            if (j+1) < Count then
              begin
                if Elev[j+1] < Bf then
                  begin
                    if Sta[j] = Sta[j+1] then
                      begin                                  (to avoid)
                        Sta[j] := Sta[j] + 0.01;             (dividing by zero)
                        Change := true;
                      end;

                    Slope := (Elev[j]-Elev[j+1])/(Sta[j]-Sta[j+1]);
                    B := Elev[j]-Slope*Sta[j];
                    LBSta := (Bf-B)/Slope;

                    for k := Count downto (j+1) do
                      begin
                        Sta[k+1] := Sta[k];
                        Elev[k+1] := Elev[k];
                      end;

                    Sta[j+1] := LBSta;
                    StaNoLB := (j+1);
                    Elev[j+1] := Bf;
                    Count := Count + 1;
                    ThalSta := ThalSta + 1;
                  end
                else
```

```
            end;
          end;

        if Elev[j] < Bf then
          begin
            if Elev[j+1] > Bf then
              begin

                if Sta[j] = Sta[j+1] then
                  begin
                    Sta[j] := Sta[j] + 0.01;                (to avoid dividing)
                    Change := true;                         (by zero          )
                  end;

                Slope := (Elev[j]-Elev[j+1])/(Sta[j]-Sta[j+1]);
                B := Elev[j]-Slope*Sta[j];
                RBSta := (Bf-B)/Slope;

                for l := Count downto (j+1) do
                  begin
                    Elev[l+1] := Elev[l];
                    Sta[l+1] := Sta[l];
                  end;

                Sta[j+1] := RBSta;
                StaNoRB := (j+1);
                Elev[j+1] := Bf;
                Count := Count + 1;
              end                    (end nested if then statement)
            else
          end;
          if Change = true then Sta[j] := Sta[j] - 0.01;

      end;                       (end for loop)
  end;                           (end procedure)


(*****************************************************************************)

procedure area;

  var
    A, AStaNoLB, AStaNoRBminus1       : real;
    A1, A2 : array[0..39] of real;

  begin
    i := 0;
    j := 0;
    A := 0;

  AStaNoLB := abs(0.5*(LBSta-Sta[StaNoLB+1])*(Bf-Elev[StaNoLB+1]));

    AStaNoRBminus1 := abs(0.5*(RBSta-Sta[StaNoRB-1])*
                                        (Bf-Elev[StaNoRB-1]));

    for i := (StaNoLB+1) to (StaNoRB-2) do
      begin
        if Elev[i] > Elev[i+1] then j := i;
        if Elev[i] = Elev[i+1] then j := i;
        if Elev[i] < Elev[i+1] then j := i + 1;

        A1[i] := abs(0.5*(Sta[i]-Sta[i+1])*(Elev[i]-Elev[i+1]));
        A2[i] := abs((Sta[i]-Sta[i+1])*(Bf-Elev[j]));
        A := A + A1[i] + A2[i];

      end;
    Atot := A + AStaNoLB + AStaNoRBminus1;
  end;
```

```
(*****************************************************************************)

procedure width;
  begin
    W := abs(LBSta - RBSta);
  end;

procedure depth;
  begin
    D := abs(Atot/W);
  end;

procedure form;
  begin
    F := W/D;
  end;

procedure radius;
  var
    Dist, SQX, SQY : real;

  begin

    i := 0;
    P := 0;

    for i := StaNoLB to (StaNoRB-1) do
      begin
        SQX := sqr(Sta[i]-Sta[i+1]);
        SQY := sqr(Elev[i]-Elev[i+1]);
        Dist := sqrt(SQX + SQY);
        P := P + Dist;
      end;
     R := Atot/P;
  end;

(*****************************************************************************)

procedure input2;
  begin
    writeln ('What Manning''s n-value would you like to use for the');
    write ('slope-area method of discharge calculation?   ');
    readln(N);  writeln;
    write ('What is the local slope of ', Site, '?   ');
    readln(S);
  end;

procedure discharge;
  begin
    input2;
    V := (1/N)*sqrt(S)*(exp (0.666 * ln(R)));
    Q := V*Atot;
  end;

procedure conveyance;
  begin
    CON := Q/(sqrt(S));
  end;

procedure froude;
  begin
    Fr := V/(sqrt(9.8 * D));
  end;
```

```
{*************************************************************************}

procedure writeout;

var OutputChoice, DataChoice  : string[1];

begin

writeln ('Do you want to send data to the Screen or Printer (S or P)?');
  readln(OutputChoice);
if OutputChoice = 'P' then OutputChoice := 'p';
if OutputChoice = 'p' then
  begin
  writeln ('Do you want to print the station-elevation data? (Y or N)');
    readln(DataChoice);
  if DataChoice = 'Y' then DataChoice := 'y';
  if DataChoice = 'y' then
    begin
    writeln (Lst);
    writeln (Lst, 'SITE:  ', Site);  writeln (Lst);
    writeln (Lst, 'Station no.          station (m)           elevation (m)');
    writeln (Lst, '-----------          ---------------       ---------------');

    for i := 1 to Count do
       writeln (Lst, i:6, Sta[i]:31, Elev[i]:23);
    writeln (Lst);
    end; {end datachoice if loop}

  writeln ('Do you want to print the calculated data? (Y or N)');
    readln(DataChoice);
  if DataChoice = 'Y' then DataChoice := 'y';
  if DataChoice = 'y' then
    begin
    writeln (Lst);
    writeln (Lst, 'SITE:  ', Site);  writeln (Lst);
    writeln (Lst, 'Bankfull stage (m):    ', Bf);
    writeln (Lst, 'Slope                :    ', S);
    writeln (Lst, 'Manning''s n-value :    ', N); writeln (Lst);

    writeln (Lst, '  CALCULATED DATA');
    writeln (Lst, 'Bankfull area (sq m) :      ', Atot, '      (sq ft):  ',Atot*10.76);
    writeln (Lst, 'Hydraulic radius (m) :      ', R,    '         (ft):  ',R*3.28);
    writeln (Lst, 'Wetted perimeter (m) :      ', P);
    writeln (Lst, 'Top width (m)        :      ', W);
    writeln (Lst, 'Mean depth (m)       :      ', D);
    writeln (Lst, 'Form ratio           :      ', F);
    writeln (Lst, 'Manning''s velocity (m/s) : ', V,    '       (ft/s):  ',V*3.28);
    writeln (Lst, 'Conveyance (cms)     :      ', CON,  '       (cfs):  ',CON*35.29);
    writeln (Lst, 'Bankfull discharge (cms) : ', Q,    '       (cfs):  ',Q*35.29);
    writeln (Lst);
    writeln (Lst, 'Froude number        :      ', Fr);
    end; {end datachoice=y if loop}
  end; {end outputchoice=p if loop}

if OutputChoice = 'S' then OutputChoice := 's';
if OutputChoice = 's' then
  begin
  writeln ('Do you want to print the station-elevation data? (Y or N)');
    readln(DataChoice);
  if DataChoice = 'Y' then DataChoice := 'y';
  if DataChoice = 'y' then
    begin
    writeln ('*************************************************************');
```

```
    writeln;
    writeln ('SITE:  ', Site);  writeln (Lst);
    writeln ('Station no.          station (m)          elevation (m)');
    writeln ('-----------          ----------------     ----------------');

    for i := 1 to Count do
       writeln (i:6, Sta[i]:31, Elev[i]:23);
    writeln;
    end; (end datachoice if loop)

  writeln ('Do you want to print the calculated data? (Y or N)');
    readln(DataChoice);
  if DataChoice = 'Y' then DataChoice := 'y';
  if DataChoice = 'y' then
    begin
    writeln ('Bankfull stage (m):     ', Bf);
    writeln ('Slope                :     ', S);
    writeln ('Manning''s n-value :     ', N); writeln (Lst);

    writeln ('  CALCULATED DATA');
    writeln ('Bankfull area (sq m) :      ', Atot, '     (sq ft):  ',Atot*10.76);
    writeln ('Hydraulic radius (m) :      ', R,    '       (ft):  ',R*3.28);
    writeln ('Wetted perimeter (m) :      ', P);
    writeln ('Top width (m)        :      ', W);
    writeln ('Mean depth (m)       :      ', D);
    writeln ('Form ratio           :      ', F);
    writeln ('Manning''s velocity (m/s) : ', V,    '      (ft/s):  ',V*3.28);
    writeln ('Conveyance (cms)     :      ', CON,  '      (cfs):  ',CON*35.29);
    writeln ('Bankfull discharge (cms) : ', Q,    '      (cfs):  ',Q*35.29);
    writeln;
    writeln ('Froude number        :      ', Fr);
    end; (end datachoice=y if loop)
  end; (end outputchoice=s if loop)
end;

(*****************************************************************************)

  BEGIN
    input1;
    stage;
    area;
    width;
    depth;
    form;
    radius;
    discharge;
    conveyance;
    froude;
    writeout;
  END.
```

APPENDIX C

Classification and field descriptions of soils

in the Rio Hondo and Rio Pueblo de Taos valleys

below the Sangre de Cristo mountain front, near Taos, New Mexico

Soil Classification

At Taos, mean annual precipitation and temperature are 315 mm and 8.6 C, respectively (State Engineer Office, 1956). Below the mountain front, where all of the soil profiles were described, a pinyon-juniper-sagebrush vegetation assemblage exists. Soil temperature regime is probably mesic; soil moisture regime is probably aridic, but may border on ustic.

In the Taos area, diagnostic horizons for soil classification (Soil Survey Staff, 1975) include the cambic, argillic, and calcic horizons. Soils of units Qlp and Qt2 are tentatively classified as Petrocalcic Paleargids, based on presence of argillic and petrocalcic horizons. Soils of units Qt3, Qt4, and Qt5 appear to be Typic Paleargids, and soils of unit Qt6 appear to be Typic Haplargids. Typic Cambiorthids characterize surface Qt7, and modern floodplain (unit Q8) soils are classified in the Torrifluvent great group.

Key to Appendix

HORIZON BOUNDARIES

Distinctness	Topography
a-abrupt	s-smooth
c-clear	w-wavy
g-gradual	i-irregular
d-diffuse	b-broken

SOIL TEXTURE

c-cobbly	S-sand	SCL-sandy clay loam
p-pebbly	LS-loamy sand	CL-clay loam
g-gravelly	SL-sandy loam	SiCl-silty clay loam
	L-loam	SC-sandy clay
	SiL-silt loam	C-clay
	Si-silt	SiC-silty clay

SOIL STRUCTURE

Grade	Size	Type
ma-massive	vf-very fine	cr-crumb (granular)
sg-single grained	f-fine	pl-platy
vwk-very weak	m-medium	pr-prismatic
wk-weak	c-coarse	cpr-columnar
m-moderate	vc-very coarse	abk-angular blocky
str-strong		sabk-subangular blocky

SOIL CONSISTENCE

Dry	Wet	
lo-loose	ns-non-sticky	np-non-plastic
so-soft	ss-slightly sticky	sp-slightly plastic
sh-slightly hard	s-sticky	p-plastic
h-hard	vs-very sticky	vp-very plastic
vh-very hard		
eh-extremely hard		

CARBONATE

Effervescence	-----Coatings ----- Frequency	Thickness	Morphology
vs-very slight	vd-very discontinuous	t-thin	b-bottoms of clasts
s-slight	d-discontinuous	m-moderate	s-sides of clasts
str-strong	c-continuous	th-thick	t-tops of clasts
vio-violent		vth-very thick	p-ped faces
			surr-surrounds grains

Cementation	---------In fine grained material---------		
wc-weak continuous	f-few	vf-very fine	d-disseminated in matrix
sc-strong continuous	c-common	f-fine	f-filaments
	m-many	m-medium	n-nodules
		c-coarse	m-mottles

CLAY FILMS

Frequency	Thickness	Morphology
vd-very discontinuous	t-thin	pw-coatings on pore walls
d-discontinuous	m-moderate	pf-coatings on ped faces
c-continuous	th-thick	cl-coatings on clasts

ROOTS AND PORES

Abundance	Size	Pore shape	Root orientation
vf-very few	vf-very fine	t-tubular	h-horizontal
f-few	f-fine	i-irregular	v-vertical
c-common	m-medium	ves-vesicular	
m-many	c-coarse		
vm-very many			

Field descriptions of Rio Hondo soils

Map unit	Sample Number	Horizon	Depth (cm)	Lower Boundary	Dry Color	Moist Color	Texture	Structure	Consistence Dry	Consistence Wet
Qt4	SP1	Ak1	0-8	c,w	10YR 5/4	10YR 4/4	SL	vwk,m,cr	so	ss,sp
		Ak2	8-14	c,w	10YR 5/4	10YR 4/4	SL	wk,m,sabk	so	ss,sp
elev. 6780 ft 2066 m		Btk1	14-26	a,w	10YR 6/3	10YR 5/4	SiCL	m,c,sabk	sh	s,sp
36°31'46" 105°41'34"		Btk2	26-50	c,w	10YR 7/3	10YR 6/3	CL	m,m-c,abk	sh	s,p
2.0 km SW of Arroyo Hondo		Btk3	50-73	c,w	10YR 7/3	10YR 6/3	CL	m,m-c,abk	sh	s,sp
		Bk	73-83	c,w	10YR 6/4	10YR 6/4	SiL	wk,m,sabk	h	ss,sp
		2Ck	83-110+	--	10YR 7/3	10YR 5/6	LS	sg	lo	ns,np
Qt3	SP2	Ak1	0-5	c,w	10YR 4/4	10YR 4/4	SiL	wk,f,cr	so	ss,sp
		Ak2	5-13	c,w	10YR 5/4	10YR 4/3	SiL	vwk,f,sabk	sh	ss,sp
elev. 6810 ft 2076 m		Btk1	13-28	c,w	8.25YR 5/4	10YR 4/4	SiCL	vwk,m,sabk	sh	s,p
36°31'45" 105°41'40"		Btk2	28-37	c,w	10YR 7/4	10YR 6/3	CL	m,m,abk	h	s,p
2.2 km SW of Arroyo Hondo		Bk1	37-47	g,w	10YR 7/4	10YR 7/3	SiCL	m,m-c,abk	h	ss,sp
		Bk2	47-69	g,w	10YR 6/3	10YR 6/3	LS	m,m,abk	sh	ns,np
		CBk	69-85	g,w	2.5Y 7/2	2.5Y 4/2	LS	sg;wk,m,sab	lo;sh	ns,np
		Ck	85-96+	--	2.5Y 7/2	2.5Y 5/3	LS	sg	lo	ns,np
Qt5	SP3	Ak1	0-4	c,w	10YR 4/4	10YR 3/3	SiL	wk,m,cr	so	ss,sp
		Ak2	4-11	c,w	10YR 5/4	10YR 4/3	SiL	wk,m,sabk	sh	s,p
elev. 6770 ft 2063 m		Btk1	11-22	c,w	10YR 5/4	10YR 4/3	SiCL	m,m-c,sabk	sh	s,p
36°31'46" 105°41'22"		Btk2	22-36	g,w	10YR 6/3	10YR 5/3	SiCL	m,m,sabk	sh	ss,p
1.7 km SW of Arroyo Hondo		Btk3	36-73	g,w	10YR 7/4	10YR 6/3	SiCL	m,m,sabk	sh	s,p
		Ck	73-110+	--	10YR 7/3	10YR 5/4	L	vwk,f,sabk	sh	s,sp
Qt5	SP4	Akp1	0-5	c,w	10YR 4/3	10YR 3/2	SiCL	lo	so	s,sp
		Akp2	5-21	c,w	10YR 4/3	10YR 3/3	L	m,m-c,sabk	sh	ss,sp
elev. 7005 ft 2135 m		Akp3	21-28	a,w	10YR 4/3	10YR 3/2	L	m,m,sabk	h	ss,sp
36°31'57" 105°38'46"		2Btk1	28-55	g,w	7.5YR 6/5	7.5YR 5/4	CL	str,c,sabk	h	s,p
0.4 km SE of Our Lady of Sorrows Church		2Btk2	55-80	c,w	7.5YR 7/4	7.5YR 5/4	CL	m,m-c,sabk	sh	s,p
		2Ck	80-98+	--	10YR 7/4	10YR 4/3	LS	vwk,f,sabk	lo	ns,np
Qt3	SP5	A	0-5	c,w	10YR 5/4	10YR 4/3	SiL	wk,f,cr	so	ss,sp
		Bt	5-18	c,s	7.5YR 4/4	7.5YR 3.5/4	SiC	wk,m-c,sabk	h	s,p
elev. 6970 ft 2124 m										
36°32'20" 105°39'59"		Btk1	18-30	c,s	7.5YR 4/6	7.5YR 4/4	SiC	str,m,sabk	h-vh	vs,p
0.5 km NE of Arroyo Hondo		Btk2	30-39	c,w	7.5YR 7/4	7.5YR 5/4	CL	m,f,abk	vh	s,p
		Ka1	39-49	c,w	10YR 7/4	10YR 7/4	SL	str,c,abk	vh-eh	ss,sp
		Ka2	49-87	g,w	10YR 8/3	10YR 7/3	L	str,c,abk	h-vh	ss,sp
		Ck	87-106+	--	10YR 7/3	10YR 5/4	LS	sg	lo	ns,np

Sample Number	Horizon	Effer-vescence	Carbonate Coatings	Carbonate in matrix	Carb. Cement	Clay Films	Roots	Pores	Remarks
SP1	Ak1	str	--	d	--	--	m,m,v	--	
	Ak2	str	--	d	--	--	c,vf-m,v	vf,f,t	
	Btk1	str	d,t,b	d; f,f,n	--	c,t,pw; d,t,pf; vd,t,cl	c,vf-f,v	c,f,t	
	Btk2	str	c,t-m,b	d	--	c,t,pw; d,t,pf; vd,t,cl	vf,f-m,v	f,f-m,t	
	Btk3	str-vio	c,m,b	d	--	c,t,pf	vf,vf,v	--	
	Bk	str	d,m,b	d	--	--	f,vf-m,v	f,f-m,t	
	2Ck	s	c,t,b	d	--	--	vf,m,v	--	
SP2	Ak1	str	--	d	--	--	c-m,f-m,v	vf,f-m,t	
	Ak2	str	vd,t,b	d; vf,vf,n	--	--	c,f,v	f,f,t	
	Btk1	str	c,m,b; d,t,s; d,t,t	vf,f,n	--	c,t,pf; c,t,pw; d,t,cl	c,vf-m,v	c,f-m,t	
	Btk2	vio?	c,vth,b; c,m,t	f,m,n	--	c,t,pf; d,t,cl	f,vf-f,v	f,f,t	
	Bk1	vio	c,th,b; d,m,t	vf,f,n	--	--	vf,vf,v	f,f,t	carb. in clast fractures (c,th)
	Bk2	vio	c,t,b; d,m,s	--	--	--	f,f-m,v	--	
	CBk	str?	c,t-m,b; vd,t,s; vd,t,t	--	--	--	vf,f-m,v	vf,f,t	carb. in clast fractures (vd,t)
	Ck	str	c, th, b	--	--	--	vf,f,v	--	
SP3	Ak1	str	--	d; vf,f,n	--	--	m,vf-m,v	c,f-m,t	
	Ak2	vio	d,t,b	d; f,f,n	--	--	c,vf-m,v	f,f-m,t	
	Btk1	vio	c,t,b	f,f,n	--	c,t,pw; d,t,pf; d,t,cl	c,f-m,v	vf,f,t	
	Btk2	vio	c,t,b; c,th,t	c,f-m,n	--	c,t,pw	c,vf-m,v	f,f-m,t	carb. in clast fractures (c,th)
	Btk3	vio	c,m,b; d,t,t	d	--	c,t,pw; d,t,cl	c,vf-m,v	c,vf-m,t	
	Ck	str	vd,t,b	f,f,n	--	--	c,vf-m,v	vf,f,t	clasts not as altered as SP1&2
SP4	Akp1	s	--	d	--	--	m,vf-m,v	--	plowed?
	Akp2	str	d,t,b	vf,f,n	--	--	m,vf-m,v	--	plowed?
	Akp3	str	d,t,b	f,f,n	--	d,t,pf	m,vf-f,v	f-m,f,t	sherd @ 25cm
	2Btk1	str	c,t,b	f,f,n	--	c,t,pw; d,t,pf; d,t,cl	f,vf-f,v	f,f,t	vf,m,v krotovina (10YR 4/3d)
	2Btk2	str	d,t,b	f,f,f; vf,f,n	--	c,t,pw; d,t,pf; d,t,cl	c,vf-m,v	c,vf-f,t	
	2Ck	s	d,t,b	vf,f,f	--	--	--	--	
SP5	A	--	--	--	--	--	m,f-m,v	--	
	Bt	--	--	--	--	c,t,pw; d.t,pf d,t,cl	m,vf-m,v	f,f,t	
	Btk1	vs	vd,t,b	--	--	c.th,pw; c,th,pf; c,t,cl	m,vf-f,v	m,vf-f,t	
	Btk2	vio	c,m,b	--	--	c,t,pw; d,t,cl	c,vf-f,v	f,vf-f,t	
	Km1	vio	c,th,b; c,th,s; c,m,t	--	sc	--	vf,f,v	f,f.t	granites are grussified
	Km2	vio	c,vth,b; c,vth,s; c,t,t	--	wc	--	vf,f,v	f,vf-f,t	carb. in clast fractures (c,t-m)
	Ck	str-vio	c,m,b	--	--	--	f,vf-f,v	--	carb. in clast fractures (c,m)

Map unit	Sample Number	Horizon	Depth (cm)	Lower Boundary	Dry Color	Moist Color	Texture	Structure	Consistence Dry	Consistence Wet
Qt6	SP6	A	0-3	c,w	10YR 4/4	10YR 4/4	SiCL	wk,m,sabk	lo	s,p
		Bt1	3-28	g,w	7.5YR 5/6	7.5YR 4/6	SiCL	str,m,sabk	h	s,vp
elev. 7485 ft 2281 m										
36° 32' 13" 105° 35' 09"		Bt2	28-56	g,w	10YR 5/4	10YR 4/4	CL	m,m,sabk	h	ss,sp
0.4 km NW of Valdez		Btk	56-70	c,w	10YR 5/4	10YR 4/4	L	m,m-c,sabk	sh	ss,sp
		Bk	70-100	c,w	10YR 8/2	10YR 6/3	SL	wk,m,sabk	vh	ss,sp
		Ck	100-200+	--	2.5Y 7/4	10YR 4/3	LS	wk,m,sabk	sh	ns,np
Qt6	SP7	A	0-3	c,s	10YR 5/4	10YR 4/3	LS	vwk,f,cr	so	ns,np
		Bw	3-11	c,s	10YR 5/3	10YR 4/3	SiL	wk,m-c,sabk	sh	ss,sp
elev. 7130 ft 2173 m		Bt	11-25	c,w	7.5YR 5/4	7.5YR 4/6	SiCL	m,c,sabk	h	s,p
36° 32' 30" 105° 37' 48"		Bk1	25-44	g,w	10YR 7/3	10YR 6/3	L	wk,m,sabk	sh	s,sp
		Bk2	44-63	c,i	10YR 8/2	10YR 6/3	LS	wk,m-c,sabk	sh-h	ss,np
0.4 km NW of Valdez										
		Ck	63-100+	--	10YR 7/2	10YR 6/3	S	sg	lo	ns,np
Qt5	SP9	Ak1	0-2	c,w	10YR 5/4	10YR 4/3	SiL	wk,m,sabk	so	ss,sp
		Ak2	2-8	c,w	10YR 5/4	10YR 4/3	SiL	wk,m-c,sabk	so-sh	ss,sp
elev. 7290 ft		Btk1	8-31	a,w	10YR 4/3	10YR 4/3	SiL	m,m-c,sabk	sh	ss,sp
2222 m		Btk2	31-53	g,w	10YR 7/3	10YR 5/3	SiCL	m,m,sabk	sh	s,p
36° 32' 17" 105° 36' 47"		Bk	53-73	g,w	10YR 6/3	10YR 5/3	L	m,m,sabk	sh	ss,sp
0.4 km NW of Valdez		2Ck	73-100+	--	10YR 5/4	10YR 4/4	LS	sg	lo	ns,np
Qt4	SP10	A1	0-2	c,w	10YR 4/3	10YR 3/3	SiL	vwk,m,sabk	so	ss,sp
		A2	2-6	c,s	10YR 4/4	10YR 3/3	SiL	m,m-c,sabk	sh	ss,sp
elev. 7210 ft		Btk1	6-29	c,s	8.25YR 4/4	8.25YR 3/4	SiCL	wk,m,sabk	sh-h	s,p
2198 m										
36° 32' 15" 105° 37' 29"		Btk2	29-55	c,w	10YR 5/4	10YR 4/4	CL	vwk,m,sabk	sh	s,p
3.7 km W of Valdez		Km	55-93	g,w	10YR 6/3	10YR 5/3	SL	sg	h-vh	ns,np
		Ck	93-200+	--	10YR 7/3	10YR 5/4	LS	sg	lo	ns,np
Qt7	SP11	A1	0-4	c,s	10YR 5/3	10YR 3/2	SL	sg	lo	ns,np
elev. 7060 ft		A2	4-18	c,s	10YR 4/4	10YR 3/3	SL	wk,m-c,sabk	sh	ss,np
2152 m										
36° 32' 29" 105° 37' 51"		Bw	18-53	a,s	10YR 4/3	10YR 3/2	SL	m,m-c,sabk	sh	ss,np
		C	53-95	--	10YR 6/3	10YR 4/3	S	sg	lo	ns,np
Qt3	SP12	A	0-5	c,s	10YR 5/4	10YR 4/3	SiL	wk,m,sabk	so-sh	ss,sp
		Btk1	5-20	a,s	7.5YR 4/4	7.5YR 4/6	SiC	m,m-c,sabk	h	vs,p
elev. 7040 ft 2237 m										
36° 32' 36"		Btk2	20-28	c,s	10YR 6/3	10YR 5/4	SiCL	m,m,sabk	h	s,p
105° 36' 47"		Bk	28-80	g,s	10YR 6/3	10YR 6/3	CL	m,abk-pl	h	ss,p
2.9 km NW of Valdez		Ck	80-98+	--	10YR 6/3	10YR 5/4	SL	vwk,f,sabk	h	ns,np
Q8	SP13	Cn	0-25	a,i	10YR 6/3	10YR 4/3	LS	sg	so	ns,np
elev. 7080 ft 2158 m		2Cn	25-50+	--	10YR 6/3	10YR 4/3	LS	sg	lo	ns,np
36° 32' 33" 105° 37' 35"										

Sample Number	Horizon	Effer-vescence	Carbonate Coatings	Carbonate in matrix	Carb. Cement	Clay Films	Roots	Pores	Remarks
SP6	A	--	--	--	--	--	m,vf-f,v	--	
	Bt1	--	--	--	--	c,m,pw; c,m,pf; d,t,cl	f,f-m,v	m,f-m,t	
	Bt2	--	--	--	--	d,t,pw; d,t,pf; vd,t,cl	vf,f-m,v	f,f,t	
	Btk	s	--	f,f,f	--	c,t,pf; d,t,cl	vf,f-m,v	f,f,t	
	Bk	str	c,t,b; d,t,t	d	--	--	vf,vf-m,v	f,f,t	
	Ck	str	--	f,f,f	--	--	f,f-m,v	f,f,t	
SP7	A	--	--	--	--	--	f,f,h	--	
	Bw	--	--	--	--	--	f,f-m,h	m,vf-f,t	
	Bt	--	--	--	--	c,t,pw; d,t,pf; d,t,cl	m,vf-c,h	f,f,t	
	Bk1	vio	c,th,b	d	--	--	m,vf-m,h	vf,f,t	
	Bk2	vio	c,th,b; c,th,s; c,t,t	d	--	--	f,f-m,h	--	vf,c krotovina (10YR 4/3 m)
	Ck	str	c,t,b	--	--	--	c,f-m,h	--	
SP9	Ak1	str	--	d	--	--	m,vf-f,h	f,f,t	
	Ak2	str	--	d	--	--	m,f-m,h	f,f,t	
	Btk1	str	--	vf,f,n	--	c,t,pw	f,f-m,h	f,f-m,t	
	Btk2	str	c,t,b	d; vf,f,f	--	c,t,pw; d,t,pf	c,f-c,h	f,f-m,t	
	Bk	str	c,t,b	d; vf,m-c,n	--	--	c,f-c,h	--	
	2Ck	str	d,m,b; d,t,t	--	--	--	vf,f,h	--	
SP10	A1	--	--	--	--	--	vf,f,h	--	
	A2	--	--	--	--	--	c,f-m,h	--	
	Btk1	--	c,t,b	--	--	c,t,pw; c,t,cl	m,f-c,h	f,f-m,t	
	Btk2	--	c,m,b; c,t,cl	--	--	d,t,pf; c,t,cl	m,vf-m,h; m,vf-m,v	m,i	
	Km	vio	c,m,surr	--	mc	--	f,f-m,v	--	
	Ck	str	c,t,b; d,t,pf	--	--	--	vf,f-m,v	--	
SP11	A1	--	--	--	--	--	m,vf-f,v	--	few mica specks
	A2	--	--	--	--	--	c,vf-m,h; c,vf-m,v	--	few mica specks
	Bw	--	--	--	--	--	c,vf-m,v	f,f,t	few mica specks
	C	--	--	--	--	--	vf,vf,v	--	few mica specks
SP12	A	--	--	--	--	--	m,vf-f,v	--	
	Btk1	--	c,t,b	--	--	c,t,pw; c,t,pf; d,t,cl	m,vf-m,h; m,vf-m,v	f,f,t	
	Btk2	vio	c,m,b	d	--	vd,t,cl	vf,vf-m,h	--	
	Bk	str	c,m-th,b; c,m,t	d	--	--	vf,f-m,h	vf,f,t	
	Ck	str	d,m,b	--	--	--	vf,vf,v	vf,f,t	
SP13	Cn	--	--	--	--	--	vm,f-vc,v; vm,f-vc,h	--	silty floodplain deposit
	2Cn	--	--	--	--	--	m,vf-m,v	-	

Map unit	Sample Number	Horizon	Depth (cm)	Lower Boundary	Dry Color	Moist Color	Texture	Structure	Consistence Dry	Consistence Wet
Qlp	SP14	A1	0-4	c,s	10YR 4/3	10YR 3/3	SiL	ma	so	ss,sp
		A2	4-13	c,s	8.25YR 3/3	10YR 4/3	SiCL	vwk,m,sabk	sh	s,p
elev. 7130 ft 2173 m		Bt1	13-30	c,w	8.25YR 4/4	10YR 4/4	SiCL	m,m,abk	h	s,p
36° 31' 09" 105° 39' 26"		Bt2	30-42	a,w	10YR 5/4	10YR 5/3	CL	vwk,vf,sabk	h	vs,p
2.2 km SE of Arroyo Hondo		Km1	42-66	a,w	10YR 8/2	10YR 7/3	LS	m,pl	eh	ns,np
		Km2	66-84	a,w	10YR 8/2	N/A	N/A	c,pl	eh	N/A
		Km3	84-128	c,i	10YR 7/2	10YR 5/3	LS	m,m,sabk	h	ns,np
		Ck	128-140+	--	10YR 6/3	10YR 5/3	LS	sg	lo	ns,np
Qt5	SP15	A	0-10	c,s	10YR 4/3	10YR 3/3	SiL	vwk,m,sabk	sh	s,sp
		Bwk	10-18	c,s	10YR 4/4	10YR 3/3	SiL	wk-m,m,sabk	sh	s,sp
elev. 6765 ft 2062 m		Bk1	18-31	g,s	10YR 4/4	10YR 3/3	L	vwk,m,sabk	sh	ss,sp
36° 32' 03" 105° 41' 14"		Bk2	31-55	g,i	10YR 7/2	2.5Y 6/2	L	wk,f-m,sabk	sh	ss,sp
		Ck1	55-70	g,i	10YR 7/2	2.5Y 6/2	LS	sg	lo	ns,np
		Ck2	70-85+	--	2.5Y 7/2	2.5Y 5/2	LS	sg	lo	ns,np
1.6 km E of Arroyo Hondo										

Field descriptions of Rio Pueblo de Taos soils

Map unit	Sample Number	Horizon	Depth (cm)	Lower Boundary	Dry Color	Moist Color	Texture	Structure	Dry	Wet
Qt4	SP16	Ak	0-30	a,i	10YR 5/4	10YR 4/4	SiL	wk,m,sabk	sh	ss,sp
elev. 6675 ft 2035 m		2Kmb	30-73	g,w	10YR 8/2	10YR 6/4	LS	N/A	eh	ns,np
36° 22' 31" 105° 40' 11"		2Ckb	73-95+	--	10YR 6/4	2.5Y 4/4	LS	sg	lo	ns,np
Q8	SP17	Cn	0-80+	--	10YR 6/3	10YR 5/3	SL	sg	lo	ns,np
elev. 6630 ft, 2021 m		36 22 48, 105 39 48								
Qt4	SP18	A1	0-5	c,s	10YR 5/4	10YR 4/3	SiL	ma	so	ss,np
		A2	5-11	c,s	10YR 5/4	10YR 4/3	SiCL	wk,f-m,sabk	sh	s,p
elev. 6690 ft 2039 m		Bt	11-27	c,s	10YR 4/4	10YR 4/4	SiC	m,m,sabk	h	vs,p
36° 22' 36" 105° 40' 03"		Btk	27-37	c,w	10YR 5/4	10YR 4/4	SiC	m,m,sabk	h-vh	vs,p
2.0 km SW of Los Cordovas		Bk	37-54	a,w	10YR 8/3	10YR 5/4	CL	str,f,abk	h-vh	s,p
		Km1	54-72	g,w	10YR 9/2	10YR 7/3	SiL	str,f-m,abk	vh	ss,sp
		Km2	72-100	g,i	10YR 7/3	10YR 6/3	L	str,f,abk	vh	ns,np
		Ck	100-110+	--	10YR 8/3	10YR 4/3	LS	sg	lo	ns,np
Qt2	SP19	Avk	0-2	a,s	10YR 5/4	10YR 4/3	SiL	wk,f-m,sabk	sh	ss,sp
		Ak	2-12	c,s	10YR 5/4	10YR 4/3	L	wk,m,sabk	sh	ss,sp
elev. 6765 ft 2062 m		Bk1	12-27	c,s	10YR 5/4	10YR 4/3	SiCL	wk,f-m,sabk	sh	s,p
36° 32' 30" 105° 39' 15"		K1	27-46	a,s	10YR 8/2	10YR 6/4	LS	ma	h	ss,np
		K2	46-81	c,w	10YR 9/2	N/A	N/A	str,pl	eh	N/A
2.0 km SW of Los Cordovas		Ck	81-160	g,i	10YR 8/3	10YR 3/3	LS	sg	lo	ns,np
		C	160-350+	--	10YR 6/3	10YR 3/3	LS	sg	lo	ns,np

Sample Number	Horizon	Effer-vescence	Carbonate Coatings	Carbonate in matrix	Carb. Cement	Clay Films	Roots	Pores	Remarks
SP14	A1	--	--	--	--	--	m,vf,v	--	
	A2	--	--	--	--	d,t,cl	m,f-c,v	vf,f,t	
	Bt1	--	--	--	--	c,t,pw; d,m,pf; d,t,cl	c,vf-m,h	f,f-m,t	
	Bt2	--	--	--	--	c,m,pw; c,m,pf; d,m,cl	f,vf-m,h	f,f,t	
	Km1	vio	c,th,b; c,m,s; c,m,t	--	sc	--	c,m,h	--	
	Km2	vio	surr	--	sc	--	--	--	laminar carb.
	Km3	vio	c,m,b; c,m,t	--	wc	--	f,vf-f,v	--	
	Ck	s	d,t,b	--	--	--	--	--	
SP15	A	--	--	vf,f,n	--	--	vm,vf-m,v	--	
	Bwk	s	c,t,b	vf,f,n	--	d,t,cl	m,vf-m,v	--	
	Bk1	vio	c,m,b; c,t,t	--	--	--	vm,vf-f,v	--	
	Bk2	vio	c,m-th,b	d	--	--	vf,f,v	--	
	Ck1	vio	c,m,b	--	--	--	vf,vf,v	--	
	Ck2	str	c,m,b	--	--	--	--	--	

Sample Number	Horizon	Effer-vescence	Carbonate Coatings	Carbonate in matrix	Carb. Cement	Clay Films	Roots	Pores	Remarks
SP16	Ak	s	c,th,b	--	--	--	m,vf-f,v; f,m,h	--	
	2Kmb	vio	c,m-th,b; c,m-th,s; c,m-th,t	--	wc	--	vf,vf-f,v	-	
	2Ckb	str	c,m,b	--	--	--	vf,vf-f,v	--	
SP17	C	s	--	d	--	--	--	--	modern alluvium
SP18	A1	--	--	--	--	--	m,vf-m,v	--	
	A2	--	--	--	--	--	m,f-m,v	vf,f,t	
	Bt	--	d,t,b	--	--	c,t,pw; d,t,pf; c,m,cl	c,vf-f,v	c,vf-f,t	carb. coatings on large clasts only
	Btk	str	c,m,b	d; f,f,n	--	d,t,pf; c,m,cl	c,vf-f,v	vf,f,t	
	Bk	vio	c,m-th,b; d,t,t	d	--	--	vf,vf,v	--	
	Km1	vio	c,m-th,b; c,t,t	--	wc	--	--	--	
	Km2	vio	c,m-th,sur	--	wc	--	vf,f,v	--	
	Ck	vio	c,m,b	--	--	--	--	--	
SP19	Avk	str	--	d	--	--	f,f,v	vm,vf-m,ves	
	Ak	str	--	d	--	--	c,vf-m,v	vf,f,t	
	Bk1	str	c,m,b; d,t,t	f,f,n	--	--	m,f-m,v	--	
	K1	vio	c,m-th,b; d,t,t	--	wc	--	vf,vf-f,v	--	
	K2	vio	c,th,surr	--	sc	--	vf,f,h	--	laminar carb.
	Ck	s	c,m,b	--	--	--	--	--	
	C	--	--	--	--	--	--	--	

Map unit	Sample Number	Horizon	Depth (cm)	Lower Boundary	Dry Color	Moist Color	Texture	Structure	Dry	Wet
Qt2	SP20	Av	0-8	a,s	10YR 6/3	10YR 4/3	SiL	m,c,sabk	sh	ss,sp
		Bt	8-26	c,s	7.5YR 4/4	7.5YR 4/6	C	str,f-m,abk	h	vs,vp
elev. 7020 ft 2140 m										
36°26'04" 105°37'24"		Btk1	26-56	g,w	7.5YR 7/6	10YR 4/6	SiC	m,m,abk	h	s,p
5.5 km NW of Taos		Btk2	56-92	g,i	7.5YR 4/4	7.5YR 5/4	CL	m,m,sabk	h	s,p
		Km	92-104	c,i	10YR 8/0	10YR 8/3	SL	m,f-c,sabk	h	ss,sp
		Ck	104-120+	--	7.5YR 6/6	7.5YR 5/6	LS	sg	lo	ss,np
Qt4	SP21	Av	0-4	c,s	10YR 6/3	10YR 5/3	SiL	wk,m,sabk	so	ss,sp
		Bt	4-16	c,s	7.5YR 6/4	7.5YR 5/4	SiC	m,m,sabk	h	vs,p
elev. 6780 ft 2067 m										
36°23'31" 105°37'58"		Btk1	16-27	c,s	7.5YR 6/4	7.5YR 5/4	SiCL	m,m,abk	h	s,p
		Btk2	27-61	c,s	8.25YR 5/4	8.25YR 4/4	SiCL	m,m,sabk	h	s,p
0.7 km NE of Los Cordovas		K	61-75+	--	10YR 8/2	10YR 7/3	L	str,f,abk	vh	ss,sp
Qt4	SP22	Av	0-10	a,s	10YR 5/4	10YR 4/3	SiL	m,c,sabk	sh	ss,sp
		Bt	10-30	g,s	7.5YR 4/4	10YR 4/5	C	str,m,abk	h	vs,vp
elev. 6980 ft 2128 m										
36°25'58" 105°37'12"		Btk1	30-42	g,s	7.5YR 4/4	7.5YR 4/5	SiC	m,m,sabk	sh	vs,p
5.1 km NW of Taos		Btk2	42-70	c,s	7.5YR 4/4	7.5YR 4/4	SiC	m,f-m,sabk	h	s,p
		Km	70-130+	--	7.5YR 8/2	7.5YR 6/4	L	wk-m,m-c, sabk	h	ss,sp
Qt6	SP23	A	0-8	c,s	10YR 5/4	10YR 3/3	SiL	wk,m,sabk	sh	ss,sp
		Btk1	8-19	g,s	10YR 4/3	10YR 3/3	SiC	m,m-c,sabk	h-vh	vs,p
elev. 6750 ft 2057 m										
36°23'11" 105°37'40"		Btk2	19-34	g,s	10YR 6/3	10YR 5/3	SiC	wk,m,sabk	h	vs,p
		Btk3	34-53	g,s	10YR 5/4	10YR 4/4	SiCL	m,m,abk	h	s,p
0.8 km E of Los Cordovas		Bk	53-87	g,s	10YR 6/3	10YR 5/4	SiCL	m,m,abk	h	s,p
		Ck	87-120+	--	2.5Y 7/2	10YR 5/3	SiL	ma	sh	s,sp
Qa8?	SP24	Akb	0-22	c,s	10YR 4/3	10YR 3/3	SiL	m,m,sabk	sh	s,sp
(underlain by Qt6? and Qt4?)		2Btk1b	22-40	c,s	8.25YR 5/4	8.25YR 4/4	SiCL	m,m,sabk	h	s,p
		2Btk2b	40-60	g,s	7.5YR 4/4	8.25YR 3/4	SiCL	wk,m,abk	vh	s,p
elev. 7050 ft 2149 m										
36°[illegible] 105°[illegible]		2CBkb	60-78	g,w	8.25YR 5/4	10YR 4/3	LS	sg	lo	ns,np
		2Ckb	78-105	g,w	10YR 4/4	10YR 4/3	LS	sg	lo	ns,np
2.9 km SE of Taos		2Cb	105-137	a,i	10YR 4/3	10YR 4/3	LS	sg	lo	ns,np
		3Kb	137-170	g,w	10YR 7/2	10YR 6/3	SL	str,m,abk	vh	ss,np
		3Ckb	170-180+	--	10YR 5/3	10YR 4/3	LS	sg	lo	ns,np

Sample Number	Horizon	Efferv-escence	Carbonate Coatings	Carbonate in matrix	Carb. Cement	Clay Films	Roots	Pores	Remarks
SP20	Av	--	--	--	--	--	m,f,v	vm,f,ves	polygonal peds
	Bt	--	--	--	--	c,m,pw; c,m,pf; d,t,cl	f,vf-f,v; f,vf-f,h	m,vf-f,t	
	Btk1	s-vio	d,t,b	f,m,n; f,c,m	--	c,m,pw; c,m,pf; d,t,cl	vf,vf,v	m,f,t	10% vert. mottles (7.5YR 7/6d)
	Btk2	s-vio	c,m,b	m,f-m,n; m,c,m	--	d,m,pf	--	f,f,t	70% mottles (7.5YR 7/4d)
	Km	vio	c,m,b; c,t,t	--	sc	--	--	--	
	Ck	str	d,t,b	--	--	--	--	--	
SP21	Av	--	--	--	--	--	N/A	m,f-c,ves	
	Bt	s	--	d	--	c,t,pw; d,t,pf; d,t,cl	N/A	c,f,t	
	Btk1	str	c,t,b; d,t,s	c,f,m	--	c,t,pw	N/A	c,f,t	
	Btk2	str	c,m,b; d,t,s	d; f,f,n	--	d,t,pw	N/A	c,f,t	
	K	vio	c,th,b; c,m,s; c,m,t	--	--	--	N/A	--	carb. dominates matrix
SP22	Av	--	--	--	--	--	c,vf-f,v	vm,f,ves	
	Bt	--	--	--	--	c,m,pw; c,m,pf; c,t,cl	c,vf-f,v	c,f,t	
	Btk1	s-vio	d,t,b; d,t,t	f,m,m	--	c,m,pw; d,m,pf; d,t,cl	f,vf-f,v	f,f,t	10% mottles
	Btk2	s-vio	c,t,b	c,f,f; c,m,m	--	c,t,pw; d,m,pf; d,t,cl	vf,vf,v	c,f,t	20% mottles
	Km	vio	surr	--	wc	--	--	--	carb. dominates matrix
SP23	A	--	--	--	--	--	m,f-m,v	vf,f,ves	
	Btk1	str	c,t-m,b	vf,f,n	--	c,t,pw; d,t,pf; c,t,cl	m,vf-m,h; m,vf-m,v	m,vf-f,t	
	Btk2	vio	c,m,b	vf,f,n	--	c,t,pw; d,t,cl	m,vf-f,h; m,vf-f,v	m,vf-f,t	
	Btk3	vio	c,m,b	f,f,f	--	c,t,pw	c,vf-f,v	c,f,t	
	Bk	vio	c,m,b; d,t,t	c,f,f	--	--	vf,f,v	--	disting. from Bk1 by % filaments
	Ck	str	d,t,b; d,t,s	d	--	--	--	--	
SP24	Akb	str	d,t,b	--	--	--	m,vf-f,v	c,f,t	charcoal, tin can
	2Btk1b	str	d,t,b	--	--	c,t,pw; c,t,pf; d,t,cl	c,vf-m,v	c,f-m,t	
	2Btk2b	str	d,t,b	--	--	c,m,pw; c,m,pf; d,t,cl	f,vf-m,v	f,f,t	
	2CBkb	s	d,m,b; d,t,s	--	--	d,t,cl	f,vf-m,v	--	
	2Ckb	s	d,t,b	--	--	--	f,f-m,v	--	
	2Cb	--	--	--	--	--	f,vf-m,v	--	
	3Kb	vio	c,th,b; c,th,s; c,th,t	--	wc	--	--	--	carb. dominates matrix
	3Ckb	--	d,t,b; d,t,s; d,t,t	--	--	--	--	--	

Map unit	Sample Number	Horizon	Depth (cm)	Lower Boundary	Dry Color	Moist Color	Texture	Structure	Consistence Dry	Consistence Wet
?	SP25	Ak	0-20	c,s	10YR 5/4	10YR 4/3	SiL	wk,m,sabk	so	ss,sp
elev. 7000 ft 2134 m 36° 22' 04" 105° 34' 54"		Btk	20-35	c,s	8.25YR 5/4	8.25YR 5/4	SiCL	m,m,abk	vh	s,p
		Bk1	35-82	g,s	8.25YR 8/3	8.25YR 7/3	L	m,m,sabk	vh	s,sp
2.4 km NE of Ranchos de Taos		Bk2	82-165	g,s	7.5YR 7/4	7.5YR 5/4	SiCL	str,m,sabk	eh	s,p
		2Ck	165-192	a,i	10YR 6/5	10YR 4/4	SL	sg	lo	ns,np
		3Btkb	192-233	c,s	7.5YR 5/4	7.5YR 4/4	SiCL	m,m,sabk	h	s,p
		3Kb	233-264	g,s	10YR 8/2	10YR 6/4	L	str,m-c,abk	eh	s,sp
		3Ckb	264-300+	--	10YR 6/4	10YR 4/3	LS	sg	sh	ns,np
		p.m. for Ak2-->Bk2			8.25YR 5/6	8.25YR 4/4	L	ma	lo	s,sp
		p.m. for Ck			10YR 5/4	10YR 4/4	LS	sg	lo	ns,np
		modern alluvium			10YR 6/3	10YR 4/3	LS	sg	lo	ns,np

Sample Number	Horizon	Effervescence	Carbonate coatings	Carbonate matrix	Carb. Cement	Clay Films	Roots	Pores	Remarks
SP25	Ak	str	--	d; vf,f,	--	--	m,f-c,h; m,f-c,v	vf,f,t	
	Btk	str	--	c,f,f; m,c,m	--	c,t,pw; c,m,pf; d,t,cl	m,f-c,h; m,f-c,v	f,f,t	m,c krotovina
	Bk1	vio	--	--	wc	--	f,vf-f,v	f,f,v	m,m krotovina carb. dominates matrix
	Bk2	vio	d,t,b; d,t,s	m,f,f; f,m,n	--	--	--	c,f,t	m,m krotovina
	2Ck	vio	vd,t,b	c,f-m,n	--	--	--	--	
	3Btkb	str	--	f,f,n	--	d,t,pw; c,t,pf; d,t,cl	--	m,f,t	
	3Kb	vio	c,m,b; c,m,s; c,m,t	--	wc	--	--	m,f,ves	f,c krotovina carb. dominates matrix
	3Ckb	vio	--	f,f,f; c,m,m	--	--	--	--	
		--	--	--	--	--	--	--	
		--	--	--	--	--	--	--	
		--	--	--	--	--	--	--	

Appendix D. Method of calculating normalized values for carbonate morphology in the Relative Profile Development index (Harden, 1982).

1) Most horizons had carbonate as coatings on clasts and as nodules or filaments; therefore distinction was made between "gravelly" and "non-gravelly" material.
   a) for "gravelly" material, calculate points for coatings on bottoms, sides, or tops of clasts:

frequency	thickness	location
very discontinuous (10)	thin (10)	bottoms (10)
discontinuous (20)	medium (20)	sides (20)
continuous (30)	thick (30)	tops (30)
	very thick (40)	ped faces (10)

   e.g., for continuous, medium coatings on bottoms of clasts, 30 + 20 + 10 = 60.

   b) for "non-gravelly" material, calculate points for mottles, nodules, or filaments:

frequency	size	morphology
very few (10)	fine (10)	disseminated (10)
few (20)	medium (20)	filaments (20)
common (30)	coarse (30)	nodules (30)
many (40)		mottles (40)

   e.g., if there are few, medium nodules, then points equal 20 + 20 + 20 = 60

2) Tabulate all points for all types of carbonate, "gravelly" and "non-gravelly". For the type with the highest points multiply by 1.0, for all others multiply by 0.5.

3) Sum all of these weighted points.

4) The highest points possible for non-cemented profiles in this study was 325; thus weakly-cemented horizons were assigned 330 points, and strongly-cemented horizons were assigned 340 points.

5) Add points for effervescence to weighted sum:
   very slight (10)
   slight (20)
   strong (30)
   violent (40)

6) Maximum points in a horizon = 340 + 40 = 380, for strongly cemented, violently effervescent horizon.

FOR EXAMPLE, profile SP2, horizon Btk1 (13-28 cm)

	points		weighted points
continuous, medium coatings on bottoms of clasts (c,m,b):	30 + 20 + 10 = 60	x 1.0 =	60
discontinuous, thin coatings on sides of clasts (d,t,s) :	20 + 10 + 20 = 50	x 0.5 =	25
discontinuous, thin coatings on tops of clasts (d,t,t) :	20 + 10 + 30 = 60	x 0.5 =	30
very few, fine nodules (vf,f,n) :	10 + 10 + 30 = 50	x 0.5 =	25
			140

add points for effervescence (strong = 30); total points = 140 + 30 = 170

RPD index is 170/380 = 0.45, this normalized value used in RPD calculations.

Appendix E. Mean annual discharges of selected U. S. Geological Survey streamflow gaging stations in Colorado, Utah, Wyoming, and New Mexico.

DRAINAGE AREA AND MEAN ANNUAL DISCHARGE (Qa) FOR STREAMS UNDERLAIN BY CRYSTALLINE ROCK TYPES IN COLORADO, UTAH, WYOMING, AND NEW MEXICO

USGS #	USGS station name	Drainage area (km^2)	Qa (m^3/s)
9352900	Vallecito Cr nr Bayfield, CO	187	3.99
8304300	Little Tesuque Cr Tributary #3 nr Santa Fe, NM	1.68	0.001
8304200	Little Tesuque Cr Tributary #4 nr Santa Fe, NM	1.79	0.003
8304100	Little Tesuque Cr nr Santa Fe, NM	1.66	0.004
8302400	South Fork Tesuque Cr nr Santa Fe, NM	1.22	0.006
8302300	Middle Fork Tesuque Cr nr Santa Fe, NM	1.11	0.008
8302200	North Fork Tesuque Cr nr Santa Fe, NM	4.14	0.040
8295200	Rio En Medio nr Santa Fe, NM	1.63	0.207
8294300	Rio Nambe at Nambe Falls, NM	65.0	0.303
8291000	Santa Cruz River at Cundiyo, NM	220	0.824
8263000	Latir Cr nr Cerro, NM	25.9	0.171
8240500	Trinchera Cr abv Turners Ranch, CO	117	0.634
7089000	Cottonwood Cr blw Hot Springs, nr Buena Vista, CO	168	1.56
6748600	South Fork Cache la Poudre R nr Rustic, CO	239	1.80
6733000	Big Thompson River at Estes Park, CO	486	3.57
6730300	Coal Cr nr Plainview, CO	39.1	0.128
6716500	Clear Cr nr Lawson, CO	381	3.88
6710500	Bear Cr at Morrison, CO	425	1.51
6707000	North Fork South Platte R at South Platte, CO	1240	4.33
6706000	North Fork South Platte R blw Geneva Cr, at Grant, CO	329	1.98
6700500	Goose Cr abv Cheesman Lake, CO	224	0.799
6623800	Encampment R abv Hog Park Cr nr Encampment, WY	188	3.28
8267500	Rio Hondo nr Valdez, NM	93.8	0.963
8271000	Rio Lucero nr Arroyo Seco, NM	43	0.611

Appendix E. (continued)

DRAINAGE AREA AND MEAN ANNUAL DISCHARGE (Qa) FOR STREAMS UNDERLAIN BY SEDIMENTARY ROCK TYPES IN COLORADO, UTAH, WYOMING, AND NEW MEXICO

USGS #	USGS station name	Drainage area (km^2)	Qa (m^3/s)
9378700	Cottonwood Wash nr Blanding, UT	531	0.256
9372000	McElmo Cr nr CO-UT stateline, CO	896	1.29
9337500	Escalante R nr Escalante, UT	829	0.439
9308000	Willow Cr nr Ouray, UT	2320	0.753
9307500	Willow Cr abv Diversions, nr Ouray, UT	769	0.606
9306410	Evacuation Cr abv Missouri Cr, nr Dragon, UT	259	0.066
9306255	Yellow Cr nr White River, CO	679	0.054
9306242	Corral Gulch nr Rangley, CO	81.8	0.038
9306235	Corral Gulch blw Water Gulch, nr Rangley, CO	22.3	0.006
9306222	Piceance Cr at White River, CO	1630	0.702
9306200	Piceance Cr blw Ryan Gulch, CO	1310	0.564
9306061	Piceance Cr abv Hunter Cr, nr Rio Blanco, CO	800	0.459
9306058	Willow Cr nr Rio Blanco, CO	125	0.056
9306022	Stewart Gulch abv West Fork, nr Rio Blanco, CO	114	0.044
9306007	Piceance Cr blw Rio Blanco, CO	458	0.334
9184000	Mill Cr nr Moab, UT	194	0.405
9183000	Courthouse Wash nr Moab, UT	420	0.053
9168100	Dissappointment Cr nr Dove Creek, CO	381	0.496
9163310	East Salt Cr nr Mack, CO	510	0.165
9163400	West Salt Cr nr Mack, CO	435	0.025
9095000	Roan Cr nr De Beque, CO	831	1.20
9093500	Parachute Cr at Parachute, CO	513	0.875
9093000	Parachute Cr nr Parachute, CO	365	0.679
8284500	Willow Cr nr Park View, NM	500	0.608
8284200	Willow Cr nr Heron Reservoir, nr Los Ojos, NM	290	0.297
7126200	Van Bremer Arroyo nr Model, CO	435	0.071
7126100	Luning Arroyo nr Model, CO	233	0.050
7124500	Purgatoire R at Trinidad, CO	2060	2.36
7124200	Purgatoire R at Madrid, CO	1420	1.88
7114000	Cucharas R at Boyd Ranch, nr La Veta, CO	145	0.632
7111000	Huerfano R at Manzanares Crossing, nr Redwing, CO	189	0.878
6712000	Cherry Cr nr Franktown, CO	438	0.254
8275000	Rio Fernando de Taos near Taos, NM	186	0.178
8275500	Rio Grande del Rancho near Talpa, NM	210	0.558
8275600	Rio Chiquito near Talpa, NM	95.8	0.225
8269000	Rio Pueblo de Taos nr Taos, NM	172	0.796

REFERENCES: Barker (1969), Cashion (1973), Dane and Bachman (1965), Hackman and Wyant (1973), Hayes et. al. (1972), Johnson (1969), Lovering and Goddard (1950), Scott (1968), Steven et. al. (1974), Tweto (1976), Tweto et. al. (1976), and Williams (1964).

Appendix F. Mean monthly snowmelt, rainfall, evapotranspiration, runoff and storage changes in six drainage basins near Taos, NM.

Basin	Snowmelt (cm)				Rainfall (cm)				Runoff (cm)				Evapotranspiration loss (cm)			
	April	May	June	July	April	May	June	July	April	May	June	July	April	May	June	July
RH	4.8	12.5	14.6	3.4	4.6	5.8	5.1	14.4	2.5	7.7	8.7	3.8	0.0	0.6	2.7	5.2
RL	3.9	12.0	20.7	5.3	3.7	5.1	5.3	15.4	3.7	10.4	12.1	5.3	0.0	0.4	2.4	4.9
RPT	6.8	6.7	4.9	1.0	6.1	5.7	4.3	11.7	1.8	5.2	3.1	1.0	0.0	1.3	3.6	6.1
RFT	9.1	11.9	2.7	0.0	7.4	6.5	4.6	12.7	0.5	1.1	0.3	0.0	0.0	0.9	3.3	5.8
RC	7.7	7.1	0.5	0.0	7.0	5.9	4.1	11.0	1.1	2.9	1.3	0.5	0.0	1.4	3.8	6.3
RGR	5.7	6.6	2.5	0.2	6.0	5.7	4.0	10.7	1.0	3.1	1.7	0.5	0.0	1.5	3.9	6.4

	Storage change (cm)			
	April	May	June	July
RH	6.8	10.0	8.3	8.7
RL	3.9	6.3	11.5	10.6
RPT	11.0	6.1	2.4	5.6
RFT	16.0	16.4	3.6	6.8
RC	13.7	8.8	-0.6	4.2
RGR	10.6	7.7	0.9	3.9

RH : Rio Hondo
RL : Rio Lucero
RPT : Rio Pueblo de Taos
RFT : Rio Fernando de Taos
RC : Rio Chiquito
RGR : Rio Grande del Rancho

APPENDIX G

Number and lengths of stream links in six small drainage basins

near Taos, New Mexico

Basin	1st order n	1st order L	1st order $\bar{x}$	2nd order n	2nd order L	2nd order $\bar{x}$	3rd order n	3rd order L	3rd order $\bar{x}$	4th order n	4th order L	4th order $\bar{x}$
Rio Hondo	281	123.1	0.4	65	41.9	0.6	16	20.3	1.3	4	10.0	2.5
Rio Lucero	71	35.2	0.5	23	14.2	0.6	5	7.2	1.4	1	6.7	6.7
Crystalline terrane	352	158.3	0.5	88	56.1	0.6	21	27.5	1.3	5	16.7	3.3
Rio Fernando de Taos	522	233.3	0.4	115	92.6	0.8	25	44.5	1.8	3	8.5	2.8
Rio Chiquito	352	140.0	0.4	80	56.4	0.7	14	20.1	1.4	2	16.8	8.4
Rio Grande del Rancho	428	162.6	0.4	105	65.9	0.6	25	41.1	1.6	6	23.5	3.9
Rito de la Olla	224	94.0	0.4	58	45.9	0.8	11	18.5	1.7	1	17.9	17.9
Sedimentary terrane	1526	629.9	0.4	358	260.8	0.7	75	124.2	1.7	12	66.7	5.6
Rio Hondo	47	23.9	0.5	10	12.6	1.3	3	5.8	1.9	--	--	--
Rio Lucero	37	11.5	0.3	8	5.6	0.7	1	3.7	3.7	--	--	--
Rio Grande del Rancho	39	21.0	0.5	9	11.6	1.3	2	2.6	1.3	--	--	--
Glacial deposits	123	56.4	0.5	27	29.8	1.1	6	12.1	2.0	--	--	--

KEY: n: number of stream links of specified order
L: total stream length of specified order (km)
$\bar{x}$: mean stream length of specified order (km)

Basin	5th order n	5th order L	5th order $\bar{x}$	6th order n	6th order L	6th order $\bar{x}$	Σn	ΣL (km)	Area (km^2)	F (#/km^2)	Dd (km/km^2)
Rio Hondo	1	10.7	10.7	--	--	--	367	206.0	66.5	5.52	3.10
Rio Lucero	--	--	--	--	--	--	100	63.3	25.9	3.86	2.44
Crystalline terrane	1	10.7	10.7	--	--	--	467	269.3	92.4	5.05	2.91
Rio Fernando de Taos	1	22.1	22.1	--	--	--	666	401	156.7	4.25	2.56
Rio Chiquito	1	5.7	5.7	--	--	--	449	239	98.8	4.54	2.42
Rio Grande del Rancho	2	8.5	4.3	1	3.0	3.0	567	304.6	112.7	5.03	2.70
Rito de la Olla	--	--	--	--	--	--	294	176.3	89.9	3.27	1.96
Sedimentary terrane	4	36.3	9.1	1	3.0	3.0	1976	1120.9	458.1	4.31	2.45
Rio Hondo	--	--	--	--	--	--	60	42.3	28.8	2.08	1.47
Rio Lucero	--	--	--	--	--	--	46	20.8	17.6	2.61	1.18
Rio Grande del Rancho	--	--	--	--	--	--	50	35.2	21.8	2.29	1.61
Glacial deposits	--	--	--	--	--	--	156	98.3	68.2	2.29	1.44

APPENDIX H

Calculations of the Relative Profile Development index (Harden, 1982)

for soil profiles described in the Rio Hondo

and Rio Pueblo de Taos valleys

Note: Normalized data in each table calculated by three techniques:

A, the quantified property is divided by its maximum quantity;

B, for clay films only, 20 points subtracted from quantified property, which is then divided by maximum;

C, for dry consistence only, quantified property is divided by twice the maximum (see Harden, 1982).

Appendix H. Calculations of the Relative Profile Development index (Harden, 1982) for soil profiles described in the Rio Hondo and Rio Pueblo de Taos valleys.

SOIL PIT: 1 PIT DEPTH: 110 cm PROFILE INDEX: 23.99 (unit-cm)

NORMALIZED DATA PROPERTY	MAXIMUM	TECHNIQUE	HORIZONS Ak1	Ak2	Btk1	Btk2	Btk3	Bk	Ck
RUBIFICATION	140	A	0.14	0.14	0.07	0.00	0.00	0.14	0.00
TEXTURE	100	A	0.30	0.30	0.50	0.70	0.60	0.40	0.00
CLAY FILMS	155	B	0.00	0.00	0.48	0.48	0.26	0.00	0.00
STRUCTURE	60	A	0.25	0.50	0.67	0.67	0.67	0.50	0.00
DRY CONSISTENCE	50	C	0.10	0.10	0.20	0.20	0.20	0.30	0.00
MELANIZATION	50	A	0.20	0.20	0.00	0.00	0.00	0.00	0.00
CARBONATE	380	A	0.11	0.11	0.24	0.24	0.26	0.22	0.20
COLOR-LIGHTENING	60	A	0.00	0.00	0.50	0.50	0.50	0.33	0.33
SUM			1.10	1.35	2.66	2.79	2.49	1.90	0.53
SUM/n			0.14	0.17	0.33	0.35	0.31	0.24	0.07
(SUM/n)*THICKNESS			1.10	1.01	3.99	8.36	7.15	2.37	1.79

SOIL PIT: 2 PIT DEPTH: 96 cm PROFILE INDEX: 20.59 (unit-cm)

NORMALIZED DATA PROPERTY	MAXIMUM	TECHNIQUE	HORIZONS Ak1	Ak2	Btk1	Btk2	Bk1	Bk2	CBk	Ck
RUBIFICATION	140	A	0.14	0.07	0.18	0.07	0.07	0.00	0.00	0.00
TEXTURE	100	A	0.40	0.40	0.80	0.70	0.60	0.00	0.00	0.00
CLAY FILMS	155	B	0.00	0.00	0.58	0.42	0.00	0.00	0.00	0.00
STRUCTURE	60	A	0.33	0.42	0.42	0.67	0.67	0.67	0.25	0.00
DRY CONSISTENCE	50	C	0.10	0.20	0.20	0.30	0.30	0.20	0.10	0.00
MELANIZATION	50	A	0.40	0.20	0.20	0.00	0.00	0.00	0.00	0.00
CARBONATE	380	A	0.11	0.24	0.45	0.49	0.41	0.33	0.34	0.26
COLOR-LIGHTENING	60	A	0.00	0.00	0.00	0.50	0.67	0.33	0.17	0.33
SUM			1.48	1.52	2.82	3.14	2.71	1.53	0.86	0.60
SUM/n			0.19	0.19	0.35	0.39	0.34	0.19	0.11	0.07
(SUM/n)*THICKNESS			0.93	1.52	5.29	3.54	3.39	4.20	1.72	0.82

SOIL PIT: 3 PIT DEPTH: 110 cm PROFILE INDEX: 24.15 (unit-cm)

NORMALIZED DATA PROPERTY	MAXIMUM	TECHNIQUE	HORIZONS Ak1	Ak2	Btk1	Btk2	Btk3	Ck
RUBIFICATION	140	A	0.07	0.07	0.07	0.00	0.07	0.07
TEXTURE	100	A	0.40	0.60	0.80	0.70	0.80	0.50
CLAY FILMS	155	B	0.00	0.00	0.52	0.19	0.35	0.00
STRUCTURE	60	A	0.33	0.50	0.67	0.67	0.67	0.42
DRY CONSISTENCE	50	C	0.10	0.20	0.20	0.20	0.20	0.20
MELANIZATION	50	A	0.60	0.20	0.20	0.00	0.00	0.00
CARBONATE	380	A	0.20	0.30	0.30	0.49	0.36	0.25
COLOR-LIGHTENING	60	A	0.00	0.00	0.00	0.17	0.50	0.33
SUM			1.70	1.87	2.76	2.42	2.95	1.77
SUM/n			0.21	0.23	0.34	0.30	0.37	0.22
(SUM/n)*THICKNESS			0.85	1.64	3.79	4.24	13.64	8.19

SOIL PIT: 5 PIT DEPTH: 106 cm PROFILE INDEX: 34.80 (unit-cm)

NORMALIZED DATA PROPERTY	MAXIMUM	TECHNIQUE	HORIZONS A	Bt	Btk1	Btk2	K1	K2	Ck
RUBIFICATION	140	A	0.07	0.29	0.43	0.29	0.14	0.00	0.07
TEXTURE	100	A	0.30	0.80	0.90	0.70	0.30	0.40	0.00
CLAY FILMS	155	B	0.00	0.52	0.81	0.35	0.00	0.00	0.00
STRUCTURE	60	A	0.33	0.50	0.83	0.67	0.83	0.83	0.00
DRY CONSISTENCE	50	C	0.10	0.30	0.35	0.40	0.45	0.35	0.00
MELANIZATION	50	A	0.20	0.50	0.40	0.00	0.00	0.00	0.00
CARBONATE	380	A	0.00	0.00	0.11	0.26	1.00	0.97	0.25
COLOR-LIGHTENING	60	A	0.00	0.00	0.00	0.33	0.67	0.83	0.33
SUM			1.00	2.90	3.82	3.00	3.39	3.39	0.65
SUM/n			0.13	0.36	0.48	0.38	0.42	0.42	0.08
(SUM/n)*THICKNESS			0.63	4.72	5.74	3.38	4.24	16.10	1.56

SOIL PIT: 7 PIT DEPTH: 100 cm PROFILE INDEX: 16.21 (unit-cm)

NORMALIZED DATA PROPERTY	MAXIMUM	TECHNIQUE	HORIZONS A	Bw	Bt	Bk1	Bk2	Ck
RUBIFICATION	140	A	0.07	0.00	0.43	0.00	0.00	0.00
TEXTURE	100	A	0.00	0.40	0.80	0.50	0.10	0.00
CLAY FILMS	155	B	0.00	0.00	0.52	0.00	0.00	0.00
STRUCTURE	60	A	0.25	0.50	0.67	0.50	0.50	0.00
DRY CONSISTENCE	50	C	0.10	0.20	0.30	0.20	0.25	0.00
MELANIZATION	50	A	0.20	0.20	0.20	0.00	0.00	0.00
CARBONATE	380	A	0.00	0.00	0.00	0.30	0.51	0.21
COLOR-LIGHTENING	60	A	0.00	0.00	0.00	0.50	0.67	0.50
SUM			0.62	1.30	2.91	2.00	2.03	0.71
SUM/n			0.08	0.16	0.36	0.25	0.25	0.09
(SUM/n)*THICKNESS			0.23	1.30	5.09	4.76	4.82	3.29

SOIL PIT: 9 PIT DEPTH: 100 cm PROFILE INDEX: 18.83 (unit-cm)

NORMALIZED DATA PROPERTY	MAXIMUM	TECHNIQUE	HORIZONS Ak1	Ak2	Btk1	Btk2	Bk	2Ck
RUBIFICATION	140	A	0.07	0.07	0.00	0.00	0.00	0.14
TEXTURE	100	A	0.40	0.40	0.40	0.80	0.40	0.00
CLAY FILMS	155	B	0.00	0.00	0.19	0.35	0.00	0.00
STRUCTURE	60	A	0.50	0.50	0.67	0.67	0.67	0.00
DRY CONSISTENCE	50	C	0.10	0.15	0.20	0.20	0.20	0.00
MELANIZATION	50	A	0.20	0.20	0.40	0.00	0.00	0.20
CARBONATE	380	A	0.11	0.11	0.18	0.26	0.30	0.30
COLOR-LIGHTENING	60	A	0.00	0.00	0.00	0.33	0.17	0.00
SUM			1.38	1.43	2.04	2.62	1.74	0.65
SUM/n			0.17	0.18	0.26	0.33	0.22	0.08
(SUM/n)*THICKNESS			0.34	1.07	5.88	7.20	4.34	2.16

SOIL PIT: 10 PIT DEPTH: 200 cm PROFILE INDEX: 24.44 (unit-cm)

NORMALIZED DATA PROPERTY	MAXIMUM	TECHNIQUE	HORIZONS A1	A2	Btk1	Btk2	K	Ck
RUBIFICATION	140	A	0.00	0.07	0.21	0.14	0.00	0.07
TEXTURE	100	A	0.40	0.40	0.80	0.70	0.00	0.00
CLAY FILMS	155	B	0.00	0.00	0.42	0.45	0.00	0.00
STRUCTURE	60	A	0.42	0.67	0.50	0.42	0.00	0.00
DRY CONSISTENCE	50	C	0.10	0.20	0.25	0.20	0.35	0.00
MELANIZATION	50	A	0.60	0.60	0.60	0.20	0.00	0.00
CARBONATE	380	A	0.00	0.00	0.13	0.24	0.97	0.26
COLOR-LIGHTENING	60	A	0.00	0.00	0.00	0.00	0.17	0.33
SUM			1.52	1.94	2.92	2.35	1.49	0.67
SUM/n			0.19	0.24	0.36	0.29	0.19	0.08
(SUM/n)*THICKNESS			0.38	0.97	8.38	7.63	7.08	8.93

SOIL PIT: 11 PIT DEPTH: 95 cm PROFILE INDEX: 9.63 (unit-cm)

NORMALIZED DATA PROPERTY	MAXIMUM	TECHNIQUE	HORIZONS A1	A2	Bw	C
RUBIFICATION	140	A	0.00	0.07	0.00	0.00
TEXTURE	100	A	0.00	0.10	0.10	0.00
CLAY FILMS	155	B	0.00	0.00	0.00	0.00
STRUCTURE	60	A	0.00	0.50	0.67	0.00
DRY CONSISTENCE	50	C	0.00	0.20	0.20	0.00
MELANIZATION	50	A	0.40	0.60	0.60	0.00
CARBONATE	340	A	0.00	0.00	0.00	0.00
COLOR-LIGHTENING	60	A	0.00	0.00	0.00	0.00
SUM			0.40	1.47	1.57	0.00
SUM/n			0.05	0.18	0.20	0.00
(SUM/n)*THICKNESS			0.20	2.58	6.85	0.00

SOIL PIT: 12 PIT DEPTH: 98 cm PROFILE INDEX: 25.04 (unit-cm)

NORMALIZED DATA PROPERTY	MAXIMUM	TECHNIQUE	HORIZONS A	Btk1	Btk2	Bk	Ck
RUBIFICATION	140	A	0.07	0.43	0.07	0.00	0.07
TEXTURE	100	A	0.40	0.90	0.80	0.60	0.00
CLAY FILMS	155	B	0.00	0.58	0.13	0.00	0.00
STRUCTURE	60	A	0.50	0.67	0.67	0.75	0.42
DRY CONSISTENCE	50	C	0.15	0.30	0.30	0.30	0.30
MELANIZATION	50	A	0.20	0.40	0.00	0.00	0.00
CARBONATE	380	A	0.00	0.13	0.28	0.39	0.21
COLOR-LIGHTENING	60	A	0.00	0.00	0.17	0.33	0.17
SUM			1.32	3.41	2.41	2.37	1.17
SUM/n			0.17	0.43	0.30	0.30	0.15
(SUM/n)*THICKNESS			0.83	6.39	2.41	15.41	2.62

SOIL PIT: 15 PIT DEPTH: 85 cm PROFILE INDEX: 15.02 (unit-cm)

NORMALIZED DATA PROPERTY	MAXIMUM	TECHNIQUE	HORIZONS A	Bwk	Bk1	Bk2	Ck1	Ck2
RUBIFICATION	140	A	0.00	0.07	0.07	0.00	0.00	0.00
TEXTURE	100	A	0.50	0.50	0.40	0.40	0.00	0.00
CLAY FILMS	155	B	0.00	0.19	0.00	0.00	0.00	0.00
STRUCTURE	60	A	0.42	0.50	0.42	0.50	0.00	0.00
DRY CONSISTENCE	50	C	0.20	0.20	0.20	0.20	0.00	0.00
MELANIZATION	50	A	0.60	0.60	0.60	0.00	0.00	0.00
CARBONATE	380	A	0.11	0.24	0.37	0.29	0.26	0.24
COLOR-LIGHTENING	60	A	0.00	0.00	0.00	0.50	0.50	0.33
SUM			1.82	2.30	2.06	1.89	0.76	0.57
SUM/n			0.23	0.29	0.26	0.24	0.10	0.07
(SUM/n)*THICKNESS			2.28	2.30	3.34	5.67	1.43	1.07

SOIL PIT: 18 PIT DEPTH: 110 cm PROFILE INDEX: 35.10 (unit-cm)

NORMALIZED DATA PROPERTY	MAXIMUM	TECHNIQUE	HORIZONS A1	A2	Bt	Btk	Bk	K1	K2	Ck
RUBIFICATION	140	A	0.07	0.07	0.14	0.14	0.07	0.00	0.00	0.00
TEXTURE	100	A	0.30	0.80	0.90	0.90	0.70	0.40	0.20	0.00
CLAY FILMS	155	B	0.00	0.00	0.65	0.48	0.00	0.00	0.00	0.00
STRUCTURE	60	A	0.00	0.50	0.67	0.67	0.83	0.83	0.83	0.00
DRY CONSISTENCE	50	C	0.10	0.20	0.30	0.35	0.35	0.40	0.40	0.00
MELANIZATION	50	A	0.20	0.20	0.40	0.20	0.00	0.00	0.00	0.00
CARBONATE	380	A	0.00	0.00	0.11	0.32	0.37	0.97	0.97	0.26
COLOR-LIGHTENING	60	A	0.00	0.00	0.00	0.00	0.17	0.83	0.50	0.00
SUM			0.67	1.77	3.16	3.06	2.49	3.44	2.91	0.26
SUM/n			0.08	0.22	0.39	0.38	0.31	0.43	0.36	0.03
(SUM/n)*THICKNESS			0.42	1.33	6.32	3.82	5.29	7.74	10.17	0.33

SOIL PIT: 20 PIT DEPTH: 120 cm PROFILE INDEX: 41.73 (unit-cm)

NORMALIZED DATA PROPERTY	MAXIMUM	TECHNIQUE	HORIZONS Av	Bt	Btk1	Btk2	K	Ck
RUBIFICATION	140	A	0.00	0.43	0.57	0.29	0.00	0.57
TEXTURE	100	A	0.40	1.00	0.80	0.70	0.30	0.10
CLAY FILMS	155	B	0.00	0.68	0.68	0.26	0.00	0.00
STRUCTURE	60	A	0.67	0.83	0.67	0.67	0.67	0.00
DRY CONSISTENCE	50	C	0.20	0.30	0.30	0.30	0.30	0.00
MELANIZATION	50	A	0.00	0.40	0.00	0.40	0.00	0.00
CARBONATE	380	A	0.00	0.00	0.41	0.53	0.34	0.18
COLOR-LIGHTENING	60	A	0.00	0.00	0.17	0.17	1.00	0.17
SUM			1.27	3.64	3.59	3.31	2.61	1.02
SUM/n			0.16	0.45	0.45	0.41	0.33	0.13
(SUM/n)*THICKNESS			1.27	8.19	13.46	14.90	3.91	2.04

SOIL PIT: 23 PIT DEPTH: 110 cm PROFILE INDEX: 27.41 (unit-cm)

NORMALIZED DATA PROPERTY	MAXIMUM	TECHNIQUE	HORIZONS A	Btk1	Btk2	Btk3	Bk	Ck
RUBIFICATION	140	A	0.07	0.00	0.00	0.14	0.07	0.00
TEXTURE	100	A	0.40	0.90	0.90	0.80	0.80	0.50
CLAY FILMS	155	B	0.00	0.58	0.35	0.19	0.00	0.00
STRUCTURE	60	A	0.50	0.67	0.50	0.67	0.67	0.00
DRY CONSISTENCE	50	C	0.20	0.35	0.30	0.30	0.30	0.20
MELANIZATION	50	A	0.40	0.60	0.00	0.20	0.00	0.00
CARBONATE	380	A	0.00	0.28	0.32	0.30	0.41	0.28
COLOR-LIGHTENING	60	A	0.00	0.00	0.17	0.00	0.17	0.33
SUM			1.57	3.37	2.54	2.61	2.41	1.31
SUM/n			0.20	0.42	0.32	0.33	0.30	0.16
(SUM/n)*THICKNESS			1.57	4.64	4.76	6.19	10.25	5.40

REFERENCES

Andrews, E. D., 1979, Hydraulic adjustment of the East Fork River, Wyoming, to the supply of sediment: *in* Rhodes, D. D., and Williams, G. P. (eds.), *Adjustments of the Fluvial System*: Kendall-Hunt, Dubuque, Iowa, p. 69-94.

_____, 1984, Bed-material entrainment and hydraulic geometry of gravel-bed rivers in Colorado: Geological Society of America Bulletin, v. 95, p. 371-378.

Bagnold, R. A., 1966, An approach to the sediment transport problem from general physics: U. S. Geological Survey Professional Paper 422-I, 37 p.

_____, 1977, Bed load transport by natural rivers: Water Resources Research, v. 13, no. 2, p. 303-312.

Baker, V. R., 1977, Stream channel response to floods with examples from central Texas: Geological Society of America Bulletin, v. 88, p. 1057-1071.

Baker, V. R., and Ritter, D. F., 1975, Competence of rivers to transport coarse bedload material: Geological Society of America Bulletin, v. 86, p. 975-978.

Barker, F., 1969, Precambrian geology of the Needle Mountains, southwestern Colorado: U. S. Geological Survey Professional Paper 644-A, 35 p.

Barnes. H. H., 1967, Roughness characteristics of natural channels: U. S. Geological Survey Water Supply Paper 1849.

Begin, Z. B., Meyer, D. F., and Schumm, S. A., 1981, Development of longitudinal profiles of alluvial channels in response to base-level lowering: Earth Surface Processes, v. 6, p. 49-68.

Benson, M. A., and Dalrymple, T., 1967, General field and office procedures for indirect discharge measurements: Techniques of Water-Resources Investigations of the United States Geological Survey, chapter A1, book 3, 30 p.

Birkeland, P. W., 1984, *Soils and geomorphology*: Oxford University Press, New York, 372 p.

Born, S. M., and Ritter, D. F., 1970, Modern terrace development near Pyramid Lake, Nevada, and its geologic implications: Geological Society of America Bulletin, v. 81, p. 1233-1242.

Brayshaw, A. C., 1985, Bed microtopography and entrainment thresholds in gravel-bed rivers: Geological Society of America Bulletin, v. 96, p. 218-223.

Brush, L. M., 1961, Drainage basins, channels, and flow characteristics

of selected streams in central Pennsylvania: U. S. Geological Survey Professional Paper 282-F, 181 p.

Brush, L. M., and Wolman, M. G., 1960, Knickpoint behavior in noncohesive material: a laboratory study: Geological Society of America Bulletin, v. 71, p. 59-74.

Bull, W. B., 1979, Threshold of critical power in streams: Geological Society of America Bulletin v. 90, p. 453-464.

Bull, W. B., and McFadden, L. D., 1977, Tectonic geomorphology north and south of the Garlock fault, California: Eighth Annual Geomorphology Symposia Series, Binghampton, NY, p. 115-137.

Cashion, W. B., 1973, Geologic and structure map of the Grand Junction Quadrangle, Colorado and Utah: U. S. Geological Survey Miscellaneous Investigations Map I-736, scale 1:250,000.

Chapin, C. E., and Seager, W. R., 1975, Evolution of the Rio Grande Rift in Socorro and Las Cruces area: New Mexico Geological Society 26th Field Conference Guidebook, p. 297-321.

Clark, K. F., and Read, C. B., 1972, Geology and ore deposits of the Eagle Nest area, New Mexico: New Mexico Bureau of Mines and Mineral Resources Bulletin 94, 152 p.

Costa, J. E., 1983, Paleohydraulic reconstruction of flash-flood peaks from boulder deposits in the Colorado Front Range: Geological Society of America Bulletin, v. 94, p. 986-1004.

Dalrymple, T., and Benson, M. A., 1967, Measurement of peak discharge by the slope-area method: Techniques of Water-Resource Investigations of the United States Geological Survey, chapter A2, book 3, 12 p.

Dane, C. H., and Bachman, G. O., 1965, Geologic Map of New Mexico: U. S. Geological Survey, scale 1:500,000.

Dixon, H. W., 1962, Vegetation, pollen rain, and pollen preservation, Sangre de Cristo Mountains, New Mexico: Unpublished M. S. Thesis, University of New Mexico, Albuquerque, 69 p.

Dunne, T., and Black, R. D., 1970, Partial area contributions to storm runoff in a small New England watershed: Water Resources Research, v. 6, p. 1296-1311.

Dunne, T., and Leopold, L. B., 1978, *Water in Environmental Planning*: W. H. Freeman and Company, San Francisco, 818 p.

Fahnestock, R. K., 1963, Morphology and hydrology of a glacial stream-White River, Mount Ranier, Washington: U. S. Geological Survey Professional Paper 422-A, 70 p.

Gilbert, G. K., 1877, Geology of the Henry Mountains (Utah): U. S. Geographical and Geological Survey of the Rocky Mountain Region,

Washington, D. C.: U. S. Government Printing Office.

Gile, L. H., Peterson, F. F., and Grossman, R. B., 1966, Morphological and genetic sequences of carbonate accumulation in desert soils: Soil Science, v. 101, p. 347-360.

Gillam, M. L., Moore, D. W., and Scott, G. R., 1984, Quaternary deposits and soils in the Durango area, southwestern Colorado: *in* Brew, D. C. (ed.), Geological Society of America Rocky Mountain Section 37th Annual Meeting Field Trip Guidebook, p. 149-182.

Gillam, M. L., Blair, R. W., and Johnson, M. D., 1985, Geomorphology and Quaternary geology of the Animas River valley, Colorado and New Mexico: Friends of the Pleistocene, Rocky Mountain Cell, Field Trip Guidebook.

Goudie, A., 1981, *Geomorphological Techniques*: George Allen & Unwin, London, 395 p.

Gruner, J. W., 1920, Geologic reconnaissance of the southern part of the Taos Range, New Mexico: Journal of Geology, v. 28, p.731-742.

Hack, J. T., 1957, Studies of longitudinal stream profiles in Virginia and Maryland: U. S. Geological Survey Professional Paper 294-B, 54 p.

Hackman, R. J., and Wyant, D. G., 1973, Geology, structure and uranium deposits of the Escalante Quadrangle, Utah and Arizona: U. S. Geological Survey Miscellaneous Investigations Map I-744, scale 1:250,000.

Harden, J. W., 1982, A quantitative index of soil development from a chronosequence in central California: Geoderma, v. 28, p. 1-28.

Hayes, D. D., Vogel, J. D., and Wyant, D. G., 1972, Geology, structure, and uranium deposits of the Cortez Quadrangle, Colorado and Utah: U. S. Geological Survey Miscellaneous Investigations Map I-629.

Hely, A. G., and Olmstead, F. H., 1963, Some relations between streamflow characteristics and the environment in the Delaware River region: U. S. Geological Survey Professional Paper 417-B.

Horton, R. E., 1933, The role of infiltration in the hydrological cycle: American Geophysical Union Transactions, v. 14, p. 446-460.

Izett, G. A., Obradovich, J. D., Naeser, C. W., and Cebula, G. T., 1981, Potassium-Argon and fission-track zircon ages of Cerro Toledo Rhyolite tephra in the Jemez Mountains, New Mexico: U. S. Geological Survey Professional Paper 1199-D, p. 37-43.

Johnson, R. B., 1969, Geologic map of Trinidad Quadrangle, south-central Colorado: U. S. Geological Survey Miscellaneous Investigations Map I-558, scale 1:250,000.

Kelley, V. C., 1956, The Rio Grande depression from Taos to Santa Fe: New

Mexico Geological Society 7th Field Conference Guidebook, p. 109-114.

Knox, J. C., 1976, Concept of the graded stream: Seventh Annual Geomorphology Symposia Series, Binghampton, NY, p. 169-198.

Kottlowski, F. E., 1958, Geologic history of the Rio Grande near El Paso: West Texas Geological Society Guidebook of the Franklin and Hueco Mountains, p. 46-54.

Lambert, P. W., 1966, Notes on the late Cenozoic geology of the Taos-Questa area, New Mexico: New Mexico Geological Society 17th Field Conference Guidebook, p. 43-50.

Lane, E. W., 1953, Design of stable channels: American Society of Civil Engineers, Proceedings, v. 79, p. 1-31.

Langbein, W. B., and Schumm, S. A., 1958, Yield of sediment in relation to mean annual precipitation: American Geophysical Union Transactions, v. 39, no. 6, p. 1076-1084.

Leininger, R. L., 1982, Cenozoic evolution of the southernmost Taos Plateau, New Mexico: Unpublished M. A. thesis, University of Texas at Austin, 110 p.

Leopold, L. B., and Bull, W. B., 1979, Base level, aggradation and grade: Proceedings of the American Philosophical Society, v. 123, no. 3, p. 168-202.

Leopold, L. B., and Maddock, 1953, The hydraulic geometry of stream channels and some physiographic implications: U. S. Geological Survey Professional Paper 252, 57 p.

Leopold, L. B., and Wolman, M. G., 1957, River channel patterns: braided, meandering and straight: U. S. Geological Survey Professional Paper 282-B, 85 p.

Leopold, L. B., Wolman, M. G., and Miller, J. P., 1964, *Fluvial processes in geomorphology*: W. H. Freeman, San Fransisco, 522 p.

Limerinos, J. T., 1970, Determination of the Manning coefficient from measured bed roughness in natural channels: U. S. Geological Survey Water-Supply Paper 1898B, 47 p.

Lipman, P. W., and Mehnert, H. H., 1979, The Taos Plateau volcanic field, northern Rio Grande rift, New Mexico: *in* Riecker, R. E. (ed.), *Rio Grande rift--tectonics and magmatism*: American Geophysical Union, Washington, D. C., p. 289-311.

Lovering, T. S., and Goddard, E. N., 1950, Geology and ore deposits of the Front Range, Colorado: U. S. Geological Survey Professional Paper 223, 319 p.

Mackin, J. H., 1948, Concept of a graded river: Geological Society of America Bulletin, v. 59, p. 463-511.

Maizels, J. K., 1983, Paleovelocity and paleodischarge determination for coarse gravel deposits: *in* Gregory, K. J. (ed.), *Background to Paleohydrology*: John Wiley & Sons, Ltd., New York, p. 101-139.

Manley, K., 1979, Stratigraphy and structure of the Espanola Basin, Rio Grande Rift, New Mexico: *in* Riecker, R. E. (ed.), *Rio Grande Rift--tectonics and magmatism*: American Geophysical Union, Washington, D. C., p. 71-86.

----------, 1982, Geologic map of the Broke Off Mountain quadrangle, Rio Arriba County, New Mexico: U. S. Geological Survey Miscellaneous Field Studies Map MF-1450.

McCalpin, J. P., 1982, Quaternary geology and neotectonics of the west flank of the northern Sangre de Cristo Mountains, south-central Colorado: Colorado School of Mines Quarterly, v. 77, no. 3, 98 p.

Melton, M. A., 1958, Geometric properties of mature drainage systems and their representation in E_4 phase space: Journal of Geology, v. 66, no. 1, p. 35-56.

Mendenhall, W., and Sincich, T., 1984, *Statistics for the Engineering and Computer Sciences*: Dellen, Santa Clara, CA, 884 p.

Menges, C. M., in preparation, Tectonic geomorphology of mountain front landforms, northern Rio Grande rift, north-central New Mexico: Unpublished Ph. D. dissertation, University of New Mexico, Albuquerque.

Miller, J. P., 1958, High mountain streams: effects of geology on channel characteristics and bed material: New Mexico Bureau of Mines and Mineral Resources Memoir 4, 53 p.

Miller. J. P., Montgomery, A., and Sutherland, P. K., 1963, Geology of part of the southern Sangre de Cristo Mountains, New Mexico: New Mexico Bureau of Mines and Mineral Resources Memoir 11, 106 p.

Morisawa, M. E., 1964, Development of drainage systems on an upraised lake floor: American Journal of Science, v. 262, p. 340-354.

Muehlberger, W. R., 1979, The Embudo fault between Pilar and Arroyo Hondo, New Mexico: an active intracontinental transform fault: New Mexico Geological Society 30th Field Conference Guidebook, p. 77-82.

Parker, G., 1978, Self-formed rivers with equilibrium banks and mobile beds-Part II, The gravel river: Journal of Fluid Mech., v. 89, p. 127-148.

Personius, S. F., and Machette, M. N., 1984, Quaternary and Pliocene faulting in the Taos Plateau region, northern New Mexico: New Mexico Geological Society 35th Field Conference Guidebook, p. 83-90.

Peterson, C. M., 1981, Late Cenozoic stratigraphy and structure of the Taos Plateau, northern New Mexico: Unpublished M. A. thesis,

University of Texas at Austin, 57 p.

Pickup, G., 1975, Downstream variations in morphology, flow conditions and sediment transport in an eroding channel: Zeit. Geomorph., v. 19, no. 4, p. 443-459.

Porter, S. C., Pierce, K. L., and Hamilton, T. D., 1983, Late Wisconsin mountain glaciation in the western United States: *in* Porter, S. C. (ed.), *Late Quaternary environments of the United States, Volume 1: The Late Pleistocene*: University of Minnesota Press, Minneapolis, p. 71-110.

Reed, J. C., Lipman, P. W., and Robertson, J. R., 1983, Geologic map of the Latir Peak and Wheeler Peak Wilderness and Columbine-Hondo Wilderness Study Area, Taos County, New Mexico: U. S. Geological Survey Miscellaneous Field Investigations Map MF-1570-B, scale 1:50,000.

Richards, K., 1982, *Rivers: Form and process in alluvial channels*: Methuen, London, 358 p.

Richmond, G. M., 1962, Correlation of some glacial deposits in New Mexico: U. S. Geological Professional Paper 450-E, p. E121-125.

_____, 1965, Glaciation of the Rocky Mountains: *in* Wright, H. E., and Frey, D. G. (eds.), *The Quaternary of the United States*: Princeton University Press, Princeton, New Jersey, p. 217-230.

Ritter, D. F., 1978, *Process Geomorphology*: Wm. C. Brown, Dubuque, Iowa, 603 p.

Rubey, W. W., 1952, Geology and mineral resources of the Hardin and Brussels quadrangles (in Illinois): U. S. Geological Survey Professional Paper 218, 175 p.

Schumm, S. A., 1956, Evolution of drainage systems and slopes in badlands at Perth Amboy, New Jersey: Geological Society of America Bulletin, v. 67, p. 597-646.

_____, 1965, Quaternary paleohydrology: *in* Wright, H. E., and Frey, D. G. (eds.): *The Quaternary of the United States*: Princeton University Press, Princeton, New Jersey, p. 783-794.

_____, 1968, River adjustment to altered hydrologic regimes, Murrumbidgee River and paleochannels, Australia: U. S. Geological Survey Professional Paper 598.

_____, 1973, Geomorphic thresholds and complex responses of drainage systems: *in* Morisawa, M. E. (ed.): *Fluvial Geomorphology*: State University of New York, Binghampton Publinations in Geomorphology, 4th Annual Meeting, p. 299-310.

_____, 1977, *The fluvial system*: John Wiley & Sons, Ltd.,New York, 338 p.

Schumm, S. A., and Hadley, R. F., 1957, Arroyos and the semiarid cycle of erosion: American Journal of Science, v. 255, p. 161-174.

Schumm, S. A., and Lichty, R. W., 1965, Time, space and causality in geomorphology: American Journal of of Science, v. 263, p. 110-119.

Schumm, S. A., and Parker, R. S., 1973, Implications of complex response of drainage systems for Quaternary alluvial stratigraphy: Nature (Physical Science), v. 243, p. 99-100.

Scott, G. R., 1968, Geologic and structure contour map of the La Junta Quadrangle, Colorado and Kansas: U. S. Geological Survey Miscellaneous Investigations Map I-560, scale 1:250,000.

Scott, K. M., and Gravlee, G. C., 1968, Flood surge on the Rubicon River, California: hydrology, hydraulics, and boulder transport: U. S. Geological Survey Professional Paper 422-M, 40 p.

Selby, M. J., 1982, *Hillslope materials and processes*, Oxford University Press, Oxford, 264 p.

Shepherd, R. G., 1979, River channel and sediment responses to bedrock lithology and stream capture, Sandy Creek drainage, central Texas: *in* Rhoades, D. D., and Williams, G. P. (eds.), *Adjustments of the fluvial system*: Kendall-Hunt, Dubuque, Iowa, p. 255-275.

----------, 1985, Regression analysis of river profiles: Journal of Geology, v. 93, p. 377-384.

Shields, A., 1936, Application of similarity principles and turbulence research to bed-load movement: M. H. Preuss, Verchanst, Berlin, Wasserbau Schittbau, *in* Ott, W. P., and Uchelon, J. C. (translators): Pasadena, California Institute of Technology, W. M. Kech Laboratory of Hydraulics and Water Resources, Report Number 167.

Soil Survey Staff, 1975, *Soil Taxonomy*: U. S. Department of Agriculture, Agricultural Handbook Number 436, U. S. Government Publishing Office, Washington, D. C., 754 p.

State Engineer Office, 1956, Climatological summary, New Mexico, 1894-1954: State of New Mexico, Technical Reports 5 and 6.

Steven, T. A., Lipman, P. W., Hail, H. J., Jr., Barker, F., and Luedke, R. G., 1974, Geologic map of the Durango Quadrangle, southwestern Colorado: U. S. Geological Survey Miscellaneous Investigations Map I-764, scale 1:250,000.

Strahler, A. N., 1952, Hypsometric (area-altitude) analysis of erosional topography: Geological Society of America Bulletin, v. 63, p. 1117-1142.

----------, 1957, Quantitative analysis of watershed geomorphology:

American Geophysical Union Transactions, v. 38. p. 913-920.

Todd, D. K., 1980, *Groundwater Hydrology*: John Wiley & Sons, New York, 535 p.

Tweto, O., 1976, Preliminary geologic map of Colorado: U. S. Geological Survey Miscellaneous Field Map MF-788.

Tweto, O., Steven, T. A., Hail, W. J., Jr., and Moench, R. F., 1976, Preliminary geologic map of the Montrose 1 x 2 Quadrangle, southwestern Colorado: U. S. Geological Survey Miscellaneous Investigations Map MF-761, scale 1:250,000.

U. S. Army Corps of Engineers, 1956, *Snow Hydrology: Summary report of snow investigations*: North Pacific Division, Portland, OR, 437 p.

U. S. Bureau of Reclamation, 1968, Definite plan report, San Juan-Chama Project, Colorado-New Mexico, Volume II - Tributary units: unpublished report.

Upson, J. E., 1939, Physiographic subdivisions of the San Luis Valley, southern Colorado: Journal of Geology, v. 47, p. 721-736.

Viessman, W., Jr., Knapp, J. W., Lewis, G. L., and Harbaugh, T. E., 1977, *Introduction to Hydrology, 2nd ed.*: Harper & Row, New York, 704 p.

Washichek, J. N., Moreland, R. E., and Teilborg, J., 1972, Summary of snow survey measurements, Colorado and New Mexico, 1936-1972: Soil Conservation Service, Denver, CO, 208 p.

Washichek, J. N., Shafer, B. A., and Teilborg, J., 1978, Summary of snow survey measurements Colorado and New Mexico, 1971-1977: Soil Conservation Service, Denver, CO, 128 p.

Wells, S. G., and Jercinovic, D. E. 1983, Applications of geomorphology to surface coal-mining reclamation, northwestern New Mexico: *in* Wells, S. G., Love, D. W. and Gardner, T. W., (eds.), *Chaco Canyon Country*: American Geomorphological Field Group 1983 Field Trip Guidebook, p. 133-148.

Wheeler, D. A., 1979, The overall shape of longitudinal profiles of streams: *in* Pitty, A. F. (ed.), *Geographical Approaches to Fluvial Processes*: Norwich, Geobooks, p. 241-260.

Williams, G. P., 1978, Bankfull discharge of rivers: Water Resources Research, v. 14, p. 1141-1154.

Williams, P. J., 1964, Geology, structure, and uranium deposits of the Moab Quadrangle, Colorado and Utah: U. S. Geological Survey Miscellaneous Geological Investigations Map I-360, scale 1:250,000.

Wolman, M. G., 1954, A method of sampling coarse river-bed material: American Geophysical Union Transactions, v. 35, p. 951-956.

Womack, W. R., and Schumm, S. A., 1977, Terraces of Douglas Creek, northwestern Colorado: An example of episodic erosion: Geology, v. 5, p. 72-76.

Yair, A., and Lavee, H., 1985, Runoff generation in arid and semi-arid zones: *in* Anderson, M. G., and Burt, T. P. (eds.), *Hydrological Forecasting*: John Wiley & Sons, Ltd., New York, p. 183-220.

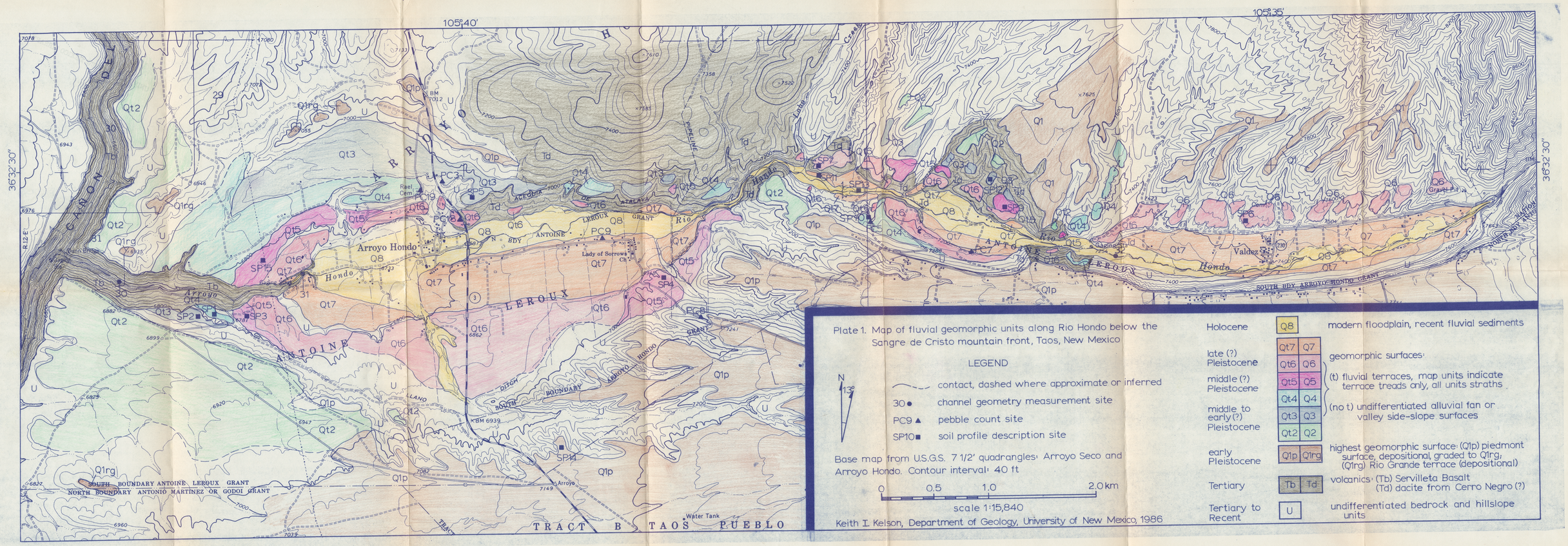

Plate 1. Map of fluvial geomorphic units along Rio Hondo below the Sangre de Cristo mountain front, Taos, New Mexico

LEGEND

- contact, dashed where approximate or inferred
- 30● channel geometry measurement site
- PC9▲ pebble count site
- SP10■ soil profile description site

Base map from U.S.G.S. 7 1/2' quadrangles: Arroyo Seco and Arroyo Hondo. Contour interval: 40 ft

0 0.5 1.0 2.0 km

scale 1:15,840

Keith I. Kelson, Department of Geology, University of New Mexico, 1986

Holocene	Q8	modern floodplain, recent fluvial sediments
late (?) Pleistocene	Qt7 Q7	geomorphic surfaces: (t) fluvial terraces, map units indicate terrace treads only, all units straths. (no t) undifferentiated alluvial fan or valley side-slope surfaces
middle (?) Pleistocene	Qt6 Q6	
	Qt5 Q5	
middle to early (?) Pleistocene	Qt4 Q4	
	Qt3 Q3	
	Qt2 Q2	
early Pleistocene	Q1p Q1rg	highest geomorphic surface: (Q1p) piedmont surface, depositional, graded to Q1rg; (Q1rg) Rio Grande terrace (depositional)
Tertiary	Tb Td	volcanics: (Tb) Servilleta Basalt (Td) dacite from Cerro Negro (?)
Tertiary to Recent	U	undifferentiated bedrock and hillslope units

Plate 3. Map of fluvial geomorphic units along Rio Grande del Rancho between the Sangre de Cristo mountain front and Ojo Sarco Canyon, near Taos, New Mexico

LEGEND

Holocene	Q8	modern floodplain, recent sediments
late (?) Pleistocene	Qt7 Q7	geomorphic surface: (t) fluvial terrace: map units indicate terrace treads only
	Qt6	
middle (?) Pleistocene	Qt4	
middle to early (?) Pleistocene	Qt2	(no t) undifferentiated alluvial fan or valley side-slope surfaces
Mississippian to Recent	U	undifferentiated bedrock and hillslope units

contact, dashed where approximate or inferred

Base map from U.S.G.S. 7 1/2' quadrangle Ranchos de Taos

Keith I. Kelson, Department of Geology, University of New Mexico, 1986

105°32'30"
36°17'30"

FEET 446 — TRES RITOS 15 MI / MORA 34 MI — 35' — 448 — 449 (TRES RITOS) 4856 II NE — 450 — 451 — 32'30"

SCALE 1:24000

1 MILE
7000 FEET
1 KILOMETER

CONTOUR INTERVAL 40 FEET
DATUM IS MEAN SEA LEVEL

GN MN 0°20' 6 MILS 13° 231 MILS

UTM GRID AND 1964 MAGNETIC NORTH DECLINATION AT CENTER OF SHEET

Plate 2 Map of fluvial geomorphic units along Rio Pueblo de Taos, Arroyo Seco, Rio Grande del Rancho, and Rio Fernando de Taos near Taos, New Mexico.

Legend

Holocene
- Q8 — modern floodplain,recent fluvial sediments

late (?) Pleistocene
- Qt6 — geomorphic surfaces:

middle (?) Pleistocene
- Qt4 — (t) fluvial terraces map units indicate terrace treads only, all units strattns

middle to early (?) Pleistocene
- Qt3 Qt2 Q2 — (no t) undifferentiated alluvial fan or valley side-slope surfaces

early Pleistocene
- Qlp Qtrg — highest geomorphic surface, (Qlp) piedmont surface, depositional, graded to (Qtrg) Rio Grande terrace (depositional), (Qtf) alluvial fan and fluvial deposits
- Qtf

Pleistocene(?) to Recent(?)
- Qt — alluvial fan deposits between Taos and Talpa, undifferentiated, contains many buried soils, ages unknown

Tertiary
- Tb — Servilleta Basalt

Mississippian to Recent
- U — undifferentiated bedrock and hillslope units

- contact, dashed where approximate or interred
- fault, dotted where buried, dashed where approximate, ball on downthrown side
- 33 ● — channel geometry measurement site
- PC11 ▲ — pebble count site
- SP21 ■ — soil profile description site
- ⊙ — sample locality, Tsankawi Pumice, 1.2±0.03 Ma (Izett et al.,1981)

Base map from U.S.G.S. 7 1/2' quadrangles: Taos, Ranchos de Taos, Los Cordovas, and Taos SW. Contour interval: 40 ft, except on Los Cordovas sheet (20 ft)

0 0.5 1.0 2.0 km

scale 1:15,840

Keith T Kelson, Department of Geology, University of New Mexico, 1986